UNIVERSITY OF
NEWCASTLE

Residual Stress Distributions in Injection Mouldings

by

Satoshi Hirosawa

A Thesis submitted in partial fulfilment of the requirements for the Degree of Doctor of Philosophy

Department of Mechanical, Materials and Manufacturing Engineering

The University of Newcastle upon Tyne

2001

For all knowledge and wonder (which is the seed of knowledge) is an impression of pleasure in itself.

Francis Bacon

PREFACE

This thesis describes original work which has not been submitted for a degree at any university.

The investigations were carried out in the Materials Division of the Department of Mechanical, Materials and Manufacturing Engineering of the University of Newcastle upon Tyne, United Kingdom under the supervision of Professor J. R. White.

This thesis describes an investigation into the computations of residual stress distributions in injection Mouldings.

ACKNOWLEDGEMENTS

I am heartily grateful to Professor J. R. White for his supervision, continued support and kind help during the research.

I wish to express my gratitude to the technical staff of the Divisional workshop for constant help and useful advice. I also thank A. A. Da Silva, Dr T. J. Turton and other fellow research students for their help and kindness.

I would also like to record my appreciation of Dr Li Tong, Professor Ichiro Muramatsu, Professor Susumu Furuichi and the friends in England for their support.

Lastly, but not least, I am grateful to my parents Setsuzo, Fumiko and my fiancée Shinju Takeyasu for their continued support and patience during the research.

Abstract

Residual stress distributions in injection moulded polystyrene plaques have been computed using various calculation methods based on procedures from the literature. Some of the mathematical procedures have been extended to provide improved analysis of the process. The results have been compared with measured distributions obtained using the layer removal technique. The purpose of this work was to resolve some of the disagreements between the measured residual stress distributions in injection moulded parts and those predicted by computations made in the literature.

The calculations are made using the general purpose software "Mathcad". Various temperature, time and pressure dependent material models have been used to calculate the residual stress and they are compared. Special attention has been paid to choosing boundary conditions that match the moulding parameters used in the manufacture of the injection mouldings on which the measurements were made. Similarly, care has been taken to choose boundary conditions that correspond with the different actual storage times before analysis for the samples and also boundary conditions that correspond with the post-moulding conditioning.

Measurements of residual stresses distributions were made on mouldings produced under conditions chosen to simplify the modelling requirements. The sensitivity of the calculations to the materials property data and to the boundary conditions used have been examined. The experimental verification includes examination of the post-moulding changes.

The predicted residual stress distributions over the entire moulding and post-moulding history have been found to be in generally good agreement with the corresponding experimental results under various processing conditions and post-moulding changes. In particular, kinematic boundary conditions for the moulding conditions and the post-moulding conditions, due to different temperatures and relaxation times of the polymer, have been found to be critical ingredients in the calculation of the residual stress distributions.

Glossary

Latin symbols

$a(T,T_g)$ is the shift factor between the temperature T and the glass transition temperature T_g

A is a mechanical parameter defined as $\frac{\alpha_g \times E_g}{1-\nu_g}$

B is the quantity between 0.08 and 1 defined as follows when T is below the glass transition temperature: $B=\frac{30-\ln q}{T}$

C represents constants

e is the thickness of sample

$E(t)$ is the time-dependent Young's modulus

$f(z,t)$ is the dimensionless function defined in a way similar to the temperature difference ratio in the Fourier heat transfer analysis

$G(t)$ is the time-dependent shear modulus

$h(z)$ is a periodic step function

$H(t)$ is the position of the solidification or glass transition plane

k represents Boltzmann's constant

$K(t)$ is the time-dependent bulk modulus

L is the length of sample bars used in the experimental part

m is the exponent parameter in the KWW equation

P is the pressure

q is the local cooling rate $q=\dot{T}(z,t)$

R is a mechanical parameter defined as follows $R = \frac{E}{1-\nu}$

t is time

T is the temperature

$\dot{T}(z,t)$ is the cooling rate

$\dot{T}$ stands for the differentiation of temperature with respect to time

V is the volume

W is the width of sample bars

x is the coordinate measured along the length of samples

y is the coordinate measured in the width direction of samples

z is the coordinate measured in the normal direction to the plane faces of the bars

Latin and subscript symbols

a_n, b_n, a'_n and b'_n are Fourier sum coefficients

a_{0s}, a_{0m}, a_{1s}, a_{1m}, b_s, b_m are the constants in the Tait equations

A_r is a mechanical parameter defined as $\frac{\alpha_g \times E_g}{1-\nu_g} = \alpha_r \cdot R_r$

C_1 and C_2 are universal constants that appear in the WLF equation

C_p is the specific heat at constant pressure

E_0 is the unrelaxed Young's modulus (Sections 2.3.1, 2.3.2 and 3.5.1)

E_0 is the reference Young's modulus (Section 3.5.2)

E_r is the Young's modulus in the rubbery core

$g_1(z,t) = u_i(z) \cdot v_i(t)$ where $v_i(t)$ is an exponential decay function and $u_i(z)$ is a cosine function

J_r is the relaxed compliance as expressed in the single relaxation time model

J_u is the unrelaxed compliance as expressed in the single relaxation time model

$$k_1 = k \cdot \left(\frac{\pi}{e}\right)^2$$

K_1 (z, t_2) is a bulk modulus

P_0 is the packing pressure

P_1 is the atmospheric pressure

$$R_r = \frac{E_r}{1-\nu_r}$$

$t_0(T)$ is the relaxation time at the temperature T that appears in the KWW equation

$t_1(z)$ is the time at which the solidification plane reaches the position z

t_{dem} is the cooling time after demoulding

t_g is defined as the time at which solidification of the whole moulding is just complete, that is the time at which the material which cools most slowly just reaches T_g

T_0 is the initial temperature of the molten polymer within the mould cavity walls

T_∞ is the temperature at the cold cavity walls

T_{dem} (z,t) is the temperature distribution after demoulding

T_g is the glass transition temperature

$T_{g1}(t_1)$ is the glass transition temperature when $t = t_1$

T_m is the melt temperature

$T_m(z,t_n)$ is the melt temperature when t is t_n

T_{melt} is the melt temperature

T_r is the reference temperature

T_{room} is the room temperature

z_0 is the half thickness of samples

Greek symbols

$\alpha(T)$ is the temperature-dependent thermal expansion coefficient

β is a variable

ΔH is the activation energy of a secondary relaxation process

$\Delta(z,t,\psi)=\phi(z,t)-\phi(z,\psi)$

ε and ε' are respectively the strains in the glassy shell and in the rubbery core

ϕ is the heat flux vector

$\phi(z,t)$ is the reduced time

κ is the thermal diffusivity of the polymer

λ is the coefficient of heat conduction

θ is an integration variable or an angle used

ρ is the density

τ is the relaxation time in the single relaxation time model

ξ is a space integration variable

$f(t)$ and $\varphi(z,t)$ are unknown functions

Greek and subscript symbols

α_g is the thermal expansion coefficient in the glassy shell

α_r is the thermal expansion coefficient in the rubbery region

α_v volumetric thermal expansion

ΔP_1 is the average pressure drop

ΔV_1 is the volumetric change in an element of material at z

ΔT_1 is the temperature defined as $T_1(z,t_1)$-$T_2(z,t_2)$

$\varepsilon_{xx}(t)$ is the strain in the x-direction

$\dot{\varepsilon}_{xx}(t)$ is the strain rate in the x-direction

ν_g is the Poisson's ratio in the glassy shell

ν_r is the Poisson's ratio in the rubbery core

V_s is the measured specific volume at temperature T

V_0 is the occupied volume

$\rho_n(t_n,P=0,z)$ is the density when the pressure is atmospheric

$\rho_n(t_n,P=0,z)$ is the density when the pressure is atmospheric

$\rho_{n+1}(t_{(n+1)}, P_n, z)$ is the density when the temperature has fallen to below T_g at all locations

ρ_x and ρ_y are the components of curvature in the x and y directions

σ_t is the true stress for a simple extension

$\sigma_{xx}(z,t)$, $\sigma_{yy}(z,t)$, $\sigma_{zz}(z,t)$, represent the equi-biaxial stress distribution

$\dot{\sigma}(z,t)$ is the normal stress rate according to the x-direction

$\dot{\sigma}_{xx}(t)$ is the stress rate in the x-direction

$\dot{\sigma}_{xxmelt}(t)$ is the stress rate in the x-direction

Miscellaneous symbols

∇ is the 3-dimensional delta operator

CONTENTS

CHAPTER 1

INTRODUCTION

1.1 Research objective

Polymers are one of the most important families of materials and widely used in engineering structures. Residual stresses are known to occur in injection moulded polymers. They can influence the mechanical properties and also cause warping and other changes in dimensions of mouldings.

The surface regions of the moulding cool and solidify before the interior cools significantly. The subsequent thermal shrinkage of the material in the interior causes the formation of tensile stresses there and of compressive stresses near to the surface. In the case of parts made by moulding operations that involve flow in the melt state, there may be an additional contribution to the residual stresses related to the thermo-mechanical history prior to solidification. Changes in residual stresses can occur after the moulding is made. In some polymers, the magnitude of the residual stresses may even change significantly on ageing at room temperature. Larger and more rapid changes occur as the result of ageing at elevated temperature or application of a temperature gradient. The reasons for the changes in stress distribution are many and will be discussed in this thesis.

Mathematical models have been proposed and widely developed by various research groups for the residual stress computations. The purpose of this study is to resolve some

of the disagreements between the measured residual stress distributions in injection moulded parts and those predicted by computations made in the literature.

1.2 The research programme

The samples used in this study were injection moulded bars made of polystyrene (PS). Polystyrene was moulded into ASTM D638 type I tensile test bars and straight test bars (190×12.7×3.2mm) with a deep gate system (2.5mm) and a shallow gate system (0.5mm). The test methods applied and the properties measured include (i) The layer removal procedure to determine the residual stress distribution; (ii) stress relaxation tests at constant strain at a constant temperature.

Residual stress distributions in injection moulded polystyrene plaques were computed using various calculation methods from the literature. The calculations were made using the general purpose software "Mathcad". Various temperature, time and pressure dependent material models were used in the calculation of the residual stress and the results obtained from the different methods are compared.

1.3 Outline of this thesis

The literature survey in chapter 2 deals with mechanical, thermal properties and analytical descriptions of polymer behaviour which form the basis of the calculations presented in Chapter 3. Reviews of computer-aided calculations are covered here.

Chapter 3 deals with modelling of residual stress distributions. Calculations are divided into two procedures: firstly, using the procedure based on Struik's method (Method A), and secondly, using the new procedure (Method B) developed during this research, in

which the pressure profile was calculated and used to estimate density distributions through the depth and the stress distribution.

Chapter 4 deals with residual stress calculations performed using both Method A and Method B. Various temperature, time and pressure dependent material models were used. Special attention was paid to choosing boundary conditions that match the moulding parameters used in the manufacture of the injection mouldings on which the measurements were made. Similarly, care was taken to choose boundary conditions that correspond with the different actual storage times before analysis for the samples and also boundary conditions that correspond with the post-moulding conditioning.

The layer removal procedure and the stress relaxation tests are discussed in Chapter 5. Chapter 6 covers the experimental results. The results include residual stress distributions and stress relaxation.

Chapter 7 contains general discussion covering comparisons between the experiments and the calculations. Some of the disagreements between the measured residual stress distributions in injection moulded parts and those predicted by computations are discussed. The main conclusions are given in Chapter 8.

CHAPTER 2

LITERATURE SURVEY

This chapter is divided into eleven sections. Sections 2.1 and 2.2 begin with very general introductions to injection moulding and the properties of polystyrene.

Sections 2.3 and 2.4 review the literature about the time and temperature dependence of Young's modulus of polymers, in particular near the glass transition temperature. Section 2.5 deals with temperature and pressure dependence of specific volume.

Section 2.6 describes rate of heat transport in polymers. Section 2.7 deals with thermal residual stress. Section 2.8 describes effect of moulding conditions on residual stress. The analytical description of polymer behaviour developed in the literature in Sections 2.3 to 2.8 form the basis of the calculations presented in Chapter 3. Section 2.9 shows post moulding changes in residual stress. Section 2.10 outlines computer-aided calculations. Section 2.11 deals with residual stress measurement.

2.1 The injection moulding process

A simplified sketch of an injection moulding machine is given in Fig. 2.1.1 The material is inserted into the hopper and fed into the extruder where it is mixed and heated with the intention to obtain a melt which is as homogeneous as possible, with respect to temperature and mixture, and to transport it towards the nozzle. The screw is allowed to travel backwards (away from the mould) and a charge accumulates in front of it. When there is sufficient charge to fill the mould cavity the screw is propelled forward and the material is injected into the mould at a very high speed at very high pressures (up to 250 MPa). After the product has cooled down sufficiently in the mould, it is ejected.[1]

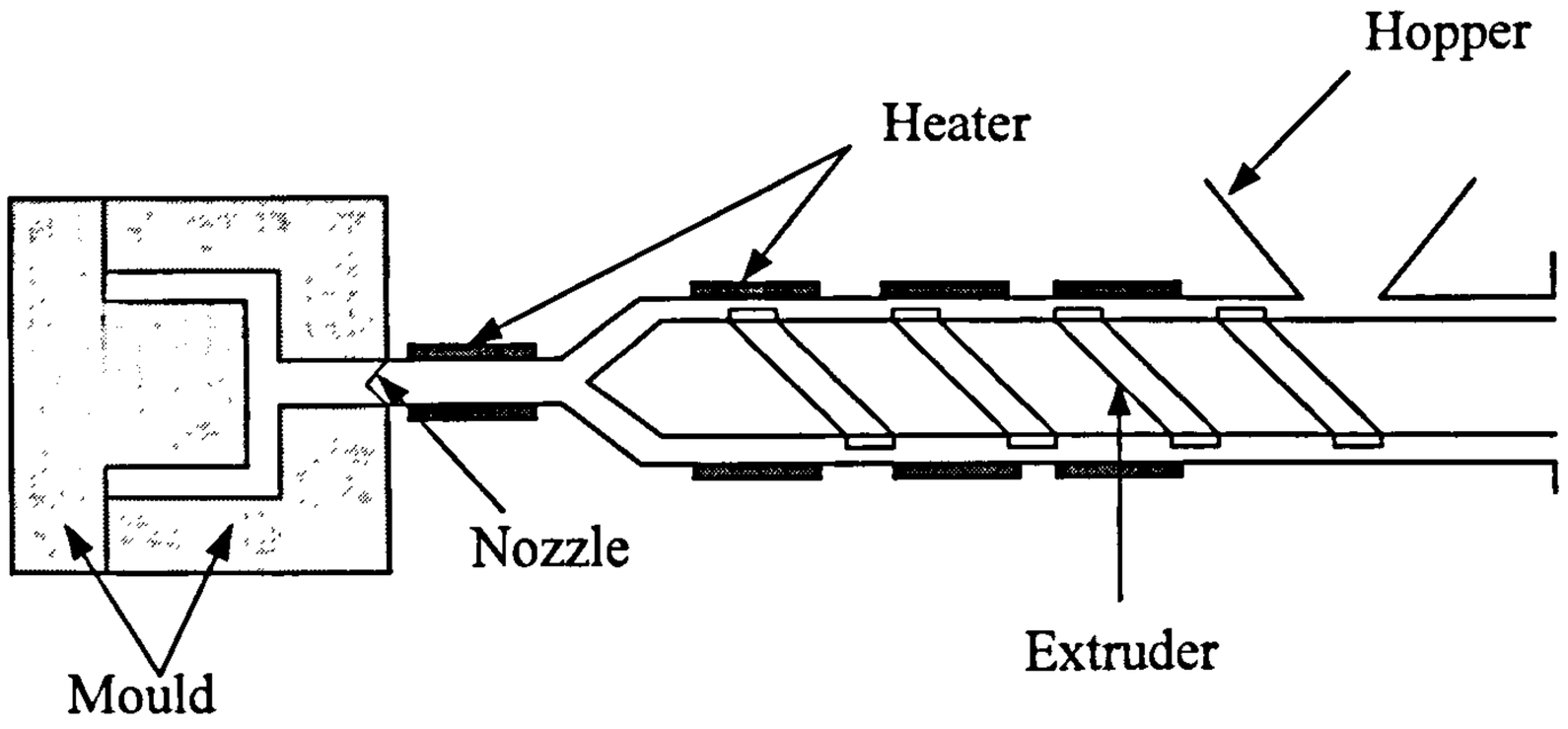

Fig. 2.1.1 Schematic presentation of moulding machine

A typical pressure profile at a certain position in the cavity is shown in Fig. 2.1.2. From a conceptual point of view, three stages are defined. First, the injection stage, with moderate pressures. Thereafter follows the compression stage in which the material is compressed to conform to the mould cavity. After compression the post-filling stage begins, the high pressure at the entrance of the cavity allows material to flow into the cavity as the polymer cools down, again with the purpose to compensate for the thermal shrinkage. Eventually, the gate freezes off and no more material flows into the cavity. This stage is also referred to as the cooling stage.[1]

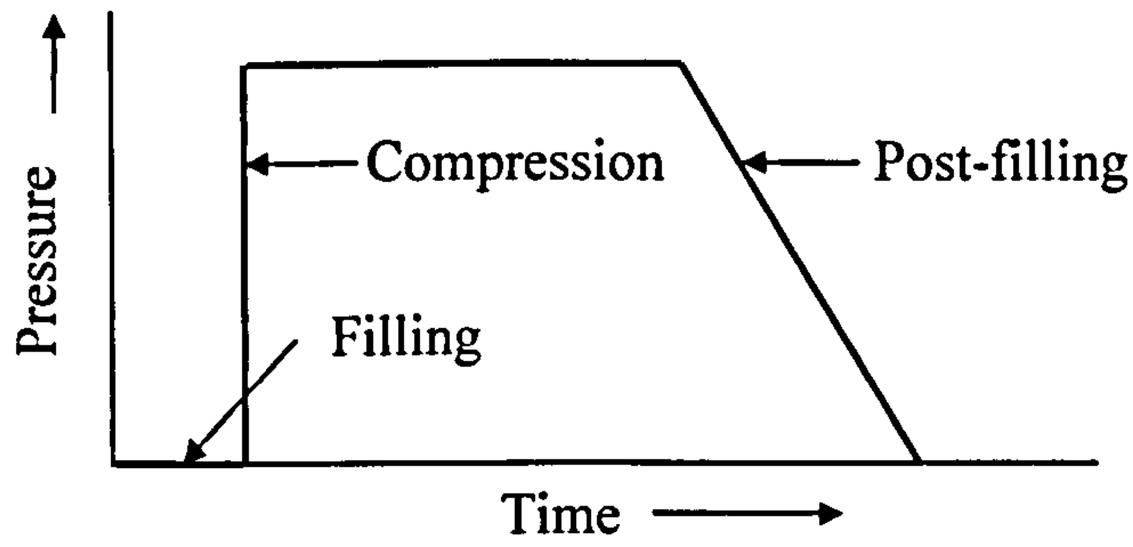

Fig. 2.1.2 Pressure trace in a cavity during the injection moulding cycle

2.2 Properties of Polystyrene

Many polymers show regions of high order and should be considered as semi-crystalline[2]. The major factor which is determining whether a polymer can crystallise depends on the occurrence of successive units in the chain in a configuration of high structural regularity. If the chain elements are small as in linear polyethylene (see Fig. 2.2.a), crystallinity is highly developed. If the chain elements are complex, containing bulky side groups (see Fig. 2.2.b), as in polystyrene (PS), the material can crystallise only if these substitute groups are arranged in an ordered or tactic configuration.[3]

In linear thermoplastic semi-crystalline polymers, it is possible to identify a melting temperature (T_m). Above this melting temperature, the polymer may be liquid, viscoelastic or rubbery according to its molecular mass. However, below it, in the high molecular mass range, it will tend to act like a viscoelastic solid down to the glass transition temperature.[4]

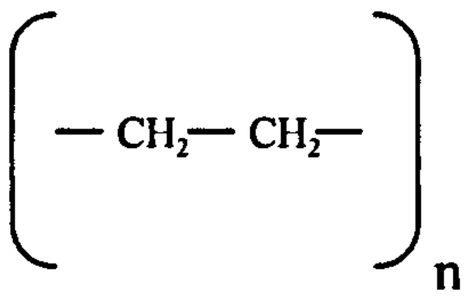

Fig. 2.2.a the structure of polyethylene

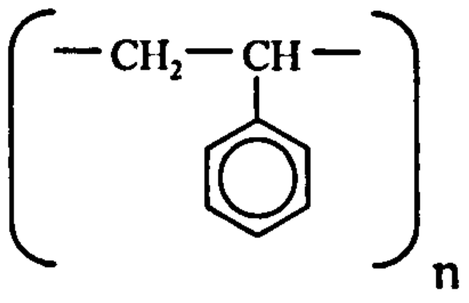

Fig. 2.2.b the structure of polystyrene

The semi-crystalline melting point (T_m) is theoretically the highest temperature at which polymer crystallites can exist. Normally, polymer crystallises in a certain temperature range. Secondary semi-crystalline transitions (below T_m) occur if the material transforms from one type of crystal to another. These transitions, like the melting point, are thermodynamic first-order transitions. In crystalline polymers, T_m rather than T_g

determines the upper service temperature of plastics and the lower service temperature of rubbers, T_g is still very important. The reason is that between T_g and T_m the polymer is likely to be tough; the best use region of the polymer may therefore be expected at the lower end of the leathery range (Fig. 2.2.1). Below the glass transition temperature, many polymers tend to be brittle, especially if the molecular weight is not very high. Secondary transitions may be responsible if a rigid material is tough rather than brittle[5].

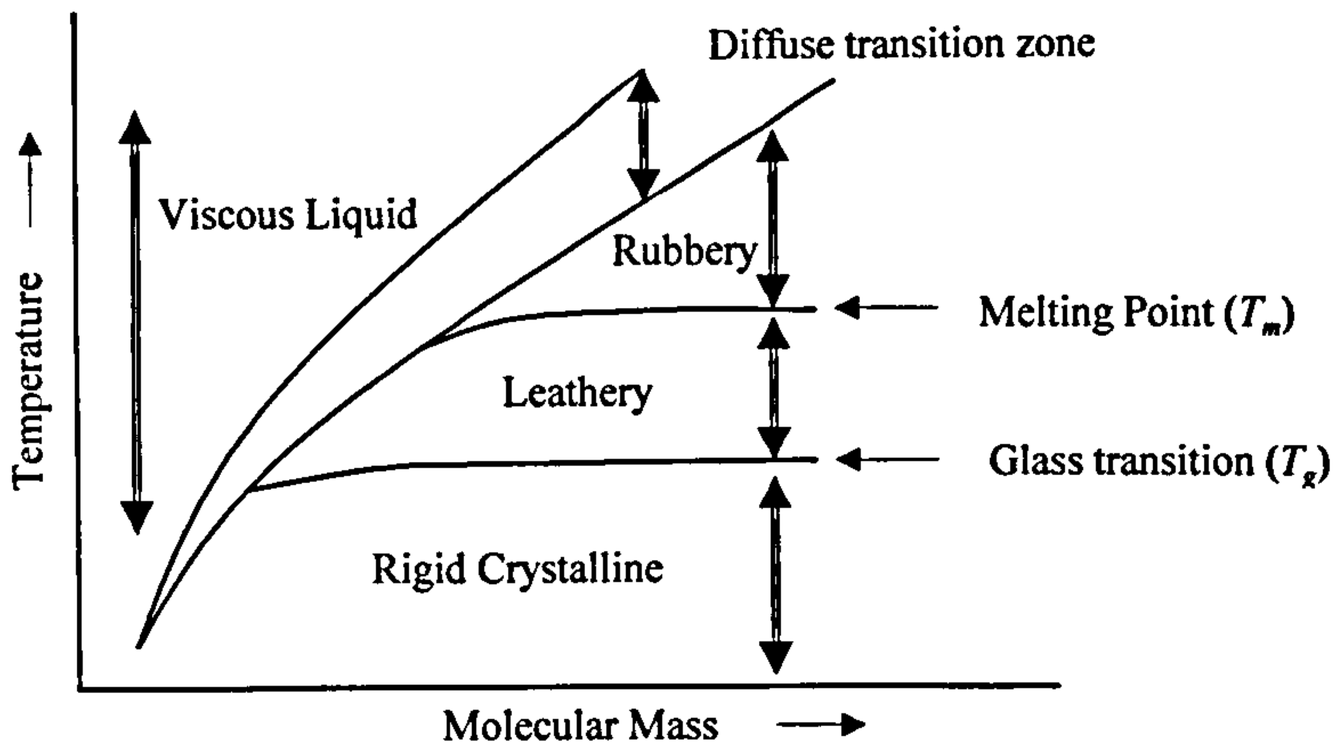

Fig. 2.2.1 T-M Diagram for semi crystalline polymers[13]

Temperature-Molecular Diagram for semi crystalline polymers. Leathery range is shown in between two curves (melting point and glass transition)

Polystyrene is regarded as an amorphous glassy thermoplastic. Because of its atacticity,

Polystyrene is unlikely to crystallise even if it is drawn to give molecular alignment, as happens in the soft blocks in copolymers of polyurethane. The mechanical properties and integrity are due to entanglements among the main chains. The density of entanglements is high below the glass transition temperature and decreases as the temperature rises. The drop in the Young's modulus when the temperature increases is connected to this decrease of the density of entanglements below T_g. As polystyrene

does not have cross-links, which are permanent covalent bonds connecting adjacent main chains, at high temperatures, it may not display an elastic behaviour when being stretched, for the density of entanglements is too low. Consequently, it can be assumed that the Young's modulus of PS will totally vanish when the polymer flow is liquid-like (above T_g)[4]. There is no residual mechanical integrity due to cross-links. Such an assumption is a premise for Lodge's constitutive model of a rubber-like liquid[6].

2.3 Time and temperature dependence of Young's modulus

The Young's modulus of polystyrene and other thermoplastics is time-dependent and changes continuously as temperature changes and it is required to chose a suitable expression to represent it that can be inserted into computations[7,8,9,10,11].

Materials have non-elastic properties under certain circumstances. This is especially the nature of polymers. They may show non-elastic deformation under conditions in which other materials may be regarded as purely elastic.[4] It can be said that viscoelastic deformations cover for all deformations that are not purely elastic. This means that viscoelasticity deals with a number of quite different phenomena. Viscoelasticity is the combination of viscous and elastic properties[4].

2.3.1 Stress relaxation

Stress relaxation is the time-dependent change in stress at a constant deformation and temperature. It is common use to call the momentary ratio of tensile stress to strain the "relaxation modulus" (E_{rl}) and to present the results of the experiments in the form of E_{rl} as a function of time. The stress-relaxation behaviour of polymers is extremely temperature-dependent, especially in the region of the glass transition temperature.

2.3.1.1 The single relaxation time model

The single relaxation time model due to Nowick (1953)[12] is introduced which permits derivation of an expression for the time-dependent compliance:

$$J(t) = J_u + (J_R - J_u) \cdot \left(1 - \exp\left(-\frac{t}{\tau}\right)\right) \qquad (2.3.1)$$

where

J_U, J_R are the unrelaxed and the relaxed compliance respectively and τ is the characteristic relaxation time.

When $t << \tau$, $J(t)=J_u$ and when $t >> \tau$, $J(t)=J_R$. In the same way, the Young's modulus can be written: $E_0 \cdot \exp\left(\frac{-t}{\tau}\right)$ where E_0 stands for the unrelaxed modulus. Here the relaxed modulus ($t \to \infty$)equals zero. Such relationships include the decay of the Young's modulus controlled by a single relaxation time present in an exponential function and approximate the behaviour of thermoplastics shown by experimental data (Fig. 2.3.1[22]).

Great care has to be taken to describe theoretically the true shape (sigmoid curve) of the time-dependence of the Young's modulus. A model taking into an account a distribution of relaxation times has also been developed to better match the experimental data.[4,22]

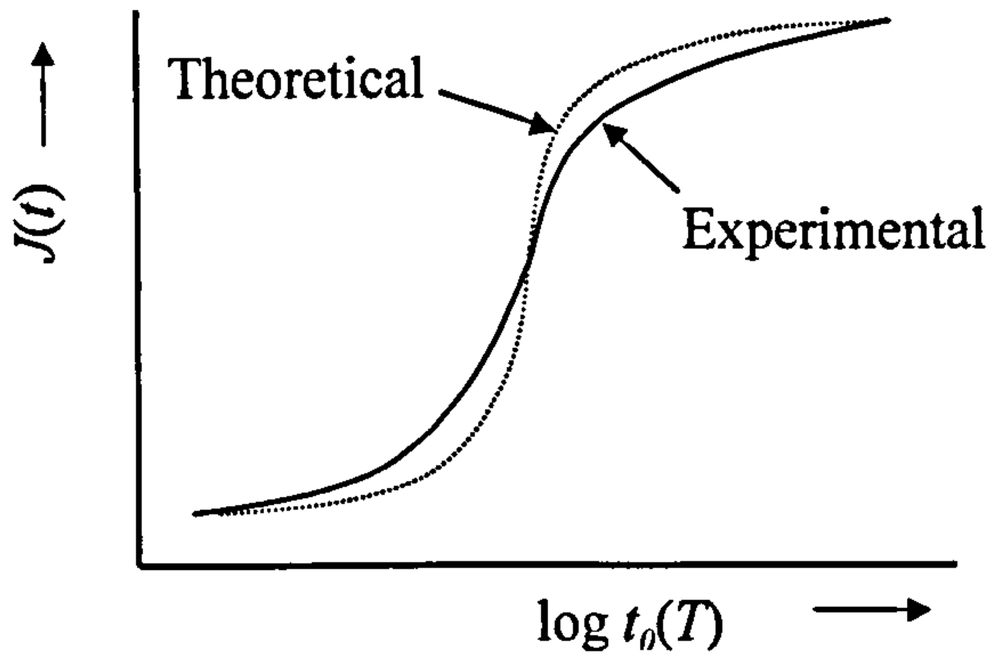

Fig. 2.3.1 Compliance of PS showing the glass transition[22]

2.3.1.2 Struik's adapted equation

In the transition region a plot of the logarithm of the tensile relaxation function ($\sigma(t)/\varepsilon_{0}$,) against the logarithm of time is nearly a straight line with a negative slope; at both higher and lower temperatures the slope becomes less steep[13].

This behaviour can be approximated by the Maxwell model:

$$\frac{\sigma(t)}{\varepsilon_0} \equiv E_{r1}(t) = E_0 \exp\left(\frac{-t}{\Theta_{r1}}\right) \qquad (2.3.2)$$

where

Θ_{rl} is the relaxation time, i.e. the time necessary to reduce σ to a fraction 1/e of its original value and ε_0 is the applied strain.

Eq. 2.3.1 is valid only in a rather limited time interval. If the behaviour over a longer time period must be described, a number of equations of this type can be superposed, each with a different relaxation time. Ultimately, a whole relaxation spectrum is developed[14].

The formulae for stress relaxation which give best agreement with measured time dependent behaviour were proposed by Struik (1978)[15].

$$\frac{\sigma(t)}{\varepsilon_0} \equiv E_{rl}(t) = E_0 \cdot \exp\left(-\frac{t}{t_0}\right)^m \qquad (2.3.3)$$

and for long-term tests

$$\frac{\sigma(t)}{\varepsilon_0} \equiv E_{rl}(t) = E_0 \cdot \exp\left[\left(-\frac{t_e}{t_0}\right)^m \cdot \left[\ln\left(1+\frac{t}{t_e}\right)\right]^m\right] \qquad (2.3.4)$$

where

t_0 is a characteristic constant for the material, dependent on T. t_e is an ageing time of

polymer, elapsed after quenching of melt and m is a constant with a value about 1/3

2.3.1.3 Kohlrausch-Williams-Watts equation

The single relaxation time model can be modified by an empirical formula of general applicability[16], the Kohlrausch-Williams-Watts (KWW)[17] equation, as follows:

$$E(T,t) = E(T_g, at) = E_0 \cdot \exp\left[-\left(\frac{at}{t_0(T_g)}\right)^m\right] \tag{2.3.5}$$

where

$E(T,t)$ is the time-dependent Young's modulus at temperature T

a is the shift factor describing displacement along the time axis and is a function of temperature

$t_0(T)$ is the associated relaxation time at the same temperature and has the same significance as τ in Eq. 2.3.1. and m is a parameter different from unity

Consequently, the KWW equation introduces a departure from the single relaxation time model. This equation has come closer to agreement with the experimental measurements. Actually, m is considerably smaller than unity (e.g. 1/3-1/2)[18] and many materials show very similar m-values. For all these materials the shape of the time-dependent stress-relaxation curve is roughly the same[15]. This can be readily understood, for the shape of the curve is determined by the development of the main chain-diffusion process at a long range scale; which main chains actually diffuse is obviously of less importance.

$t_0(T)$ is temperature-dependent and does not follow an Arrhenius law with constant activation energy, $t_0(T)$ is expected instead to obey the WLF equation (see later). The definition of the glass transition temperature may be ambiguous because it is reported[18]

to be the temperature at which the associated relaxation time in the KWW equation is within the interval 1s-100s[18]. The latter interval has a length of two orders of magnitude, which is the upper tolerance as regards the intervals of values for $t_0(T_g)$. In these calculations, the latter relaxation time is assumed to equal to either 1s or 100s. In the article written by Gortemaker *et al* (1974)[19], when the shear rate is less than 10^{-2} s^{-1}, the time for the adjustment of a steady flow is controlled by a relaxation time equal to 100s. When the shear rate is about 1 s^{-1}, this relaxation time becomes very small (1s or less than 1s). It seems that an accurate value for $t_0(T_g)$ will depend on the nature of the problem (e.g. thermal stress calculations or relaxation of the first normal stress difference after steady shear flow) and the previous applied shear rate 1 s^{-1}.

2.3.2 Time-temperature superposability (T.T.S) of Polymers

Struik (1990)[16] developed the time-temperature superposability of polymers which considers both the KWW and the WLF equations. The plots representing the Young's modulus at various temperatures versus logarithmic time can be superimposed by shifting according to a horizontal shift factor. If the mastercurve is taken at the reference temperature equal to the glass transition temperature, it can be seen that:

$$E(T,t) = E(T_g, a(T,T_g)\cdot t) \tag{2.3.6}$$

where

$a(T,T_g)$ is the shift factor between T and T_g which will be given by Eq. 2.3.10.

When $T>T_g$, $a(T,T_g)>1$. When $T<T_g$, $a(T,T_g)<1$. Finally when $T=T_g$, $a(T,T_g)=1$ (Fig. 2.3.1).

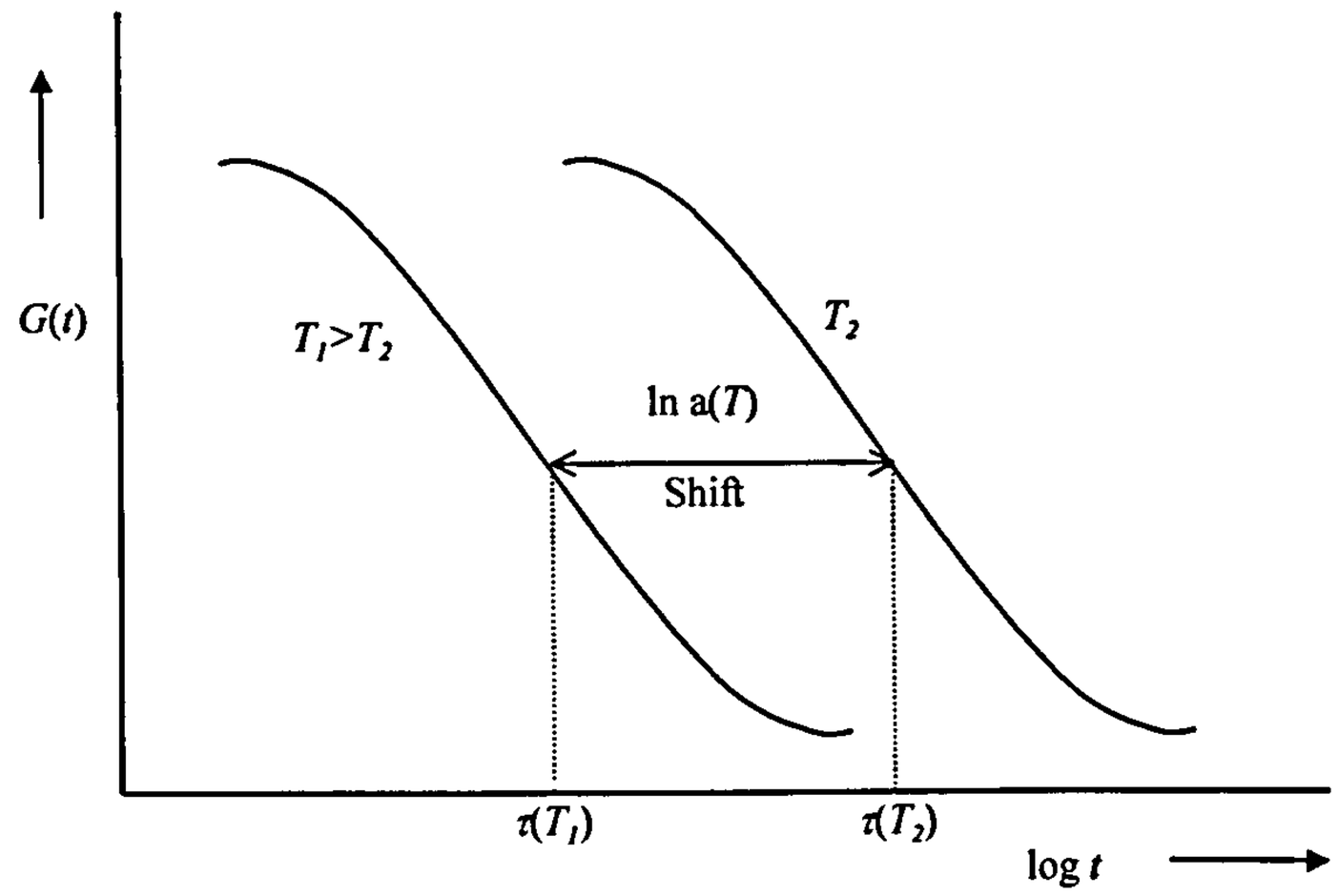

Fig. 2.3.1 Stress relaxation and the effect of temperature[16]

The two curves (the mastercurve at T_g and the curve at temperature T) are superimposed when a translation, for which the translation vector is $\ln(a(T,T_g))$, is performed. Such a behaviour is said to be thermorheologically simple and was first observed in the 1940s and 1950s[26,27]. Its interpretation is that temperature only affects the position of the relaxation curve, the shape of this curve being independent of temperature.

The KWW equation at T_g gives:

$$E(T_g,t) = E_0 \cdot \exp\left[-\left(\frac{t}{t_0(T_g)}\right)^m\right] \tag{2.3.7}$$

By applying the T.T.S principle, it follows from Eq. 2.3.5

$$E(T,t) = E(T_g, a(T,T_g)\cdot t) = E_0 \exp\left[-\left(\frac{a(T,T_g)\cdot t}{t_0(T_g)}\right)^m\right] = E_0 \cdot \exp\left[-\left(\frac{t}{t_0(T)}\right)^m\right] \tag{2.3.8}$$

This yields

$$-\ln\left[\frac{t_0(T)}{t_0(T_g)}\right]=\ln\left(a\left(T,T_g\right)\right) \tag{2.3.9}$$

Now the WLF expression for time-temperature superposition can be applied

$$\ln\left(a\left(T,T_g\right)\right)=\exp\left[\frac{-C_1(T-T_g)}{C_2+(T-T_g)}\right] \tag{2.3.10}$$

where T represents a modified temperature field, for the latter equation is only valid for a limited temperature range around the glass transition temperature. For the purpose of moulding solidification in moulding operations, this modified temperature field can be allowed to take all values above T_g for the shift factors between the mastercurve and the curve of the time dependence of Young's modulus (this is the method adopted in Section 4.4.2). In the case of polystyrene, Struik allowed the temperature to drop until it reached 350K (23 degrees below T_g). According to the authors[4] the WLF equation is only valid for a limited temperature range below T_g, and this is why a limited drop of amplitude 23 degrees has been chosen[16]. A new temperature field $S(t)$ was then defined as follows:

if $T(t)>350$K then $T(t)=S(t)$

if $T(t)\leq 350$K, then $S(t)=350$K

If such a limit is not imposed, the viscosity as predicted by the WLF equation becomes infinite, which is contrary to observation even with a polymer in its glassy state.

Combination of Eq. 2.3.8, Eq. 2.3.9 and Eq. 2.3.10 gives

$$E(T,T_g,t)=E_0\cdot\exp\left[-\left(\frac{\exp\left(\frac{C_1\cdot(T-T_g)}{C_2+(T-T_g)}\right)\cdot t}{t_0(T_g)}\right)^m\right] \tag{2.3.11}$$

2.3.3 Creep (elasto-plasticity)

Long term dimensional stability under force is one of the most important properties of solid materials, but few materials are perfect in this respect. Creep is the time-dependent (also temperature dependent) relative deformation under a constant force (tension, shear or compression). In contradistinction to stress relaxation, creep is in general a combination of relaxation and viscous deformation phenomena. For small deformations (i.e. under the influence of small forces) relaxation phenomena predominate. It is under these conditions that stress relaxation and creep can be quantitatively correlated. As the amount of deformation increases, viscous phenomena become increasingly important. At a given moment, the specimen may show yielding, i.e. rapid viscous deformation.

The results of creep experiments are usually expressed as the quantity creep compliance, the time-dependent quotient of strain/stress. Creep properties are very much dependent upon temperature. Well below the glass-transition point, very little creep will take place, even after long periods of time. As the temperature is raised, the rate of creep increases. In the glass-transition region the creep properties become extremely temperature-dependent. In many polymers, the creep rate goes through a maximum near the glass-transition point[13].

A well-known simplified equation for the tensile creep function is the Voigt model.

$$\frac{\varepsilon(t)}{\sigma_0} \equiv S_r(t) = S_0\left[1 - \exp\left(\frac{-t}{\Theta_r}\right)\right] \qquad (2.3.12)$$

where

Θ_r is the retardation time.

In addition, in this case, several retardation phenomena with different retardation times

may be superposed[14].

Struik (1978)[15] modified the expression for creep strain in manner similar to that used to describe Young's modulus, giving a form similar to the KWW function, ie.

$$\frac{\varepsilon(t)}{\sigma_0} \equiv S(t) = S_0 \cdot \exp\left(\frac{t}{t_0}\right)^m \qquad (2.3.13)$$

and for long term experiments

$$\frac{\varepsilon(t)}{\sigma_0} \equiv S(t) = S_0 \cdot \exp\left[\left(\frac{t_c}{t_0}\right)^m \cdot \left[\ln\left(1+\frac{t}{t_c}\right)\right]^m\right] \qquad (2.3.14)$$

where

t_0 is a characteristic constant for the material, dependent on T.

t_c is an ageing time of polymer, elapsed after quenching of melt and m is a constant with a value about 1/3

2.4 Glass transition processes

The properties of polymers change very significantly as the material cools through the glass transition. This is a critical regime in the injection moulding process.

There are many theories that try to explain the glass transition process. They all emphasise a diffusion mechanism of main chains according to a long-range scale. These theories can be divided into three main groups.

2.4.1 Normal mode theories

The first group deals with normal mode theories based on the Gaussian sub-molecular model. A chain is arbitrarily divided into a number of segments or "submolecules" each

of which is sufficiently long (e.g. more than 50 monomer units) that its end-to-end distance may also be approximated by the Gaussian distribution[20]. The motion of this chain is then described as the superposition of a number of normal modes. Local motions of chain segments which are shorter than the hypothetical submolecule are excluded. The treatment of the normal mode theory as done by Rouse (1953)[21] gives the following time relaxation distribution:

$$\tau_p = z' \cdot l^2 \cdot \zeta \cdot \left[24k \cdot T \cdot \sin^2\left(\frac{p\pi}{2(\nu'+1)} \right) \right]^{-1} \qquad (2.4.1)$$

where

$z' = \frac{n}{\nu'}$: the number of links in each submolecule, n is the number of links in the overall macromolecule and ν' represents the number of sub-molecules.

l is the length of one link, π is a constant and p is the discrete index that defines the distribution.

The p^{th} mode corresponds to motions in p+1 submolecules, a mode existing between each submolecule. ζ is the frictional coefficient that appears in the definition of the frictional force $f = -\zeta v$ where v stands for the velocity of the submolecule. Other normal mode theories have been formulated[22]. They differ from each other because some take account of the effects of hydrodynamic interactions more completely than others. These interactions may be illustrated as follows: when a polymer chain segment moves relative to its liquid environment it will exert frictional forces on the surrounding liquid medium. These forces will modify the velocity distribution of the liquid medium in the vicinity of the polymer chain. This effect will, in turn, influence the motions of other segments of the same polymer coil. The treatment of Rouse does not include these hydrodynamic interactions.

2.4.2 Detailed chain dynamics theories

The second group is composed of theories that try to treat the local motions neglected by the normal mode theories because these motions are shorter than the dimensions of the corresponding submolecules. Kirkwood and Fuoss (1941)[23] considered the motions of a polymer chain in a viscous medium, neglecting the effects of hydrodynamic interaction. Their procedure involved a solution of the diffusion equation in which the time-dependent probability distribution function was expressed in a general way. Yamafuji and Ishida (1962)[24] proposed a theory for the dielectric relaxation of a linear polymer chain which also takes into account local chain motions. In order to avoid the complications of the Kirkwood and Fuoss formulation (1941)[23], they neglected translational motions of the chain dipoles on the grounds that these do not alter potential energy with regard to an external electric field. Bueche (1961)[25] suggested that the major portion of the prime dielectric dispersion might be explained by ignoring co-operative motions of a chain, considering only the motions of a single chain bond.

2.4.3 Free volume theories

The last group deals with free-volume theories. A definition of free volume often used in polymer studies is that employed by Doolittle (1951)[26,27]:

$$V_F = V_S - V_0 \tag{2.4.2}$$

where V_F is the "free volume" per unit volume, V_S represents the measured "specific volume" of the polymer at temperature T and V_0 stands for the "occupied volume". Because the temperature is above absolute zero, the links of a given main chain have oscillatory motions, whose extension above the dimensions of the links at rest defines V_0.

Doolittle found that the flow viscosity of low molecular weight hydrocarbon liquids could be represented by an empirical equation as follows: $\eta = a \cdot \exp\left(\frac{b}{f}\right)$ where a and b are constants, $f = \frac{V_F}{V_S}$ is the fractional free volume and η is the viscosity of the liquid. It follows that $f(T) = f(T_g) + \alpha_f \cdot (T - T_g)$ where $f(T_g)$ represents the fractional free volume at the glass transition temperature and α_f stands for the difference of thermal expansion coefficients above T_g and below T_g. The glass transition temperature has been chosen as the reference temperature. From this starting point, one can derive the Williams-Landel-Ferry equation[4].

$$\ln\left(\frac{\eta(T)}{\eta(T_g)}\right) = \frac{-C_1 \cdot (T - T_g)}{C_2 + (T - T_g)} \qquad (2.4.3)$$

where

C_1 and C_2 are universal constants that can be calculated from the universal values of α_f and $f(T_g)$, which are respectively equal to $4.8 \cdot 10^{-4} K^{-1}$ and to 0.025. Therefore C_1 =40 and C_2 =52. Such a formula has been experimentally verified for numerous polymers when T varies within a limited temperature range around T_g Because the viscosity is proportional to the time between two diffusional molecular group jumps and because this time is nearly equal to the average relaxation time, the WLF equation can be rewritten by quoting the average relaxation times at temperatures T and T_g:

$$\ln\left[\frac{t_0(T)}{t_0(T_g)}\right] = \frac{-C_1(T - T_g)}{C_2 + (T - T_g)} \qquad (2.4.4)$$

It has been found by Kovacs (1964)[28] that the relaxation time, which appears in the KWW equation, does not follow an Arrhenius law but obeys the WLF equation.

2.5 Specific volume

The specific volume as a function of temperature and pressure is usually given in a PVT diagram[29]. Fig. 2.5.1 gives an example for amorphous polymers and Fig. 2.5.2 for semi-crystalline polymers[30]. The volume increases by thermal expansion as temperature increases and the volume reduces as the pressure increases.

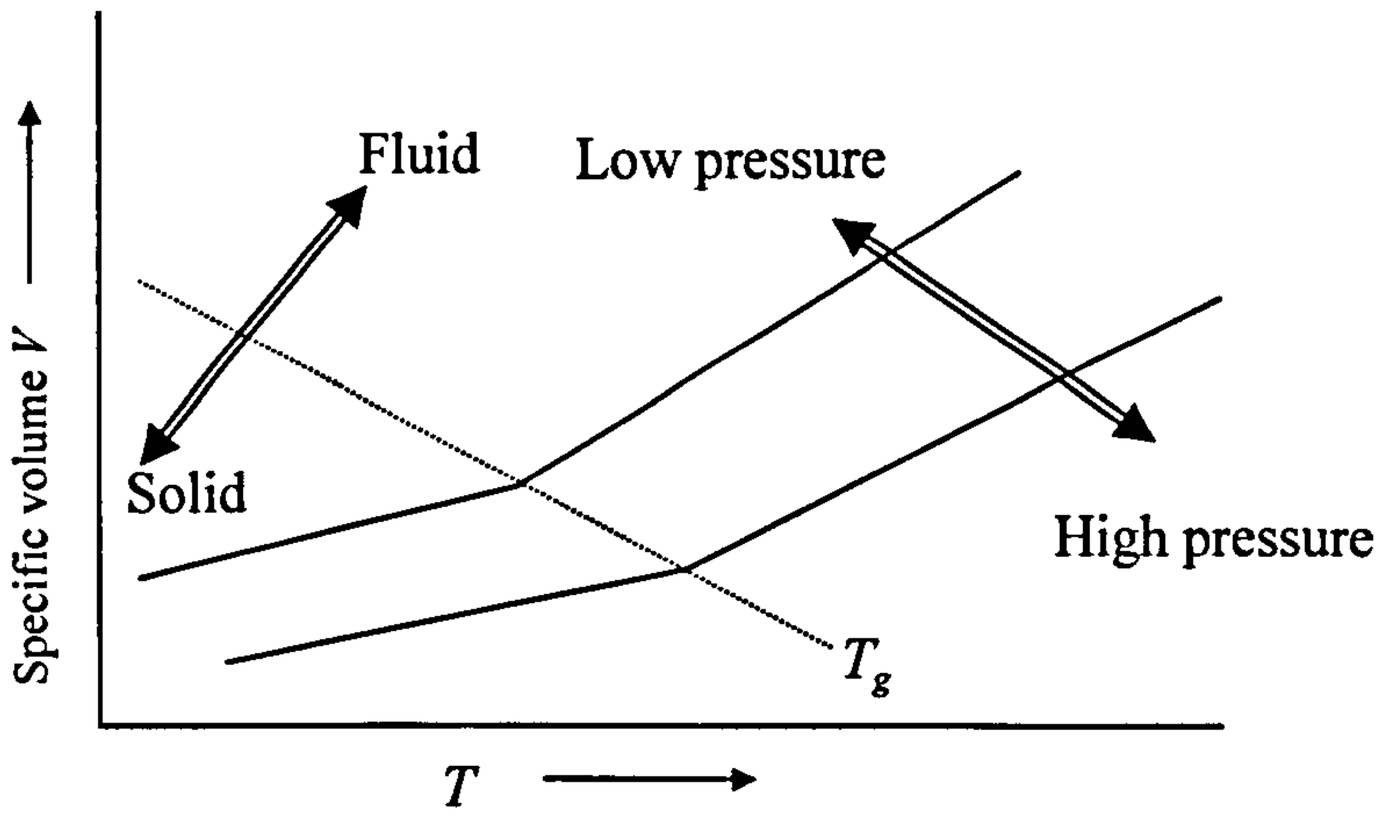

Fig. 2.5.1 PVT diagram for an amorphous polymer[29]

(T_g is glass transition temperature: depends on pressure)

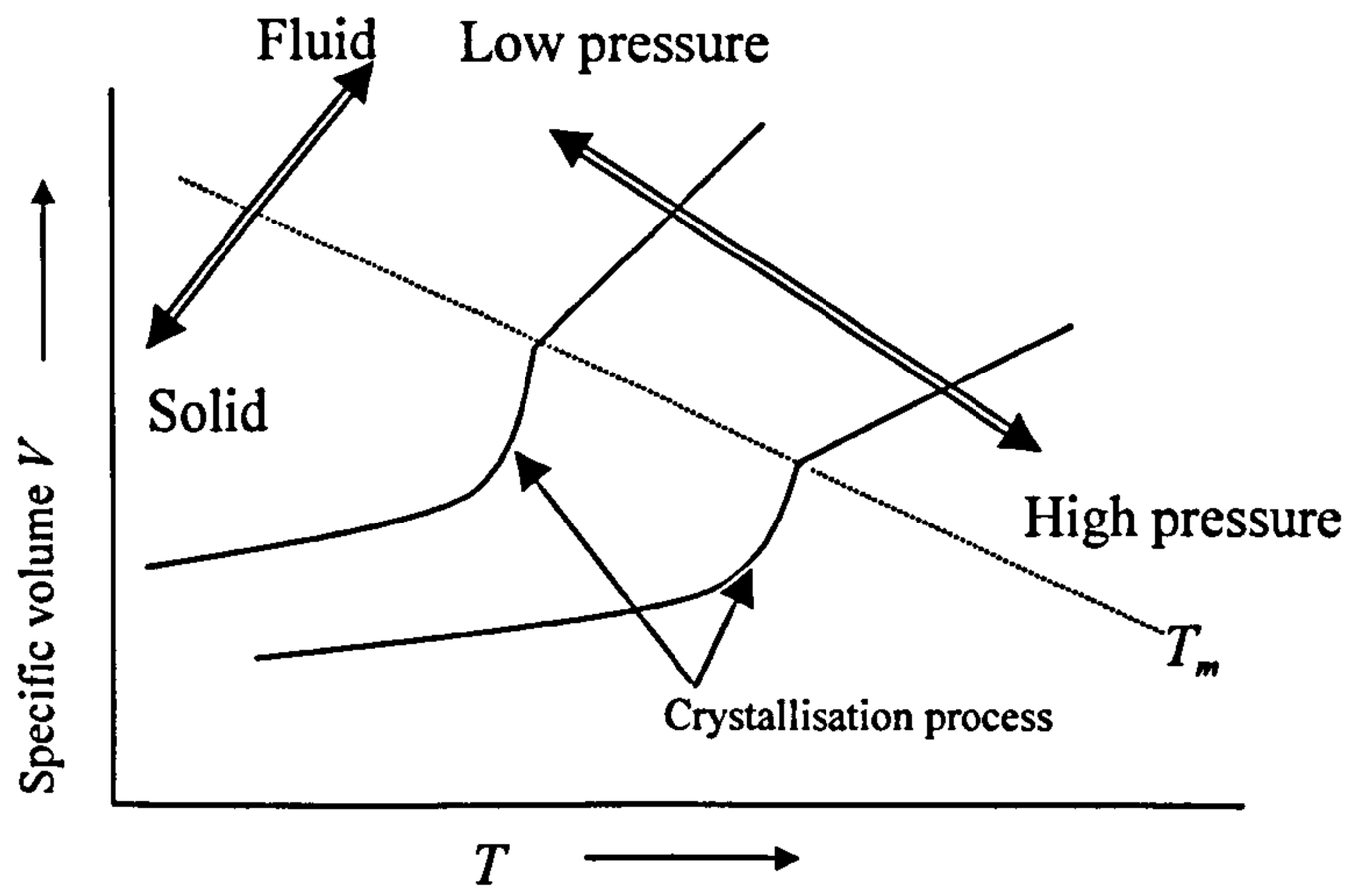

Fig. 2.5.2 PVT diagram for a semi-crystalline polymer[29]

(T_m is crystal melting temperature: depends on pressure)

2.5.1 The Spencer-Gilmore equation

Spencer and Gilmore (1949)[31,32] showed that the PVT behaviour of polymer melts can be represented reasonably well by the following modified Van der Waals equation of state[33]:

$$(P+\pi)\left(\frac{V}{M}-\omega\right)=\frac{RT}{M} \qquad (2.5.1)$$

where

P is the applied pressure

V is the specific volume of the polymer

M is the molecular weight of an interacting unit

π and ω are constants which must be determined experimentally, just as the interaction unit M. π in this equation is the internal pressure, which is independent of specific volume and, therefore, of temperature and pressure. It is obvious that the internal pressure will be related to the cohesive energy density measured in (N/m^3).

Spencer and Gilmore evaluated the constants π and M, from a series of PVT measurements at fixed temperatures. In synthetic linear polymers, M could be identified with the molecular weight of the structural unit. In this case ($M\omega = V(0)$) the equation of state becomes:

$$(P+\pi)(V-V(0))=RT \qquad (2.5.2)$$

At atmospheric conditions the internal pressure π is much greater than the external pressure P, so that for the liquid polymer[33]:

$$\pi=\frac{RT}{V(T)-V(0)}\cong\frac{R}{\alpha_1} \qquad (2.5.3)$$

where α_l is molar thermal expansivity of a liquid

The same result is obtained by differentiation of the equation of state:

$$\left(\frac{\partial V}{\partial T}\right)_P = \frac{R}{M\pi} \tag{2.5.4}$$

From the equation of state, equations for the linear thermal expansion coefficient (α) and for the compressibility (κ) can he obtained. Rearrangement of Eq. 2.5.2 gives

$$V = V(0) + \frac{RT}{P+\pi} \tag{2.5.5}$$

from which the following partial derivatives are obtained

$$\left(\frac{\partial V}{\partial T}\right)_P = \frac{R}{P+\pi} \tag{2.5.6}$$

and

$$\left(\frac{\partial V}{\partial P}\right)_T = -\frac{RT}{(P+\pi)^2} \tag{2.5.7}$$

Substitution gives[34]:

$$\alpha = \frac{1}{V}\left(\frac{\partial V}{\partial T}\right)_P = \frac{1}{T + \frac{V(0)}{R}(P+\pi)} \tag{2.5.8}$$

$$\kappa = -\frac{1}{V}\left(\frac{\partial V}{\partial P}\right)_T = \frac{1}{(P+\pi) + \frac{V(0)}{RT}(P+\pi)^2} \tag{2.5.9}$$

The compressibility κ is the reciprocal of the compression modulus or bulk modulus of the material.

2.5.2 The Tait equation

One of the most useful expressions to represent the $V(P,T)$-behaviour of liquids, including polymeric liquids, is the Tait-relation[35]:

$$\frac{V(0,T)-V(P,T)}{V(0,T)} = C \cdot \ln\left(1+\frac{P}{B(T)}\right) \qquad (2.5.10)$$

where

C is a dimensionless constant

$B(T)$ is a temperature dependent constant with the same dimension as pressure

For practical calculations $V(0,T)$ may be approximated by $V(T,\ P = 1\ \text{bar})$. This purely empirical relation was suggested by Tait.

Simha et al (1973)[36] have shown that C is almost constant (best average value C=0.0894) and that the temperature dependent factor $B(T)$ can be expressed by

$$B(T) = b_1 \exp(-b_2 T') \qquad (2.5.11)$$

where

b_1 and b_2 are empirical constants

T' is the temperature in °K

Substituting (2.5.11) into (2.5.10) gives

$$\frac{V(P_A)-V(P)}{V(P_A)} = 0.0894 \cdot \ln\left(1+\frac{P}{b_1}\exp(b_2 T')\right) \qquad (2.5.12)$$

Simha et al (1973)[36] showed that the Tait relation is also valid for polymers in the glassy state. In this case, the value of b_1 is about the same as for polymer melts, but b_2 is smaller.

2.5.3 Semi-empirical equations

There are several semi-empirical equations that have been proposed. Two of them are discussed here.

2.5.3.1 The Hartmann-Haque equation

Hartmann and Haque (1985)[37,38] combined the zero-pressure isobar of Simha and Somzynsky (1969)[39] with the theoretically derived dependence of the thermal pressure by Pastime and Warfield (1981)[40]. This led to an equation of state of a simple form

$$\tilde{P}\tilde{V}^5 = \tilde{T}^{3/2} - \ln\tilde{V} \qquad (2.5.13)$$

where

$\tilde{P}$ is the reduced pressure $= \frac{P}{B_0}$

$\tilde{V}$: is the reduced specific volume = $\frac{V}{V_0}$

$\tilde{T}$: is the reduced temperature = $\frac{T}{T_0}$

This equation was verified by application of the PVT data of the melts of 23 polymers of very different structure, adapting the reducing parameters B_0 ,V_0, and T_0, to the closest fit with the experiments. The average deviation between calculated and experimental V(P,T) data is the same as that obtained with the Tait relation. The advantage of Hartmann's equation is that it contains only 3 constants, whereas the Tait equation involves 4.

Hartmann and Haque applied their equation also to solid polymers, and with some success[37]. The reducing parameters appeared to be of the same order as for polymeric melts, but different, as would be expected. Their values are given in

Table 2.5.1.

Hartmann already pointed out that the reducing parameter B_0 is equal to the compression or bulk modulus K, extrapolated to zero temperature and pressure and that T_0 is related to the glass transition temperature. Analysing the data of Hartmann and Haque found the results shown in Table 2.5.2.

Parameters / Polymer	Melt			Solids		
	B_0 (GPa)	V_0 ($m^3 \cdot kg^{-1}$)	T_0 (K)	B_0 (GPa)	V_0 ($m^3 \cdot kg^{-1}$)	T_0 (K)
Polyethylene	2.80	1036	1203	5.59	959	1829
Polypropylene	2.05	1087	1394	-	-	-
Poly(1-butene)	2.10	1077	1426	-	-	-
Poly(4-methyl pentene-1)	1.67	1118	1423	2.61	1121	1658
poly(vinylfluoride)	-	-	-	4.86	754	1972
poly(vinylidene fluoride)	-	-	-	5 78	589	1490
Poly(trifluoro-chloro-ethene)	-	-	-	4.97	447	2373
Poly(tetrafluoro-ethene)	3.64	359	875	-	-	-
Poly(vinyl alcohol)	-	-	-	-	-	-
Poly(ethylene terephthalate)	4.14	677	1464	-	-	-
Poly(vinyl acetate)	3.82	738	1156	4.49	796	1955
Poly(methyl methacrylate)	3.84	757	1453	4.17	813	2535
Poly(butyl methacrylate)	3.10	854	1284	3.62	885	1781
Poly(cyclohexyl methacrylate)	3.14	816	1449	4.43	876	2567
Polystyrene	2.97	873	1581	4.25	919	2422
Poly(o-methyl styrene)	3.11	887	1590	4.19	936	2301
Poly(dimethyl phenylene ether)	3.10	784	1307	3.74	913	2947
Polyarylate (Ardel)	3.71	738	1590	4.58	798	2702
Phenoxy resin	4.27	776	1459	5.87	817	2425
Polycarbonate	3.63	744	1473	4.55	804	2476
polysulfone	3.97	720	1585	5.33	782	2727
poly(dimethyl siloxane)	1.85	878	999	-	-	-

Table 2.5.1

Parameter	Melts	Solid
B_0 (GPa)	2/3 K (298) (dynamic)	K (298) (dynamic)
V_0 ($m^3 \cdot kg^{-1}$)	1425 V_W /M	150 V_W/M for glasses 140 V_W/M for semi-crystalline
T_0 (K)	2.0T_g+700	5.0 T_g+500

Table 2.5.2

Hartmann and Haque also gave some useful equations for estimations:

$$\frac{R \cdot T_0}{B_0 \cdot V_0} = C \tag{2.5.14}$$

where

C: 5.4 ± 0.65 (g/mol) for amorphous solid polymers

C : 4.2 ± 1 25 (g/mol) for semi-crystalline solid polymers

From the Hartmann-Haque equation the following expressions for α and κ can be derived[13]:

$$\alpha = \frac{1}{V}\left(\frac{\partial V}{\partial T}\right)_P = \frac{\frac{3}{2}\left(\frac{T}{T_0^3}\right)}{1+5\frac{P}{B_0}\cdot\left(\frac{V}{V_0}\right)^5} \tag{2.5.15}$$

$$\kappa = -\frac{1}{V}\left(\frac{\partial V}{\partial P}\right)_T = \frac{1}{\frac{B_0}{(V/V_0)^5}+5P} \tag{2.5.16}$$

2.6 Transport of thermal energy

The rate of heat transport in polymers is important in order to obtain an accurate temperature distribution. For good thermal insulation, the thermal conductivity has to be low. On the other hand, polymer processing requires that the polymer can be heated to the processing temperature and cooled to ambient temperature in a reasonable time.

2.6.1 Thermal Conductivity

No adequate theory exists which may be used to predict accurately the thermal conductivity of polymeric melts or solids[13,41]. Most of the theoretical or semi-theoretical expressions proposed are based on Debye's treatment of heat conductivity[42], which give rise to the equation:

$$\lambda = \Lambda C_V \rho u L \qquad (2.6.1)$$

where

C_V is specific heat capacity, ρ is density, L is average free path length between the molecules, u is velocity of elastic waves, Λ is a constant in the order of magnitude of unity

Kardos (1934)[43] and, later, Sakiadis and Coates (1955)[44,45] proposed an analogous equation but redefining L as the distance between the molecules in adjacent isothermal layers.

The general shape of the λ-T curve of amorphous polymers is given in Fig. 2.6.1.a. The curve passes through a rather flat maximum at T_g and shows a gradual but slow decline in the liquid state. Also the slopes of the C_P-T (Fig. 2.6.1b), ρ-T (Fig. 2.6.1.c) and u-T (Fig. 2.6.1d) curves are shown, being the components of the λ-T curve according to Eq. 2.6.1. Multiplication of C_P, ρ and u gives the expected behaviour of λ[13,41].

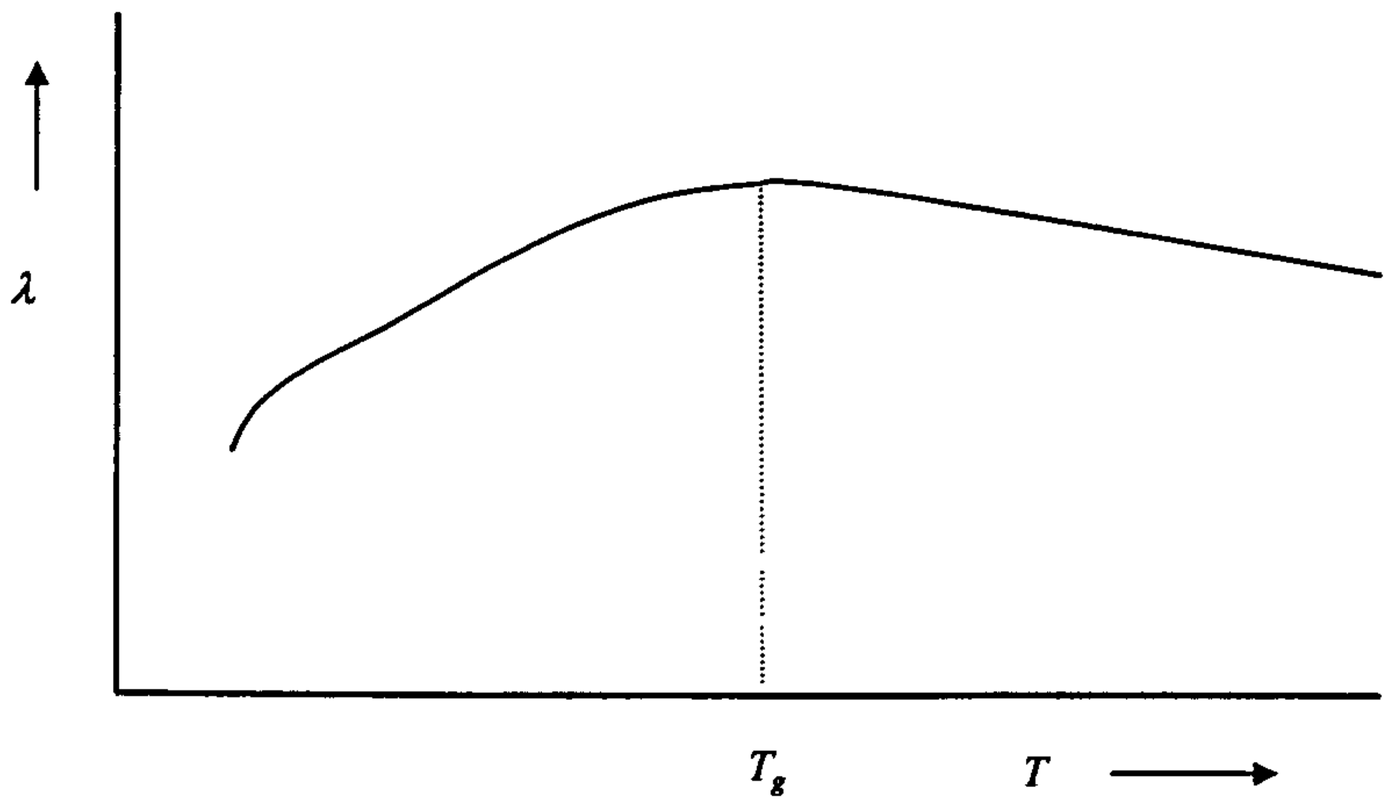

Fig. 2.6.1.a Thermal conductivity as a function of temperature[13,41]

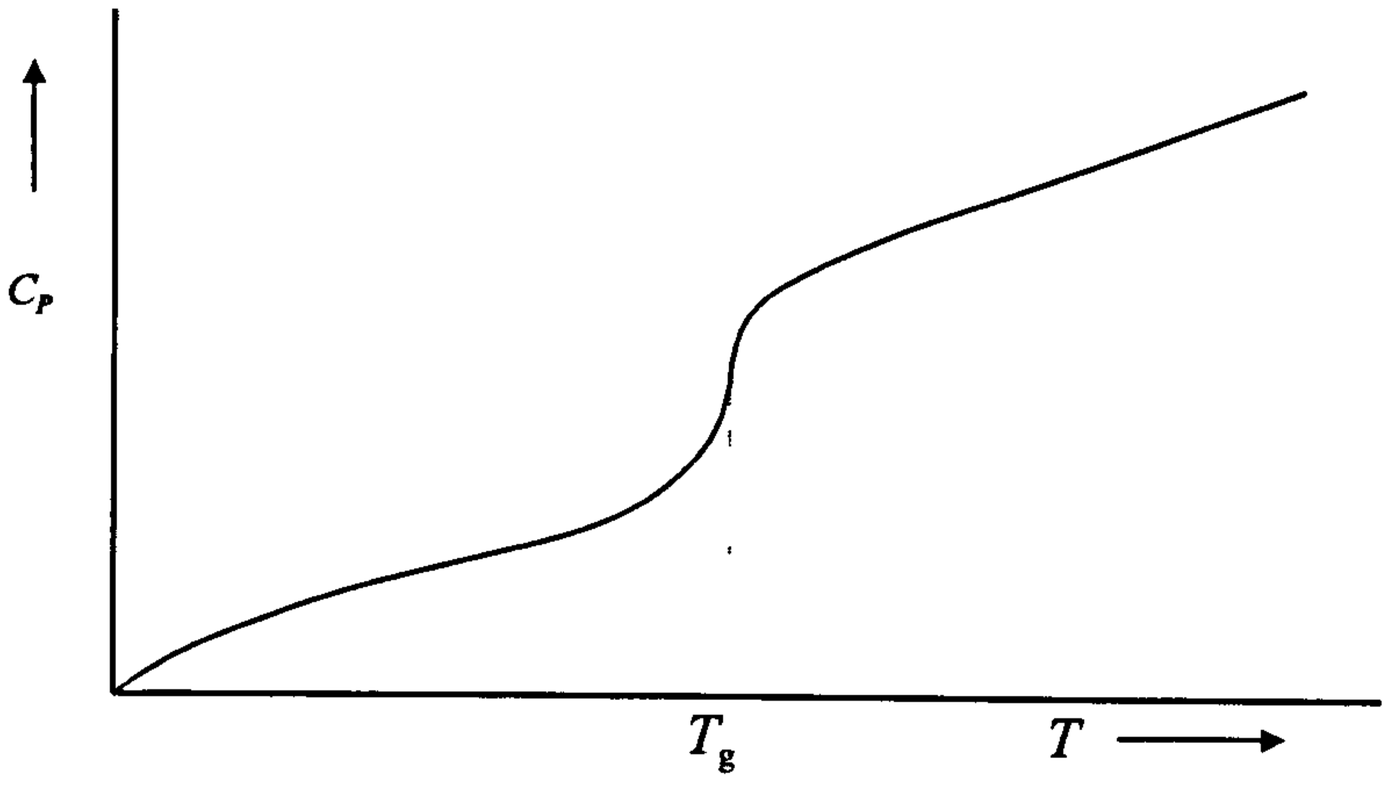

Fig. 2.6.1.b. Heat capacity as a function of temperature[13,41]

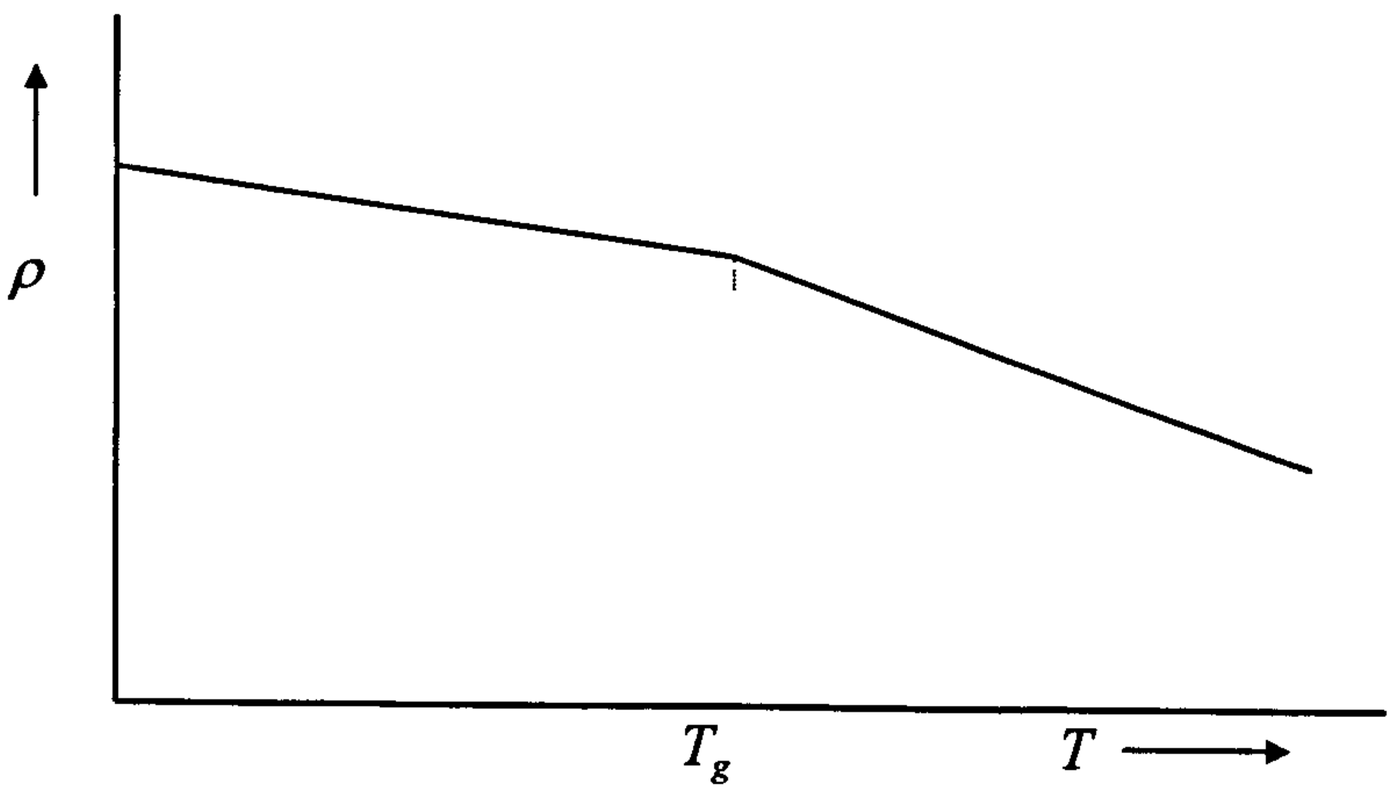

Fig. 2.6.1.c Density as a function of temperature[13,41]

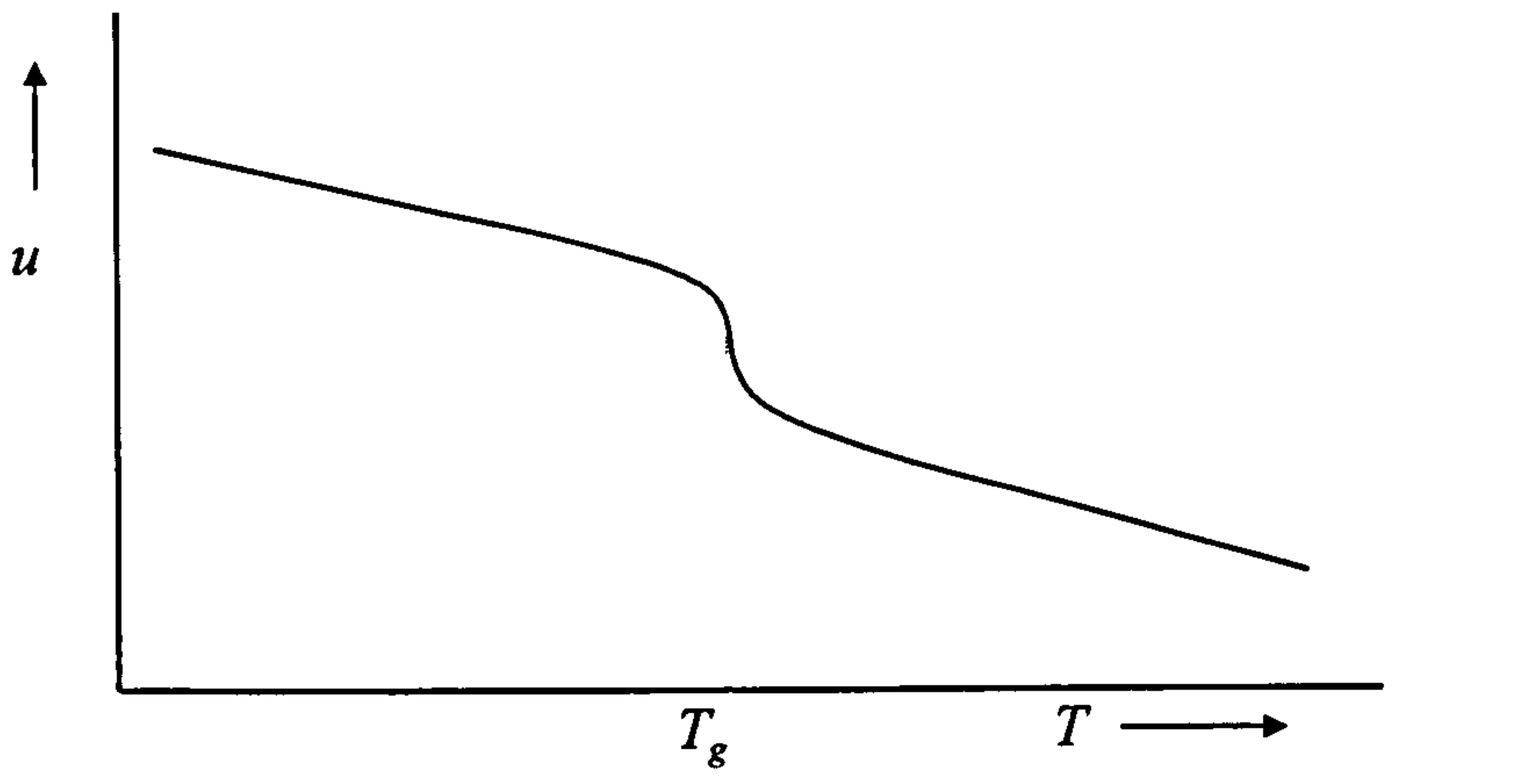

Fig. 2.6.1.d Elastic wave velocity as a function of temperature[13,41]

2.6.2 Specific heat as a function of temperature

The specific heat capacity of the crystalline component of a polymer follows the curve in Fig. 2.6.2 for the solid state to the melting point[46,47,48]. The value of C_p at T_m increases to that of the liquid polymer. The molar heat capacity of the amorphous component of the polymer follows the same curve for the solid up to the glass transition temperature, where the value increases to that of the rubbery (liquid) material.

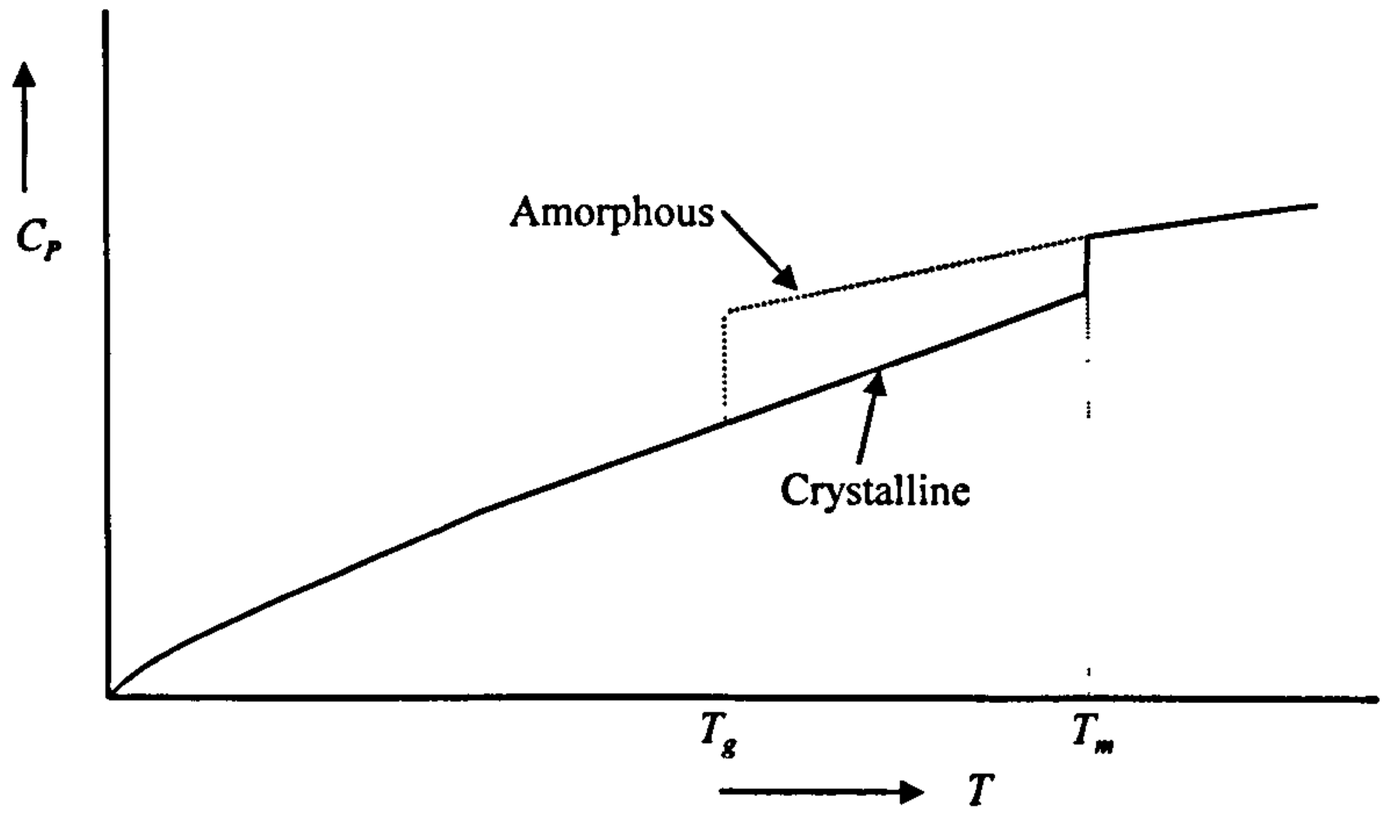

Fig.2.6.2 Heat capacity as a function of temperature[13]

2.7 Thermal residual stresses

Cooling stresses arise when a sample is cooled inhomogeneously and when the cooling causes it to stiffen. The explanation of their origin lies in the fact that no appreciable stresses are built up during the first cooling phase, when the contraction of the outside solidified layers occurs but the counteracting resistance of the core (molten) is so small that hardly any stresses are actually built up. Thermal stresses only arise when both the skin and the core are solidified (e.g. during the second phase). These stresses will now persist when cooling is completed, the skin being under compression and the core in a state of tension[49, 50]. The assessment of both transient thermal stresses (e.g. stresses that build up during the solidification) and residual thermal stresses (when t tends towards ∞) is worthwhile and forms the main subject of chapter 3. Key contributions have been made by:

Dimensional changes and residual stresses in parts which were made by solidifying molten material (not polymer) have been calculated at least since 1920. Adams and Williamson (1920)[51] calculated tempering stresses in a glass plate. The proposed parabolic, through-thickness residual stress distribution was later verified to be a good approximation for an unconstrained, rapidly solidified glass plate.

Leaderman (1958)[52] progressed in predicting residual stresses and dimensional changes caused by solidification. The prediction was closely related to the development of thermoviscoelasticity theory and to its application to inorganic glasses and thermoplastics.

Moreland and Lee (1960)[53] extended linear viscoelasticity to account for time-dependent temperature variations by introducing the concept of pseudotime or material time. The model was applied to a cylinder of incompressible linear thermorheologically

simple material. Subsequently, Lee and Rogers (1963)[54] showed that Laplace transforms can be effectively used for viscoelastic stress analysis only for a restricted class of problems. This method is utilised for a symmetrically cooled glass plate. Following Lee and Rogers, Lee et al. (1965)[55] accounted for glass relaxation effects[56]. Measured temperature-dependent relaxation characteristics of glass were used in the form of a thermorheologically simple material model. The transient stresses calculated by using a thermorheologically simple model for a glass plate quenched from above the glass temperature differed from the experimental data significantly.

The simplest basic thermo-elastic analysis can be traced back to Timoshenko and predicts the parabolic distribution given in Eq. 2.7.1 [57,58].

$$\sigma_t = \sigma_0\left(1-\frac{3z_1^2}{z_0^2}\right) \tag{2.7.1}$$

where σ_t is the residual stresses in the *x-y* plane at a distance z_1 from the mid-plane of a parallel-sided moulding of total thickness $2z_0$ and σ_0 is the stress at the midplane.

Struik (1978)[59] classified internal stresses in injection moulded thermoplastic parts into molecular orientation, physical aging and thermal stresses during part moulding. The stresses caused by molecular orientation depend not only on the level of deformation but also on the degree of intermolecular interaction for amorphous thermoplastics. Struik attributes physical aging to internal hydrostatic stresses that induce a gradual material contraction by a process of bulk creep. Finally, the stresses resulting from rapid, nonhomogeneous cooling (thermal stresses) are accounted for in an "instant freeze" theory developed by Aggarwala and Saibel (see later in this section) that neglects viscoelastic and volume relaxation effects at all temperatures. Struik applied this theory to solidifying parts of arbitrary shape to account for the temperature dependence of the

glassy state. The glassy state elastic modulus and the thermal expansion coefficient were assumed to be temperature-dependent. The solidification of semi-crystalline thermoplastics is assumed to be identical to amorphous thermoplastics. Struik did not consider latent heat effects and significant density changes[16,59].

Isayev and Crouthamel and Eduljee *et al* (1984)[60] consider that the strain during cooling has three components: an elastic component, a plastic component and a thermal component. The material is assumed to be perfectly plastic when the temperature is above T_g and perfectly elastic below T_g, and the thermal stress is proportional to the difference between the local temperature and the original temperature of the melt. It is observed that the average elastic strain through the part of the moulding that is below T_g must be zero (if the Young's modulus is uniform through the depth of this region) and it is then relatively straightforward to derive the stress distribution when the part has finally cooled to a uniform temperature[60,61]. This predicts stress distributions that are fairly close to parabolic[61].

Early attempts to take account of the relaxation effects used viscoelastic models developed originally for inorganic glasses and are reviewed by Isayev and Crouthamel (1984)[60]. More recent treatments are given elsewhere and use a range of methods to describe and account for the viscoelastic behaviour of the polymer[7],[70],[11],[9],[62]. Liu (1996)[8] calculated that the stresses should be compressive at the surface, in agreement with the results from earlier, simpler treatments, but some calculations predict that the stress very close to the surface of the moulding will be tensile (not compressive), changing to compressive a short distance from the surface [63],[69],[64]. Zoetlief *et al* (1996) calculated that the stress very close to the surface should be tensile on ejection from the mould but that the stress there will reverse, becoming compressive, when the moulding reaches a uniform temperature[80].

Wimberger-Friedl (1994)[65] compared the layer removal technique and the birefringence method for measuring flow induced stresses (see Section 2.7.3). He showed an important deficiency of the birefringence method to determine the residual stress because the birefringence from thermally induced stress was found to be of comparable magnitude to that from flow induced orientation.

Williams (1981)[66] described three major sources of residual stress. They are nonhomogeneity caused by differences in crystallinity levels between the skin and core layers, anisotropy caused by molecular orientation and thermal stresses resulting from the nonhomogeneous temperature history during solidification. Williams neglected packing-pressure effects. Lee et al. (1990)[67] also outlined the effects of the elastic properties, specimen size, and thickness on the shrinkage and warpage of injection-moulded bars of nylon 6 and poly (ethylene terephthalate). Shrinkage was found to increase with the bar thickness, both in the flow and cross-flow directions. The elastic properties of the materials, the bar thickness, and the distance from the gate had a large effect on the through-thickness shrinkage.

Santhanam (1992)[68] used a thermoviscoelastic model to assess residual stresses and post moulding deformations in injection-moulded parts. Packing-pressure effects were taken into account to specify the initial strains in the thermoplastic at the end of filling. Consequently, initial strain for a given material only depends on the melt pressure.

Bushko and Stokes (1995)[69,70,71,72] took into account a processing history that includes packing pressure and a fixed set of boundary conditions (temperature, pressure and in-plane boundary conditions i.e. fully constrained in-plane direction) for the known dependence (specific volume and relaxation effect) of residual stress and dimensional changes. The result was not compared with an experimental result.

Zoetelief, Douven and Ingen Housz (1996)[80] took into account the influence of the

holding stage with a linear viscoelastic constitutive law. The results were compared with experimental results obtained with the layer removal method. The magnitude of calculated stress was 1.0 to 3.5 times higher than the experimental results.

Jansen and Titomanlio (1994, 1996)[73,74] accounted for shrinkage anisotropy between in-plane and thickness direction, which was caused by different constraints in deformation. They used local values for temperature, pressure and crystallisation. The magnitude of their calculated stress was 2.8 to 3.6 times higher than the experimental results.

2.7.1 The thermo-elastic model

This model was first derived by Aggarwala and Saibel (1961)[75]. It neglects not only viscoelasticity (time effects in the elastic behaviour of mechanical properties) but also volume relaxation. This model assumes that mechanical parameters are constant and independent of temperature below as well as above T_g and that the changes occur only at a certain temperature T_l and are discontinuous. Moreover, the non-discrete nature of the glass transition is disregarded. For a simple geometry like an infinitely large flat sheet with a thickness e in the z direction and the coordinates x and y in directions parallel to planes of the sheet, the equi-biaxial stress distribution $\sigma_{xx}(z,t) = \sigma_{yy}(z,t)$ can be calculated by using the following equation[75,76,77]: (z is measured from the mid-plane located in the core)

$$\frac{\sigma_{xx}(z,t)}{A} = T_g - T(z,t) + \int_{H(z)}^{\frac{e}{2}} \frac{1}{\frac{e}{2} - H(\psi)} \cdot \int_{H(\psi)}^{\frac{e}{2}} \dot{T}(\xi,\psi)\, d\xi\, d\psi \qquad (2.7.2)$$

where

$H(t)$ is the position $z=H(t)$ of the solidification plane (defined by $T=T_g$) moving inwards

$t_l(z)$is the time at which this solidification plane reaches the depth z

$A=\frac{\alpha_g E_g}{1-\upsilon_g}$ (subscript g stands for glassy).α_g, E_g and υ_g are respectively the thermal expansion coefficient, the unrelaxed Young's modulus, and the Poisson's ratio in the glassy state

ξ and ψ are respectively time and space integration variables;

$\dot{T}$ is the derivative of the temperature field with respect to ψ. This solution neglects the contribution due to thermal stresses that build up in the rubbery core, for the stiffness of this core is negligible with respect to that of the solidifying glassy skin. Both transient thermal stresses and residual stresses can be assessed in this way.

2.7.2 The viscoelastic model

Struik considered a fully restrained material cooled at constant length, from initial temperature T_0 to final temperature T_∞ The tensile bar is rigidly supported and is stresses free at T_0. Tensile stresses are built up during cooling because the free thermal contraction is restrained. The thermal stresses built up at the final temperature are obtained by summing the contributions of all temperature intervals δT:

Struik's approach[16] began by calculating the incremental stress, $\delta\sigma$, when the temperature changes between T and T-δT.

$$\delta\sigma(T)=\alpha(T)\cdot E(T,\frac{1}{Bq})\delta T \qquad (2.7.3)$$

where

$\alpha(T)$ is the linear thermal expansivity at T

B is a quantity between 0.08 and 1, as follows:

when T is below the glass transition temperature $B = \frac{30 - \ln q}{T}$ [16] (see note 2.7.1),

when T is above the glass transition temperature $B = \frac{C_1 C_2}{(C_2 + (T - T_g))^2}$ [16] in which C_1 and C_2 are the constants in the WLF equation. (see earlier discussion in Section 2.5)

q is the local cooling rate: $\frac{d}{dt}T$

Note 2.7.1[16,18]: The relaxation time $\tau_k(T)$ is determined by the activation energy H_k of the process:

$$\tau_k(T) = \tau_0 \exp\left[\frac{H_k}{RT}\right] \qquad (2.7.1.1)$$

where R is the gas constant, and τ_0 is a universal constant (10^{-13}s)

For relaxation times of $1/q$ at temperature T, activation energies are given by:

$$\frac{H_K}{RT} \approx \ln\left(\frac{1}{q\tau_0}\right) = 30 - \ln q \qquad (2.7.1.2)$$

Finally, the following equations were obtained[16] that permit the calculation of thermal strains and stresses:

$$\dot{\varepsilon}_{xx}(t) \cong \frac{\int_{H(t)}^{\frac{e}{2}} R\left[T, \frac{1}{Bq}\right] \cdot \alpha(T) \cdot \dot{T}(\xi, t) d\xi}{\int_{H(t)}^{\frac{e}{2}} R\left[T, \frac{1}{Bq}\right] d\xi} \qquad (2.7.4)$$

$$\dot{\sigma}_{xx}(t) = R(T, \frac{1}{Bq})\left\{\dot{\varepsilon}_{xx}(t) - \alpha(T) \cdot T) \cdot \dot{T}\right\} \qquad (2.7.5)$$

where

$H(t)$ is the position of the solidification or glass transition plane:

R is a mechanical parameter defined as $R = \frac{E}{1 - \upsilon}$

ξ is a space integration variable on the z (coordinate) scale

2.7.3 Flow-related stresses

When the polymer melt is injected into the mould under pressure, fountain flow occurs and the melt that is deposited at the mould cavity wall is rolled into place with orientation produced by elongational flow at the (almost semi-circular) flow front[78]. The bending moment produced by the shear stresses in the half of the moulding on one side of the central plane is balanced by that in the other half. Discussion of the calculation of the flow stresses has been provided by Hieber (1987)[131] and extended by Baaijens and Douven (1991)[79], who improved the analysis by employing the compressive Leonov model to describe the behaviour of the polymer[16]. Calculations indicate that this stress is one or two orders of magnitude smaller than the thermoplastic stress[7,80] and it is quite common to neglect it when calculating stress magnitudes[69].

2.8 Effect of moulding condition on residual stress

The injection moulding process parameters that are expected to have the most important influence over the residual stresses are the melt temperature, the mould temperature and the pressure, in particular the hold pressure. The effect of all of these on mouldings made from a commercial blend of poly (phenylene oxide) with polystyrene has been investigated by Siegmann *et al* (1982) [84] They give results separately for the effect of melt temperature and mould temperature whereas it would have been more valuable to consider them together. The residual stresses were always compressive near to the surface and changed rapidly with distance from the surface whereas they were tensile and slowly varying over a large proportion of the interior. The magnitude of the stresses fell with increasing melt temperature and with increasing mould temperature (with

slight variations on this trend near to the gate). Hindle *et al* found that the residual stress magnitudes in polypropylene mouldings were slightly higher when the mould temperature was 80°C that when it was 30°C[81]. This may be because the stresses largely formed during cooling after ejection from the mould rather than during the period of residence in the mould. El-Rafey (1994) *et al*[82] found that the effect of melt temperature on residual stresses in polystyrene was different to that observed by Siegmann (1982) *et al*[84]. Liou and Suh (1989)[83] investigated the use of low-thermal-inertia mould with a passive insulation layer on the cavity surface to permit greater control over temperature during moulding and claimed that this is a promising route to the production of mouldings with low levels of residual stress.

Siegmann *et al* found that the dependence of the residual stress distribution on injection and hold pressure was fairly marked[84]. It was possible to produce tensile stresses at the surface by using high pressures though the actual values quoted by the authors for the pressures required to cause this seem to be approximately an order of magnitude too low (presumably due to their omission of an amplification factor in the injection system in their reported pressure data). The effect was not very large compared to differences observed by Kwok *et al* (1996)[86] when using different coolants. Sandilands and White (1980)[85] characterised the distribution of residual stress and the relaxation of polystyrene tensile bar specimens (190×12.5× 3 mm) using the layer removal technique. The specimens were moulded at different packing pressures ranging from a nozzle pressure of 37 MPa to 143 MPa. The residual stresses were well approximated by a parabolic distribution having characteristic tensile stresses in the core and compressive stresses in the surface layers. Moulding pressure was found to have an insignificant effect on the stress distribution. Mouldings from the same batches were tested in stress relaxation. The time variation of the average stresses which were measured at a constant

temperature of 40°C, was approximated by a power law. The exponent of the time was found to be very sensitive to the moulding pressure. It was probably significant that Sandilands and White cooled their mouldings in ice-water and stored them in liquid-nitrogen after ejection. In another set of experiments, the magnitude of stress in bars cooled in liquid nitrogen was 4.2 times higher than the value in bars cooled in ice water[86]. They gave a closely parabolic residual stress distribution, a feature that seems to be associated with this type of cooling procedure as opposed to air cooling[85,86]. The residual stresses change with distance from the gate[84] and this is probably largely due to the pressure history of the material. Pham *et al* found that the residual stress distribution reversed near to the gate in their polycarbonate mouldings[87]. The effect of oscillating packing pressures on residual stresses in very thick (40 mm) mouldings of polyethylene has been studied by Allan and Mortazavi (1985)[88]. Reversal of the sense of the usual stress distribution was possible under long packing times[88].

Siegmann *et al* (1982) also found that the residual stresses were influenced by the injection rate[84]. They used a quite wide range of injection rates and obtained compressive stresses near the surface for all but the very slowest rate, for which tensile stresses were observed there. The slowest rate (4 gs^{-1}) was much less than conventional moulding rates and does not demand close scrutiny. They noted that the injection rate influenced the Young's modulus distribution but did not attempt to allow for this when performing the residual stress analysis: this might account for some of the apparent changes in measured residual stress distribution profiles.

2.8.1 Effect of the pressure

Melt pressure has an important effect on residual stresses. Titomanlio *et al.* (1987)[89] were the first who recognised the importance in injection moulded products. They

solved the equations numerically using the same elastic model and the thermal model. There are four ways of dealing with pressure history. The most accurate method is to use a recorded pressure curve of an injection moulding experiment[90]. This is only possible if these experimental data are available and reliable[91,92,93]. Secondly, the pressure curve is predicted by numerical simulations[94,72 ,95] . Thirdly, the pressure history in the cavity is calculated from the equilibrium (PVT) equation of state for the material. And, finally, the pressure curve is approximated by dividing it into two separate periods corresponding to the filling, holding and cooling stages of the injection moulding process[96]

$$P = \begin{cases} P_p & t \le t_{gf} \\ (P_p - P_r)\exp\left[-A_p(t - t_{gf})\right] + P_r & t > t_{gf} \end{cases} \qquad (2.8.1)$$

where

P_p is the peak pressure, P_r is the residual pressure, A_p and t_{gf} (the gate freeze off time) are empirically adjusted parameters (Fig. 2.8.1)

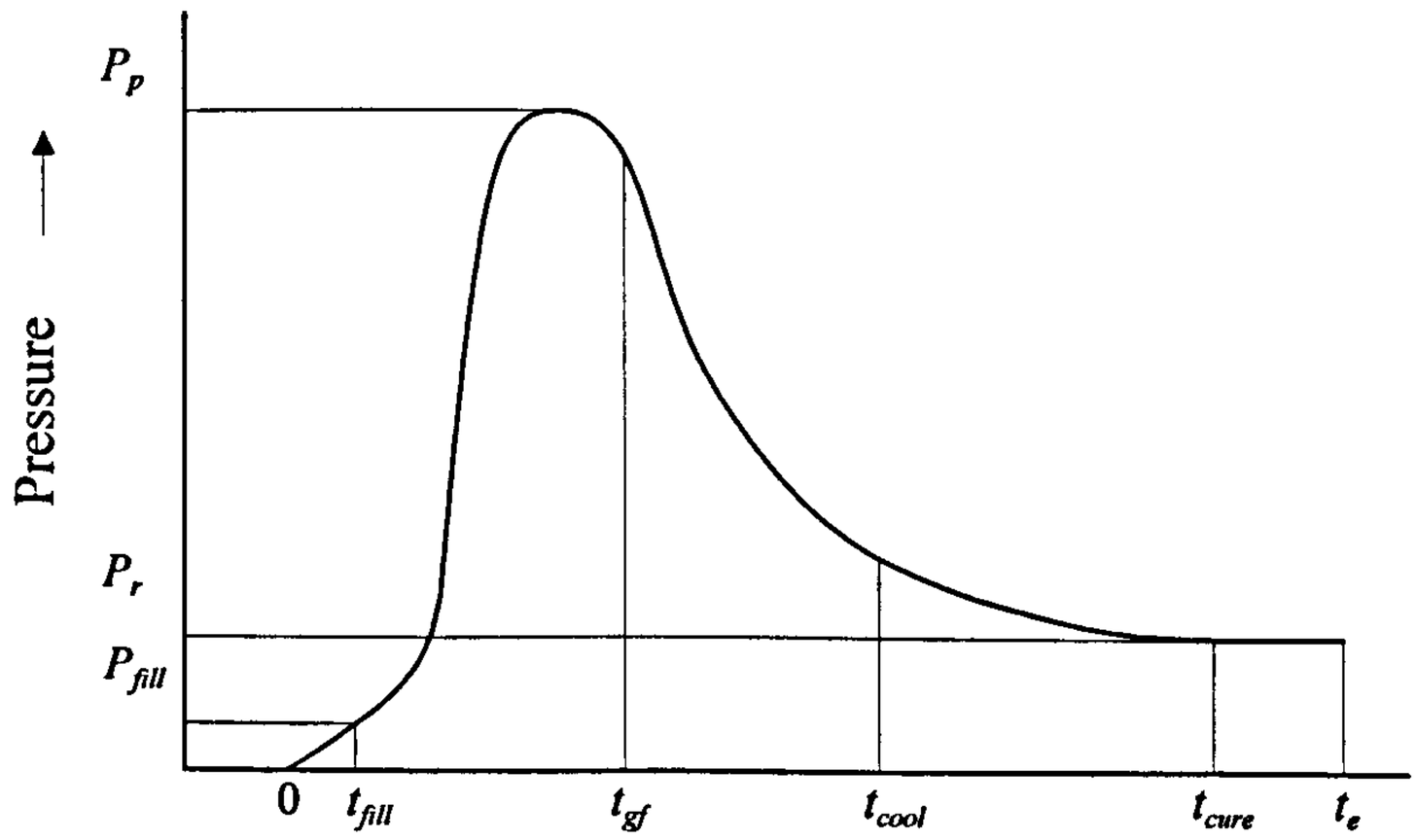

Fig. 2.8.1

A typical injection-moulding process cycle

Based on McKinney, Simha (1977)[97] and the various phenomenological studies on pressure induced densification[98,99,100], Greener (1986) [101] calculated densities at positions z (the positions within the cavity).

$$\rho_0(z) = \rho_0\left[1 + \kappa' P_f(z)\right] \qquad (2.8.2)$$

where

ρ_0 is the density of the undensified sample (the density when the pressure is zero)

κ' is the pseudo compressibility determined by $\kappa' = -\left(\frac{1}{V}\right)\left(\frac{\partial V}{\partial P_f}\right)_{T,P,\dot{T}}$

P_f is the formation pressure

2.8.2 Effect of boundary conditions

The magnitudes of the stresses depend on the moulding conditions, in particular on the surface temperature of the mouldings during solidification[61,70,84]. Many of the calculations appear to give overestimates of the stress magnitudes when compared with experimental measurements. This is probably because of relaxation effects[8]. Another effect that is often not taken into account when modelling the residual stresses in injection moulding is shrinkage within the mould (before ejection). It is usually assumed that the material in contact with the mould cavity at the surface does not slip[64]. The effect of this has been considered by Bushko and Stokes (1995)[70]. Agreement is better when the calculated predictions are compared with residual stress distributions measured in quenched slabs. This is because the boundary conditions during cooling match those used in the calculations much more closely than occurs in the injection moulding process. The same applies to residual stress distributions measured on injection mouldings ejected into a quenching medium[86]. They also show reasonable

agreement with those calculated using procedures which do not allow for the temperature rise in the mould or for the thermal resistance of the air gap when shrinkage away from the mould occurs because these effects are less important in this case.

2.9 Post moulding changes in residual stresses

Residual stresses may change considerably after the moulding operation is complete and the part has established thermal equilibrium with the surroundings. If the residual stresses have an influence on properties, it is necessary to consider the effect of the service environment on their magnitude and distribution as well as their state in the as-moulded condition.

2.9.1 Aging and annealing

In most thermoplastics creep and stress relaxation proceed at fairly significant rates at room temperature. Therefore, it can be expected that residual stress will relax during ageing at room temperature[60,81,102,153]. It is not expected that the residual stress will relax away completely[103,104,150].

On the other hand, El-Rafey *et al* found that the stress distribution in polystyrene injection mouldings reversed after an extended period of room temperature ageing[105]. Their mouldings had an approximately parabolic residual stress distribution with compressive stresses near to the surface one day after moulding but after periods of 30, 60 and 300 days ageing at room temperature the stress reversed becoming progressively more tensile as the ageing period increased.

Relaxation can be accelerated by annealing at an elevated temperature and this method is sometimes used to reduce the residual stresses[81,106,15,107].

The detailed consideration has been given to these processes in Section 2.3.

2.9.2 Temperature gradient conditioning

If the stresses relax non-uniformly there will be a change in the residual stress distribution when the moulding is returned to uniform temperature. This has been discussed elsewhere by White and co-workers who conducted laboratory experiments to investigate the effect[50,108,109]. They showed that, after returning the moulding to a uniform temperature, tensile stresses could develop at the surface that had been held at the higher temperature, reminiscent of observations made in polymer mouldings after a period of weathering in a hot climate[109,110]. Surface tensile stresses are especially unwelcome because they may assist cracking and the imbalance in the stress change causes warping.

2.10 Computer-aided calculations

Mathematical models have been proposed and widely developed by various research groups for the cavity-filling analysis. Many researchers[111,112,113,114,115] analysed simple one-dimensional flow behaviour in rectangular and centre-gated disk-shaped thin cavities in the 1960s and 1970s. During the 1970s and early 1980s, many papers[116,117,118,119,120] were published concerning flow in thin cavities of arbitrary planar geometry based on a Hele-Shaw type of flow[121].

The Finite Element Method (FEM) is a computational technique that started early in the 1950s[122,123] as a tool for the structural and stress analysis of complex shapes. Later, in the 1960s and 1970, its connections with the fundamental principles of mechanics were established[124,125]. As a result, FEM has become a versatile computational tool in several branches of engineering. In the 1980s, the era of engineering work stations (DEC, SUN,

HP and so on) started. This increased the commercial ability for applications of use of FEM in Computer Aided Engineering (CAE) [126]. In the mid-eighties, Wang *et al* combined the FEM and Finite Difference Method (FDM) formulation for generalised Hele-Shaw flow[127].

Calculation of residual stress distributions requires that the temperature distribution and the changes in pressure are followed throughout the solidification process and that the relaxation at all locations is taken into account while simultaneously satisfying the boundary conditions and the conditions for force equilibrium[96,128,129,130,131,132]. Examples of how the different components of the computations can be coupled together are given by Wang and co-workers (1991, 1992, 1993)[133,134,135].

Akay *et al* found that some of the measured values of warpage in ABS and polycarbonate mouldings made with quite large temperature gradients in the mould agreed reasonably well with values predicted by a commercial software package whereas in other parts the predicted warpage was actually in the opposite sense to that observed[136]. Ni and Wang (1993)[137] claim better success with their comparison, using a different software package. Gennari similarly provides an optimistic view, though his paper deals mainly with the related but less sensitive property of shrinkage[138].

In the case of fibre-reinforced mouldings the calculations must also include prediction of the fibre orientation distribution[139,140,141,142,143,144,145]. Notable contributions to this area have been made by Tucker and co-workers (1992)[143,144,146,147].

2.11 Residual stress measurements

There are several experimental methods that can be employed to measure residual stress[60,148,155]. The layer removal technique is one of the most useful methods. It was introduced by Treuting and Read (1951)[149] for metals. The detail of the removal

process for determining residual stress distribution for polymers can be found in White's review (1984)[150]. The method essentially is to remove uniform thin layers from mouldings in the shape of rectangular parallelepipeds[148,155]. After each layer removal, the curvature of the unloaded moulding is measured. The curvature-depth plots can be converted to calculate the stress-depth profile. The curvature measurement is an important procedure in layer removal method.

Akay and Ozden (1994)[151] have compared the advantages and disadvantages of different methods of curvature measurement that cover the dial gauge method, optical lever method, curvature measurement with a coordinate machine, laser beam scan method, then recommended that the bending moment measurement is a more accurate method to estimate of residual stress in plastics moulding because the layer removal method is time consuming, fiddly and so on. The bending moment method presents experimental difficulties and in this research work, an optical method was used to measure the curvature.

White (1996)[49] highlighted the disadvantage of the bending moment method because simple loading arrangements may result in the bar taking up an "S" shape, making it difficult to determine the position at which the internal bending moment due to the imbalanced residual stresses is exactly matched by the externally applied moment.

2.11.1 The layer removal technique

This technique is the method most frequently employed to measure the residual stresses in polymeric bars or sheets through their thickness. The analysis was introduced by Treuting and Read[149] for measurement of residual stresses in metal plates and improved for different plastics by White and co workers[152,153,154,155]. Successive uniform layers are machined from one side of the sample in the form of a rectangular trapezoid and the

measurement of the resulting curvature arising from the force imbalance thus created allows the determination of the residual stresses. Treuting and Read derived the general equation:

$$\sigma_{xx} = -\frac{E}{6(1-\nu^2)}\left[(z_0+z_1)^2\left\{\frac{d\rho_x(z_1)}{dz_1}+\frac{\nu d\rho_y(z_1)}{dz_1}\right\}\right. \qquad (2.11.1)$$
$$\left. +4(z_0+z_1)\{\rho_x(z_1)+\nu\rho_y(z_1)\}-2\int_{z_1}^{z_0}\{\rho_x(z)+\nu\rho_y(z)\}dz\right]$$

where

$\sigma_{xx}(z_1)$ is the residual stress in the x direction at the plane $z = z_1$

z_0 is the half-thickness of the bar or plate. (=e/2 in other parts of this thesis; z_0 is used here for consistency with the literature: it is the symbol used by the majority of authors in this subject area).

E and ν are assumed uniform throughout the sample.

ρ_x and ρ_y are the components of curvature in the x and y directions respectively

The Treuting and Read treatment is for biaxial in-plane stresses. Sometimes it is possible to make simplifying assumptions that permit an approximate solution to be obtained using measurements of curvature in one direction only.

Consideration of the injection direction (x-axis) and the contribution to the residual stresses of randomisation of flow-oriented molecules[20] leads to the expectation that the transverse stress, σ_{yy} , and ρ_y will be less, possibly much less, than ρ_x in some cases. If Eq. 2.10.1 is modified with the condition ρ_y =0, it follows that:

$$\sigma_{xx}(z_1)=-\frac{E}{6(1-\nu^2)}\left[(z_0+z_1)^2\frac{d\rho}{dz_1}+4(z_0+z_1)\rho-2\int_{z_1}^{z_0}\rho dz\right] \qquad (2.11.2)$$

For this equation to be valid, it is necessary for the specimen to be in a state of pure bending i.e. to form the arc of a circle after the removal of each layer. Moreover, the

machining process should not introduce new stresses into the specimen.

The Curvature ρ versus the sample depth (z_0-z_1, Fig. 2.11.1) can be converted to a stress versus (z_0-z_1) profile using Eq. 2.11.1 and Eq. 2.11.2.

When the stresses are caused by isotropic thermal shrinkage only, giving an equi-biaxial stress distribution[152,155]. Therefore,

$$\sigma_{xx}(z_1) = -\frac{E}{6(1-\nu)}\left[(z_0+z_1)^2\frac{d\rho}{dz_1} + 4(z_0+z_1)\rho - 2\int_{z_1}^{z_0}\rho dz\right] \qquad (2.11.3)$$

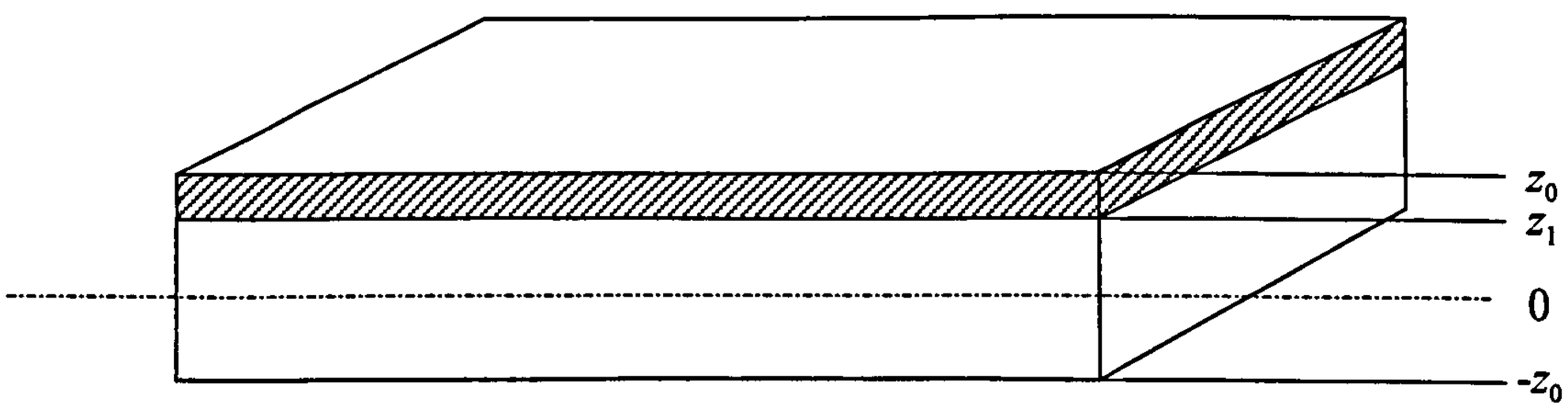

Fig. 2.11.1 The test sample and the cordinate system

CHAPTER 3

MODELLING OF RESIDUAL STRESS CALCULATIONS

This chapter deals with modelling of residual stress distributions. Section 3.1 gives the geometry used for the calculations. Section 3.2 deals with the principles of development of thermal residual stresses. Section 3.3 gives the basic assumptions in order to make the problem solvable. Section 3.4 gives the solution for the temperature distributions that arise in a sample of material, initially at constant temperature, sandwiched between two infinitely large, parallel plates constrained at a different constant temperature. This solution follows a Fourier treatment. Section 3.5 deals with representation of Young's modulus for amorphous polymers, in particular near the glass transition temperature. Section 3.6 gives the temperature and the pressure dependent thermal expansion. Section 3.7 discuss the T_g-plane position during cooling. Section 3.8 to 3.10 deal with the calculations of the residual stress using the procedure based on Struik's method (Method A). Section 3.11 gives the new procedure (Method B) developed during this research, in which the pressure profile was calculated and used to estimate density distributions through the depth and the stress distribution.

3.1 Geometry

The geometry, as shown in Fig. 3.1, is analysed in order to predict the residual stress of a simple injection-moulded plastic part. The cavity geometry consists of an ASTM D638 type I tensile test bar.

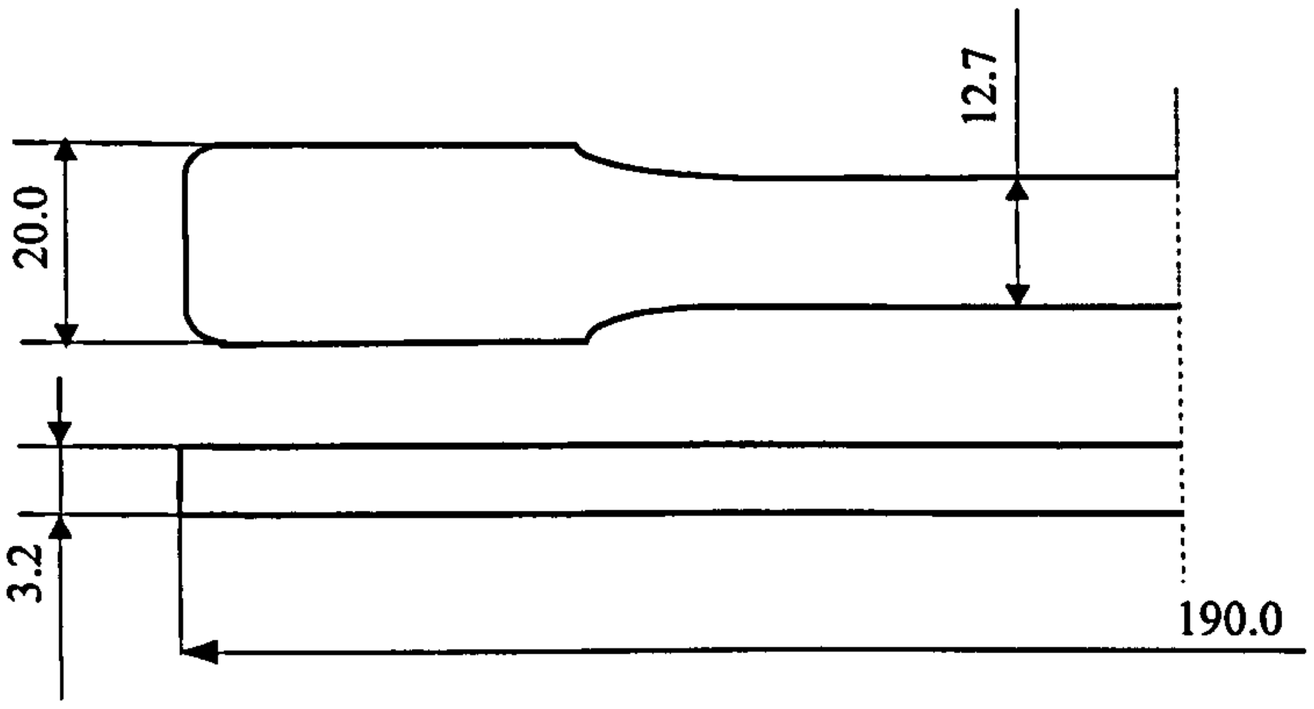

(The dimensions are in mm)

Fig. 3.1 Geometry of tensile bars used in the experiments

3.2 Development of the thermal residual stresses

The principles of the development of thermal residual stresses are illustrated in Fig. 3.2. Cooling is idealised in five steps in which the pressure varies as a function of time. As the cooling front moves inwards, the temperature drops from T_0, through T_g, to T_∞. It is assumed that the material behaves as an ideal fluid when $T > T_g$. Therefore, $\sigma = -P_0$ in the region where $T > T_g$ and P_0 is the packing pressure.

At time $t=t_0$ the mould is completely filled. For $t > t_0$, the residual thermal stress develop as follows:

1) $t=t_0$: The temperature is homogeneous and equal to T_0, The pressure is zero and the material is free of stresses.

2) $t=t_1$: The outer layers are constrained by the non slip condition at the mould walls. A small tensile stress σ_{xx} is introduced in the solidified outer shells. If the stresses are due to thermal contraction alone, they will be equi-biaxial in the xy plane, i.e. $\sigma_{xx}=\sigma_{yy}$.

3) $t=t_2$: An injection pressure P acts on the melt resulting in a compressive stresses $\sigma = -P_0$, compressing the rigid shell. If all displacements in the x-direction in the shell

are suppressed, the stress in the layers is decreased by $\Delta\sigma = \frac{\nu P_0}{1-\nu}$.

4) $t=t_3$: The pressure remains constant during the holding stage, while the material solidifies layer by layer during the time interval t_2 to t_3. Contraction of the newly cooled material decreases the compressive stresses in the surface layers.

5) $t=t_4$: The pressure is set to zero and the stresses in the melt disappear. The stresses in the rigid shell falls as moulding continue to cool.

6) $t=t_5$ Finally, the product is released from the mould. Further cooling is similar to a free quench. This results in tensile stresses in the core that are in equilibrium with the stresses in the outer shells.

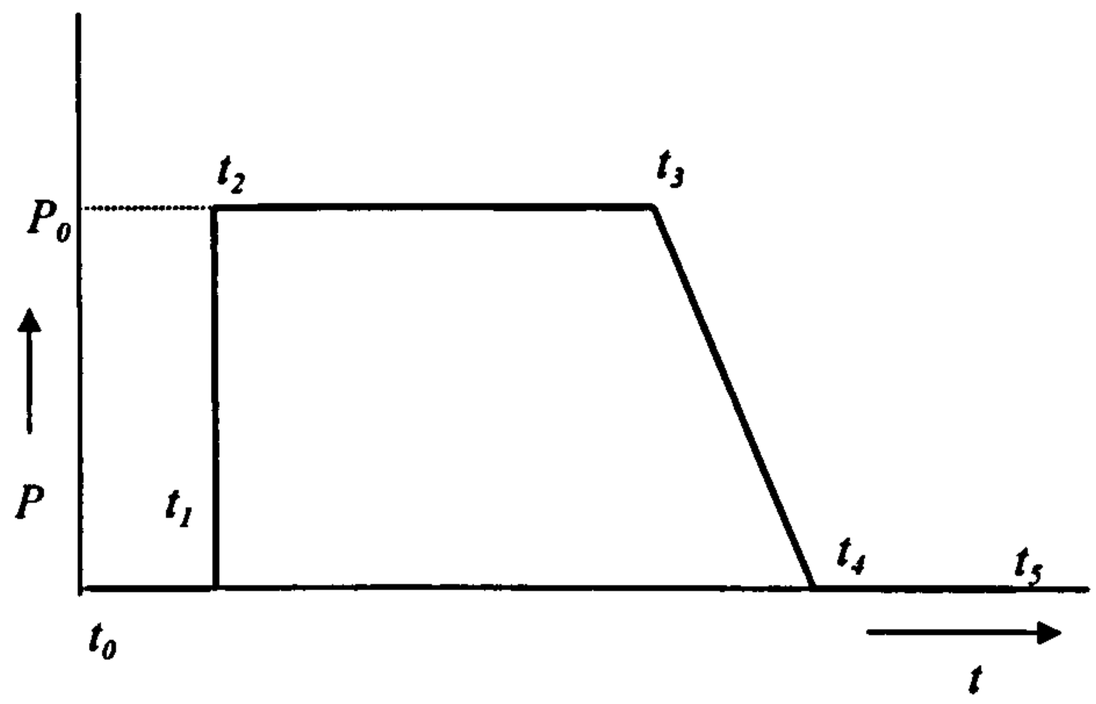

(a) Pressure trace in the cavity during the injection moulding

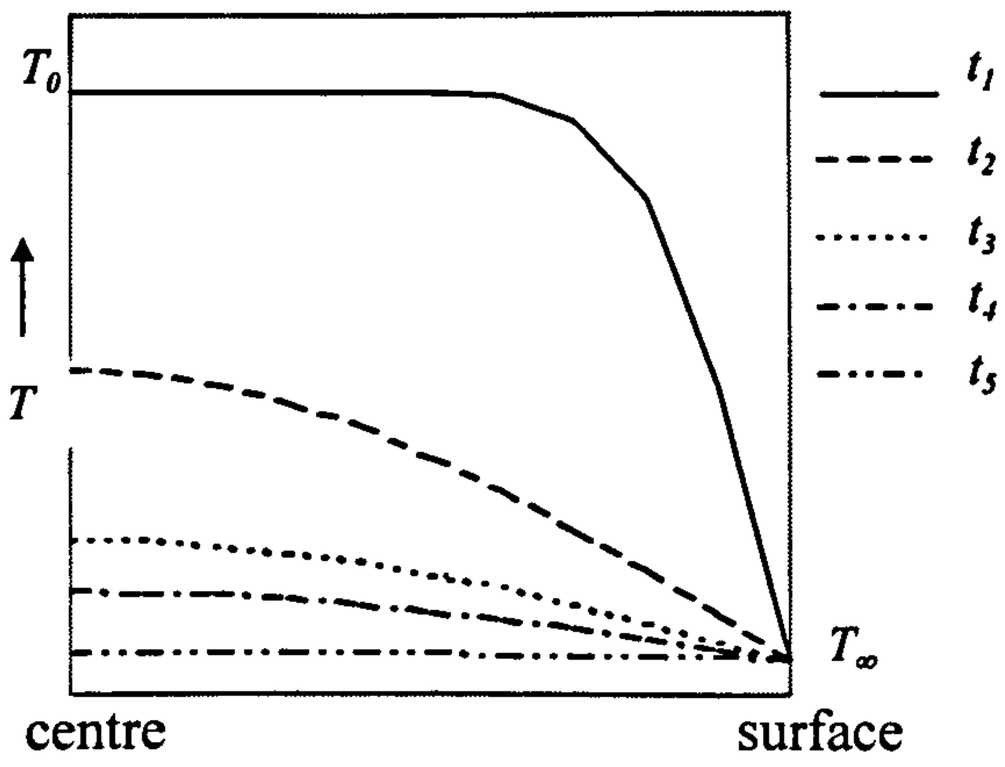

(b) Temperature

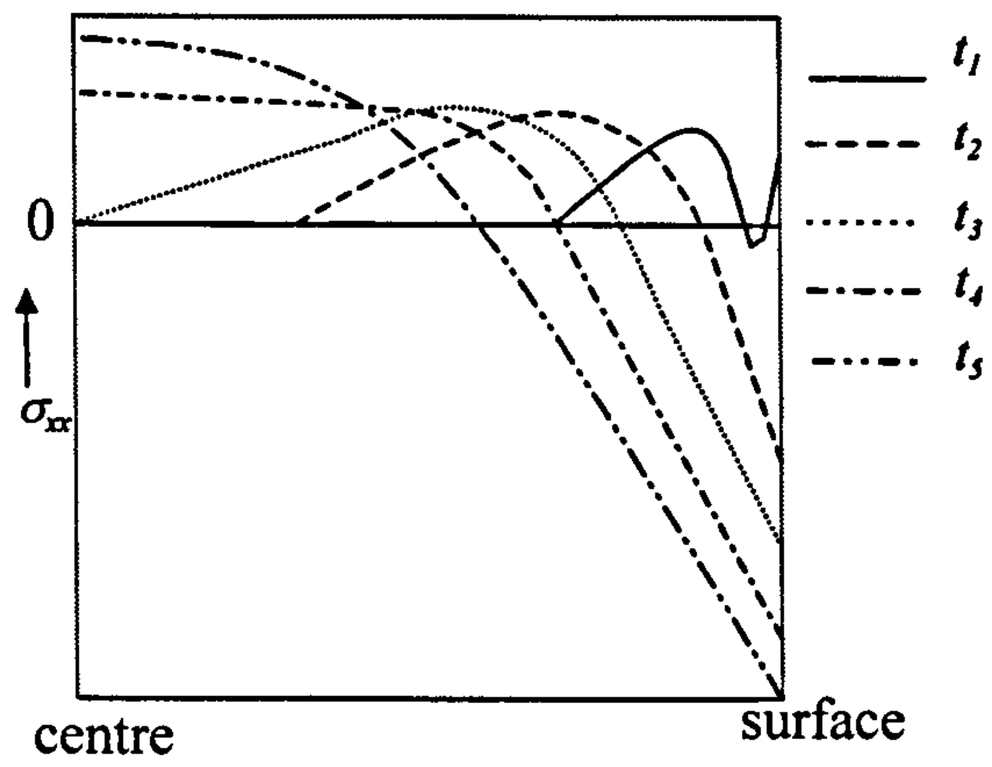

(c) Residual stresses distributions

Fig. 3.2 Residual stresses development

3.3 Basic assumptions

In order to make the problem solvable, some assumptions have to be made

1) The heat conduction problem can be solved independently of the thermal stress problem.

2) It assumed that no gap will develop between the product surface and the mould wall.

3) Calculations for a flat sheet will be made because the only important dimension will be thickness of the sample bar.

4) The solid polymer is assumed to be elastic.

5) Flow induced stresses will be neglected.

3.4 Temperature distribution

We consider a heat conduction problem of the geometry shown in Fig. 3.4.1 in a slab of thickness e, initially at the uniform temperature T_0, and exchanging heat by conduction at $z=-e/2$ and $z=e/2$ and a final equilibrium constant temperature, T_∞

The fundamental equation for this case is the Fourier conduction equation.

$$\frac{\partial T}{\partial t} = -k\nabla^2 T \tag{3.4.1}$$

Where

$$\nabla^2 = \frac{\partial^2}{\partial x^2} + \frac{\partial^2}{\partial y^2} + \frac{\partial^2}{\partial z^2} \tag{3.4.2}$$

The geometry is shown in Fig. 3.4.1. The polymer is bounded by mould surfaces at $z=\pm e/2$. The initial temperature of the melt is T_0, and final equilibrium temperature of the moulding is T_∞. Thus for one-dimensional flow, we have

$$\frac{\partial T}{\partial t} = k\frac{\partial^2 T}{\partial z^2} \qquad (-e/2<z<e/2) \qquad (3.4.3)$$

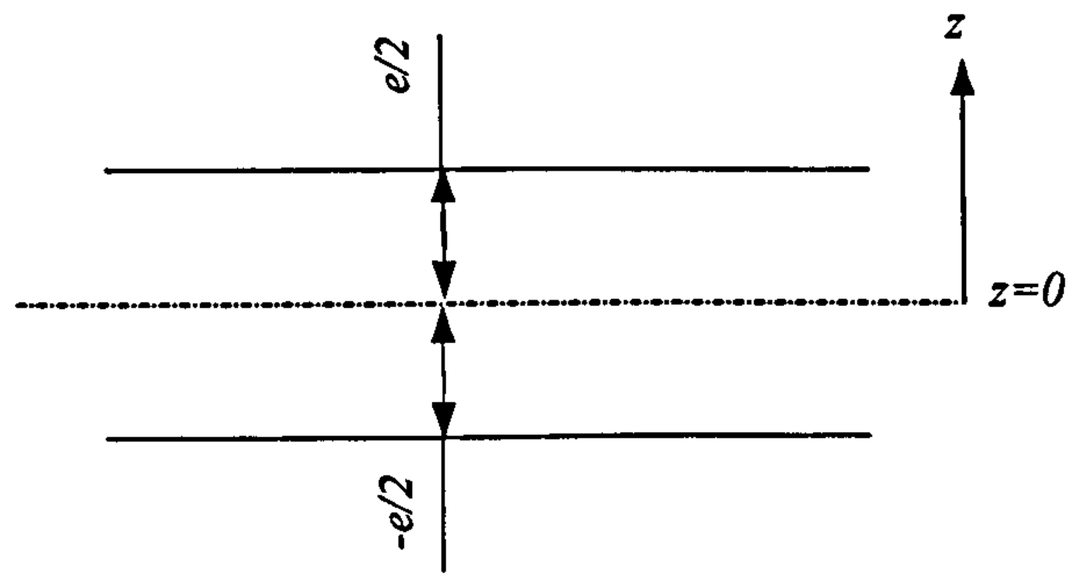

Fig. 3.4.1 The geometry of the melt

Following the procedure used by Carslaw[156], a dimension-less function *f(z,t)* is defined in a similar way to ΔT in the Fourier heat transfer analysis,

$$\text{i.e. } f(z,t) = \frac{T(z,t)-T_\infty}{T_0-T_\infty} = \Delta T \qquad (3.4.4)$$

with boundary conditions

(1) For all z within $-e/2 \le z \le e/2$, at time $t=\infty$: $T(z,t=\infty)=T_\infty$

$$f(z,t\to\infty) = \frac{T_\infty - T_\infty}{T_0 - T_\infty} = 0 \qquad (3.4.5)$$

(2) For all z within $-e/2 \le z \le e/2$, at time $t=0$: $T(z,t=0)=T_0$

$$f(z,t) = \frac{T_0 - T_\infty}{T_0 - T_\infty} = 1 \qquad (3.4.6)$$

(3) At $z = \pm\frac{e}{2}$, for all times $t \ge 0$: $T(\pm (e/2),t)=T_\infty$

therefore

$$f(\pm (e/2),t)=\frac{T_\infty - T_\infty}{T_0 - T_\infty} = 0 \qquad (3.4.7)$$

The solution to the heat equation can be described as a linear superposition of fundamental and harmonic sine modes corresponding to standing waves. $f(z,t)$ is then represented by:

$$f(z,t) = \sum_i g_i(z,t) \qquad (3.4.8)$$

where i goes over the whole ensemble of integers (i.e. $i=0 \rightarrow +\infty$). Furthermore, the spatial and time parts can be dealt with independently so that each g_i function is equal to $u_i(z) \cdot v_i(t)$ where the functions $u_i(z)$ and $v_i(t)$ are not known.

The next task is to work out the g_i functions to ensure that the first boundary condition ((i), above) is obeyed; it is assumed that, for all i values, $v_i(t)$ is not divergent, $v_i(t) \rightarrow 0$ when $i \rightarrow +\infty$. To fulfil the third boundary condition, $u_i(z)$ is represented by a cosine function, i.e.

$$u_i(z) = \cos\left(\frac{(2i+1)\cdot \pi z}{e}\right) \qquad (3.4.9)$$

will obey this condition, as the heat conduction equation is linear.

Now, we consider the function $f(z,t)$ defined by the series

$$f(z,t) = \sum_i a_{2i+1} \cdot \cos\left((2i+1)\frac{\pi z}{e}\right) \cdot \exp\left(-k_{2i+1}t\right) \qquad (3.4.10)$$

This series owes its convergence to the factor $\exp\left(-k_{2i+1}t\right)$ which is uniformly convergent. The coefficients a_{2i+1} are determined by using the second boundary condition and standard Fourier analysis.

$$g_i(z,t) = \cos\left(\frac{(2i+1)\pi z}{e}\right) \cdot \exp(-k_{2i+1}t) \tag{3.4.11}$$

$$\frac{\partial g_i}{\partial t} = \cos\left(\frac{(2i+1)\pi z}{e}\right) \cdot \exp(-k_{2i+1}t) \cdot \left(-k_{2i+1}\right) \tag{3.4.12}$$

$$\frac{\partial g_i}{\partial z} = \exp(-k_{2i+1}t) \cdot \left(\left(-\frac{(2i+1)\pi}{e}\right) \cdot \sin\left(\frac{(2i+1)\pi z}{e}\right)\right) \tag{3.4.13}$$

$$\frac{\partial^2 g_i}{\partial z^2} = \exp(-k_{2i+1}t) \cdot \left(-\left((2i+1)\frac{\pi}{e}\right)^2 \cdot \cos\left((2i+1)\frac{\pi}{e}z\right)\right) \tag{3.4.14}$$

if g_i is a solution of the heat equation, then

$$\frac{\partial g_i}{\partial t} = k\frac{\partial^2 g_i}{\partial z^2} \text{ and } k_{2i+1} = k \cdot \left(\frac{(2i+1)\pi}{e}\right)^2 \tag{3.4.15}$$

For t=0, $f(z,0) = \sum_i a_{2i+1} \cos\left((2i+1)\frac{\pi}{e}z\right)$ is a Fourier sum

A periodic function $h(z)$ is defined

$z \xrightarrow{h} h(z)$ (the period is $2e$ (Fig. 3.4.2))

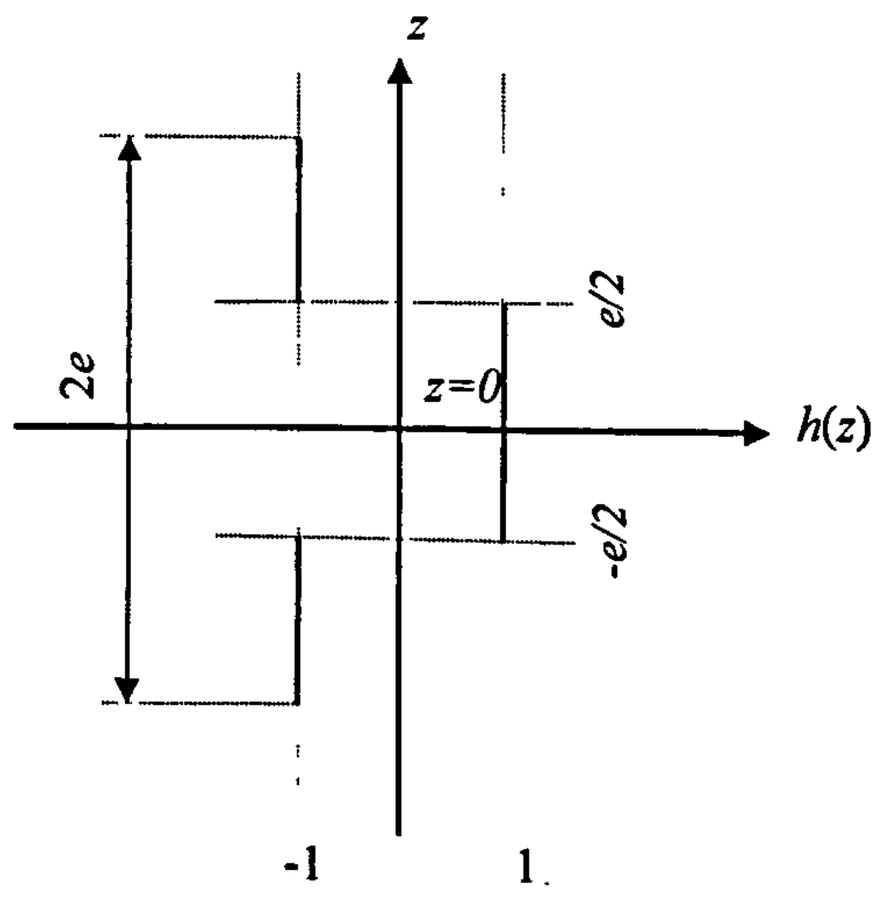

Fig. 3.4.2 Definition of the function $h(z)$

so that

$h(z)$ can be written as a Fourier sum.

$$h(z) = a_0' + \sum_{n=1}^{+\infty}\left(a_n' \cos\left(\frac{n\pi z}{e}\right) + b_n' \sin\left(\frac{n\pi z}{e}\right)\right) \tag{3.4.16}$$

where $a_0' = 0$ and for all positive integers, (n): $b_n' = 0$ because $h(z)$ is symmetrical.

The Fourier sum simply converges towards the function $h(z)$ for all z except at the discontinuities at $z = \pm\left(\frac{e}{2} + ne\right)$ (n = positive integer) Actually this sum will converge towards $\frac{1}{2}(h(z^+) + h(z^-))$ which is half of the sum of limits just to the left and just to the right of any given discontinuous point, e.g. at $z=-\frac{e}{2}$ or $z=\frac{e}{2}$.

Since $h\left(\frac{-e}{2^+}\right) = +1$, $h\left(\frac{-e}{2^-}\right) = -1$ and $h\left(\frac{+e}{2^+}\right) = -1$, $h\left(\frac{+e}{2^-}\right) = +1$

the sum will converge to 0 at $z = \pm\frac{e}{2}$. The function $h(z)$ at these points was defined as zero and was chosen so that there may be complete equality in the associated Fourier sum. Because this $h(z)$ function is written in terms of a Fourier sum that obeys both the second and the third boundary conditions for t=0 ($h(z)$=$f(z,t)$), the coefficients of the latter sum are the same as those of $f(z,0)$.

For all positive integer values

$$\text{i: } a_{2i+1} = \frac{2}{T}\int_T \cos\left((2i+1)\frac{\pi z}{e}\right)\cdot h(z)dz = \frac{1}{e}\int_{-e}^{+e}\cos\left((2i+1)\frac{\pi z}{e}\right)h(z)dz$$

$$= -\frac{1}{e}\int_{-e}^{-\frac{e}{2}}\cos(2i+1)\frac{\pi z}{e}dz + \frac{1}{e}\int_{-\frac{e}{2}}^{\frac{e}{2}}\cos(2i+1)\frac{\pi z}{e}dz - \frac{1}{e}\int_{\frac{e}{2}}^{e}\cos(2i+1)\frac{\pi z}{e}dz$$

$$=\frac{4}{\pi(2i+1)}\sin\left(\frac{\pi(2i+1)}{2}\right) \tag{3.4.17}$$

where

$$\sin\left(\frac{\pi(2i+1)}{2}\right)=(-1)^i,\ \ (a_{2i+1})=(a'_{2i+1}),\ a_{2i+1}=\frac{4\cdot(-1)^i}{\pi(2i+1)}$$

Then, the temperature field is finally, for the region $-e/2 < z < e/2$ and $0 \le t$

$$f(z,t)=\frac{4}{\pi}\sum_{i=1}^{\infty}\frac{(-1)^i}{2i+1}\cos\left((2i+1)\frac{\pi}{e}z\right)\exp\left(-k\left(\frac{(2i+1)\pi}{e}\right)^2 t\right) \tag{3.4.18}$$

3.5 Representation of Young's modulus

The Young's modulus of polystyrene and other thermoplastics is time dependent and changes continuously as temperature changes and it is required to chose a suitable expression to represent it that can be inserted into the computations.

3.5.1 Representation of Young's modulus using K.W.W and W.L.F equations

Struik (1978) found that the formula that best represented the short term stress relaxation of a range of polymers was the Kohlrausch-Williams-Watt formulation[14]:

$$E(T,t)=E_0\cdot\exp\left[-\left(\frac{t}{t_0(T)}\right)^m\right] \tag{3.5.1.1}$$

where E_0 is the initial value of the Young's modulus, $t_0(T)$ is a characteristic constant for the material which depends on T, and m is a constant with a value about 1/3[4]. When $T=T_g$, this takes this value

$$E(T_g,t) = E_0 \cdot \exp\left[-\left(\frac{t}{t_0(T_g)}\right)^m\right] \qquad (3.5.1.2)$$

The general shapes of the curves $E(T,t)$ and $E(T_g,t)$ versus $\ln t$ are shown in Fig. 3.5.1

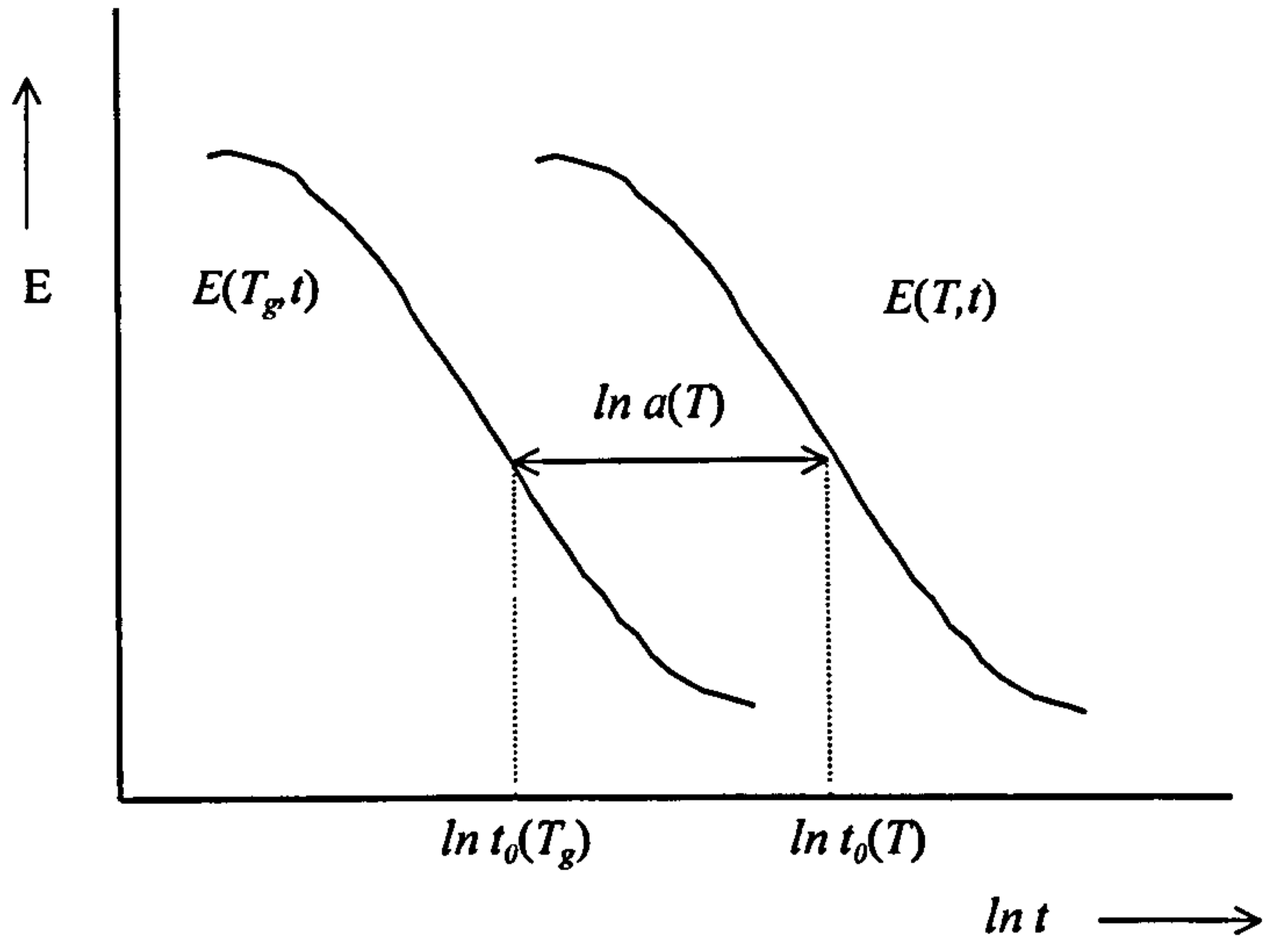

Fig. 3.5.1 Stress relaxation and the effect of temperature

It is normally found that the relaxation curves superimpose when shifted parallel to the $\ln t$ axis. Thus, we can put

$$t_0(T) = at_0(T_g) \qquad (3.5.1.3)$$

It follows that

$$E(T,t) = E(T_g,at) = E_0 \exp\left[-\left(\frac{at}{t_0(T_g)}\right)^m\right] \qquad (3.5.1.4)$$

The shift function, a, is a function of T and T_g and can be represented by the WLF expression. Also T is a function of z and t, so the shift factor can be written as

$$\ln a(z,t) = \ln\left[\frac{t_0(T(z,t))}{t_0(T_g)}\right] = \frac{C_1(T(z,t)-T_g)}{C_2+(T(z,t)-T_g)} \qquad (3.5.1.5)$$

where C_1 and C_2 are universal constants

therefore

$$a(z,t) = \exp\left[\frac{C_1(T(z,t)-T_g)}{C_2+(T(z,t)-T_g)}\right] \qquad (3.5.1.6)$$

Now, Eq. 3.5.1.6 is substituted into Eq. 3.5.1.4 and then finally

$$E(z,t) = E_0 \cdot \exp\left[-\left(\frac{t}{t_0(T_g)} \cdot \exp\left(\frac{C_1 \cdot (S(z,t)-T_g)}{C_2+(S(z,t)-T_g)}\right)\right)^m\right] \qquad (3.5.1.7)$$

3.5.2 Young's modulus represented by the Van Krevelen-Hoftyzer equations[13]

An alternative way of representing the time-temperature variation of Young's modulus has been described by Van Krevelen and Hoftyzer.

We see from Fig. 3.5.2 that at the glass transition temperature the rigidity of amorphous polymers falls rapidly. In the glassy polymers, the rigidity is obviously highly dependent on the temperature, especially near to the glass transition temperature. The empirical expressions (Eq. 3.5.2.1, Eq. 3.5.2.2) of Van Krevelen and Hoftyzer can be extended to describe the polymer rigidity as a function of temperature[Note 3.5.2].

$$\frac{T_g}{} + 2$$

$$E(z,t) = \frac{T_r}{\left(\frac{T_g}{T_r} + \frac{2T(z,t)}{T_r}\right)} \cdot E_0 \qquad (T \le T_g) \qquad (3.5.2.1)$$

$$E(z,t) = \frac{E_0}{\exp 2.65\left(\dfrac{\dfrac{T_g}{T_r} + \dfrac{T_g}{T(z,t)}}{\left(\dfrac{T_g}{T_r} - 1\right)}\right)} \qquad (T > T_g) \qquad (3.5.2.2)$$

where T_r is the reference temperature.

Note 3.5.2: As the temperature increases through the glass transition temperature, the rigidity of amorphous polymers falls rapidly.

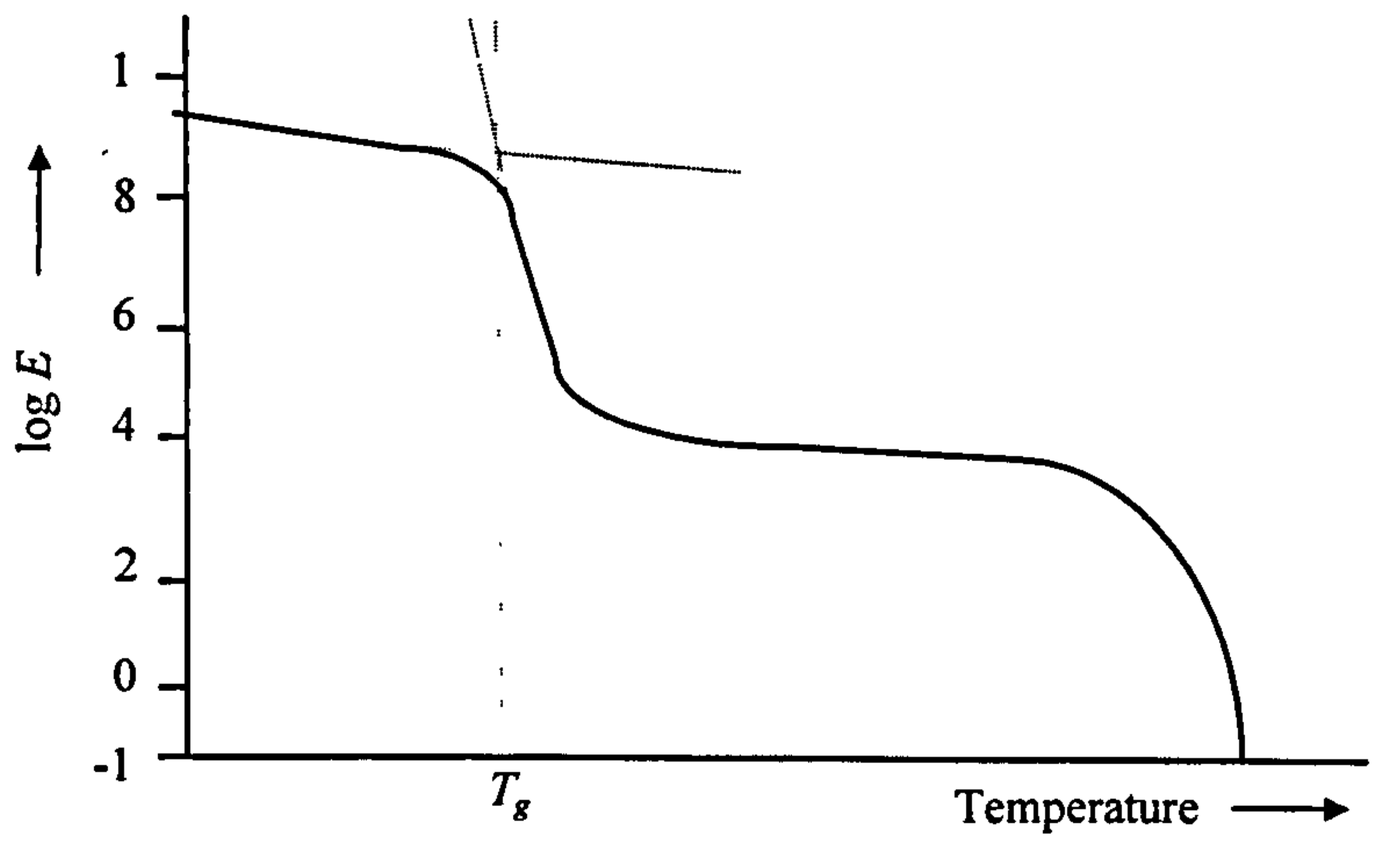

Fig. 3.5.2 Viscoelastic behaviour of a typical amorphous polymer

3.6 Calculations for the thermal expansion

The specific volume as a function of temperature and pressure is usually given on a PVT diagram[29,30] (Fig. 3.6.1). The volume increases by thermal expansion as temperature increases and the volume reduces as the pressure increased. Both effects must be dealt with by the computation.

One of the most useful representations of the $V(P, T)$-behaviour of polymeric liquids is by the Tait-equations[35]:

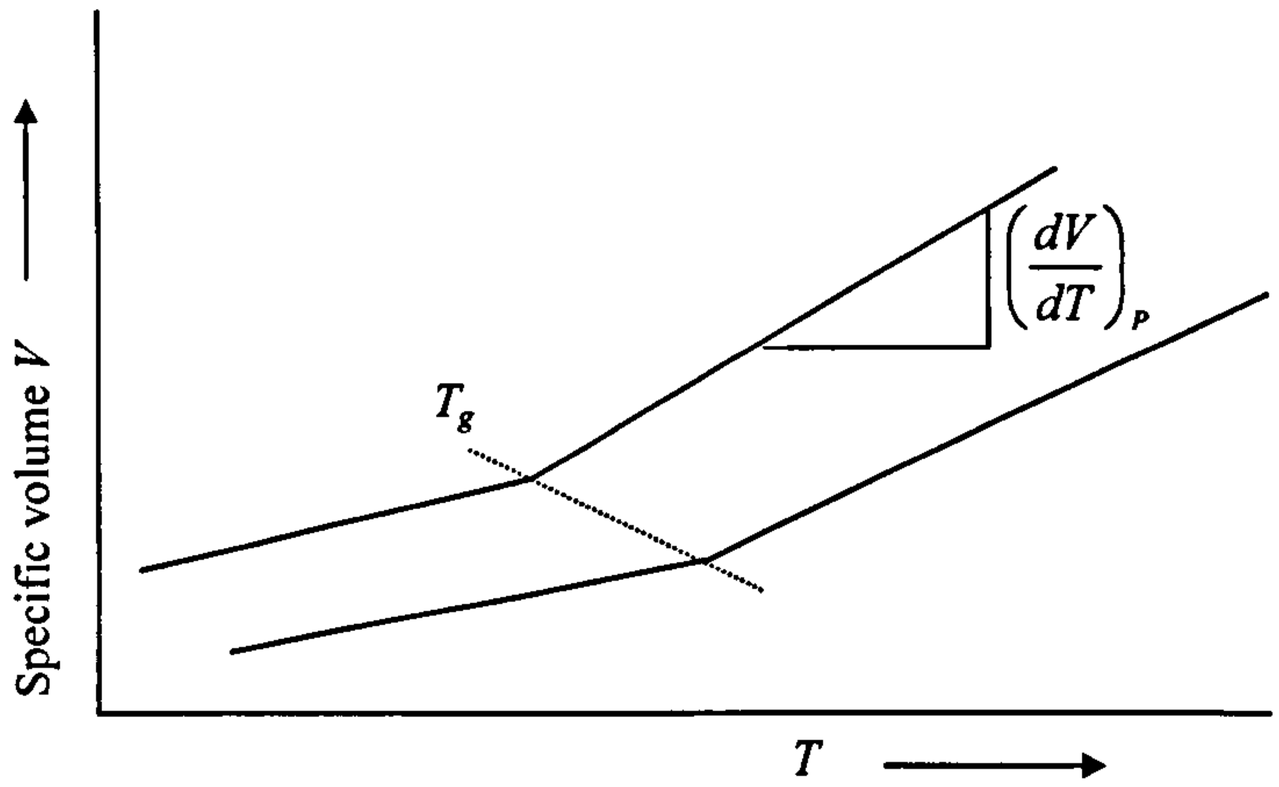

Fig. 3.6.1 PVT diagram[29]

$$V(P,T) = (a_{0s} + a_{1s}(T - T_g))\left(1 - C \cdot \ln\left(1 + \frac{P}{b_s}\right)\right) \qquad (T \le T_g) \qquad (3.6.1)$$

$$V(P,T) = (a_{0m} + a_{1m}(T - T_g))\left(1 - C \cdot \ln\left(1 + \frac{P}{b_m}\right)\right) \qquad (T > T_g) \qquad (3.6.2)$$

where

$$b_s = b_{0s} e^{-b_{1s} T(z,t)}$$

$$b_m = b_{0m} e^{-b_{1m} T(z,t)}$$

a_{0s} (m^3/kg), a_{0m} (m^3/kg), a_{1s} (m^3/kg·K), a_{1m} (m^3/kg·K), b_{0s} (Pa), b_{0m}(Pa), b_{1s} (K^{-1}), b_{1m} (K^{-1}) are constants.

Simha et al. (1973)[36] have shown that C is indeed almost constant and gave the best

average value as: C=0.0894

The fundamental equation for volumetric thermal expansion is

$$\alpha_v = \frac{1}{V} \cdot \frac{dV}{dT} \tag{3.6.3}$$

Now, Eq. 3.6.1 and Eq. 3.6.2 are applied to Eq. 3.6.3 to give the linear expansion coefficients below and above T_g as

$$\alpha(z,t) = \frac{a_{1s}}{3 \cdot (a_{0s} + a_{1s}(T(z,t) - T_g)} \qquad (T \leq T_g) \tag{3.6.4}$$

$$\alpha(z,t) = \frac{a_{1m}}{3 \cdot (a_{0m} + a_{1m}(T(z,t) - T_g)} \qquad (T \geq T_g) \tag{3.6.5}$$

Note that the linear expansion coefficients are functions of the temperature, T. They are given in the form $\alpha(z,t)$ because the temperature is uniquely defined by z and t, and because z and t are the valuables of interest in the following calculations.

3.7 Calculation of the T_g-plane position according to the time

An initial change occurs in the material within the moulding when the temperature falls below T_g. Calculations must normally be split into two parts dealing separately with changes occurring respectively at $T > T_g$ and at $T < T_g$. Thus, it is necessary to know the time at which the temperature is at T_g for all locations. For the one dimensional heat flow case examined, this amounts to following the plane of T=T_g as it travels through the moulding.

Starting with the result given already as Eq. 3.4.18

$$f(z,t)=\frac{4}{\pi}\sum_{i=1}^{\infty}\frac{(-1)^i}{2i+1}\cos\left[(2i+1)\frac{\pi}{e}z\right]\exp\left[-k\left(\frac{(2i+1)\pi}{e}\right)^2 t\right] \tag{3.4.18}$$

The first term of this series is given when i=0,

$$f_{i=1}(z,t)=\frac{4}{\pi}\cos\left(\frac{\pi}{e}z\right)\exp\left[-k\left(\frac{\pi}{e}\right)^2 t\right] \tag{3.7.1}$$

The factor $\exp\left[-k\left(\frac{(2i+1)\pi}{e}\right)^2 t\right]$ falls rapidly as i increases

A relaxation time τ can be defined for all i values:

$$\tau_{2i+1}=\frac{1}{k_{2i+1}}=\frac{1}{\left(\frac{\pi}{e}\right)^2\cdot k}\cdot\frac{1}{(2i+1)^2} \tag{3.7.2}$$

when i=0

$$\tau_{2i+1}=\tau_1=\frac{1}{\left(\frac{\pi}{e}\right)^2\cdot k} \tag{3.7.3}$$

Therefore, all τ_{2i+1} can be expressed in terms of τ_1 as $\tau_{2i+1}=\frac{\tau_1}{(2i+1)^2}$

Thus, when i=1 $\tau_3=\frac{\tau_1}{9}$ and when i=2 $\tau_5=\frac{\tau_1}{25}$ etc.

There is a further factor $\frac{1}{2i+1}$ in the summation in Eq. 3.4.18 which also falls with increasing i. Thus successive terms in Eq. 3.4.18 fall rapidly as i increases. Next the effect of terminating the sum after a small number of terms is examined.

Approximations have been calculated for the sum evaluated using one, two and three

terms respectively and they are compared in Fig. 3.7.1

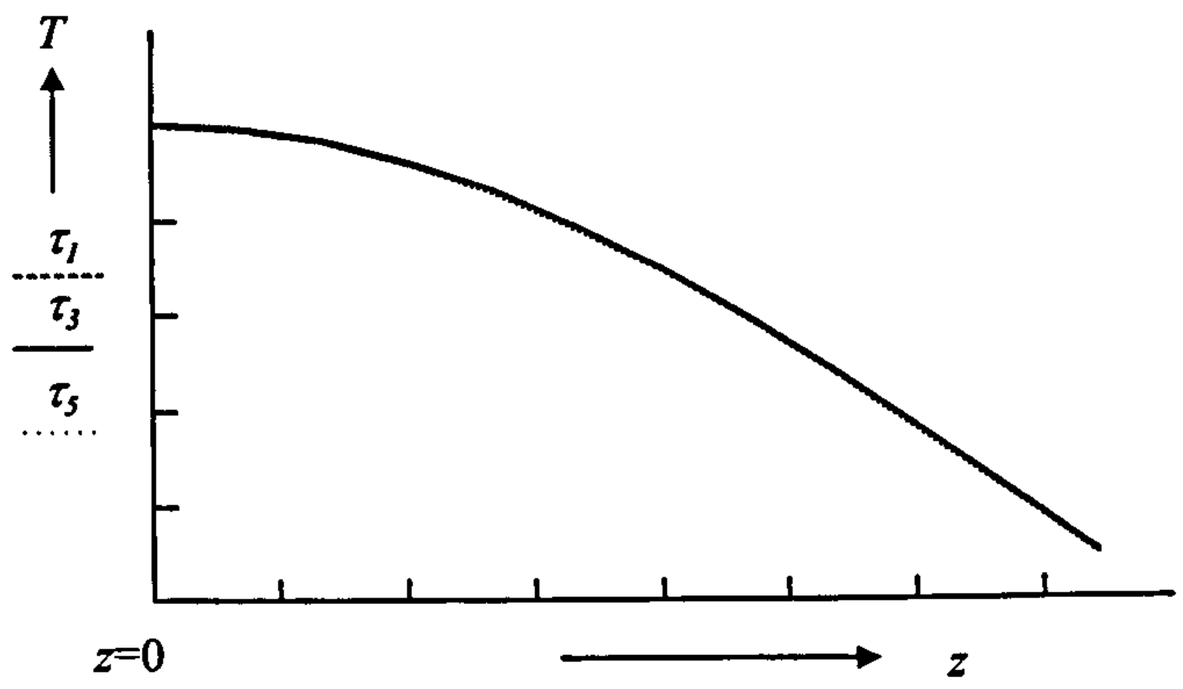

τ_1: 1st term
τ_2: sum of 1st and 2nd terms
τ_3: sum of 1st, 2nd and 3rd terms

Fig. 3.7.1

The graphs are virtually indistinguishable and therefore to a good approximation the series can be represented by the first term only,

$$\text{i.e. } f(z,t) \cong \left(\frac{T(z,t)-T_\infty}{T_0-T_\infty}\right) = \frac{4}{\pi}\cos\left(\frac{\pi}{e}z\right)\exp\left[-k\left(\frac{\pi}{e}\right)^2 t\right] \tag{3.7.4}$$

hence the position of the solidification front, i.e. of the glass transition plane is

$$H(t) = \frac{e}{\pi}\cdot\arccos\left\{\frac{\pi}{4}\left(\frac{T_0-T_\infty}{T_g-T_\infty}\right)\cdot\exp\left[k\left(\frac{\pi}{e}\right)^2 t\right]\right\} \tag{3.7.5}$$

3.8 Calculations of the residual stress using method A (based on Struik's method)

By following Lee's viscoelastic treatment[53], Struik[16] has considered a fully restrained material cooled at constant length (e.g. a bar kept at constant length), with stress-relaxation modulus $E(T,t)$ and linear thermal expansibility $\alpha(T)$. He introduces the local

cooling rate $q = -\frac{\partial T}{\partial t}$ in the time-dependent Young's moduli and states that the cooling over the interval between T and T-δ produces an incremental stress given by:

$$\delta\sigma(T) = \alpha(T) \cdot E\left(T, \frac{1}{Bq}\right)\delta T \tag{3.8.1}$$

where

$\alpha(T)$: linear thermal expansivity at T

B: quantity between 0.08 and 1, as follows:

when T is below the glass transition temperature $B = \frac{30 - \ln q}{T}$ [16],

when T is above the glass transition temperature $B = \frac{C_1 C_2}{\left(C_2 + \left(T - T_g\right)\right)^2}$ [16],

where C_1 and C_2 are the constants in the WLF equation.

$q(z,t)$ is the local cooling rate: $\frac{d}{dt}T$

Finally, the following equations were obtained that permit the calculation of thermal strains and stresses rate:

$$\dot{\varepsilon}_{xx}(t) \cong \frac{\int_{H(t)}^{\frac{e}{2}} R\left(T, \frac{1}{Bq}\right) \cdot \alpha(T) \cdot \dot{T}(\xi, t) d\xi}{\int_{H(t)}^{\frac{e}{2}} R\left(T, \frac{1}{Bq}\right) d\xi} \tag{3.8.2}$$

$$\dot{\sigma}_{xx}(t) = R\left(T, \frac{1}{Bq}\right)\left[\left(\dot{\varepsilon}_{xx}(t) - \alpha(T) \cdot T\right) \cdot \dot{T}\right] \tag{3.8.3}$$

where

$H(t)$ is the position of the solidification or glass transition plane

R is a mechanical parameter defined as $R = \frac{E}{1 - \upsilon}$

ξ is a space integration variable on the z (co-ordinate) scale

We consider the formation of cooling stresses for the geometry shown in Fig. 3.8.1 in a slab of thickness *e*, cooled symmetrically from the both surfaces, *e*/2 and –*e*/2. The temperature $T(z,t)$ depends on t and z only.

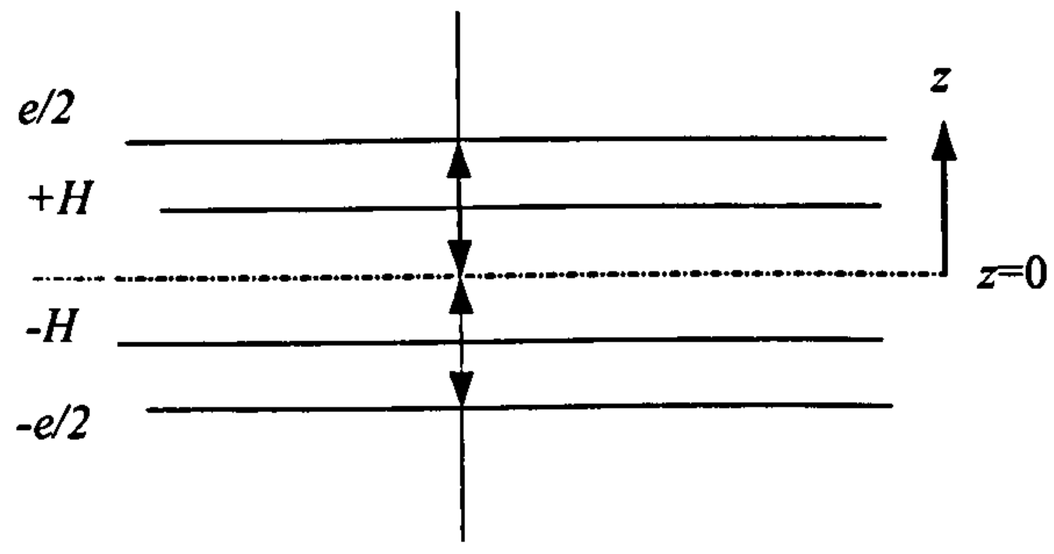

Fig. 3.8.1 The geometry of the bar

Since the temperature depends on only z and t, the stress and strain components do not depend on either x or y.

From the equations of equilibrium[157, 158] then the shear stresses τ_{xz}, τ_{yz} and the normal stress σ_{zz} must be independent of z, x or y. Since there are no forces normal to the surfaces at $z=-e/2$ and $z=e/2$,

$$\tau_{xz} = \tau_{yz} = \sigma_{zz} = 0 \tag{3.8.4}$$

In the thermo-elastic range, strain $\gamma_{xz}(z,t)$ depends on only τ_{xz} or $\tau_{xz}(z,t)$ for $\tau \le t$. From similar considerations, Eq. 3.8.4 implies that

$$\gamma_{xz} = \gamma_{yz} = 0 \tag{3.8.5}$$

Since the bar remains flat, the displacement w in the z direction cannot depend on x or y. Therefore, together with Eq. 3.8.5, and the definition of the strain tensor[157,158], it is evident that ε_{xx} and ε_{yy} do not depend on z. Thus, ε_{xx} and ε_{yy} depend only on time and,

by the symmetry of this problem, ε_{xx} is equal to ε_{yy} and γ_{xy} is zero. Consequently, τ_{xy} will be zero too. The only non-vanishing stress components are therefore σ_{xx} and σ_{yy}; for symmetry reasons they must be equal and they do not depend on x and y. We obtain

$$\varepsilon_{xx} = \varepsilon_{yy} = f(z,t) \tag{3.8.6}$$

$$\sigma_{xx} = \sigma_{yy} = \phi(z,t) \tag{3.8.7}$$

$$\tau_{xy} = \tau_{zy} = \tau_{zx} = \sigma_{zz} = \gamma_{xy} = \gamma_{zy} = \gamma_{zx} = 0 \tag{3.8.8}$$

Let us now apply this result to the inhomogeneously cooled bar. The incremental temperature changes $\partial T(z,t)$ occurring between t and $t+\partial t$, according to Hooke's law, produces a stress change $\partial\sigma_{xx}(z,t) = \partial\sigma_{yy}(z,t)$ given by

$$\partial\sigma_{xx}(z,t) = R[\partial\varepsilon_{xx}(z,t) - \alpha(z,t)\partial T(z,t)]; H < |z| < \frac{e}{2} \tag{3.8.9}$$

$$\partial\sigma_{xx}(z,t) = R_r[\partial\varepsilon'_{xx}(z,t) - \alpha_r(z,t)\partial T(z,t)]; 0 < |z| < H \tag{3.8.10}$$

where

ε_{xx} is the strain in the glassy shell and ε'_{xx} is the strain in the rubbery core

$$\begin{cases} R(z,t) = \dfrac{E(z,t)}{1-\nu} \;;\; B(z,t) = \dfrac{\alpha(z,t)E(z,t)}{1-\nu} = \alpha(z,t)R(z,t) \\ R(z,t)_r = \dfrac{E_r(z,t)}{1-\nu_r} \;;\; A_r(z,t) = \dfrac{\alpha_r(z,t)E_r(z,t)}{1-\nu_r} = \alpha_r(z,t)R_r(z,t) \end{cases} \tag{3.8.11}$$

where

α_r is the linear thermal expansion coefficient in the rubbery core

E_r is the Young's modulus in the rubbery core

ν_r is the Poisson ratio in the rubbery core

At the boundary between the zones, the displacements in the *x*-direction must be continuous, and therefore:

$$\partial\varepsilon_{xx}(z,t)=\partial\varepsilon'_{xx}(z,t) \tag{3.8.12}$$

The value of $\partial\varepsilon_{xx}(z,t)$ can be found when we remember that no forces are acting on the end faces of the bar. According to Saint-Venant's principle [158], it is therefore required that:

$$\int_{\frac{e}{2}}^{\frac{e}{2}}\partial\sigma_{xx}(z,t)dz=0 \tag{3.8.13}$$

Substituting Eq. 3.8.9, Eq. 3.8.10 and Eq. 3.8.12 into Eq. 3.8.13 and using the fact that $\partial\varepsilon_{xx}$ is independent of z, we find:

$$\partial\varepsilon_{xx}(z,t)=\frac{A_r\int_0^{H(t)}\partial T(\xi,t)d\xi+B\int_{H(t)}^{\frac{e}{2}}\partial T(\xi,t)d\xi}{R_rH(z,t)+R\left[\frac{e}{2}-H(z,t)\right]} \tag{3.8.14}$$

The treatment of the cooling over the interval between $T(z,t)$and $T(z,t)$-$\delta(z,t)$[16] produces an incremental stress given by:

$$\delta\sigma(z,t)=\alpha(z,t)\cdot E(z,t)\delta T \tag{3.8.15}$$

Recall that this is for the fully restrained core: the element of material at position z is not allowed to change dimension in the x-y plane.

Note that the stress-relaxation modulus $E(T,t)$ is a function of the temperature T.

It is given in the form $E(z,t)$ because the temperature is uniquely defined by z and t, and because z and t are the values of interest in the following calculations.

We consider a tensile bar cooled at constant length, from initial temperature T_0 to final temperature T_∞ The tensile bar is rigidly supported and is stress free at T_0. Tensile stresses are built up during cooling because the free thermal contraction is restrained. The thermal stresses built up at the final temperature are obtained by summing the contributions of all temperature intervals δT:

$$\sigma(T_\infty) = \int_{T_\infty}^{T_0} \alpha(z,t) \cdot E(z,t) dT \qquad (3.8.16)$$

where

$E(z,t)$: stress-relaxation modulus at temperature T

$\alpha(z,t)$: linear thermal expansivity at temperature T

These results on the constrained bar open up a new way of calculating the cooling stresses in general. We may consider the material as an elastic solid of which the elastic constants E, K, ν, $R = \frac{E}{1-\nu}$ and thermal expansivity depend on temperature. The proper values of E, K, ν, $R = \frac{E}{1-\nu}$ are found from $E(z,t)$.

To illustrate the method, we reconsider the rapidly cooled plate with the stress state described in Eq. 3.8.4 to Eq. 3.8.8. Because $R(z,t) = \frac{E(z,t)}{1-\nu(z,t)}$ is now dependent on the temperature and the relaxation time, as presented in Section 3.5.1 (Eq. 3.5.1.7), we no longer need the two stress-strain relations of Eq. 3.8.9 and Eq. 3.8.10. These are replaced by the single equation given by:

$$\partial\sigma_{xx}(z,t) = R(z,t)\{\partial\varepsilon_{xx}(z,t) - \alpha(z,t)\partial T\} \qquad (3.8.17)$$

Eq. 3.8.12 and Eq. 3.8.13 remain valid, but Eq. 3.8.14 is replaced by

$$\partial\varepsilon_{xx}(z,t)=\frac{\int_0^{\frac{e}{2}}R(z,t)\alpha(z,t)\partial T(\xi,t)d\xi}{\int_0^{\frac{e}{2}}R(z,t)d\xi} \tag{3.8.18}$$

where ξ is a space integration variable

These equations can be used to assess the importance of the viscoelastic effects above as well as below T_g. It immediately follows that the viscoelasticity of the material above T_g will slightly affect the cooling stresses. In the rubbery core R will be 100 to 1000 times smaller than in the glassy shell. Consequently, for H-values not too close to $e/2$, the contributions of the soft layers to the integrals of Eq. 3.8.18 can be neglected, and we obtain:

$$\partial\varepsilon_{xx}(z,t)=\frac{\int_{H(t)}^{\frac{e}{2}}R(z,t)\alpha(z,t)\partial T(\xi,t)d\xi}{\int_{H(t)}^{\frac{e}{2}}R(z,t)d\xi} \tag{3.8.19}$$

Now, R in Eq. 3.8.19 only refers to the glassy shell. The rubbery shell can be neglected above T_g . It directly leads to the approximated solution taking into account viscoelasticity, which can be formulated as:

$$\dot{\varepsilon}_{xx}(z,t)=\frac{\int_{H(t)}^{\frac{e}{2}}R(z,t)\alpha(z,t)\dot{T}(\xi,t)d\xi}{\int_{H(t)}^{\frac{e}{2}}R(z,t)d\xi} \tag{3.8.20}$$

where

$H(t)$ is the position of the solidification or glass transition plane:

$H(t_0) = e/2$ when $t = 0$

$H(t_g) = 0$ when $t = t_g$: defined as the time at which the centre of the moulding reaches the temperature T_g as appears in the KWW equation.

$0 < H(t) < e/2$ when $0 < t < t_g$

whilst Eq. 3.8.19 leads to the formula for the stress-production rate:

$$\dot{\sigma}_{xx}(z,t) = R(z,t)\left[\dot{\varepsilon}_{xx}(z,t) - \alpha(z,t)\dot{T}(z,t)\right] \tag{3.8.21}$$

We find $\sigma(z,t)$ by integration

$$\sigma(z,t) = \int_{t_g}^{t} \dot{\sigma}(z,t)dt \tag{3.8.22}$$

3.9 Calculation of the packing pressure induced strain

To determine the strain state in a pressurised melt, the change in the specific volume of the melt from $V(P_0,T)$ to $V(P_1,T)$ is calculated as $\frac{\delta V}{V}$. This leads to a corresponding linear strain of

$$\varepsilon_{melt} = \frac{1}{3} \times \frac{V(P_1,T) - V(P_0,T)}{V(P_0,T)} \tag{3.9.1}$$

where

P_0 is the packing pressure

P_1 is the atmospheric pressure

with respect to the specific volume at P_0. Eq. 3.9.1 is valid for infinitesimal changes in the specific volume. An analysis of pressure-volume-temperature (PVT) data for typical thermoplastics suggests that the packing pressure may change the specific volume by as much as 15%[72]. Therefore, a better definition for strain of this application is

$$\varepsilon_{melt} = \frac{1}{3} \ln\left(\frac{V(P_1,T)}{V(P_0,T)}\right) \tag{3.9.2}$$

where

$$V(P_0,T)=(a_{0s}+a_{1s}(T-T_g))\left(1-0.0894\cdot\ln\left(1+\frac{P_0}{B_s}\right)\right)\quad(T\le T_g)\qquad(3.9.3)$$

$$V(P_0,T)=(a_{0m}+a_{1m}(T-T_g))\left(1-0.0894\cdot\ln\left(1+\frac{P_0}{B_m}\right)\right)\quad(T>T_g)\qquad(3.9.4)$$

$$V(P_1,T)=(a_{0s}+a_{1s}(T-T_g))\left(1-0.0894\cdot\ln\left(1+\frac{P_1}{B_s}\right)\right)\quad(T\le T_g)\qquad(3.9.5)$$

$$V(P_1,T)=(a_{0m}+a_{1m}(T-T_g))\left(1-0.0894\cdot\ln\left(1+\frac{P_1}{B_m}\right)\right)\quad(T>T_g)\qquad(3.9.6)$$

The stress-production rate after de-moulding is calculated in the same way as in Eq. 3.8.22. Therefore,

$$\dot{\sigma}_{xx\,melt}(z,t)=R(z,t)\left[\dot{\varepsilon}_{xx}(z,t)+\dot{\varepsilon}_{xxmelt}-\alpha(z,t)\dot{T}(z,t)\right]\qquad(3.9.7)$$

We find $\sigma(z,t)$ by integration.

$$\sigma_{xxmelt}(z,t)=\int_{t_g}^{t}\dot{\sigma}_{xxmelt}(z,t)dt\qquad(3.9.8)$$

3.10 Calculation of the temperature distribution after de–moulding

The temperature distribution after de-moulding can be calculated using Eq. 3.7.4 Therefore,

$$T_{dem}(z,t)\cong\left(\frac{T_{dem}(z,t)-T_{room}}{T(z,t)-T_{room}}\right)\frac{4}{\pi}\cos\left(\frac{\pi}{e}z\right)\exp\left[-k\left(\frac{t}{e}\right)^2 t\right]\qquad(3.10.1)$$

where

T_{room} is the room temperature.

The strain-production rate can be calculated as for Eq. 3.8.20. Therefore,

$$\dot{\varepsilon}_{xx\,dem}(z,t)=\frac{\int_0^{\frac{e}{2}} R(z,t)\alpha(z,t)\dot{T}_{dem}(\xi,t)d\xi}{\int_0^{\frac{e}{2}} R(z,t)d\xi} \tag{3.10.2}$$

And the stress-production rate is

$$\dot{\sigma}_{xx\,dem}(z,t)=R(T,t)\left\{\dot{\varepsilon}_{xxdem}(z,t)-\alpha(z,t)\dot{T}_{dem}(z,t)\right\} \tag{3.10.3}$$

Finally,

$$\sigma_{xxdem}(z,t)=\int_0^{t_{dem}}\dot{\sigma}_{xxdem}(z,t)dt \tag{3.10.4}$$

where t_{dem} is the cooling time after de-moulding.

3.11 Calculation of the residual stress using method B (taking account of the pressure profile)

This section deals with residual stresses calculations performed taking account of the pressure profile. Section 3.11.1 gives the pressure history within half of the bar for different cooling times. Section 3.11.2 provides residual stresses calculations at $T=T_g$ using the pressure history. Section 3.11.3 gives residual stresses for $T<T_g$.

3.11.1 Calculations of the pressure profile

The specific volume as a function of temperature and pressure are usually given by the Tait equations. The volume decreases as the temperature decreases and the volume

increases as the pressure decreases. The pressure drop is calculated as functions of temperature and volume in this section.

3.11.1.1 Volumetric changes when T drops from T_1 to T_2

As discussed in Section 3.6, the volumetric change in an element of material at z when $T(z,t)$ drops from T_1 (z,t_1) to $T_2(z,t_2)$ is

$$\Delta V_1(z,t_1,t_2)=\begin{cases} a_{1s}\cdot\Delta T(z,t_1,t_2) & (T\le T_g) \\ a_{1m}\cdot\Delta T(z,t_1,t_2) & (T>T_g) \end{cases} \tag{3.11.1.1}$$

where

$$\Delta T_1(z,t_1,t_2)=T_1(z,t_1)-T_2(z,t_2)$$

3.11.1.2 Pseudo compressibility when $T(z,t)=T_2(z,t_2)$

From the differentiation of the Tait equation by pressure, we obtain the pseudo compressibility when the temperature is $T_2(z,t_2)$

$$\kappa'(z,t_2)=\begin{cases} -\left(a_{0m}+a_{1m}\cdot\left(T_2(z,t_2)-T_{g1}(t_1)\right)\cdot 0.0894\cdot\dfrac{e^{B_{1m}\cdot T_2(z,t_2)}}{B_{0m}+P_1\cdot e^{B_{1m}\cdot T_2(z,t_2)}}\right) & T\le T_{g1}(t_1) \\ -\left(a_{0s}+a_{1s}\cdot\left(T_2(z,t_2)-T_{g1}(t_1)\right)\cdot 0.0894\cdot\dfrac{e^{B_{1s}\cdot T_2(z,t_2)}}{B_{0s}+P_1\cdot e^{B_{1s}\cdot T_2(z,t_2)}}\right) & T>T_{g1}(t_1) \end{cases} \tag{3.11.1.2}$$

where the pressure-dependence of the glass transition temperature must be accounted for, as given by Menges[29].

$$T_{g1}(t_1)=T_g+s\cdot P_1(t_1)$$

3.11.1.3 Calculation of the pressure distributions

The volumetric changes throughout the bar are added in a short time interval and the result used to calculate the corresponding drop in pressure.

Using Eq. 3.11.1.1 and Eq. 3.11.1.2, the average pressure drop from t_1 to t_2 within the

half of the bar is given by:

$$\Delta P_1(z,t) = \frac{2}{e}\int_0^{e/2} \frac{\Delta V_1(z,t_1,t_2)}{\kappa'(z,t_2)} \cdot dz \qquad (3.11.1.3)$$

This is used to calculate the new average pressure at the end of the time interval, i.e. at $t=t_2$, i.e. the new pressure is $P_2(t_2)=P_1(t_1)+\Delta P_1(z,t)$.

Note 3.11.1: The new value of pressure, P_2, is inserted into Eq. 3.11.1.1 and 3.11.1.2 and the calculations are repeated for the next time interval (t_2 to t_3). The calculation is repeated until the bar reaches the required state, e.g. when the pressure has dropped to zero. At this condition the moulding shrinks away from the mould cavity walls and a new calculation procedure is required.

3.11.2 Calculations of the pressure induced stress at $T(z,t)=T_g(t)$

The stress present at z when the temperature falls to $T_g(t)$ is assumed to remain unchanged. There will, of course, be changes due to differential thermal contraction because of the changing temperature distribution. The material at different locations (z) solidifies at different pressures and may show different properties (e.g. density, heat content and so on) as a consequence of this.

3.11.2.1 Rate of change of specific volume at $T=T_g(t)$

From the differentiation of the Tait equation for $T \le T_g$ by pressure, we obtain the rate of change of specific volume at $T=T_g(t)$ at all locations z.

$$\left(\frac{dV}{dP}\right)_{T_g} = -0.0894 \cdot \left(a_{0m} + a_{1m}(T(t) - T_g(t)\right) \cdot \frac{e^{B_{1m} \cdot T(t)}}{B_{0s} + P(t) \cdot e^{-B_{1m} \cdot T(t)}} \qquad (3.11.2.1)$$

where

$$T_g(t) = T_g + s \cdot P(t)$$

Note: The pressure dependent glass transition temperature $T_g(P(t))$ is a function of the pressure, P. It is given in the form $T_g(t)$ because the glass transition temperature is uniquely defined by t for a given location, z.

3.11.2.2 Density at $T=T_g(t)$

From the Tait equation, the density at $T=T_g(t)$ at different cooling times is given by:

$$\rho(z,T_g(t)) = \left[\left(a_{0s} + a_{1s} \cdot \left(T(t) - T_g(t)\right)\right) \cdot \left(1 - 0.0894 \cdot \ln\left(1 + \frac{P(t)}{B_{0s} \cdot e^{-B_{1s} \cdot T(t)}}\right)\right)\right]^{-1} \quad (3.11.2.2)$$

3.11.2.3 Pressure induced stresses at $T=T_g(t)$

Using Eq. 4.11.2.1 and Eq. 4.11.2.2, the pressure induced strain is given by:

$$\varepsilon_1(z,T_g(t)) = \frac{1}{3}\left(\left(\frac{dV}{dP}\right)_T \cdot \rho(z,T_g(t)) \cdot P(t)\right) \quad (3.11.2.3)$$

and the pressure induced stress is

$$\sigma_1(z,t) = \varepsilon_1(z,T_g(t)) \cdot E(z,t) \quad (3.11.2.4)$$

where

$E(z,t)$: time and temperature dependent Young's modulus (Eq. 3.5.1.7 in Section 3.5).

3.11.3 Pressure induced stresses for $T<T_g$

When the temperature has fallen to below T_g at all locations, a new calculation

procedure is required.

3.11.3.1 Density distributions for $T<T_g$

From the Tait equations, density for $T<T_g$ is

$$\rho(z,t)=\left\{\left[a_{0s}+a_{1s}\cdot\left(T(t)-T_g(t)\right)\right]\cdot\left[1-0.0894\cdot\ln\left(1+\frac{P(t)}{B_{0s}\cdot e^{-B_{1s}\cdot T(t)}}\right)\right]\right\}^{-1} \qquad (3.11.3.1)$$

3.11.3.2 Volumetric shrinkage at $T<T_g$

$$\varepsilon_2(z,t)=\frac{1}{3}\Delta V=\frac{1}{3}\left(\frac{\rho_n(P=0,z)-\rho_{n+1}(t_{(n-1)},P_n,z)}{\rho(t_{(n-1)},P_n,z)}\right) \qquad (3.11.3.2)$$

where

$\rho_n(t_n,P=0,z)$ is the density when the pressure is atmospheric

$\rho_{n+1}(t_{(n-1)},P_n,z)$ is the density when the temperature has fallen to below T_g at all locations.

And the pressure induced stresses for $T<T_g$ can be written

$$\sigma_2(z,t)=\varepsilon_2(z,t)\cdot E(z,t) \qquad (3.11.3.3)$$

3.11.4 Temperature induced stresses

3.11.4.1 Temperature induced stresses when the temperature reaches T_g at the centre

Temperature induced stresses when the temperature has fallen to below T_g at all locations are given by:

$$\sigma_3(z,t) = \left(T_{melt} - T(T_g(t))\right) \cdot \alpha(z,t) \cdot E(z,t) \qquad (3.11.4.1)$$

where

T_{melt} is the melt temperature.

$T(T_g(t))$ is the temperature distribution when the temperature has fallen to below T_g at all locations.

$\alpha(z,t)$ is calculated by Eq. 3.6.4 and Eq. 3.6.5.

3.11.4.2 Temperature induced stresses for $T(z,t) \leq T_g$

Temperature induced stresses when the temperature has fallen to below T_g at all locations is written by:

$$\sigma_4(z,t) = \left(T(T_g(t)) - T_n(z,t_n)\right) \cdot \alpha(z,t) \cdot E(z,t) \qquad (3.11.4.2)$$

where

$T_n(z,t_n)$ is the temperature distribution when the pressure is atmospheric(see Fig. 3.11.4)

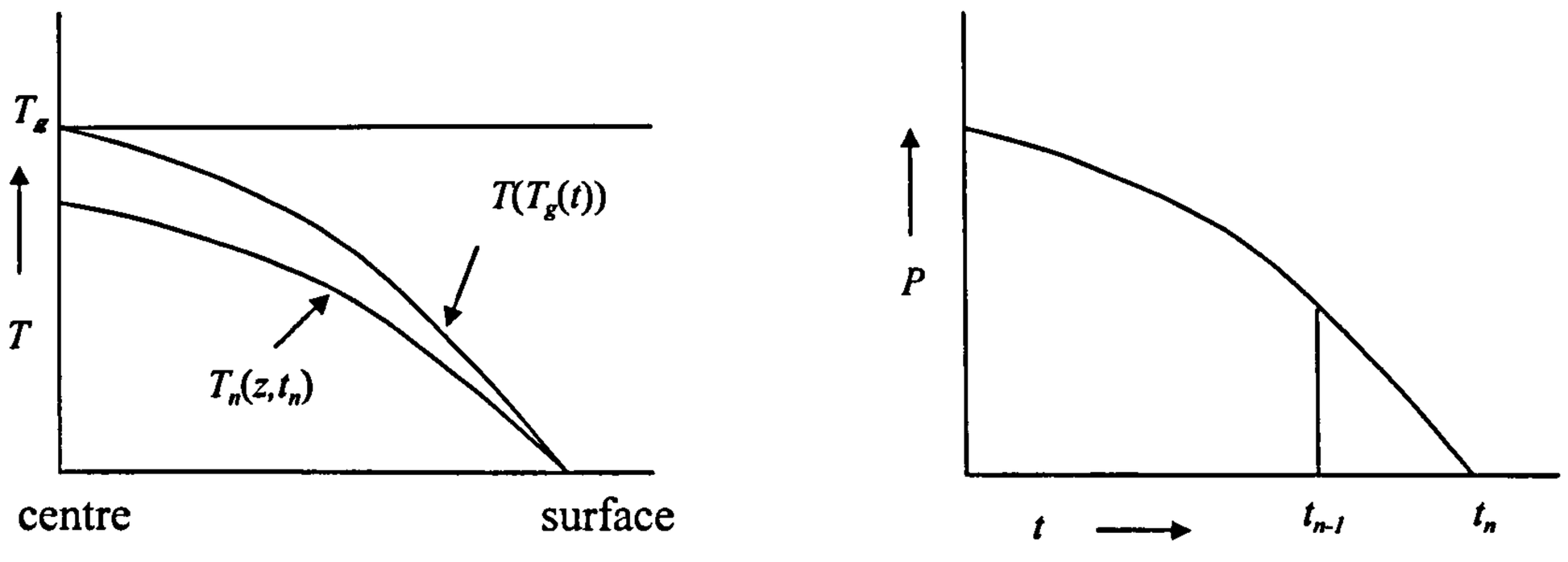

Fig. 3.11.4

t_{n-1} is the time when the temperature distribution is $T(T_g(t))$

3.11.4.3 Distributions of the stress throughout the moulding

The final result of the stress distributions is obtained using Eqs. 3.11.2.4, 3.11.3.3, 3.11.4.1 and 3.11.4.2. As the moulding shrinks away from the mould cavity walls when the pressure has dropped to zero, the integration of tensile stress and compressive stress over z is zero.

$$\sigma(z,t) = \sigma_{tot}(z,t) - \frac{1}{e}\int_0^e \sigma_{tot}(z,t) \qquad (3.11.4.3)$$

where

$$\sigma_{tot}(z,t) = \sigma_1(z,t) + \sigma_2(z,t) + \sigma_3(z,t) + \sigma_4(z,t) \qquad (3.11.4.4)$$

CHAPTER 4

RESULTS OF CALCULATIONS

This chapter deals with residual stresses calculations performed using Mathcad (mathematical software for general purpose). Section 4.1 gives the geometry used for the calculations. Sections 4.2 provide the materials data and the parameters for the calculations. Section 4.3 gives the calculations of the residual stress using method A (procedure based on Struik's method). Section 4.4 describes the new procedure method B (taking account of the pressure profile) developed during this research, in which the pressure profile was calculated and used to estimate density distributions through the depth and finally, the stress distribution. Section 4.5 gives the result of the calculations of stress relaxation after demoulding. Sections 4.6 deals with computed residual stress distributions for different boundary conditions using both method A and method B.

4.1 Geometry

The geometry is shown in Fig. 4.1 The polymer is bounded by mould surfaces at $z=\pm 1.6$ mm.

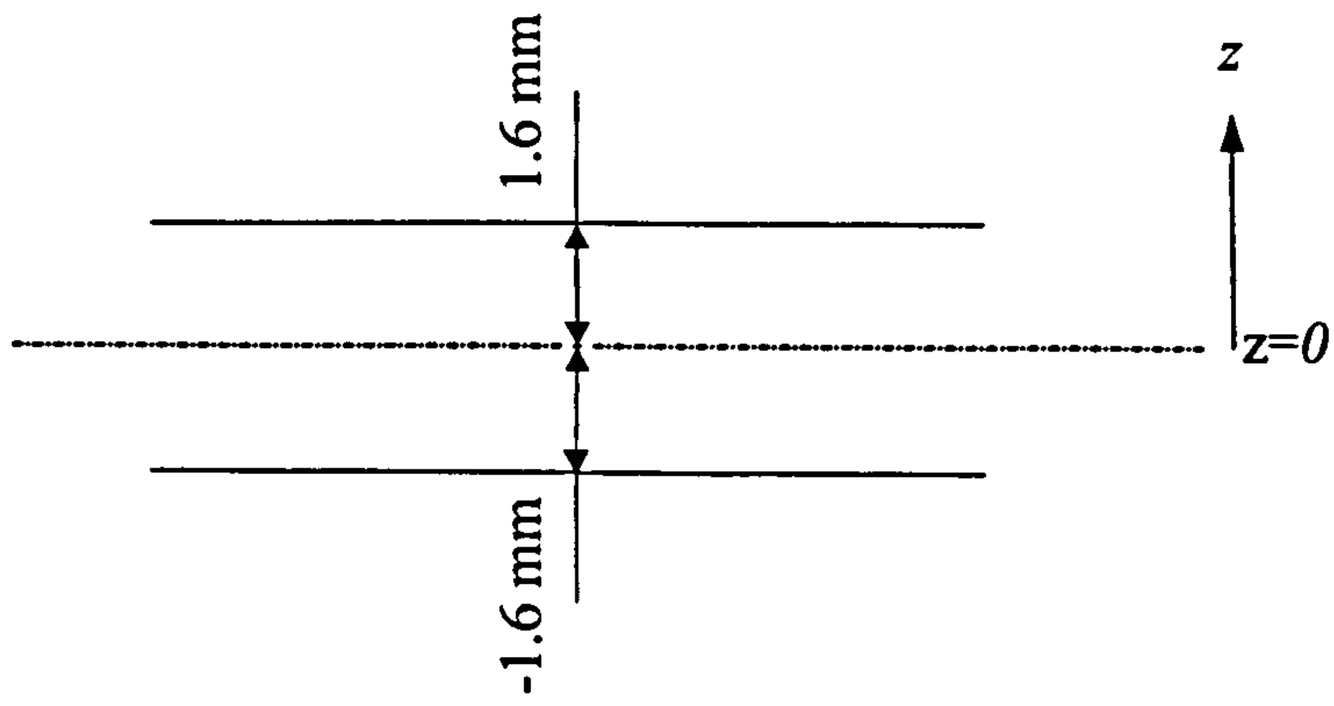

Fig. 4.1 The geometry of the melt

4.2 Material data

Table 4.2.1 shows the material properties of Dow chemical DE409 GPPS Styron 634.

These data and resin are kindly sent by Dow chemical.

Properties	constants	Note
Glass transition temperature at 0 MPa	T_g=373 (K)	
Thermal diffusivity for rubbery state	κ=7.259·10^{-8} (m^2·s^{-1})	Note 4.2.1
Thermal diffusivity for glassy state	κ=8.59·10^{-8} (m^2·s^{-1})	
Young's modules at 293 K°	E_0=3.4·10^9 (Pa)	
Poisson ratio for rubbery state	ν_r=0.5	Literature data
Poisson ratio for glassy state	ν_g=0.35	Literature data
Coefficients in the WLF equation	C_1=40	Literature data
	C_2=52 (K)	
Power index in the KWW equation	m=1/3	
Coefficients in Tait equations	a_{0s} = 9.72·10^{-4} (m^3·kg^{-1})	Note 4.2.2
	a_{0m} = 9.72·10^{-4} (m^3·kg^{-1})	
	a_{1s} = 2.42·10^{-7} (m^3·kg^{-1}·K^{-1})	
	a_{1m} = 6.25·10^{-7} (m^3·kg^{-1}·K^{-1})	
	b_{0s} = 100(Pa)	
	b_{0m} = 100 (Pa)	
	b_{1s} =10^{-3} (K^{-1})	
	b_{1m} =10^{-3} (K^{-1})	
	s=5.1·10^{-8} (K·Pa^{-1})	

Table 4.2.1 material properties of Dow chemical DE409 GPPS Styron 634

Note 4.2.1

Thermal diffusivity is calculated using $\kappa = \frac{\lambda}{\rho \cdot C_p}$

where

Thermal conductivity: λ=0.138 (W·m^{-1}·K^{-1})

Specific heat: C_p=1811 (J·kg^{-1}·K^{-1})

Density: $\rho \cong 887$ (kg·m^{-3}) ($T>T_g$)

$\rho \cong 1049$ (kg·m^{-3}) ($T \leq T_g$)

Therefore,

$\kappa \cong 7.259 \cdot 10^{-8}$ (m^2·s^{-1}) ($T>T_g$)

$\kappa \cong 8.59 \cdot 10^{-8}$ (m^2·s^{-1}) ($T \leq T_g$)

Note 4.2.2:

These constants are calculated from the PVT diagram of Dow chemical DE409 GPPS Styron 634 by comparing the measured data with the appropriate Tait equations (Section 3.6).

4.3 Result of the calculations using method A (based on Struik's method)

This section deals with stresses calculations performed using method A (based on Struik's method). Fig 4.3 (p. 105) shows the block diagram of the procedure based on Struik's method. Struik's method is based on Aggarwala and Saibel's thermo-elastic model[75]. Struik modified their model, considering viscoelasticity (time effects in the elastic behaviour of mechanical properties) and volume relaxation by following Lee's viscoelastic treatment[53]. Struik introduced the local cooling rate $q = -\frac{\partial T}{\partial t}$ in the time-dependent Young's moduli and calculated an incremental stress caused by cooling over the interval between T and T-δ. Significant modifications were made to his method and used to calculate stages ⑧, ⑨, ⑪, ⑭ and ⑯ in Fig 4.3.

Numerical calculation methods are applied to each calculation stage.

4.3.1 Process controls

The process parameters used for the calculation are shown in Table 4.3.1 and Fig. 4.3.1.

		Note
Melt temperature	433 (K)	Note 4.3.1
Mould temperature	308 (K)	
Cooling time in the mould (s)	t_c=5,10,15,20 (s)	
Packing pressure	P_0=170 (MPa)	
Atmospheric pressure	P_1=0 (MPa)	
Relaxation time at T_g (s)	$t_0(T_g)$=1.0 (sec)	
Thickness increment	z=2.0·10^{-4} (m)	Note 4.3.2

Table 4.3.1 process parameters used for the calculation

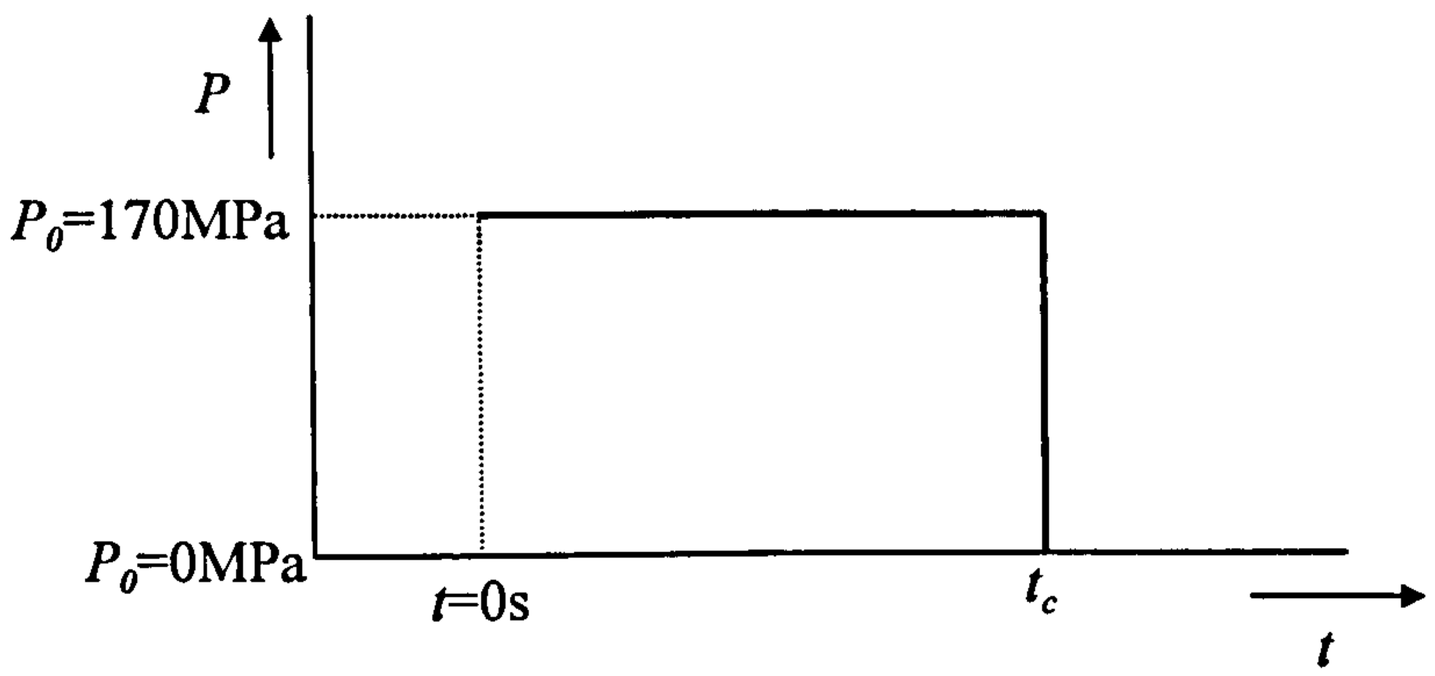

Fig. 4.3.1 Simple representation of the pressure history

Note 4.3.1:

The parameters in Table 4.3.1 correspond to the moulding conditions in the experiments.

Note 4.3.2:

The calculation points for Mathcad are defined using this control.

i.e. z=0,0.2... $1.6 \cdot 10^{-4}$ (m)

4.3.2 Temperature distributions

As explained in Section 3.4, Eq. 3.4.18 is evaluated using one, two and three terms respectively and compared in Fig. 3.7.1 (p. 62). The graphs are virtually indistinguishable and therefore a good approximation to the series can be represented by the first term only. This is of significant value as it can be used to reduce the run time in Mathcad.

This approximation is examined here again in Fig. 4.3.2 (p. 106). This graph shows that the approximation does not affect the temperature distribution when the cooling time is more than 5 seconds. However, when the cooling time is less than 3 seconds, the approximation affects the temperature distribution dramatically. Therefore,

consideration should be made when calculations are made for short cooling time, using reduced parameters[69-72, 159] and so on.

$$T(z,t)=\frac{4}{\pi}\sum_{i=0}^{\infty}\frac{(-1)^i}{2i+1}\cos\left((2i+1)\frac{\pi}{e}z\right)\exp\left[-k\left(\frac{(2i+1)\pi}{e}\right)^2 t\right](T_{ml}-T_{mo})+T_{mo} \qquad (3.4.18)$$

On the other hand, the approximation is still effective practically for the moulding conditions shown in Table 4.3.1. Therefore, Eq. 4.3.2.1 is used for this temperature distribution calculation.

$$T(z,t)=\frac{4}{\pi}\cdot\cos\left(\frac{\pi}{e}\cdot z\right)\cdot\exp\left[-k\cdot\left(\frac{\pi}{e}\right)^2\cdot t\right]\cdot(T_{ml}-T_{mo})+T_{mo} \qquad (4.3.2.1)$$

4.3.3 Distributions of the Young's modulus

There are many ways to represent temperature and time dependence of Young's modulus. Some are empirical; others have a physical origin (e.g. the WLF equation is theoretically derived from the standpoint of the free volume theory). Some of the empirical expressions are presented by Van Krevelen and Hoftyzer (Eq. 3.5.2.1 and 3.5.2.2). The WLF equation and the KWW equation are given below. These equations are compared in Fig. 4.3.3 (p. 107). The graphs represent the temperature and time dependent Young's modulus quite well and eventually both the distributions of the Young's modulus are tolerably similar. The effect of using different equations on the computed residual stress distributions is examined later.

$$E(z,t)=\frac{\frac{T_g}{T_r}+2}{\left(\frac{T_g}{T_r}+\frac{2T(z,t)}{T_r}\right)}\cdot E_0 \qquad (T\le T_g) \qquad (3.5.2.1)$$

$$E(z,t) = \frac{E_0}{\exp 2.65\left(\dfrac{\dfrac{T_g}{T_r} + \dfrac{T_g}{T(z,t)}}{\left(\dfrac{T_g}{T_r} - 1\right)}\right)} \qquad (T > T_g) \tag{3.5.2.2}$$

where T_r is the reference temperature when $E(z,t)=E_0$

$$E(z,t) = E_0 \cdot \exp\left[-\left(\frac{t}{t_0(T_g)} \cdot \exp\left(\frac{C_1 \cdot (S(z,t) - T_g)}{C_2 + (S(z,t) - T_g)}\right)\right)^m\right] \tag{3.5.1.7}$$

where $S(z,t)$ represents a modified temperature field. Since the WLF equation (Eq. 3.5.1.7) is only valid for a limited temperature range around the glass transition temperature we have

e.g. $\lim_{T \to 321^-} \exp\left(\dfrac{40 \cdot (T - T_g)}{52 + (T - T_g)}\right) = \infty$, $\lim_{T \to 321^+} \exp\left(\dfrac{40 \cdot (T - T_g)}{52 + (T - T_g)}\right) = 0$ and the table below:

Temperature (K)	314	323	330	340	350	360	370
$\exp\left(\dfrac{C_1 \cdot (T - T_g)}{C_2 + (T - T_g)}\right)$	$2.63 \cdot 10^{146} \cong \infty$	0	0	0	$1.67 \cdot 10^{-14}$	$1.62 \cdot 10^{-6}$	0.086

An approximate limited drop of amplitude 23 degrees below T_g (350K) has been chosen according to the table above. As can be seen from the table $\exp\left(\dfrac{C_1 \cdot (T - T_g)}{C_2 + (T - T_g)}\right)$ is very low and therefore $E(z,t)$ is vanishingly small for T<350K and this modified temperature field is used to save computing time with no loss of accuracy in results.

$$S(z,t) = \begin{matrix} 350 & (\mathrm{T(z,t)} < 350) \\ \mathrm{T(z,t)} & (\mathrm{T(z,t)} \geq 350) \end{matrix}$$

4.3.4 Distributions of the Poisson ratio

Poisson ratio as an affine function defined by[4]:

Poisson ratio below 343K

$$\nu(z,t)=\nu_l=0.35 \qquad (4.3.4.1)$$

Poisson ratio, linear function of the temperature above 343 (K) and below 403 (K)

$$\nu_2(z,t)=\left(\frac{\nu_r-\nu_g}{60}\cdot(T(z,t)-T_g+30)+\nu_g\right) \qquad (4.3.4.2)$$

Poisson ratio above 403K

$$\nu_3(z,t)=0.5 \qquad (4.3.4.3)$$

This result is shown in Fig. 4.3.4 (p. 108).

4.3.5 Distributions of the linear thermal expansions coefficient

Calculations of the linear thermal coefficient were made using Eq. 3.6.4 and Eq. 3.6.5 in Section 3.6. The constants a_{1s}, a_{0s}, a_{1s} and a_{1m}, a_{0m}, a_{1m} are calculated from a PVT diagram of Dow chemical DE409 GPPS Styron 634.

$$\alpha(z,t)=\frac{a_{1s}}{3\cdot\left(a_{0s}+a_{1s}\left(T(z,t)-T_g\right)\right)} \qquad (T\le T_g) \qquad (3.6.4)$$

$$\alpha(z,t)=\frac{a_{1m}}{3\cdot\left(a_{0m}+a_{1m}\left(T(z,t)-T_g\right)\right)} \qquad (T\ge T_g) \qquad (3.6.5)$$

Fig. 4.3.5 (p. 108) shows the distribution of the linear thermal expansion coefficient. After a cooling time of 10 seconds, only Eq. 3.6.4 is required for the distribution of the linear thermal expansion coefficient.

A linear thermal expansion coefficient calculated using Eq. 3.6.4 and Eq. 3.6.5 at 293K

is compared with that of DE409 GPPS Styron 634 from Dow chemical. Consequently, they are in good agreement. ($8.43 \cdot 10^{-5}$ and $8.35 \cdot 10^{-5} K^{-1}$).

4.3.6 Calculation of the T_g-plane positions according to the cooling time

As discussed in Section 3.7, T_g-plane positions at different cooling times are calculated using Eq. 3.7.5. Fig. 4.3.6 (p. 109) shows the positions of the T_g-plane at different cooling times. After a cooling time of 10 seconds, the T_g plane no longer exists within the bar: the temperature has fallen to below T_g at all locations.

$$H(t) = \frac{e}{\pi} \cdot \arccos\left(\frac{\pi}{4}\left(\frac{T_{ml} - T_{mo}}{T_g - T_{mo}}\right) \cdot \exp\left\{\kappa\left(\frac{\pi}{e}\right)^2 t\right\}\right) \qquad (3.7.5)$$

Note: Eq. 3.7.5 is derived from Eq. 3.7.1 (the first term only). Therefore, consideration should be made again (the same reason as in Section 4.3.2) when calculations are made for short cooling time, using reduced parameters [69-72, 159] and so on.

4.3.7 Calculations of the stress distributions

From Section 4.1 to Section 4.3.6, knowing the temperature field and the materials data, four series of stress calculations are made in this section. Section 4.3.7.1 gives stress calculations when the bar surfaces are fixed to the mould cavity surfaces and also examines the effect of the changes in Young's modulus described by the two different models (combination of the WLF and the KWW equations; and the Van Krevelen-Hoftyzer equations). Sections 4.3.7.2 and 4.3.7.3 deals with stress calculations when the packing pressure effect is taken into account. Section 4.3.7.4 gives residual stress distributions when the bar is not constrained by adhesion to the mould cavity walls.

4.3.7.1 Calculations of stress distributions when the bar surfaces are constrained by the mould cavity walls and the effect of the Young's modulus

As described by Eq. 3.8.20 (Section 3.8), average strain rate distributions are calculated for different cooling times (5 s, 10 s, 15 s and 20 s). In the fully constrained state, the strain in the sample when the temperature changes is zero if referred to the initial dimensions. If, instead, strain is referred to the dimensions which the moulding would have if removed from the cavity and freed from all surface tractions but with the temperature distribution at time t (within the cavity) the changes in strain can be expressed by

$$\dot{\varepsilon}_{xx}(z,t)=\frac{\int_{H(t)}^{\frac{e}{2}}R(z,t)\alpha(z,t)\dot{T}(z,t)dz}{\int_{H(t)}^{\frac{e}{2}}R(z,t)dz} \qquad (3.8.20)$$

where $H(t)$ is the position of the glass transition plane. As discussed in Section 4.3.6, the T_g plane disappears after 10 seconds since the centre of the bar has fallen to below T_g by this time. Therefore, the value for $H(t)$ is always 0 for the each cooling time after 10 seconds.

$R(z,t)$ is calculated using $R(z,t)=\frac{E(z,t)}{1-\nu}$.

$\dot{T}(z,t)$ is the cooling rate calculated using the following equation:

$$\dot{T}(z,t)=\frac{d}{dt}\left(\frac{4}{\pi}\cdot\cos\left(\frac{\pi}{e}\cdot z\right)\cdot\exp\left[-k\cdot\left(\frac{\pi}{e}\right)^2\cdot t\right]\cdot(T_{ml}-T_{mo})+T_{mo}\right) \qquad (4.3.7.1)$$

Mathcad directly solves the equation above (Eq. 4.3.7.1) and of course this result is exactly the same as for the following equation:

$$\dot{T}(z,t)=-4\cdot\pi\cdot\cos\left(\frac{\pi}{e}\cdot z\right)\cdot\exp\left(-k\cdot\left(\frac{\pi}{e}\right)^2\cdot t\right)\cdot\frac{k}{e^2}\cdot(T_{ml}-T_{mo}) \qquad (4.3.7.2)$$

When the cooling times are greater than 5 seconds, the average strain rates are shown in Table 4.3.2 and Fig. 4.3.7 (p. 109) Table 4.3.2 and Fig 4.3.7 show that the average strain rate decreases as the cooling time increases before 10 seconds and the average strain increases as the cooling time decreases after 10 seconds. Both effects are mainly due to the distributions of the linear thermal expansion coefficients (Fig. 4.3.5). The average strain rate is less significant than the local strain rate calculated using $\alpha(z,t)\dot{T}(z,t)$ (approximately 1/10 of $\alpha(z,t)\dot{T}(z,t)$).

Time (s)	Strain rate (s^{-1}) (KLV)	Strain rate (s^{-1}) (WLF)
5	$-2.75\cdot10^{-4}$	$-2.62\cdot10^{-4}$
10	$-3.13\cdot10^{-4}$	$-3.01\cdot10^{-4}$
15	$-1.92\cdot10^{-4}$	$-1.94\cdot10^{-4}$
20	$-1.19\cdot10^{-4}$	$-1.20\cdot10^{-4}$

Table 4.3.2 Distributions of the strain rate

The stress rate distributions calculated using Eq. 3.8.21 are shown in Fig. 4.3.8 (p. 110) and Fig. 4.3.9 (p. 110). As the result, when the temperature is below T_g, the stress rate distributions between using the WLF-KWW equations and the Van Krevelen-Hoftyzer equations is obviously different. However, they are quite similar after a cooling time of 15 seconds.

$$\dot{\sigma}_{xx}(z,t) = R(z,t)\left\{\dot{\varepsilon}_{xx}(z,t) - \alpha(z,t)\dot{T}(z,t)\right\} \qquad (3.8.21)$$

The stress distributions are calculated using Eq. 3.8.22 (in Section 3.8) below and the results are shown in Fig. 4.3.10 (p. 111) and Fig. 4.3.11 (p. 111). The graphs are quite similar for each cooling time.

$$\sigma(z,t) = \int_{t_g}^{t} \dot{\sigma}(z,t)dt \qquad (3.8.22)$$

Note 4.3.7.1: when the calculation is made using the Van Krevelen-Hoftyzer equations,

t_g=0 is assumed in Eq. 3.8.22.

4.3.7.2 The calculation of the packing pressure induced stress (Using the combination of the WLF and the KWW equations)

The result of the packing pressure induced stress (Using the combination of the WLF and the KWW equations is shown in Fig. 4.3.12 (p. 112).

The specific volume of the polystyrene is $9.70 \cdot 10^{-4}$ (m^3/kg) at P_0=170 (MPa) and T=433 (K) at all points within the sample because immediately after the molten polymer has been injected into the mould, the temperature distribution and packing pressure distribution are homogeneous.

The specific volume distribution is calculated at P_1=0 (MPa), $T=T(z,t)$ (the temperature distributions calculated in Section 4.3.2 are shown in Fig. 4.3.2) and cooling time=20 seconds (because only when the cooling time is 20 seconds, the pressure is assumed to be 0 (MPa)).

Note 4.3.7.2:

The cooling time 20 seconds is used to correspond with the moulding conditions in the experiments.

$$\sigma_{press} = \frac{1}{3}\ln\left(\frac{V(P_1,T)}{V(P_0,T)}\right)\cdot E_0 \qquad (3.9.2)$$

where

$$V(P_0,T) = (a_{0s} + a_{1s}(T - T_g))\left(1 - 0.0894 \cdot \ln\left(1 + \frac{P_0}{B_s}\right)\right) \qquad (T \le T_g) \qquad (3.9.3)$$

$$V(P_0,T) = (a_{0m} + a_{1m}(T - T_g))\left(1 - 0.0894 \cdot \ln\left(1 + \frac{P_0}{B_m}\right)\right) \qquad (T > T_g) \qquad (3.9.4)$$

$$V(P_1,T) = (a_{0s} + a_{1s}(T - T_g))\left(1 - 0.0894 \cdot \ln\left(1 + \frac{P_1}{B_s}\right)\right) \qquad (T \le T_g) \qquad (3.9.5)$$

$$V(P_1,T) = (a_{0m} + a_{1m}(T - T_g))\left(1 - 0.0894 \cdot \ln\left(1 + \frac{P_1}{B_m}\right)\right) \qquad (T > T_g) \qquad (3.9.6)$$

$$b_m = b_{0m} \cdot e^{-b_{1m} \cdot T} \qquad (3.9.7)$$

4.3.7.3 Residual stress distributions considering packing pressure

Equations Eq. 3.8.22 (Section 3.8), Eq. 3.9.2 (Section 3.9) and Eq. 4.3.7.2 are added to give the final stress distribution. This is shown in Fig. 4.3.13 (p. 113).

$$\sigma_{tot}(z,t) = \sigma(z,t) + \sigma_{press}(z,t) \qquad (4.3.7.3)$$

4.3.7.4 Stress distributions after demoulding

When the bar is ejected from the mould, the bar is free from frictional constraint. Therefore, the integration of tensile stress and compressive stress over z is zero.

The stress distribution in the case for which the moulding is not restrained by the mould is calculated using Eq. 4.3.7.4.

The result is shown in Fig. 4.3.14 (p. 113)

$$\sigma_{free} = \sigma_{tot}(z,t) - \frac{1}{e}\int_0^e \sigma_{tot}(z,t)dz \qquad (4.3.7.4)$$

4.4 Result of the calculations using method B (taking account of the pressure profile)

This section deals with stresses calculations performed using the Method B (taking account of the pressure profile). Fig 4.4 (p. 114) shows the block diagram of the new

procedure developed during this research, in which the pressure profile was calculated and used to estimate density distributions through the depth and, here, the stress distribution. This method starts by calculating the pressure profile and is based on the specific volume rate from the differentiation of the Tait equations by pressure. The strain as a function of pressure is calculated using the specific volume and the density. This method was used to calculate stages ②-⑨ in Fig. 4.4.

Section 4.4.1 gives the process controls used for the calculations. Section 4.4.2 provides the calculation of the pressure history. Section 4.4.3 offers the calculations of the pressure induced stress at $T(z,t)=T_g(t)$. Section 4.4.4 gives the pressure induced stress for $T<T_g$. Section 4.4.5 describes temperature induced stress. Section 4.4.6 gives the distributions of the stress through out the moulding.

4.4.1 Process controls

The parameters used for the calculation are shown Table 4.4.1

		Note
Melt temperature	433 (K)	
Mould temperature	308 (K)	
Cooling time $T>T_g$	$t(T>T_g)$=10 (s)	Note 4.4.1
Cooling time $T<T_g$	$t(T>T_g)$=1 (s)	
Packing pressure	P_0=170 (MPa)	
Atmospheric pressure	P_n=0 (MPa)	Note 4.4.2
Relaxation time at T_g (s)	$t_0(T_g)$=1.0 (sec)	

Table 4.4.1Process controls

Note 4.4.1: The total cooling time is 11 seconds.

Note 4.4.2: When the pressure reaches 0 (MPa), the cooling time is 11 seconds. This cooling time is calculated implicitly by the pressure. This calculation will be explained in the next section.

4.4.2 Calculation of the pressure history

The pressure drop is calculated as functions of both temperature and volume in this section.

4.4.2.1 Temperature distributions

As explained in Section 3.4, Eq. 3.4.18 is used to this calculation because the truncated sum does not give a good approximation when the cooling time is less then one second as is required for these calculations.

$$T(z,t)=\frac{4}{\pi}\sum_{i=0}^{\infty}\frac{(-1)^i}{2i+1}\cos\left((2i+1)\frac{\pi}{e}z\right)\exp\left[-k\left(\frac{(2i+1)\pi}{e}\right)^2 t\right](T_{ml}-T_{mo})+T_{mo} \qquad (3.4.18)$$

Also the temperature distribution calculated by Eq. 3.4.18 is compared with the result of FDM (finite difference method) in Fig. 4.4.1 (p. 115). As the result, the graphs are tolerably similar.

4.4.2.2 Distributions of the volumetric change when $T(z,t)$ drops $T(z,t)$ to T_g

Calculations of the volumetric change was made using Eq. 3.11.1.1 in Section 3.11.1.

$$\Delta V(z,t_1,t_2)=\begin{cases}a_{1s}\cdot\Delta T(z,t_1,t_2) & (T\le T_g)\\ a_{1m}\cdot\Delta T(z,t_1,t_2) & (T>T_g)\end{cases} \qquad (3.11.1.1)$$

4.4.2.3 Pseudo compressibility at $T(z,t)=T_2(z,t_2)$

Calculation of the bulk modulus was made using Eq. 3.11.1.2 in Section 3.11.1.2.

$$\kappa'(z,t_2)=\begin{cases}-\left(a_{0m}+a_{1m}\cdot\left(T_2(z,t_2)-T_{gl}(t_1)\right)\cdot 0.0894\cdot\dfrac{e^{B_{1m}\cdot T_2(z,t_2)}}{B_{0m}+P_1\cdot e^{B_{1m}\cdot T_2(z,t_2)}}\right) & T\le T_{gl}(t_1)\\ -\left(a_{0s}+a_{1s}\cdot\left(T_2(z,t_2)-T_{gl}(t_1)\right)\cdot 0.0894\cdot\dfrac{e^{B_{1s}\cdot T_2(z,t_2)}}{B_{0s}+P_1\cdot e^{B_{1s}\cdot T_2(z,t_2)}}\right) & T>T_{gl}(t_1)\end{cases} \qquad (3.11.1.2)$$

where

$$T_{g1}(t_1) = T_g + s \cdot P_1(t_1)$$

4.4.2.4 Calculation of the pressure history

As explained in Section 3.11.1.3, Eq. 3.11.1.3 was used to calculate the pressure history.

$$\Delta P_1(z,t) = \frac{2}{e}\int_0^{e/2} \frac{\Delta V_1(z,t_1,t_2)}{\kappa'(z,t_2)} \cdot dz \qquad (3.11.1.3)$$

The result is shown in Fig. 4.4.2 (p. 116)

4.4.3 Calculations of the pressure induced stress at $T(z,t)=T_g(t)$

In order to calculate the rate of change of specific volume: $\left(\frac{dV}{dP}\right)_{T_g}$ at $T=T_g(t)$ and the density at $T=T_g(t)$, the following Table (Table 4.4.2) is used to determine the relation among the cooling time T_g layer position and the pressure.

Cooling time (s)	0	1	4	6	7	8	9	10
Position of the T_g layer from the centre point (mm)	1.6	1.125	0.944	0.769	0.652	0.498	0.24	0
Pressure (MPa)	170	136	64.5	34.9	23.6	14.5	8.3	4.0

Table 4.4.2

4.4.3.1 Calculation of the specific volume rate

Calculation of the specific volume rate was made using Eq. 3.11.2.1 in Section 3.11.2.2

$$\left(\frac{dV}{dP}\right)_{T_g} = -0.0894 \cdot (a_{0m} + a_{1m}(T(t) - T_g(t)) \cdot \frac{e^{B_{1m} \cdot T(t)}}{B_{0m} + P(t) \cdot e^{-B_{1m} \cdot T(t)}} \qquad (3.11.2.1)$$

where

$$T_g(t) = T_g + s \cdot P(t)$$

The result is shown in Fig. 4.4.3 (p. 116).

Note 4.4.1: The pressure dependent glass transition temperature $T_g(P(t))$ is a function of the pressure, P. It is given in the form $T_g(t)$ because the glass transition temperature is uniquely defined by t for a given z.

4.4.3.2 Density at $T=T_g$

Calculation of the Density at $T=T_g$ was made using Eq. 3.11.2.2 in Section 3.11.2.2

$$\rho(z,T_g(t)) = a_{0s} \cdot \left(1 - 0.0894 \cdot \ln\left(1 + \frac{P(t)}{B_{0s} \cdot e^{-B_{1s} \cdot T_{g_n}}}\right)\right)^{-1} \qquad (3.11.2.2)$$

The result is shown in Fig. 4.4.4 (p. 117)

4.4.3.3 Pressure induced stress at $T=T_g$

As explained in Section 3.11.2.3, Eq. 3.11.2.3 and Eq. 3.11.2.4 were used to calculate the pressure history.

$$\varepsilon(z,T_g(t)) = \frac{1}{3}\left(\left(\frac{dV}{dP}\right)_T \cdot \rho(z,T_g(t)) \cdot P(t)\right) \qquad (3.11.2.3)$$

$$\sigma(z,T_g(t)) = \varepsilon(z,T_g(t)) \cdot E(z,t) \qquad (3.11.2.4)$$

The result is shown in Fig. 4.4.5 (p. 117).

4.4.4 Pressure induced stresses for $T<T_g$

4.4.4.1 Density distributions at $T<T_g$

As explained in Section 3.11.3, Eq. 3.11.3.1 was used to calculate the density

distribution.

$$\rho(z,t)=\left\{\left[a_{0s}+a_{1s}\cdot\left(T(t)-T_g(t)\right)\right]\cdot\left[1-0.0894\cdot\ln\left(1+\frac{P(t)}{B_{0s}\cdot e^{-B_{1s}\cdot T(t)}}\right)\right]\right\}^{-1} \quad (3.11.3.1)$$

4.4.4.2 Volumetric shrinkage at $T<T_g$ and the pressure drops from P to P=0

As explained in Section 3.11.3, Eq. 3.11.3.2 was used to calculate the volumetric shrinkage at $T<T_g$ and the pressure drops from P to P=0.

$$\varepsilon_2(z,t)=\frac{1}{3}\Delta V=\frac{1}{3}\left(\frac{\rho(t_n,P=0,z)-\rho(t_{(n-1)},P_n,z)}{\rho(t_{(n-1)},P_n,z)}\right) \quad (3.11.3.2)$$

The pressure induced stresses for $T<T_g$ is can be written

$$\sigma_2(z,t)=\varepsilon_2(z,t)\cdot E(z,t) \quad (3.11.3.3)$$

4.4.5 Temperature induced stresses

4.4.5.1 Temperature induced stresses when the temperature reaches T_g at the centre

As explained in Section 3.11.4, Eq. 3.11.4.1 was used to calculate the temperature induced stresses when the temperature reaches T_g at the centre.

$$\sigma_3(z,t)=\left(T_{melt}-T(z,t=t(T_g))\right)\alpha(z,t)\cdot E(z,t) \quad (3.11.4.1)$$

4.4.5.2 Temperature induced stresses for $T(z,t)\leq T_g$

As explained in Section 3.11.4, Eq. 3.11.4.2 was used to calculate the temperature induced stresses for $T(z,t)<T$.

$$\sigma_4(z,t)=\left(T(T_g(t))-T_n(z,t_n)\right)\cdot\alpha(z,t)\cdot E(z,t) \quad (3.11.4.2)$$

4.4.6 Distributions of the stress throughout the moulding

The result of the stress distribution through out the moulding is calculated using Eq. 3.11.4.3 in Section 3.11.4.3.

$$\sigma(z,t) = \sigma_{tot}(z,t) - \frac{1}{e}\int_0^e \sigma_{tot}(z,t) \qquad (3.11.4.3)$$

where

$$\sigma_{tot}(z,t) = \sigma_1(z,t) + \sigma_2(z,t) + \sigma_3(z,t) + \sigma_4(z,t) \qquad (3.11.4.4)$$

The result is shown in Fig. 4.4.6 (p. 118). The stress distributions are compared in Fig. 4.4.7 (p. 118) with the results obtained using Eq 4.3.7.4 in Section 4.3.7.4 and they are in good agreement.

4.5 Stress relaxation after demoulding

There are also many ways to represent stress relaxation after demoulding. Some are empirical; others are derived from theory (e.g. the WLF equation is theoretically derived from the standpoint of the free volume theory). In this section, the KWW equation is used to predict long term stress relaxation after the demoulding. The graph in Fig. 4.5.1.1 (p. 119) represents stress relaxation reasonably. The effect of using this equation on the residual stress distributions is examined with experimental data in Chapter 7.

4.5.1 Stress relaxation after demoulding

The stress relaxation after demoulding is calculated using Eq. 4.5.1. The result is shown in Fig. 4.5.1.1 (p. 119).

$$\sigma = \sigma_0 \cdot \exp(-\beta \cdot t^m) \qquad (4.5.1)$$

where

σ_0 is an initial stress

β is a constant with a value about 0.025

m is a constant with a value of 0.32

Note 4.5.1: These constants are calculated from the stress relaxation measurement of Dow chemical DE409 GPPS Styron 634 by comparing the measured data with the appropriate Eq. 4.5.1.

4.6 Computed residual stress distributions for different boundary conditions

This section deals with computations made using both method A and method B. Section 4.6.1 gives the residual stress results using method A. Section 4.6.2 shows the residual stress results using method B. Comparisons and discussions between the experimental results and both calculations are made in Chapter 7.

4.6.1 Results using method A (based on Struik's method)

The parameters used for the calculations are shown on Table 4.6.1.1. Calculations are divided into three groups in this section. Section 4.6.1.1 (K0172 and K018) calculates the effect on residual stresses of different cooling temperatures (room temperature and ice water) after de-moulding. Section 4.6.1.2 (K019 and K020) shows the effect on residual stresses of different cooling temperature (ice water and liquid nitrogen) after de-moulding. Section 4.6.1.3 (K013 and K0171) gives the difference in residual stresses obtained if the samples surfaces are friction-constrained or not constrained by the mould surfaces. Each calculation is made for a different elapsed time after demoulding obtained by measurement. These elapsed times correspond to the actual storage times

before measurement of residual stress by the layer removal analysis.

	K018	K0172	K019	K020	K013	K0171
Melt temperature (K)	443	443	488	488	443	443
Mould temperature (K)	315	315	313	313	315	315
In mould cooling time (s)	12	12	8	8	12	12
Packing pressure (MPa)	170	170	170	170	170	170
Coolant temperature (K)	293	275	77	275	275	275
Out mould relaxation time (hour)	650	216	3	168	650	650

Table 4.6.1.1 Process controls

4.6.1.1 Comparison of the effect of using different cooling temperatures, using tensile bars (K0172 and K018)

The comparison of the effect of using different cooling temperatures, using ice water and room temperature, is shown in Fig. 4.6.1.1. (p. 120) The labels in Fig 4.6.1.1 refer to the computed stress obtained using the temperature of ice water (K0172) and the stress obtained using room temperature (K018). The computed residual stress magnitude for the bars which were cooled in ice water was everywhere 1.03 times higher than the computed magnitude for bars cooled at room temperature.

4.6.1.2 Comparison of the effect of using different cooling temperatures, using tensile bars (K019 and K020)

The comparison of the effect of using different cooling temperatures, using ice water and liquid nitrogen, is shown in Fig. 4.6.1.2 (p. 120). The labels in Fig 4.6.1.2 refer to the computed stress obtained using temperature of liquid nitrogen (K019) and the computed stress obtained using the temperature of ice water (K020). The computed residual stress magnitude for the bars which were cooled in liquid nitrogen was 13.7 times higher than the computed magnitude cooled in ice water on average.

4.6.1.3 Comparison of effect of friction constraint, using straight bars (K013 and K0171)

The comparison of the effect of friction constraint for both the pressure and the temperature induced stresses in the mould are shown in Fig. 4.6.1.3 (p. 121) and Fig. 4.6.1.4 (p. 121).

It is assumed that when the pressure drops to atmospheric pressure, the friction becomes zero. This result is shown in Fig. 4.6.1.5 (p. 122). The labels in Fig 4.6.1.5 refer to the computed stress obtained without friction constraint (K013) and the computed stress obtained with friction constraint (K0171).

4.6.2 Results using method B (taking account of the pressure profile)

The parameters used for the calculations are shown on Table 4.6.2.1. Calculations are divided into three groups in this section. Section 4.6.2.1 (L006 and L007) calculates the effect of different cooling temperatures after de-moulding on residual stresses. Section 4.6.2.2 (L004 and L005) shows the difference in residual stresses when the samples surfaces are friction constrained or not fixed by the mould surfaces.

Section 4.6.2.3 (L002 and L003) gives the effect of different pressures on residual stress. Each calculation is conducted for a different time after demoulding taking into account relaxation. These times correspond to the actual storage times for samples on which layer removed analysis were made. (Section 5.3)

	L006	L007	L004	L005	L002	L003
Melt temperature (K)	488	488	443	443	503	513
Mould temperature (K)	313	313	315	315	313	313
In mould cooling time (s)	8	8	12	12	30	25
Packing pressure (MPa)	170	170	170	170	87	143
Coolant temperature (K)	77	275	275	275	287	287
Out mould relaxation time (hour)	3	168	650	216	168	168

Table 4.6.2.1 Process controls

4.6.2.1 Comparison of the effect of using different cooling temperatures, using tensile bars (L006 and L007)

This section considers the effect of cooling temperature using ice water and liquid nitrogen. The following components of the analysis are considered.

(1) Determination of the relationship between the cooling time, the T_g layer position and the pressure

In order to calculate the rate of change of specific volume: $\left(\frac{dV}{dP}\right)_{T_g}$ at $T=T_g(t)$ and the density at $T=T_g(t)$, the following Tables (Table 4.6.2.2 and Table 4.6.2.3) are used to determine the relation between the cooling time, the T_g layer position and the pressure.

Cooling time (s)	0	1.0	2.0	3.0	4.5	8.0	9.5	10.0	11.7
Position of the T_g layer (mm)	1.55	1.40	1.32	1.26	1.17	0.97	0.63	0.53	0
Pressure (MPa)	170.0	109.7	69.1	38.1	0	0	0	0	0

Table 4.6.2.2 (L006)

Cooling time (s)	0	1.0	2.0	3.0	4.5	8.0	9.5	10.0	14.2
Position of the T_g layer (mm)	1.55	1.4	1.32	1.26	1.17	0.97	0.77	0.71	0
Pressure (MPa)	170.0	109.7	69.1	38.1	0	0	0	0	0

Table 4.6.2.3 (L007)

(2) History of the pressure within half of the bar for different cooling times calculated using Eq. 3.11.1.3.

The result is shown in Fig. 4.6.2.1 (p. 123).

(3) History of the specific volume rate within half of the bar for different cooling times calculated using Eq. 3.11.2.1.

The result is shown in Fig. 4.6.2.2 (p. 123)

(4) History of the density within the half of the bar for different cooling times calculated using Eq. 3.11.2.2.

The result is shown in Fig. 4.6.2.3 (p. 124)

(5) The stress distribution throughout the moulding

The results are shown in Fig. 4.6.2.4 (p.124). The labels in Fig 4.6.2.4 refer to the computed stress obtained using the liquid nitrogen temperature (L006) and the computed stress obtained using the temperature of ice water (L007). The computed residual stress magnitude for the bars which were cooled in liquid nitrogen was 7.2 times higher than the computed magnitude for bars cooled in ice water in average. As both the calculation models, L006 and L007, used the same in-mould cooling conditions, the calculated pressure history, the specific volume rate history and the density history are the same results for them. The difference in the residual stress magnitude was mainly produced by the temperature of the cooling mediums in this case.

4.6.2.2 Comparison of effect of friction constraint, using straight bars (L004 and L005)

This section considers the effect of friction constraint on residual stress distributions when using ice water and liquid nitrogen as cooling media.

(1) Determination of the relationship between the cooling time, the T_g layer positions and the pressure

In order to calculate the rate of change of specific volume: $\left(\frac{dV}{dP}\right)_{T_g}$ at $T=T_g(t)$ and the density at $T=T_g(t)$, the following Table (Table 4.6.2.4) is used to determine the relationship between the cooling time, T_g layer position and the pressure. The same table is used for this section because L004 and L005 use the same cooling time and injection pressure.

Cooling time (s)	0	1.0	2.0	4.0	6.0	7.0	7.9	9.0	10.0	10.7
Position of the T_g layer (mm)	1.55	1.31	1.219	1.057	0.904	0.814	0.721	0.571	0.377	0
Pressure (MPa)	170.0	127.7	96.1	52.6	21.1	8.1	0	0	0	0

Table 4.6.2.4 (L004 and L005)

(2) History of the pressure within half of the bar for different cooling times calculated using Eq. 3.11.1.3.

The result is shown in Fig. 4.6.2.5 (p. 125).

Note:4.6.2.1: The result in Fig. 4.4.2 is different to Fig. 4.6.2.5 because the computations were made using different melt temperatures and mould temperatures.

(3) History of the specific volume rate within half of the bar for different cooling times calculated using Eq. 3.11.2.1.

The result is shown in Fig. 4.6.2.6 (p. 125).

(4) History of the density within the half of the bar for different cooling time calculated using Eq. 3.11.2.2.

The result is shown in Fig. 4.6.2.7 (p. 126).

(5) Pressure induced stress and temperature induced stress

The comparison of the effect of the friction constraint for both the pressure and the temperature induced stresses in the mould are shown in Fig. 4.6.2.8 (p. 127) and Fig. 4.6.2.9 (p. 127).

It is assumed that, when the pressure drops to atmospheric pressure, the friction becomes zero, because there is now no normal force at the bar surface.

(6) The stress distribution throughout the moulding

The result is shown in Fig. 4.6.2.10 (p. 128). The labels in Fig 4.6.2.10 refer to the

computed stress obtained without friction constraint (L004) and the computed stress obtained with friction constraint (L005). The computed residual stress magnitude without friction constraint was 0.66 to 0.94 times that when using friction constraint.

4.6.2.3 Comparison of effect of packing pressure, using straight bars (L002 and L003)

This section considers the effect of injection pressure using 87 (MPa) (L002) and 143 (MPa) (L003).

(1) Determination of the relation among the cooling time, the T_g layer position and the pressure

In order to calculate the rate of change of specific volume: $\left(\frac{dV}{dP}\right)_{T_g}$ at $T=T_g(t)$ and the density at $T=T_g(t)$, the following Tables (Table 4.6.2.5 and Table 4.6.2.6) are used to determine the relationship between the cooling time, T_g layer position and the pressure.

Cooling time (s)	0	1.0	1.5	2.0	2.4	4.0	10.0	12.0	14.0	14.5
Position of the T_g layer (mm)	1.55	1.42	1.38	1.34	1.32	1.23	0.88	0.68	0.3	0
Pressure (MPa)	87.0	57.2	33.7	14.6	0	0	0	0	0	0

Table 4.6.2.5 (L002)

Cooling time (s)	0	1.0	2.0	3.1	4.0	10.0	12.0	14.0	15.0
Position of the T_g layer (mm)	1.55	1.43	1.36	1.30	1.25	0.92	0.74	0.44	0
Pressure (MPa)	143.0	77.9	35.1	0	0	0	0	0	0

Table 4.6.2.6 (L003)

(2) History of the pressure within half of the bar for different cooling times calculated using Eq. 3.11.1.3.

This result is shown in Fig. 4.6.2.11 (p. 129). The labels in Fig 4.6.2.11 refer to the pressure history obtained using 143 (MPa) injection pressure (L002) and the using 87 (MPa) injection pressure (L003).

(3) History of the specific volume rate within half of the bar for different cooling times calculated using Eq. 3.11.2.1.

This result is shown in Fig. 4.6.2.12 (p. 129).

(4) History of the density within the half of the bar for different cooling times calculated using Eq. 3.11.2.2.

This result is shown in Fig. 4.6.2.13 (p. 130).

(5) The stress distribution throughout the moulding

The result is shown in Fig. 4.6.2.14(p. 130). The labels in Fig 4.6.2.14 refer to the computed stress obtained using 143 (MPa) injection pressure (L002) and the computed stress obtained using 87 (MPa) injection pressure (L003). The computed residual stress magnitude for the bars which were made using 143 (MPa) was 0.68 times the computed magnitude for bars made using 87 (MPa) on average.

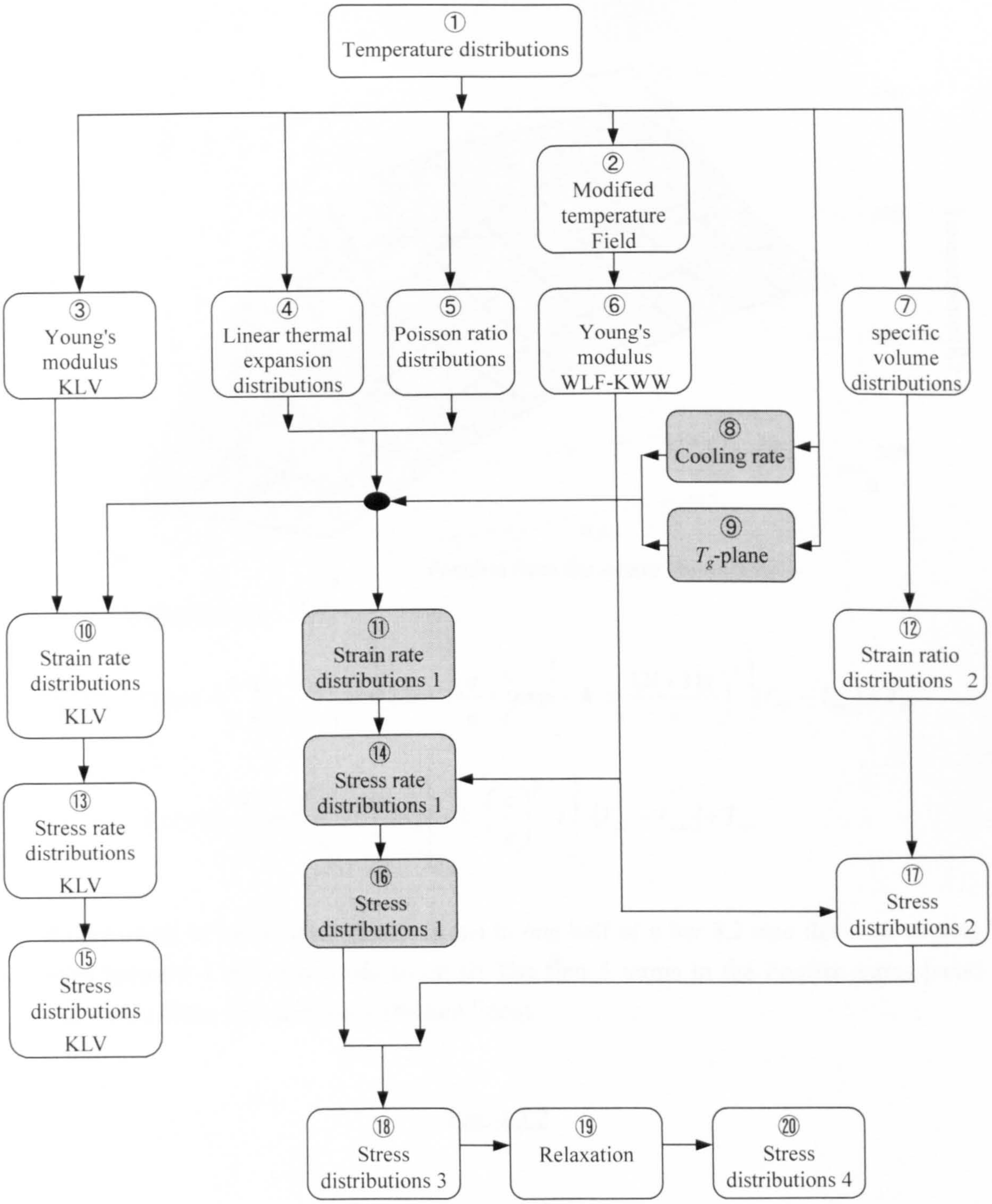

Fig. 4.3 Block diagram of the procedure (Method A)

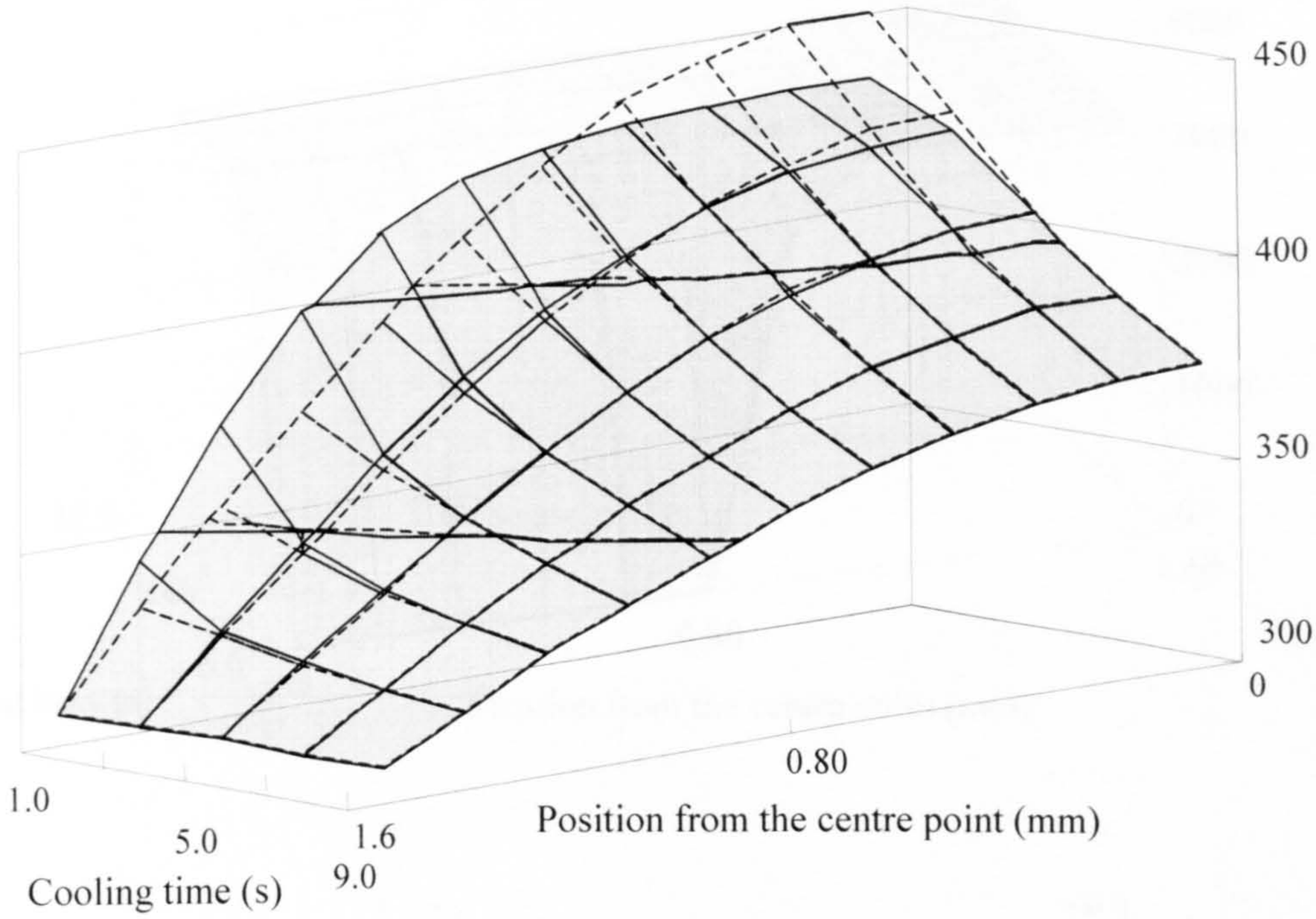

$$\square : T(z,t) = \frac{4}{\pi}\sum_{i=0}^{5}\frac{(-1)^i}{2i+1}\cos\left((2i+1)\frac{\pi}{e}z\right)\exp\left[-k\cdot t\left(\frac{(2i+1)\pi}{e}\right)^2\right](T_{ml}-T_{mo})+T_{mo}$$

$$\square : T(z,t) = \frac{4}{\pi}\cdot\cos\left(\frac{\pi}{e}\cdot z\right)\cdot\exp\left[-k\cdot\left(\frac{\pi}{e}\right)^2\cdot t\right]\cdot(T_{ml}-T_{mo})+T_{mo}$$

Comparison of temperature distributions in one half of a bar 3.2 mm thick for cooling times between 1 and 9 seconds using (i) The first 5 terms in the Fourier series (solid lines) and (ii) the first term only (broken lines)

Fig. 4.3.2

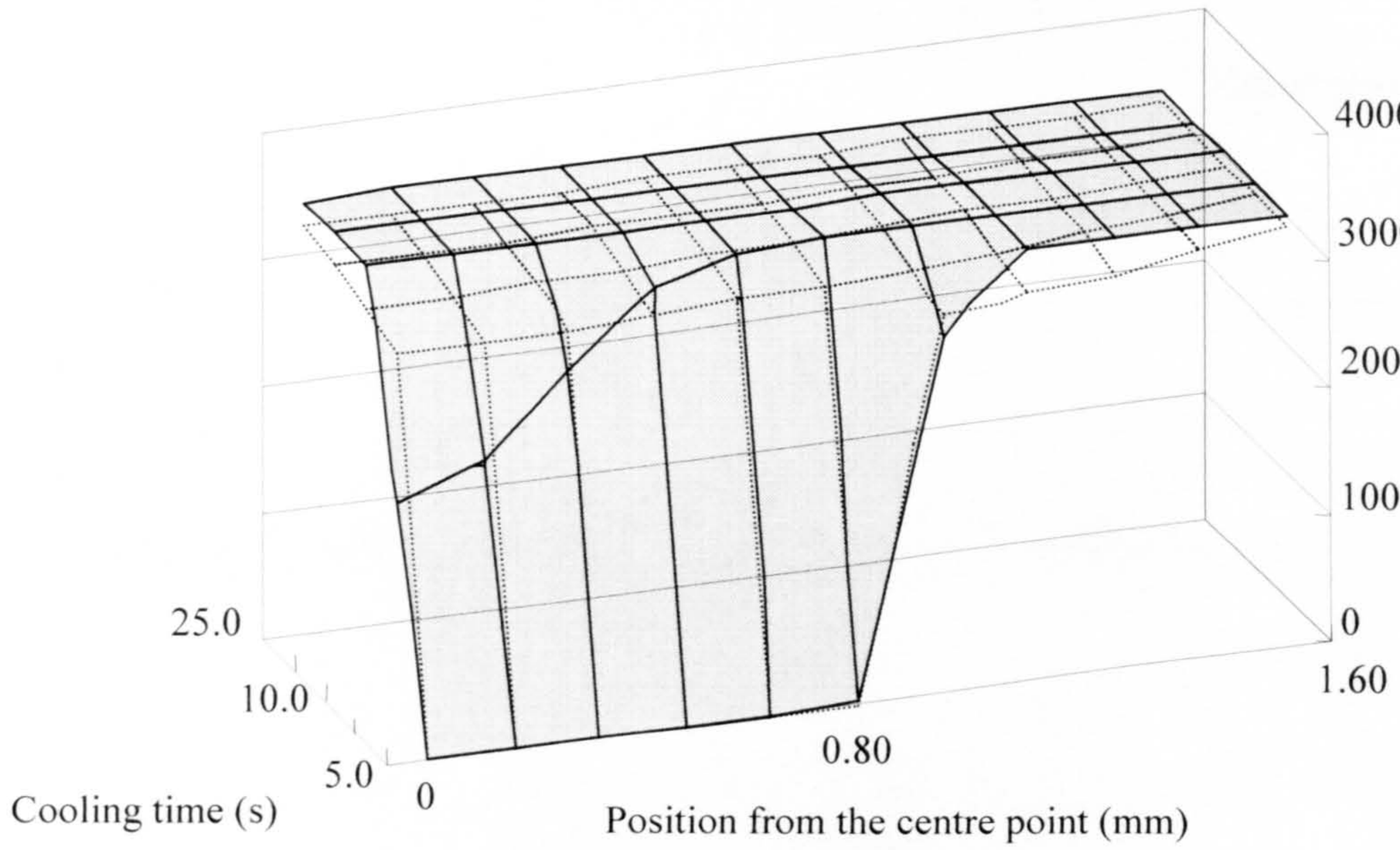

$$\square \quad : \quad E(z,t) = E_0 \cdot \exp\left[-\left[\left\{ \exp\left(\frac{C_1 \cdot (S(z,t) - T_g)}{C_2 + (S(z,t) - T_g)} \right) \right\} \cdot \frac{t}{t_0(T_g)} \right]^m \right]$$

$$\cdots\cdots \quad : \quad E(z,t) = \frac{T_r}{\frac{T_g}{T_r} + \frac{2T}{T_r}} \cdot E_0 \qquad (T \le T_g), \qquad \frac{E_0}{\exp\ 2.65 \left[\frac{\frac{T_g}{T_r} - \frac{T_g}{T}}{\left(\frac{T_g}{T_r} - 1 \right)} \right]} \qquad (T > T_g)$$

Distributions of Young's modulus within half of the bar for different cooling times, calculated using the temperature distributions obtained using (i) Eq. 3.5.1.7, from a combination of the WLF and the KWW equations (solid lines) and (ii) Eq. 3.5.2.1 and Eq. 3.5.2.2 (Van Krevelen and Hoftyzer, broken lines)

Fig. 4.3.3

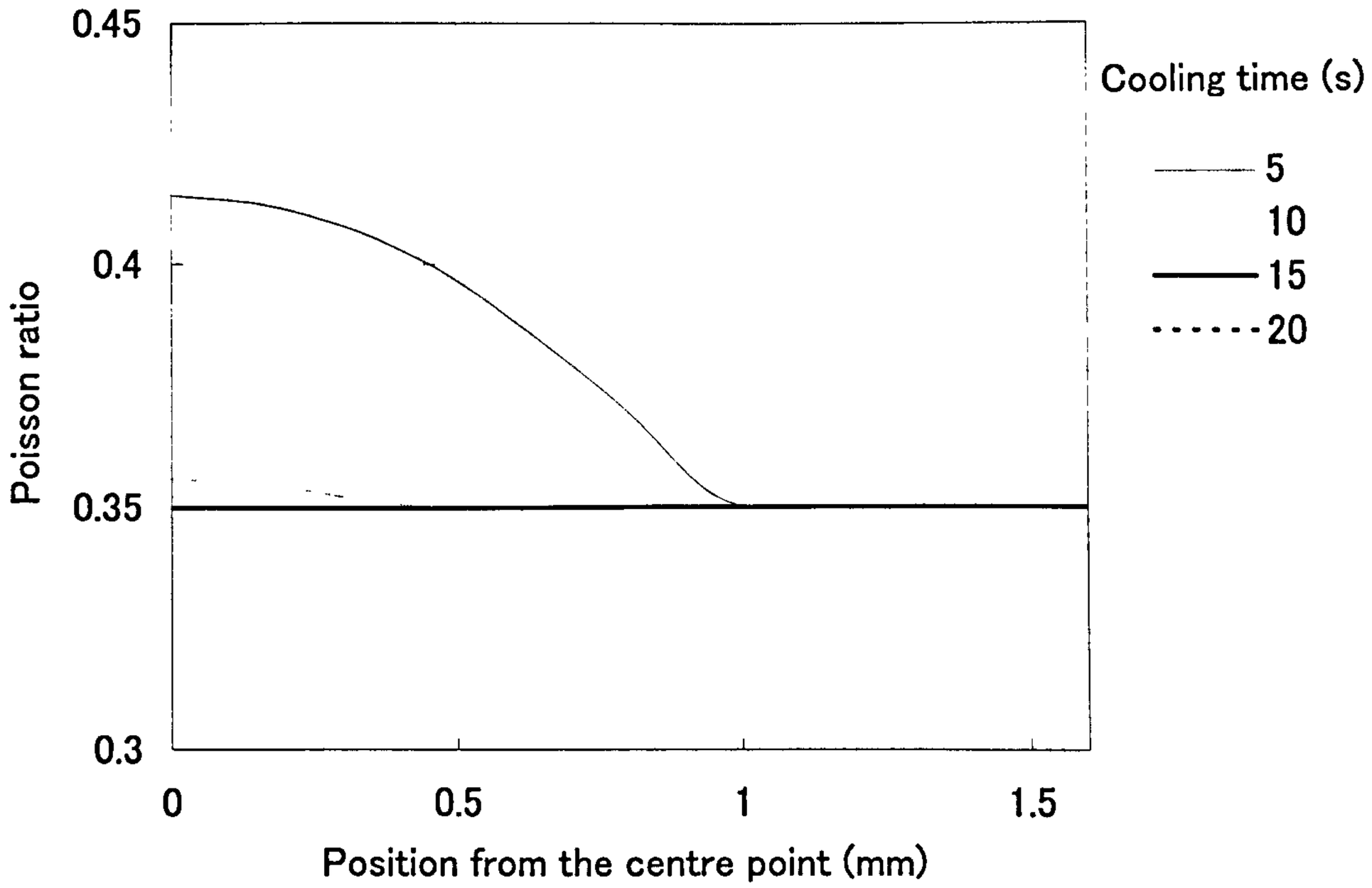

Distributions of the Poisson ratio within half of the bar for different cooling times, using the temperature distributions given by Eqs. 4.3.4.1, 4.3.4.2 and 4.3.4.3

Fig. 4.3.4 Distributions of the Posson ratio

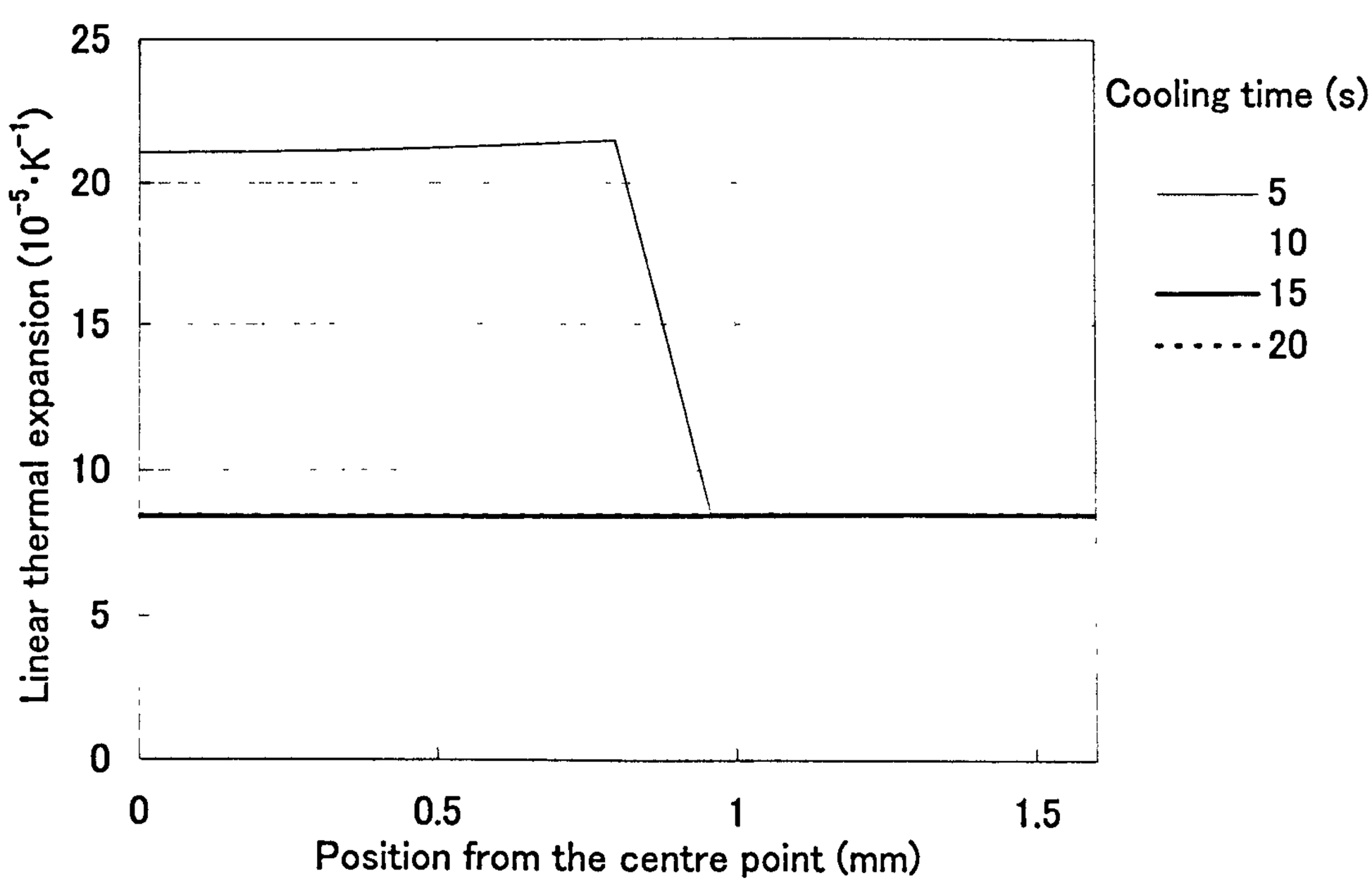

Distributions of the linear thermal expansion coefficient within half of the bar for different cooling times given by Eq.3.6.4 and Eq.3.6.5

Fig. 4.3.5 Distributions of the linear thermal expansion coefficient

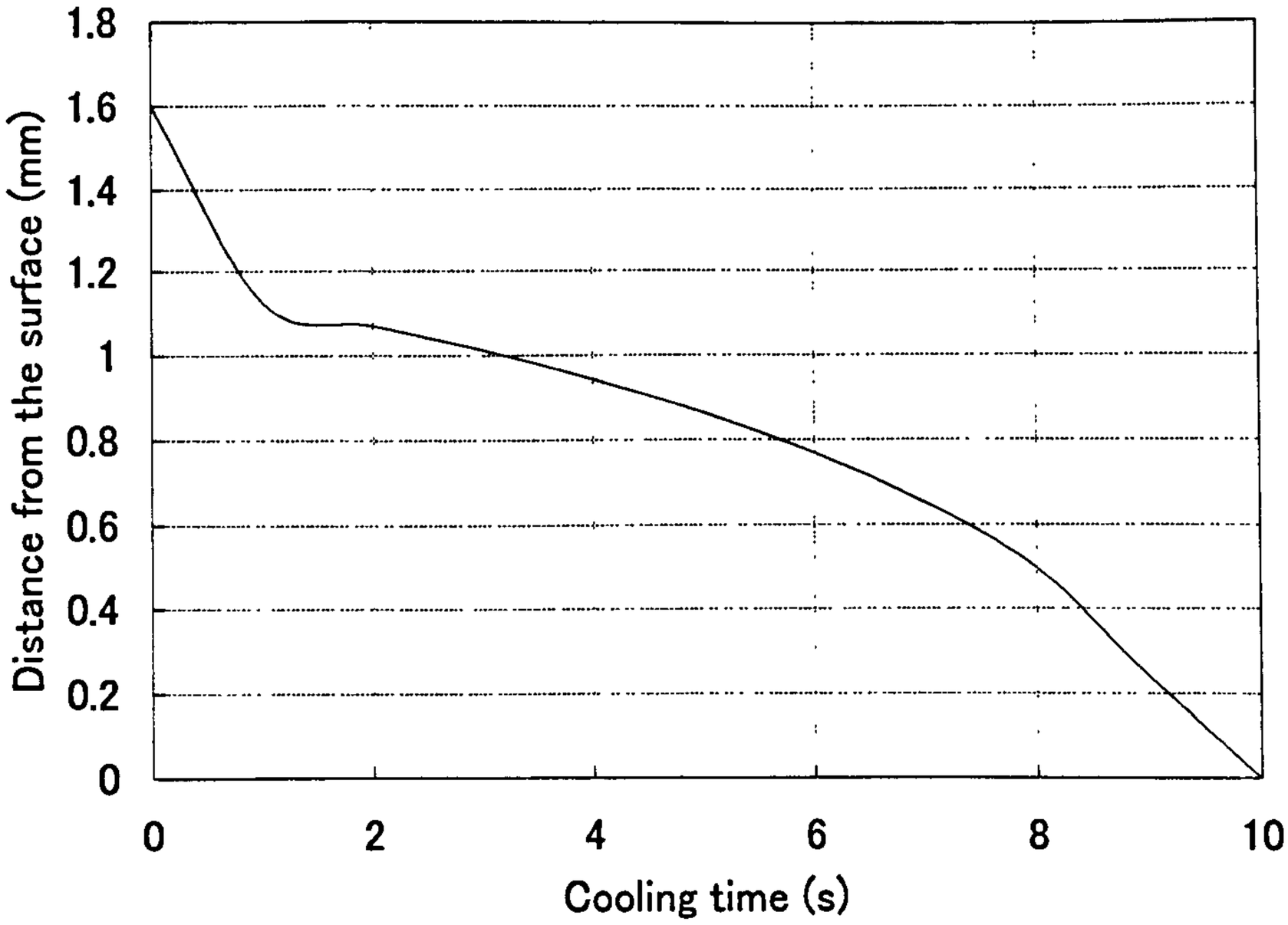

Glass transition plane positions within half of the bar for different cooling times calculated using Eq. 3.7.5.

Fig. 4.3.6 Glass transition plane position according to the cooling time

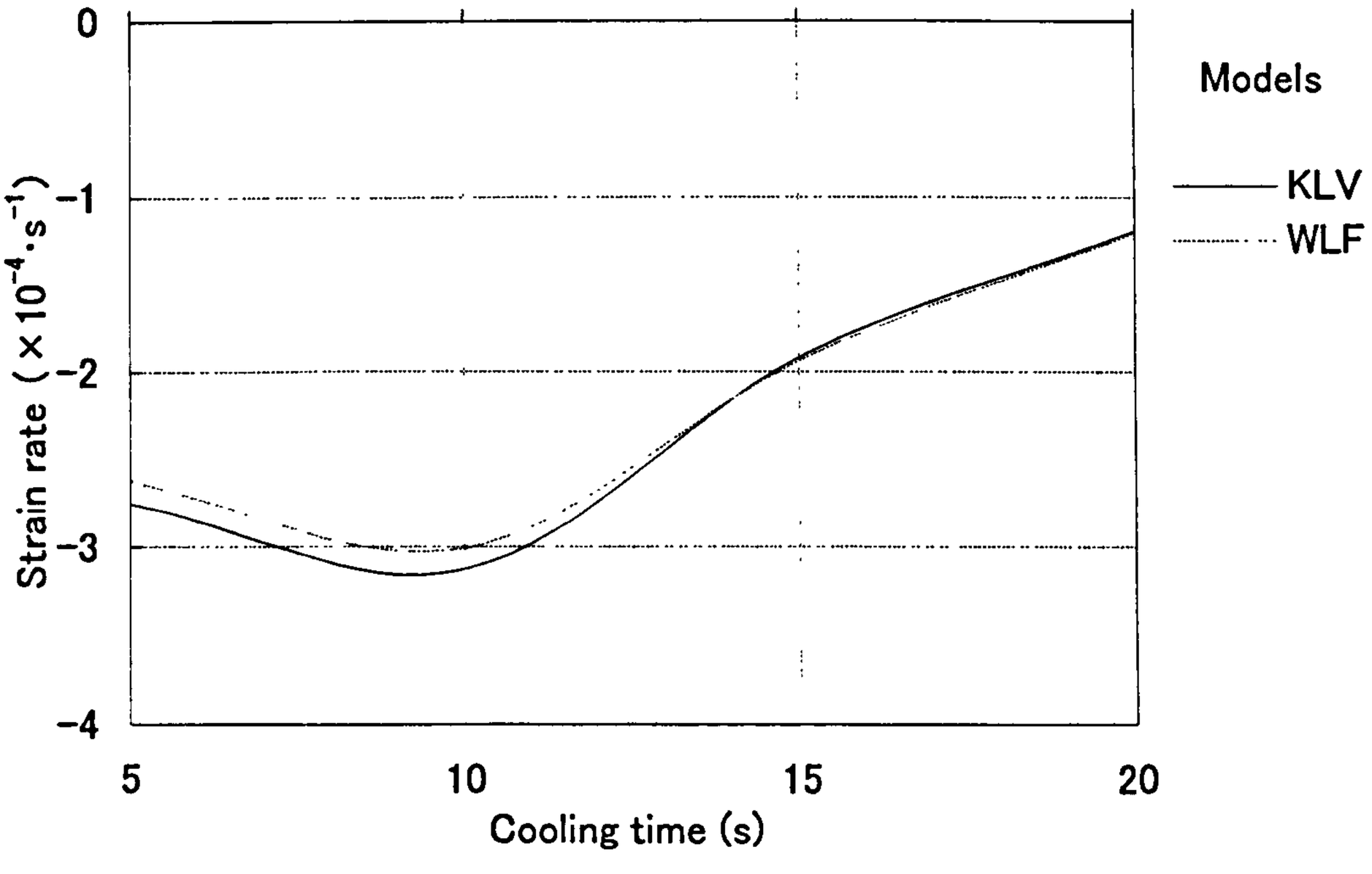

Average strain rate calculated at all points using Eq. 3.8.20. (i) Strain rate obtained using Eq. 3.5.2.1 and Eq. 3.5.2.2 (Van Krevelen and Hoftyzer, solid line). (ii) Strain rate obtained using Eq. 3.5.1.7 from a combination of the WLF and the KWW equations (broken line)

Fig. 4.3.7 Distributions of the strain rate (WLF and KWW)

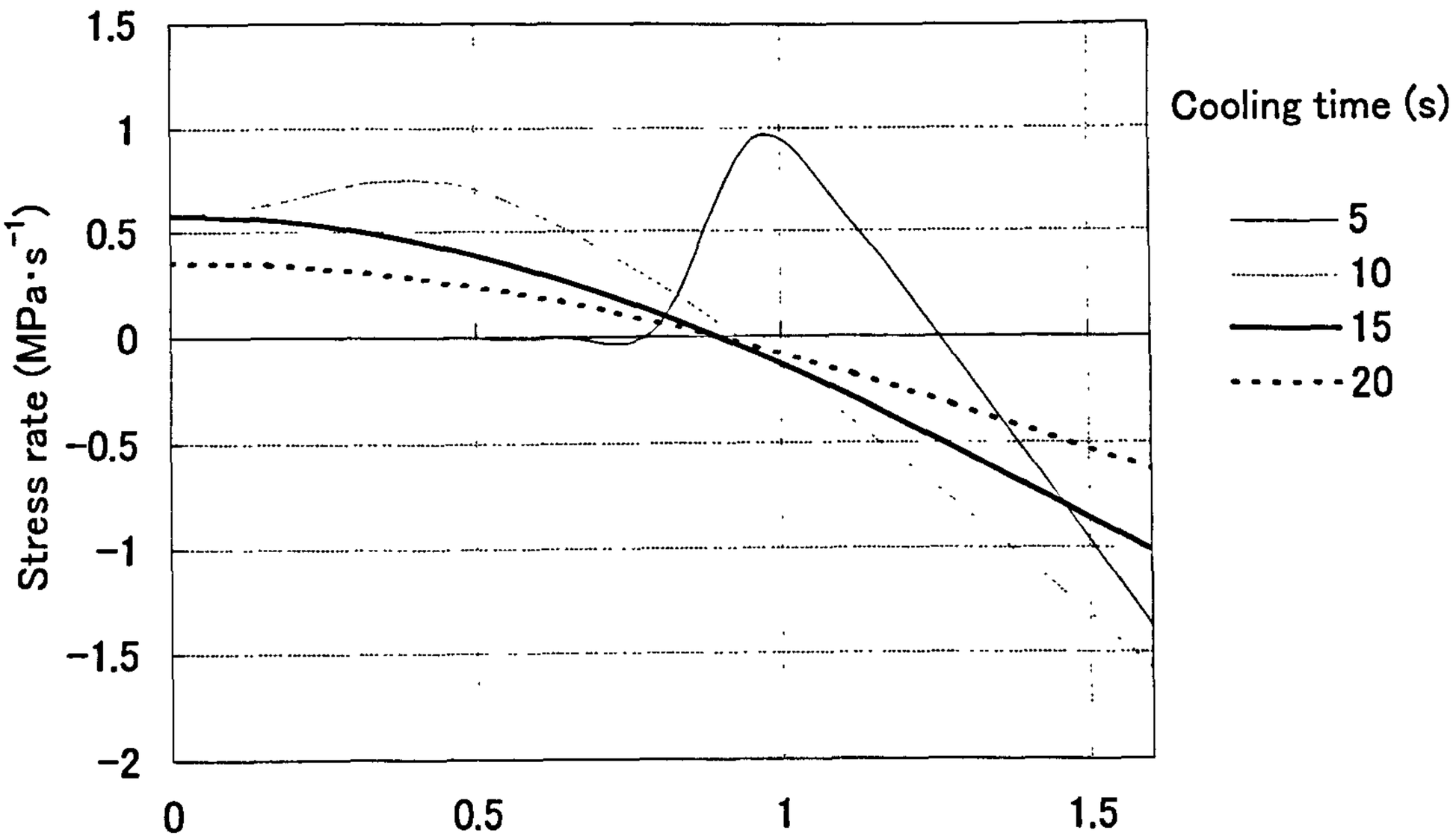

Distributions of the stress rate calculated using Eq. 3.8.21 (from the combination of the WLF and the KWW equations)

Fig. 4.3.8 Distributions of the stress rate (WLF and KWW)

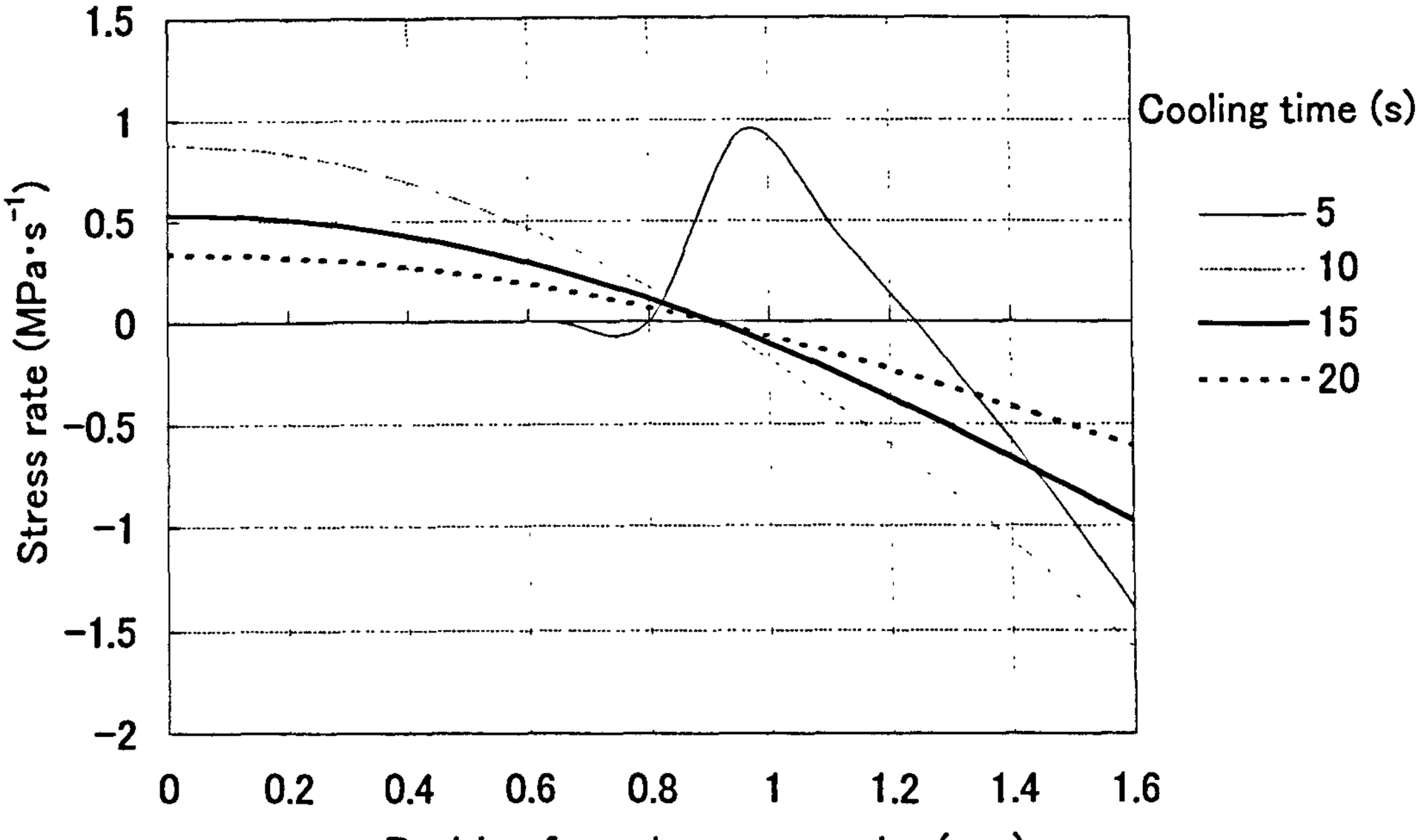

Distributions of the stress rate calculated using Eq. 3.8.21 (from the combination of the Van Krevelen and the Hoftyzer model)

Fig. 4.3.9 Distributions of the stress rate KLV)

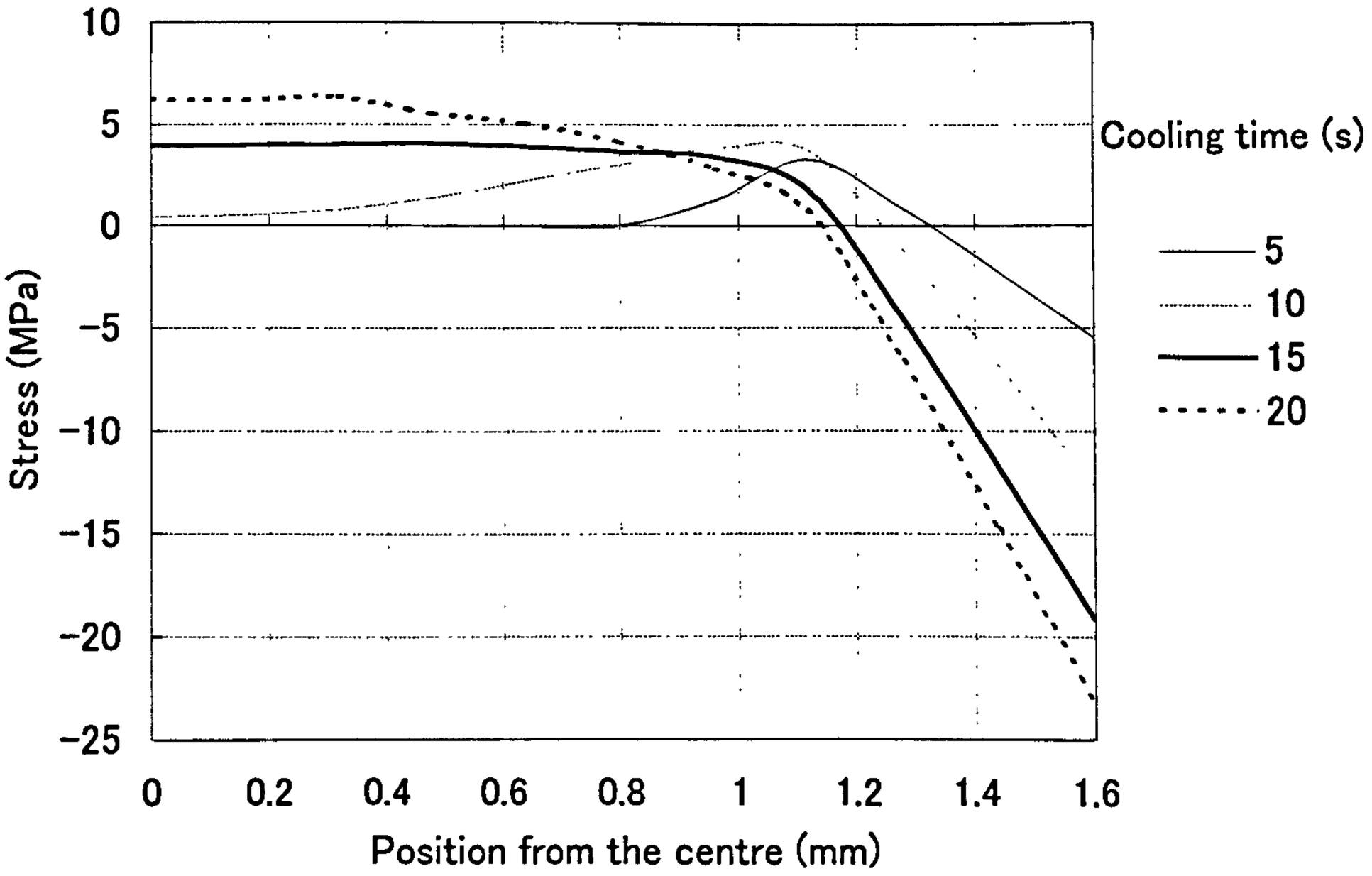

Distributions of the stresses calculated using Eq. 3.8.22. (The combination of the WLF and the KWW equation is used for the calculations)

Fig. 4.3.10 Distributions of the stress (WLF and KWW)

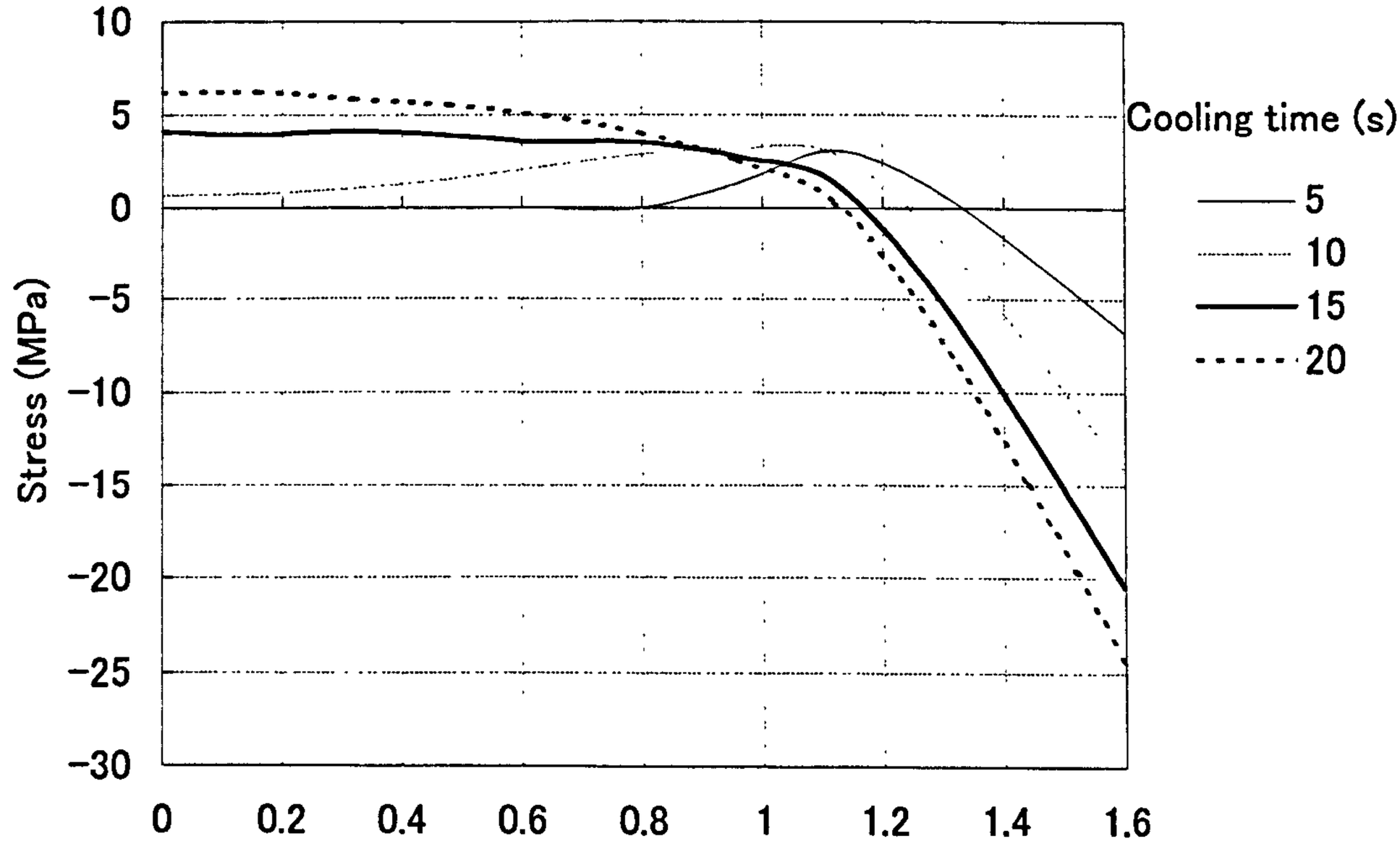

Distributions of the stress calculated using Eq. 3.8.22. The Hoftyzer and Van Krevelen equation is used for this calculations

Fig. 4.3.11 Distributions of the stresses (KLV)

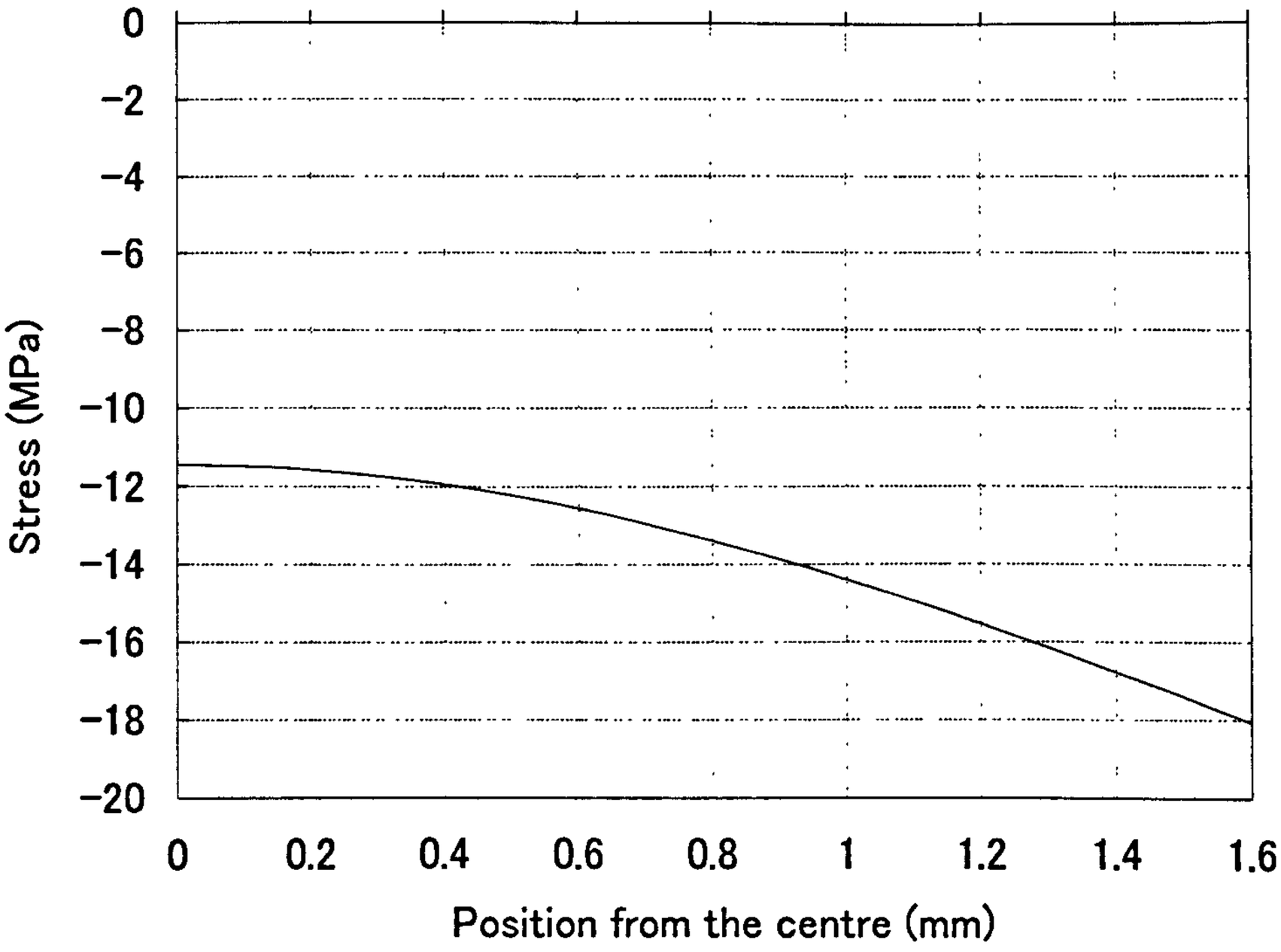

Distribution of the packing pressure induced stresses within half of the bar for the cooling time=20 s, using Eq. 3.9.2

Fig. 4.3.12 Distributions of the stress (WLF and KWW)

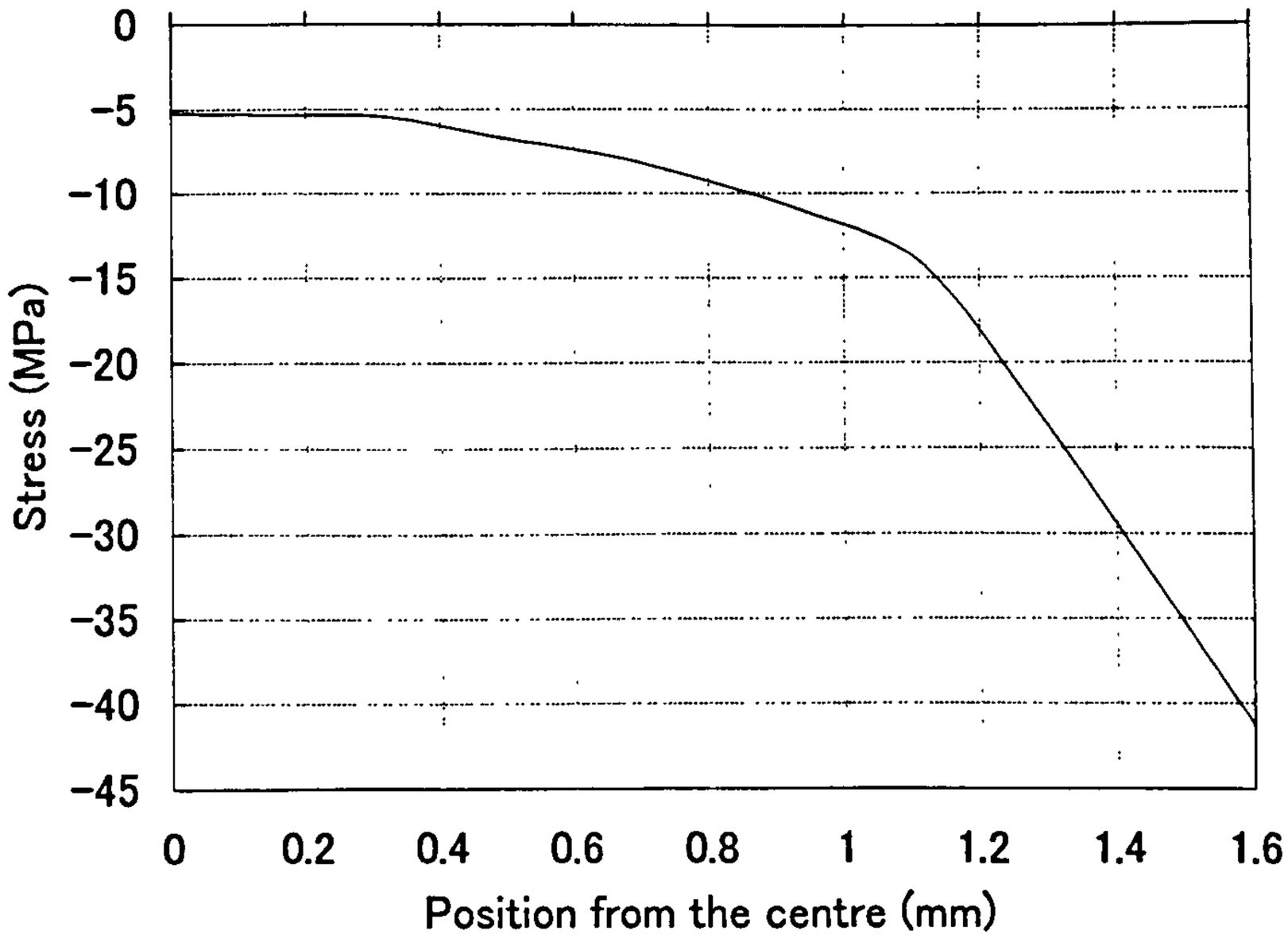

Distribution of the stresses at the cooling time=20 s, calculated using Eq. 4.3.7.3 from a combination of the WLF and the KWW equations (restrained case)

Fig. 4.3.13 Distributions of the stress (In the mould)

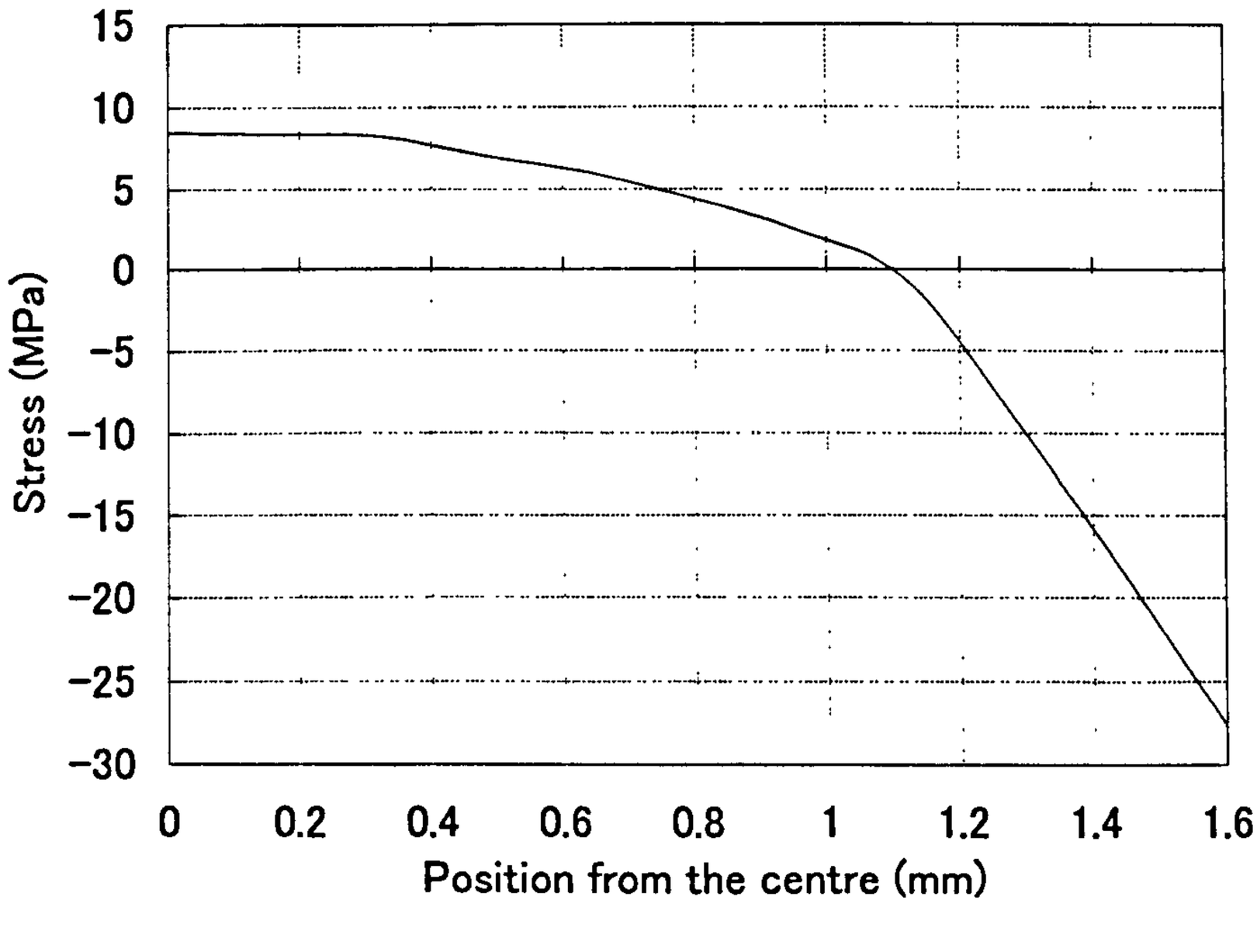

Distributions of the stress at the cooling time=20 s, calculated using Eq. 4.3.7.4, from a combination of the WLF and the KWW equations. (after demoulding)

Fig. 4.3.14 Distributions of the stress (after demoulding)

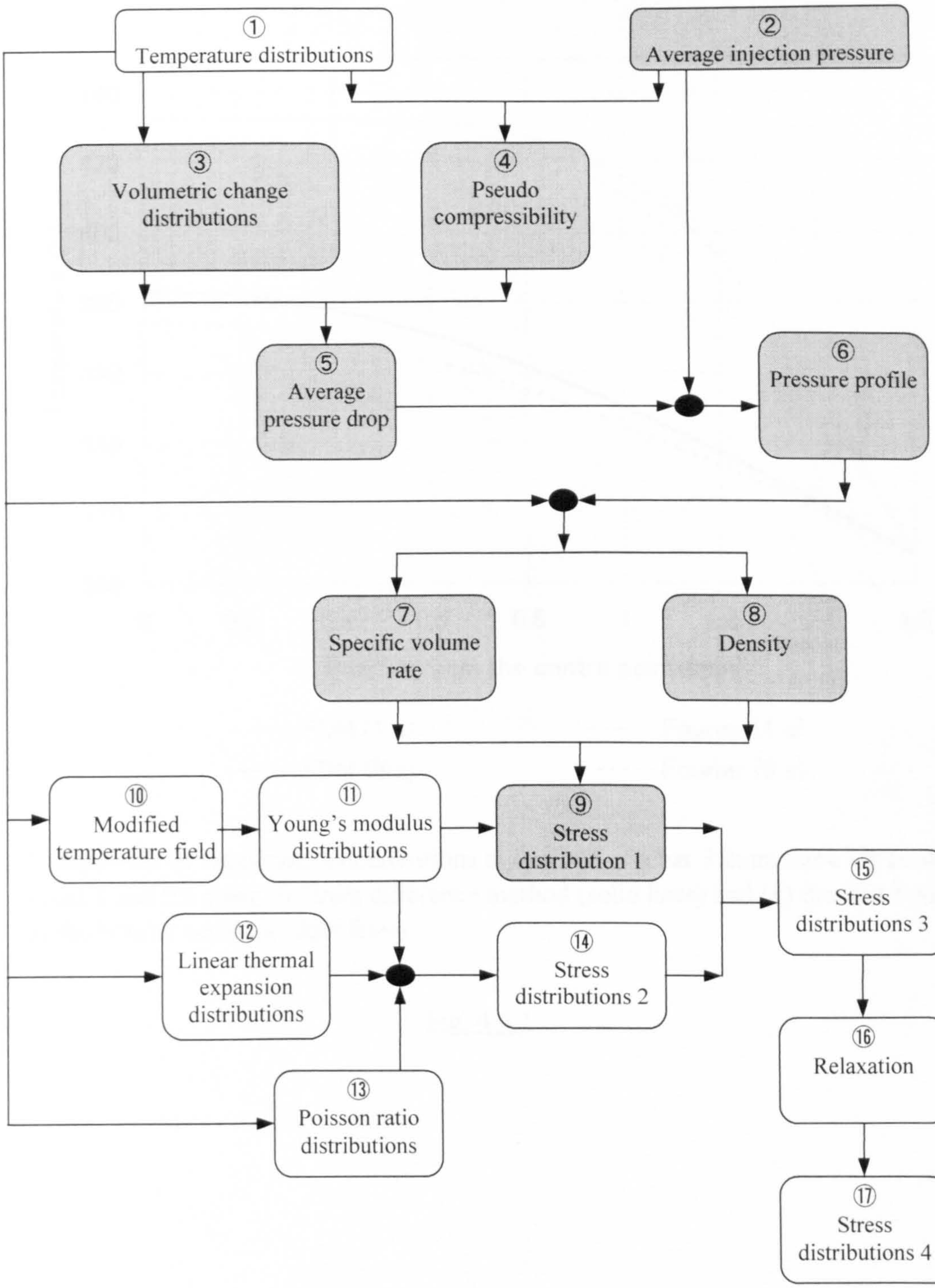

Fig. 4.4 Block diagram of the procedure (Method B)

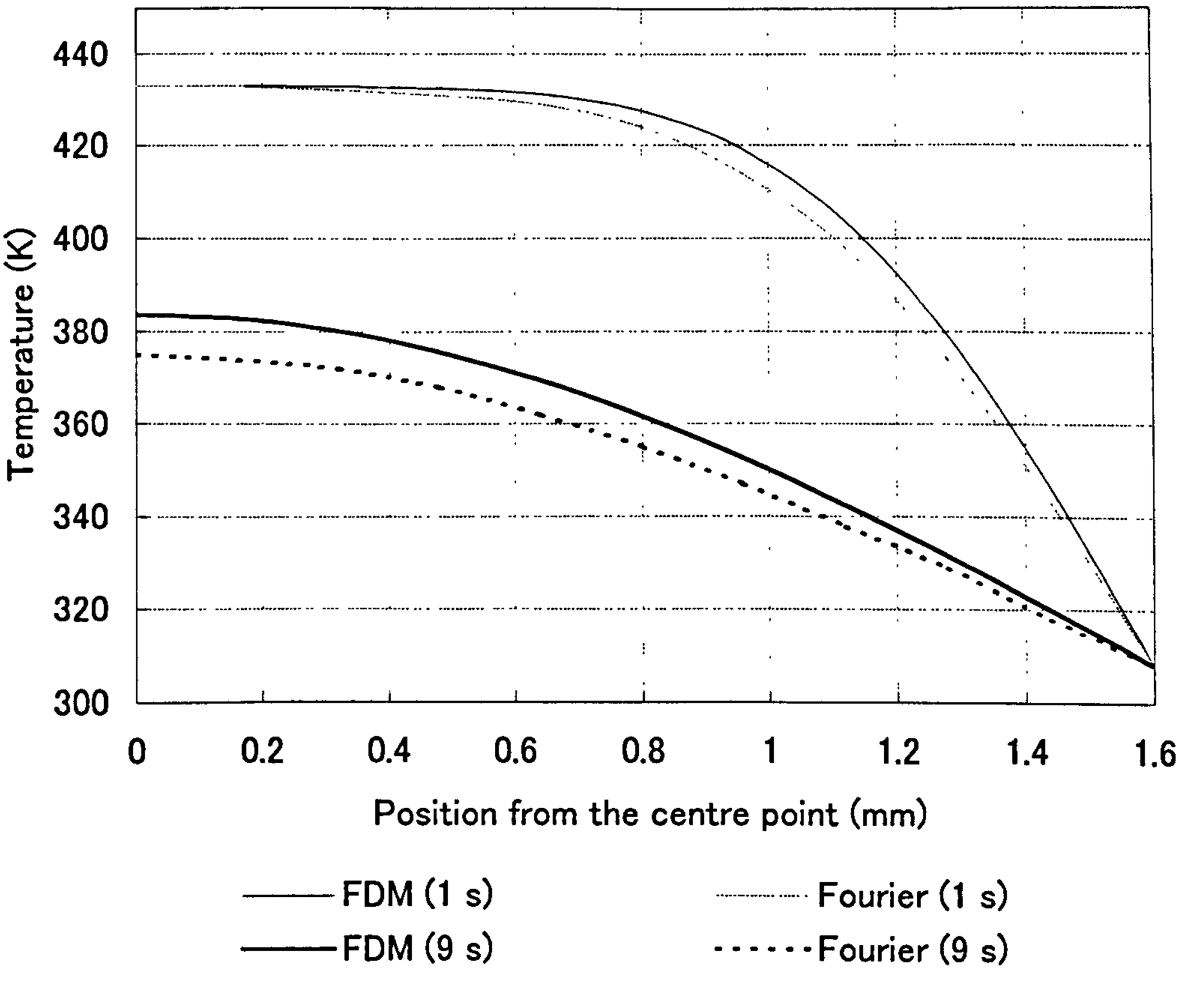

Comparison of temperature distributions in one half of a bar 3.2mm thick for cooling times 1 and 9 s using (i) Finite difference method (solid lines) and (ii) the first 5 terms in the Fourier series (broken lines)

Fig. 4.4.1

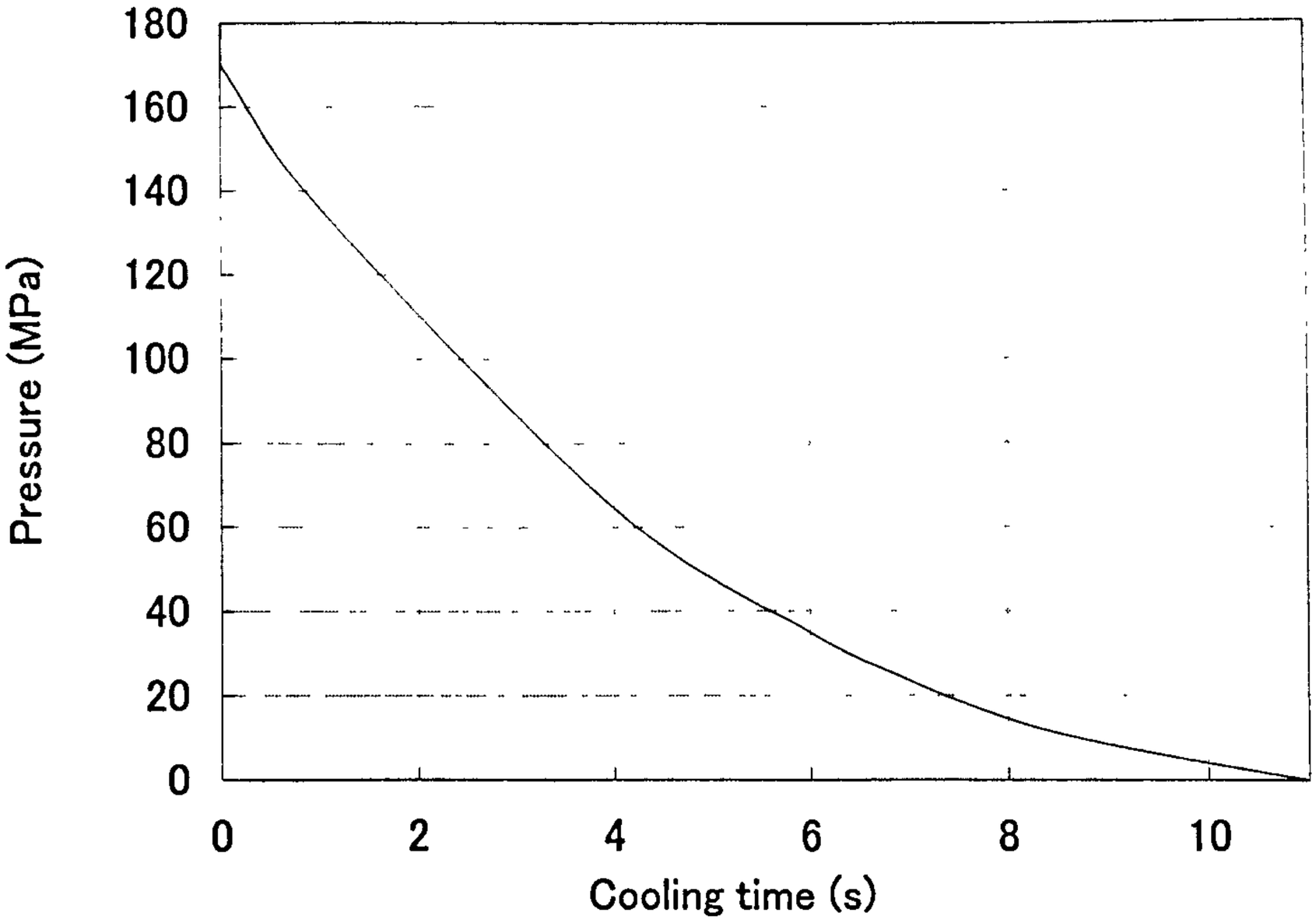

History of the pressure within half of the bar for different cooling times calculated using Eq. 3.11.1.3.

Fig. 4.4.2 Pressure history

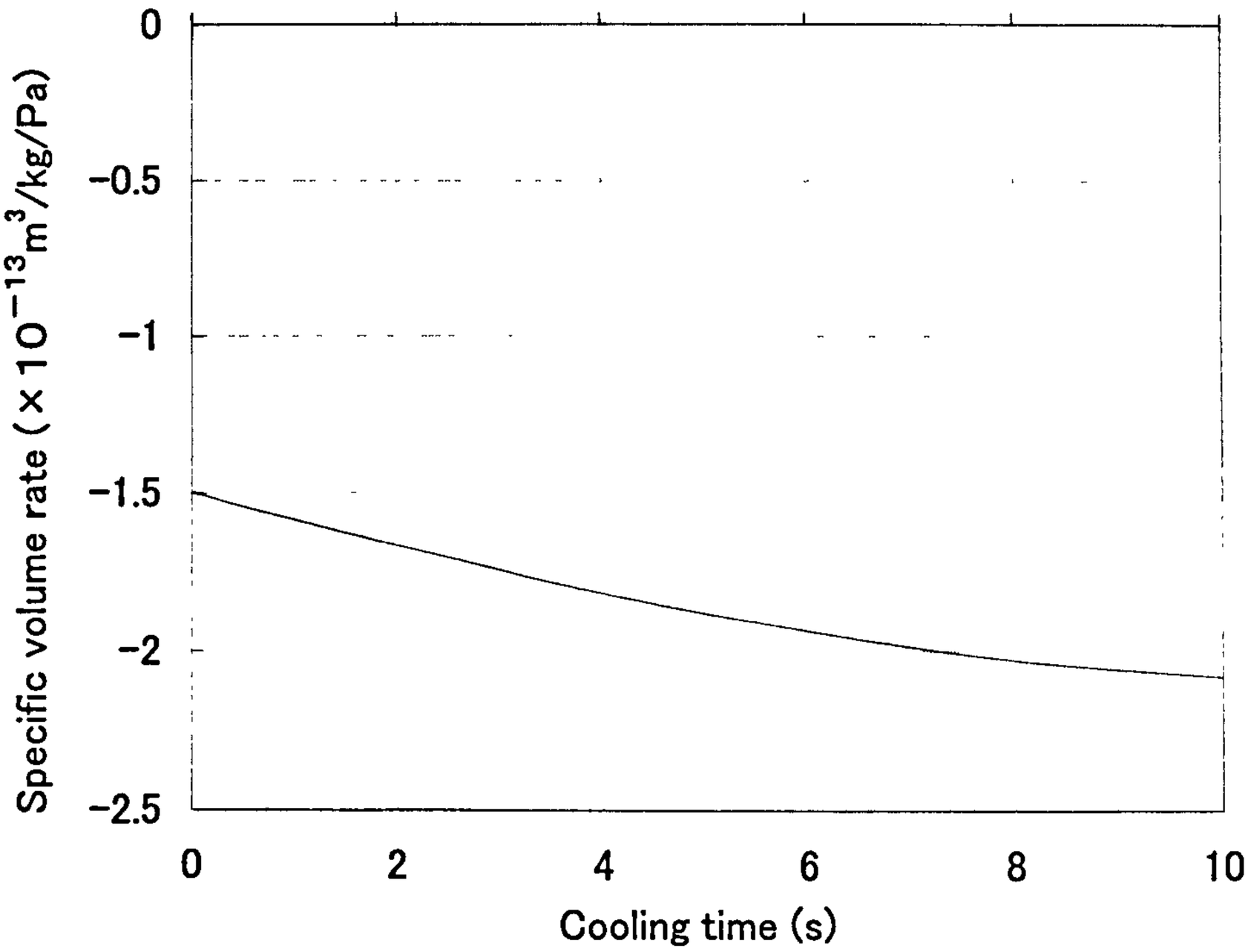

History of the specific volume rate within half of the bar for different cooling times calculated using Eq. 3.11.2.1.

Fig. 4.4.3 Specific volume rate

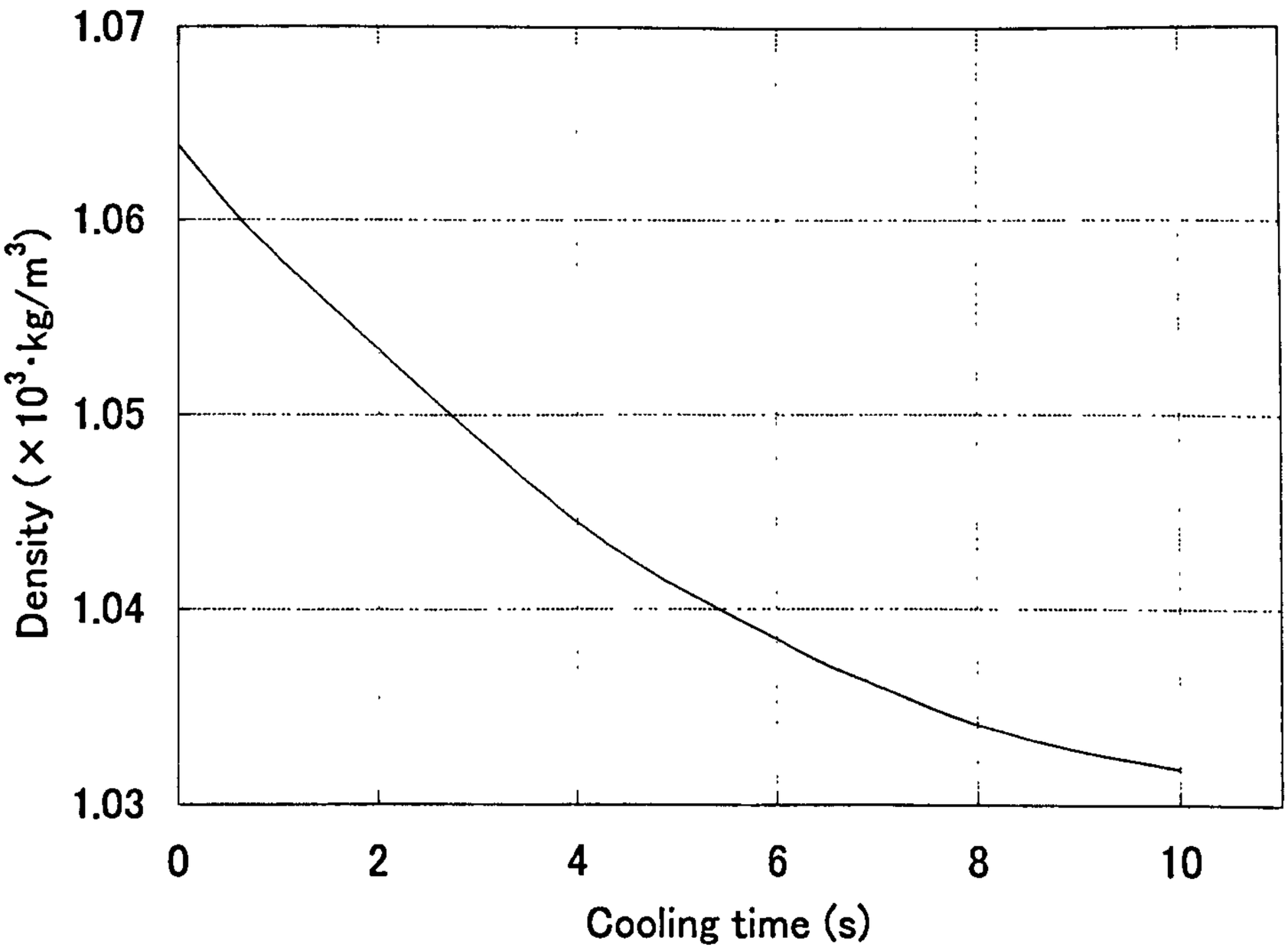

History of the density within the half of the bar for different cooling time calculated Eq. 3.11.2.2.

Fig 4.4.4 History of the density

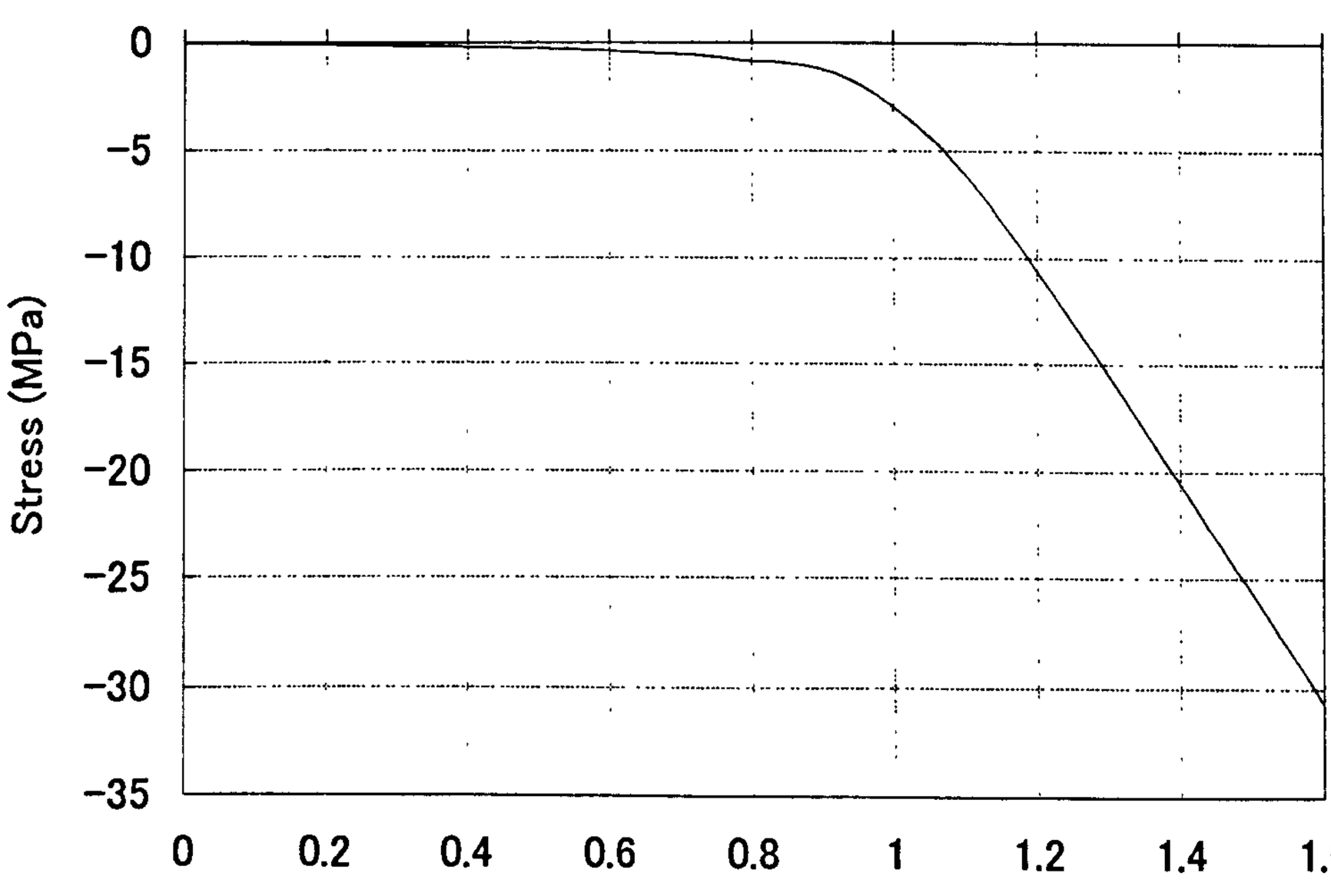

Pressure induced distribution of the stresses at $T=T_g$ and for cooling times between 0 and 10 seconds calculated using Eq. 3.11.2.2.

Fig. 4.4.5 Pressure induced distribution of the stresses at $T=T_g$

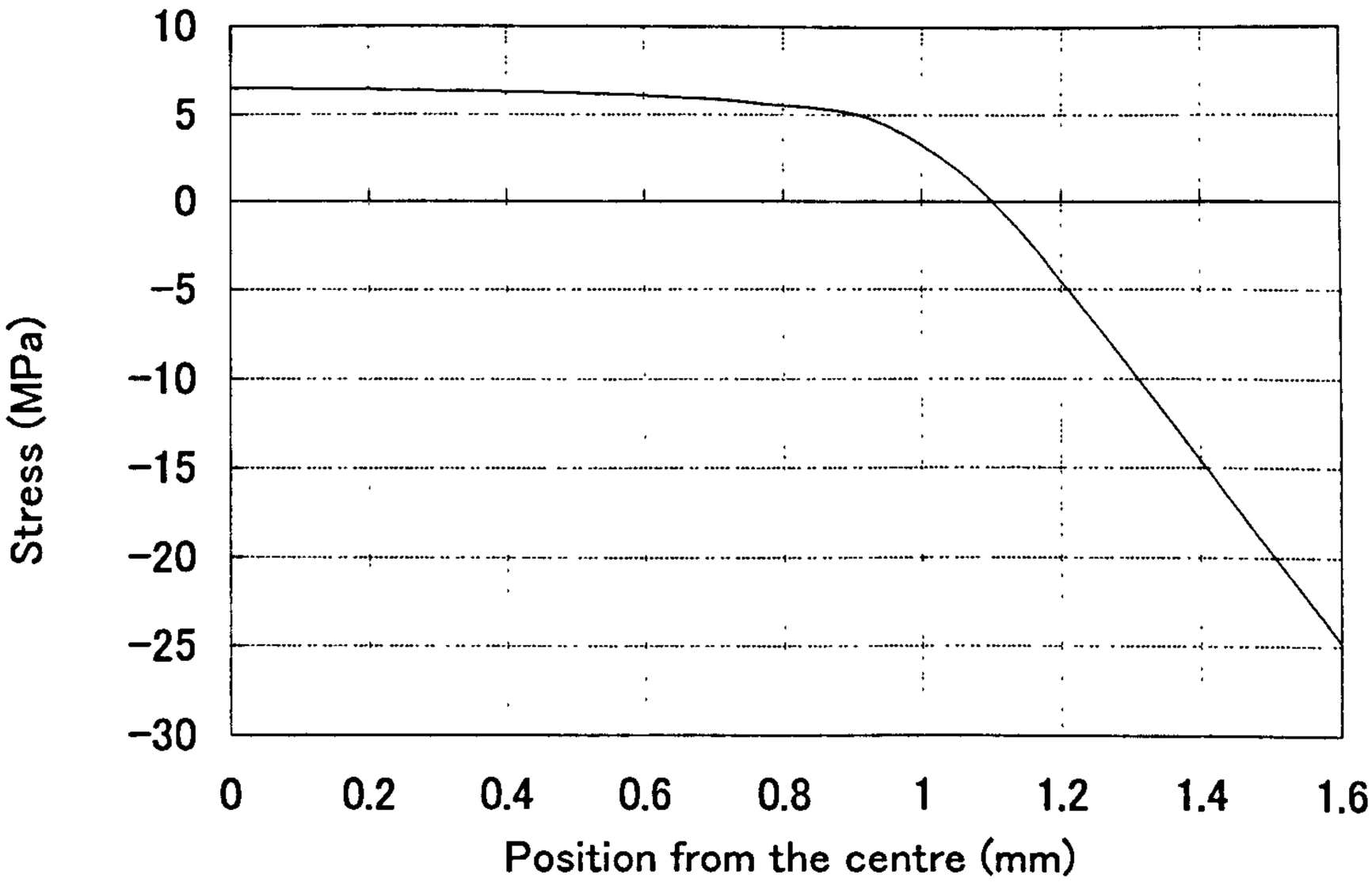

Pressure and temperature induced distribution of the stresses for cooling times between 0 and 10 seconds calculated using Eq. 3.11.4.4

Fig. 4.4.6 Distributions of the stress through out the moulding

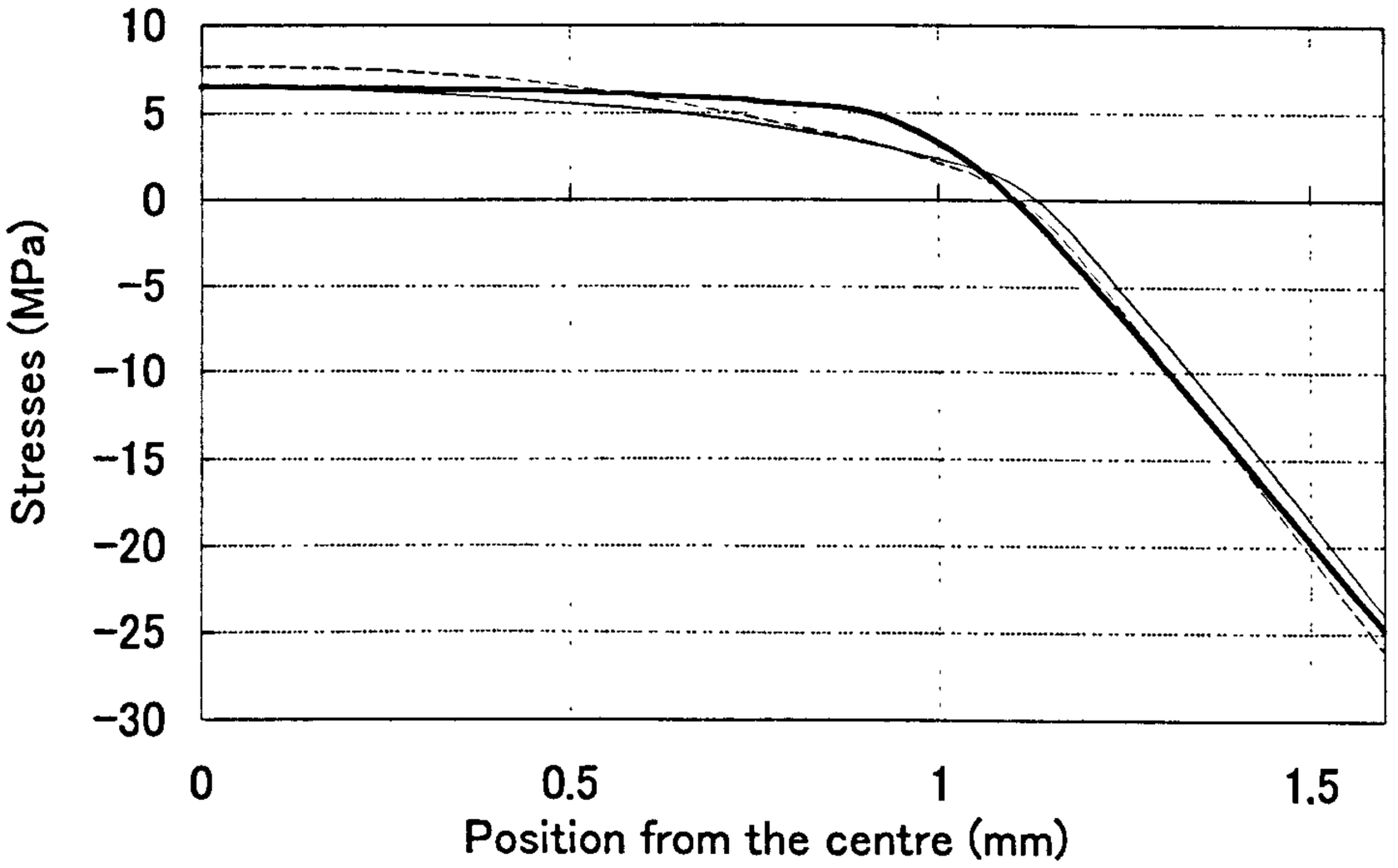

Pressure and temperature induced distribution of the stresses using (i) Eq. 3.11.4.4, (cooling times 11 seconds), (ii) Eq. 4.3.7.4 (cooling time 10 seconds) and (iii) Eq. 4.3.7.4 (cooling time 15 seconds)

Fig. 4.4.7 Distributions of the stress through out the moulding and comparison between procedure of section 4.3 and 4.4

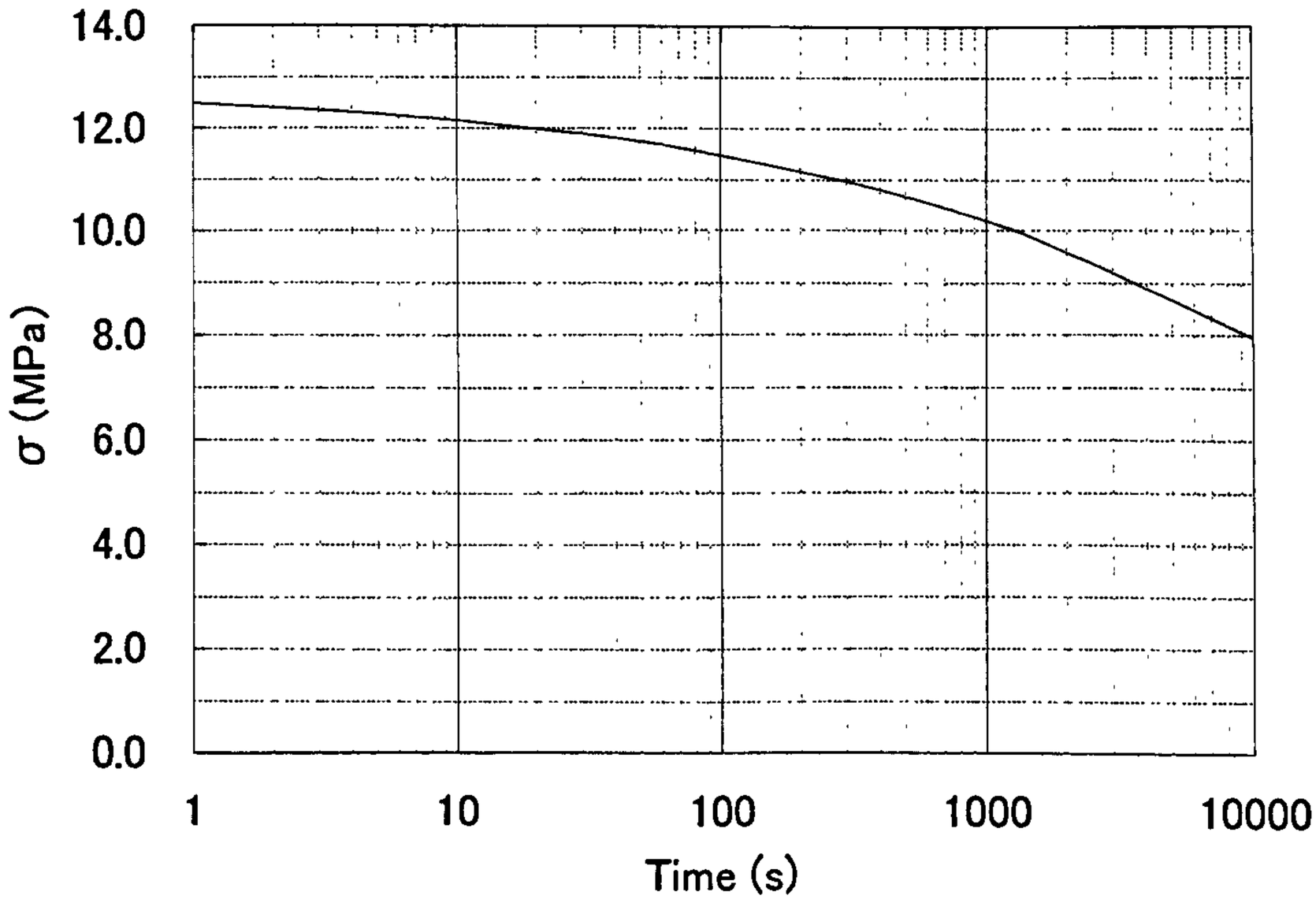

Stress relaxation after demoulding calculated using Eq .4.5.1.

Fig 4.5.1.1 Calculation of the stress relaxation after the demoulding

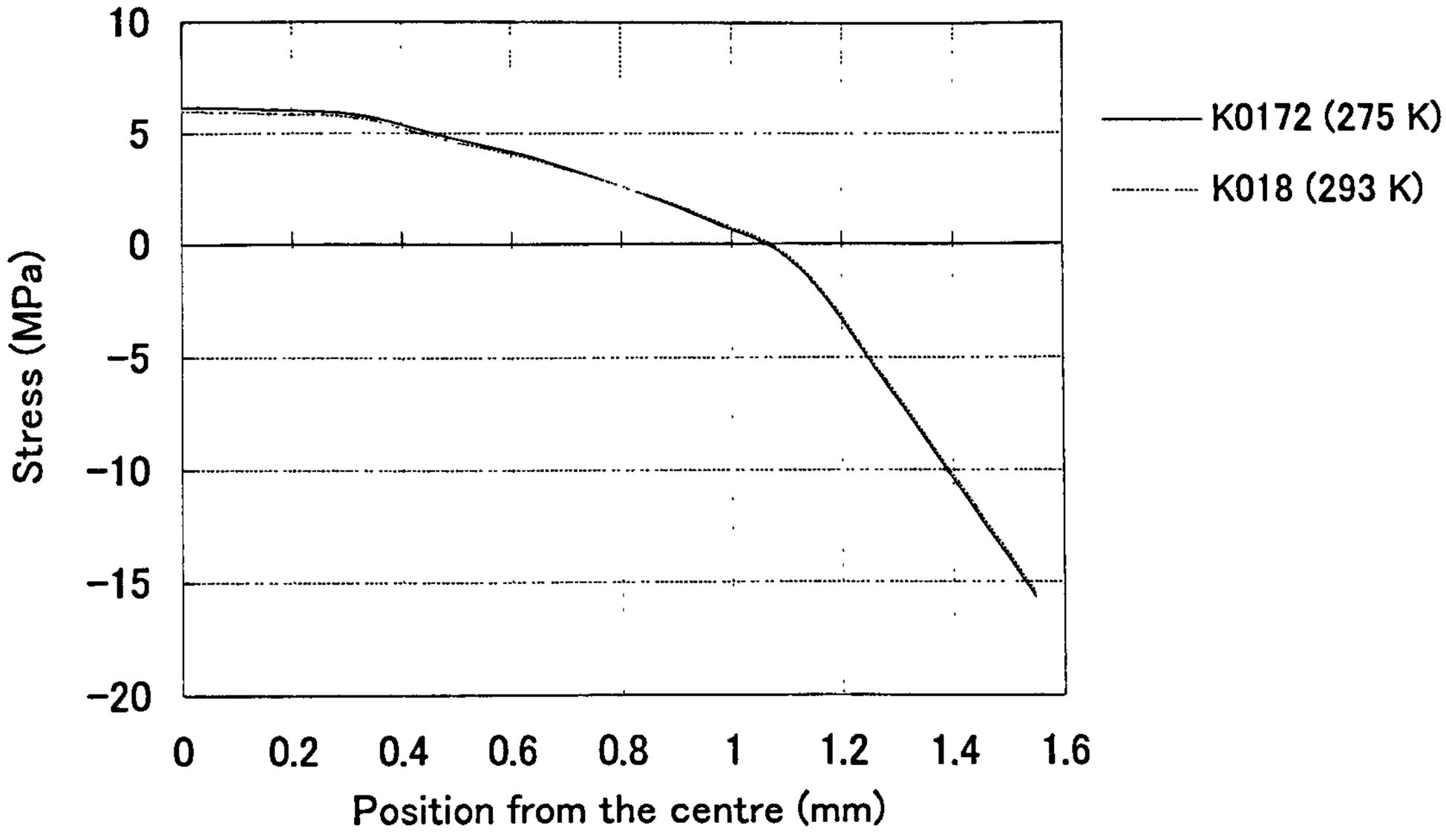

Comparison of the effect of different cooling temperatures, using tensile bars. (i) Stress obtained using ice water (K0172). (ii) Stress obtained using room temperature (K018).

Fig. 4.6.1.1 Comparison of the effect of the different cooling temperatures, using tensile bars

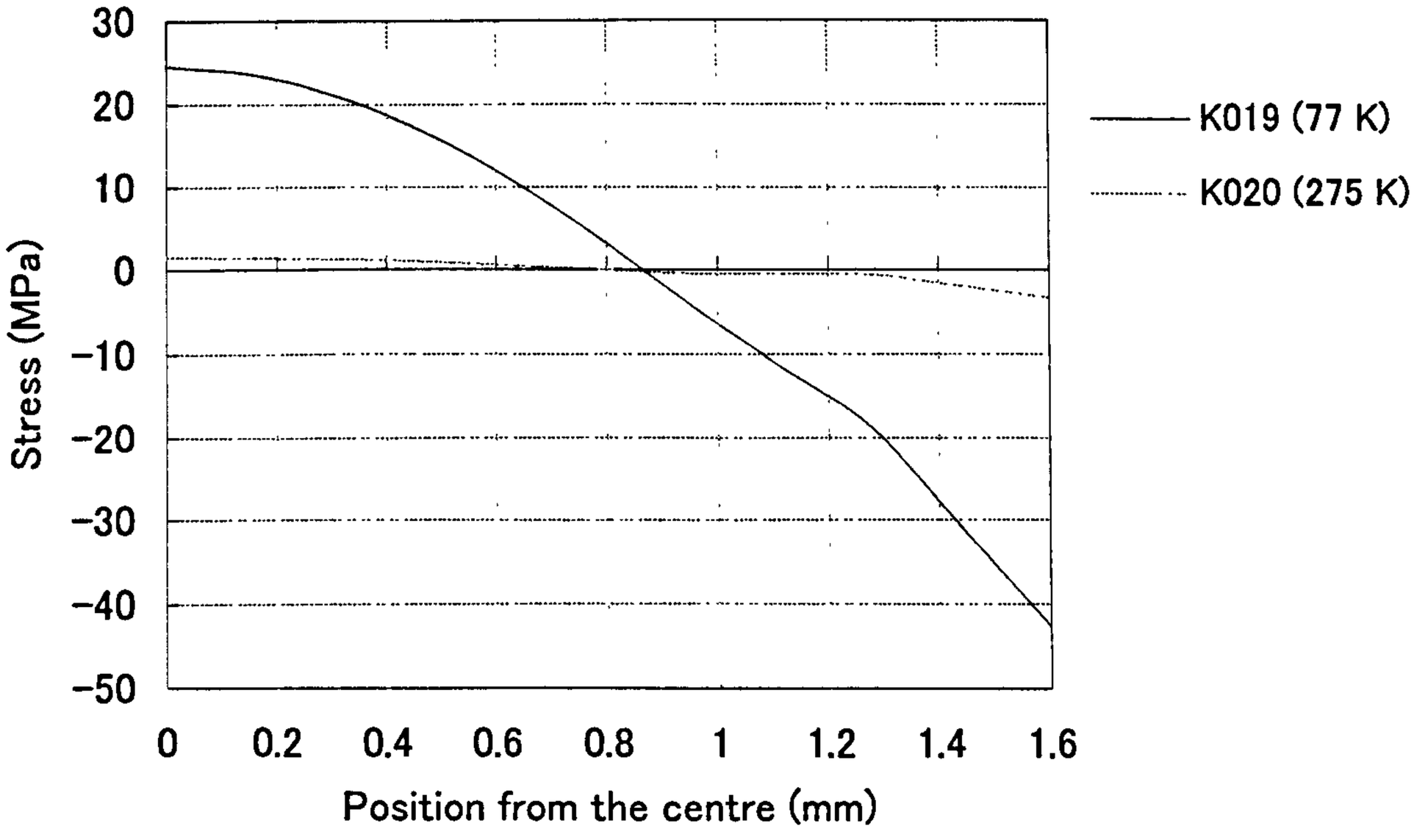

Comparison of the effect of different cooling temperatures, using tensile bars. (i) Stress obtained using liquid nitrogen (K019). (ii) Stress obtained using ice water

Fig. 4.6.1.2 Comparison of the effect of different cooling temperatures, using tensile bars

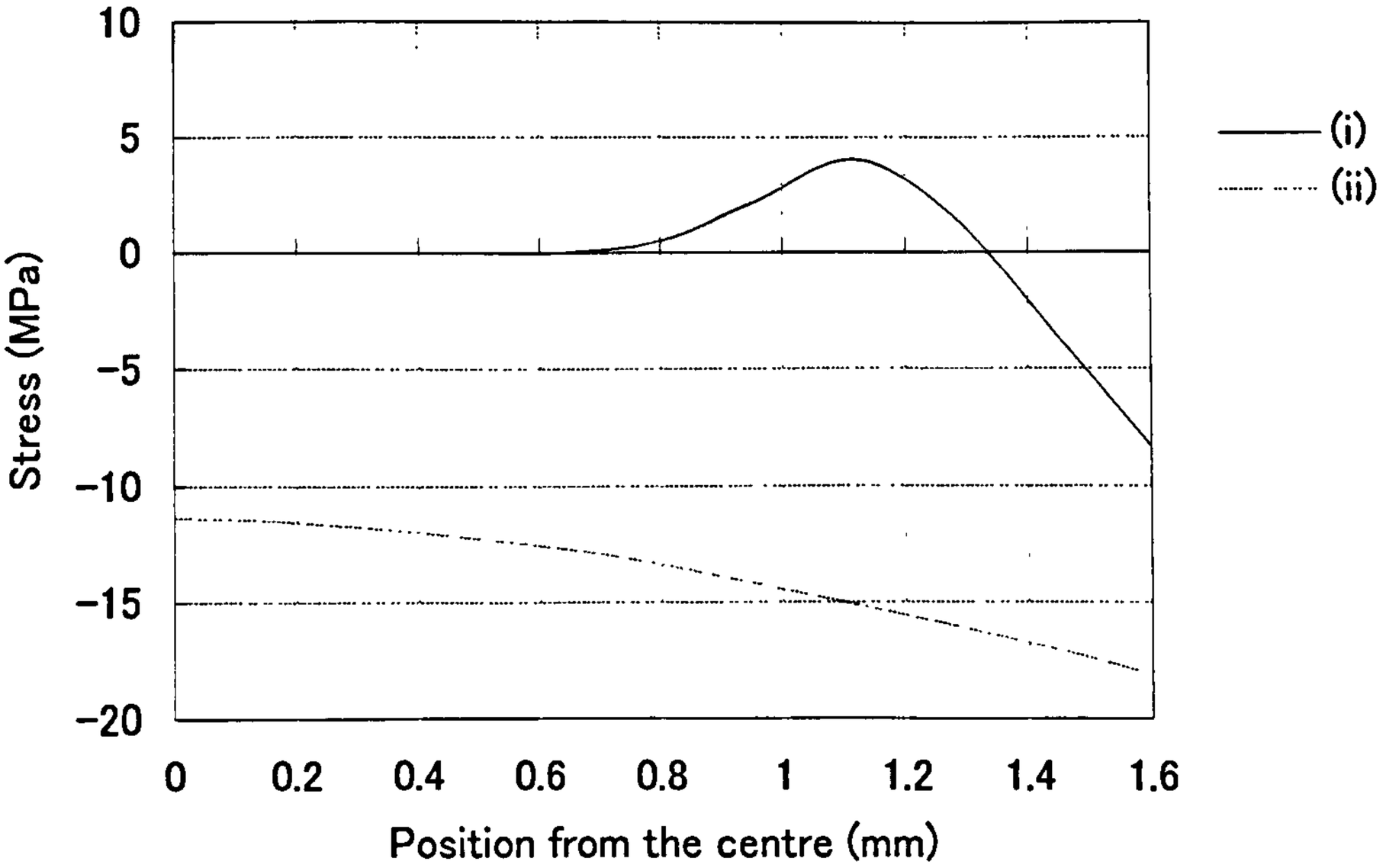

Temperature (de-mould) and pressure induced stresses. (i) Temperature induced stress in the mould. (ii) Pressure induced stress.

Fig. 4.6.1.3 Temperature (in mould) and pressure induced stresses (K013)

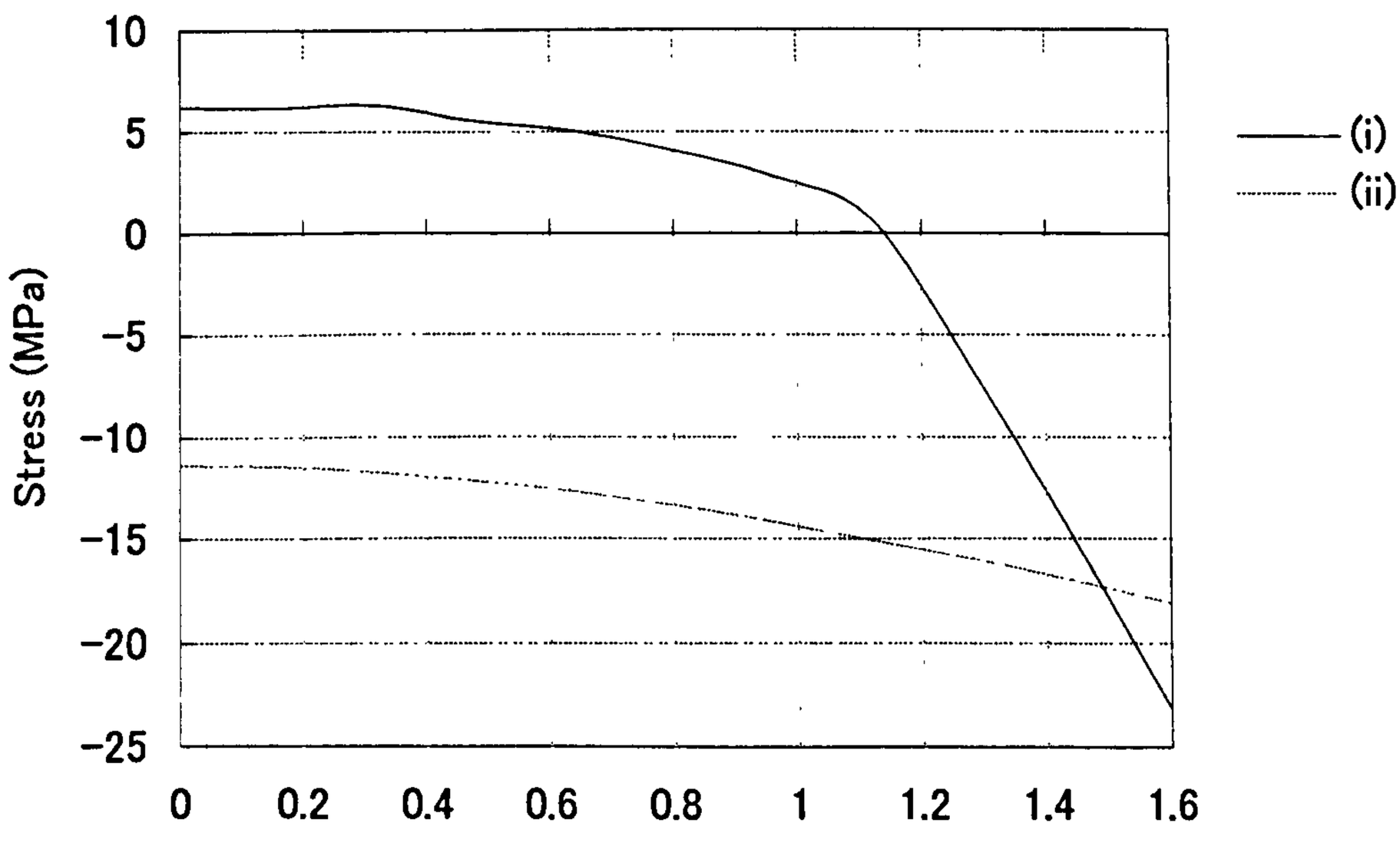

Temperature(de-mould) and pressure induced stresses. (i) Temperature induced stress in the mould. (ii) Pressure induced stress.

Fig. 4.6.1.4 Temperature (in mould) and pressure induced stresses (K0171)

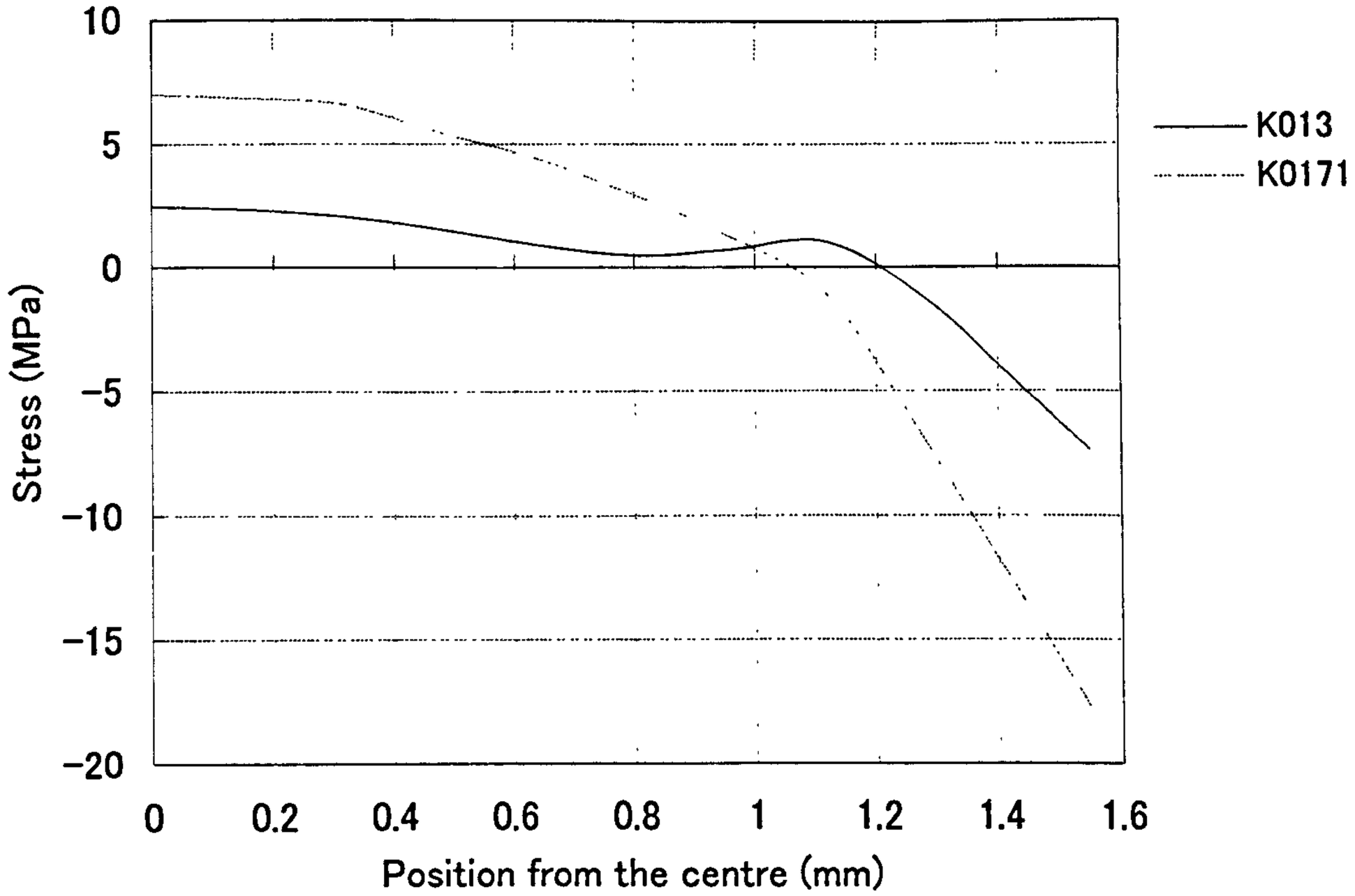

Comparison of effect of mould release agent, using straight bars. (i) Stress obtained without friction constraint (K013). (ii) Stress obtained with friction constraint

Fig. 4.6.1.5 Comparison of effect of friction constraint, using straight bars

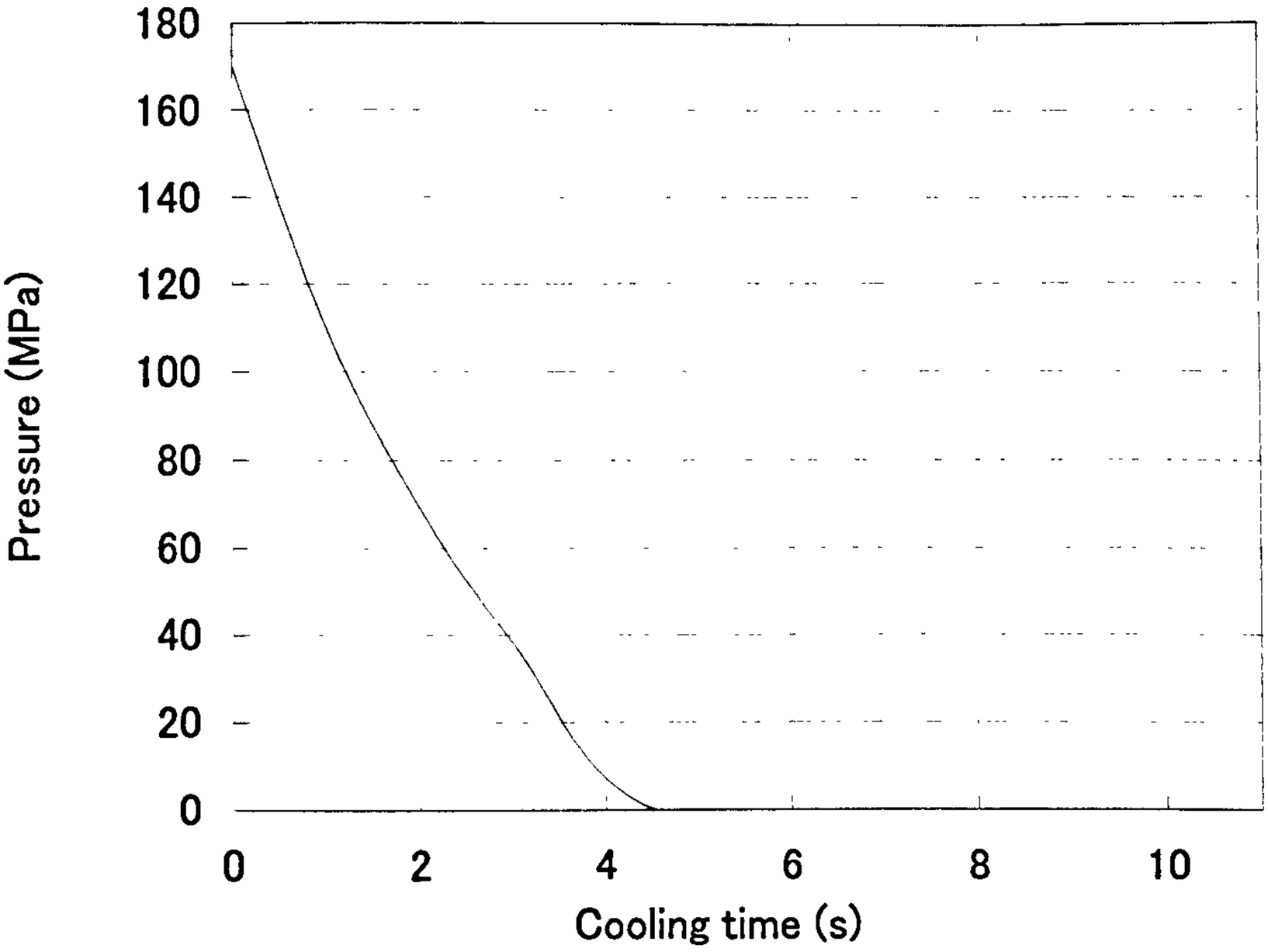

History of the pressure within half of the bar for different cooling times.

Fig. 4.6.2.1 Pressure history

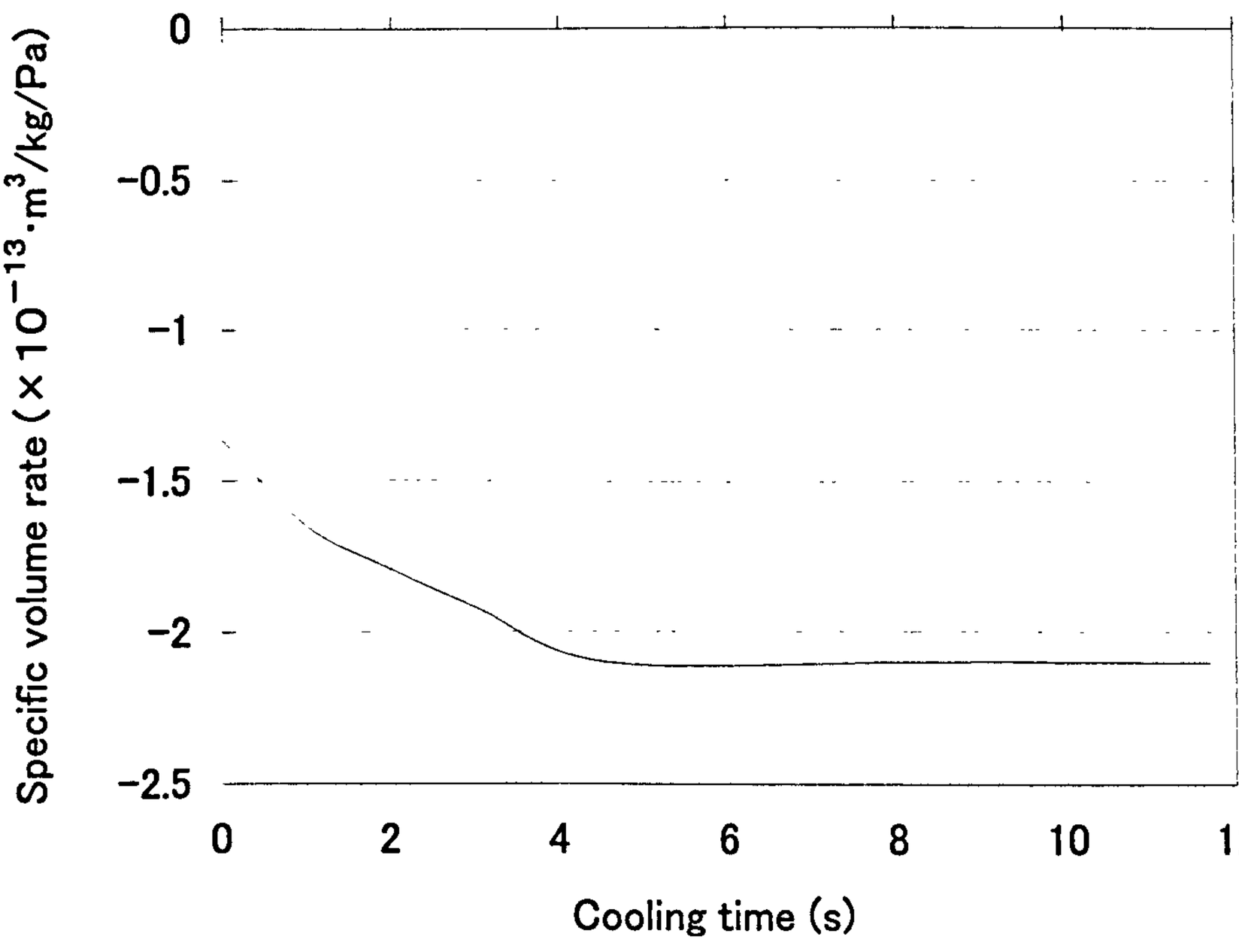

History of the specific volume rate within half of the bar for different cooling times.

Fig. 4.6.2.2 Pressure history

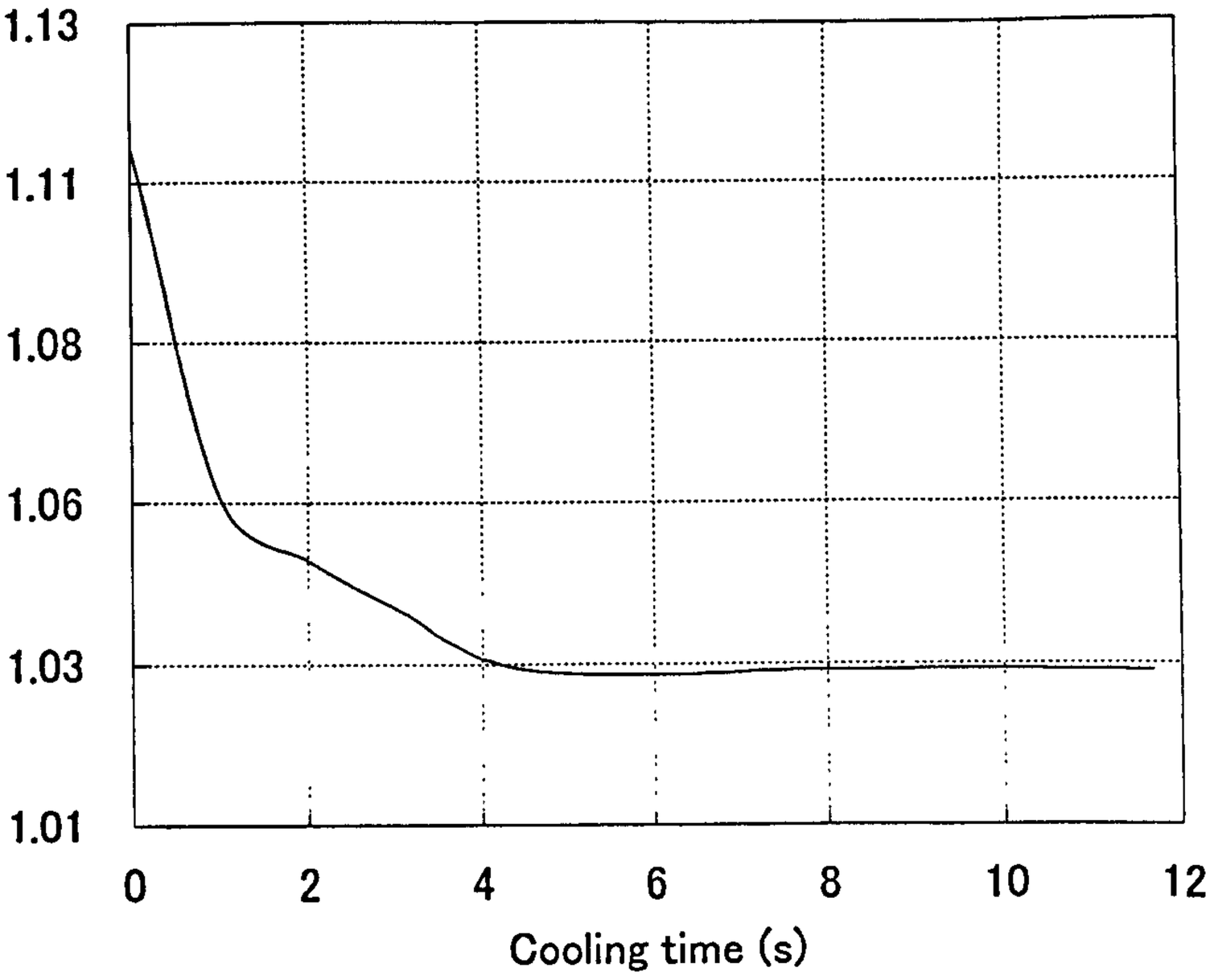

History of the density within the half of the bar for different cooling times.

Fig. 4.6.2.3 History of the density

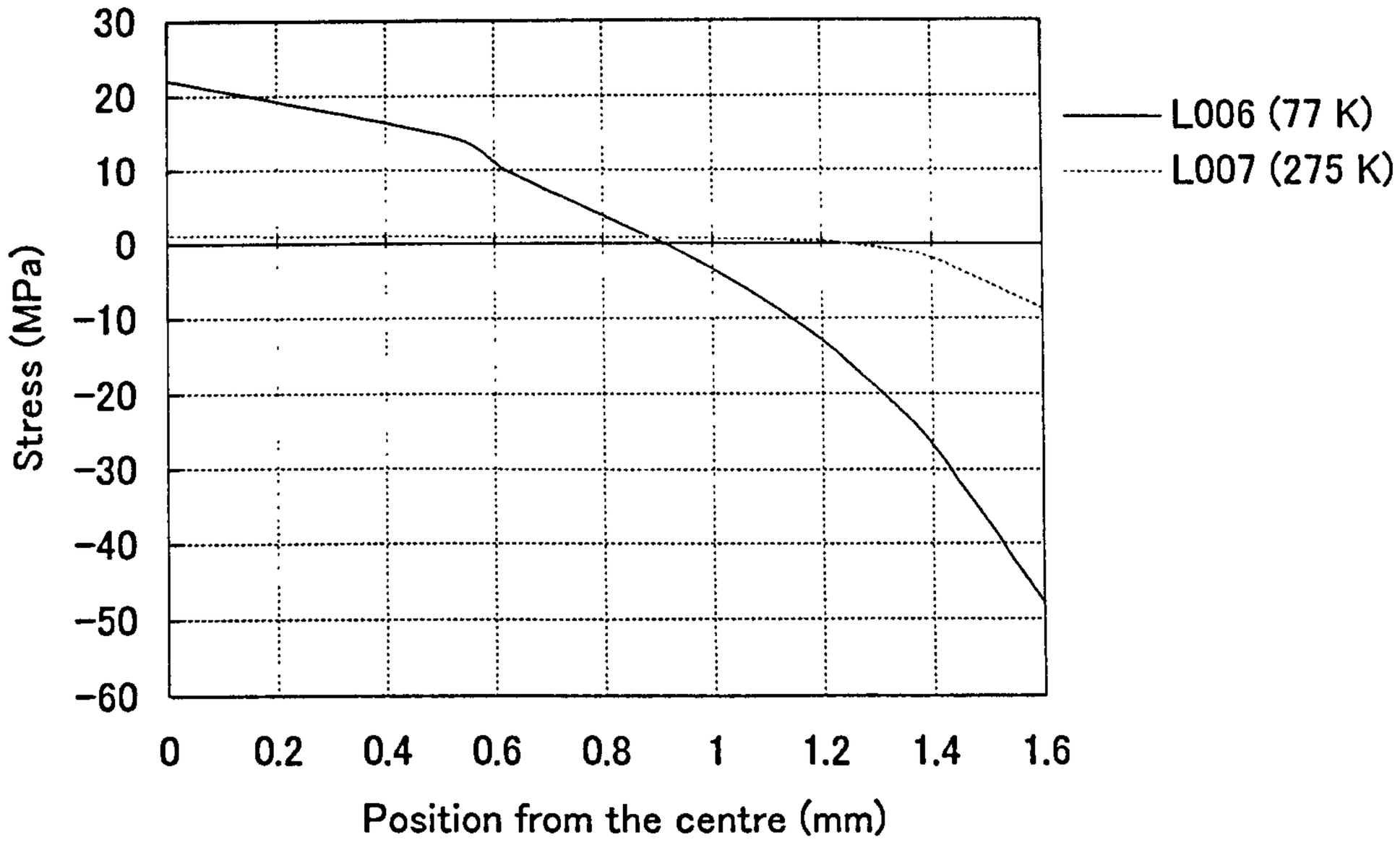

Comparison of the different cooling temperatures, using tensile bars. (i) Stress obtained using liquid nitrogen (L006). (ii) Stress obtained using ice water (L007).

Fig. 4.6.2.4 The result of the stress distribution throughout the moulding

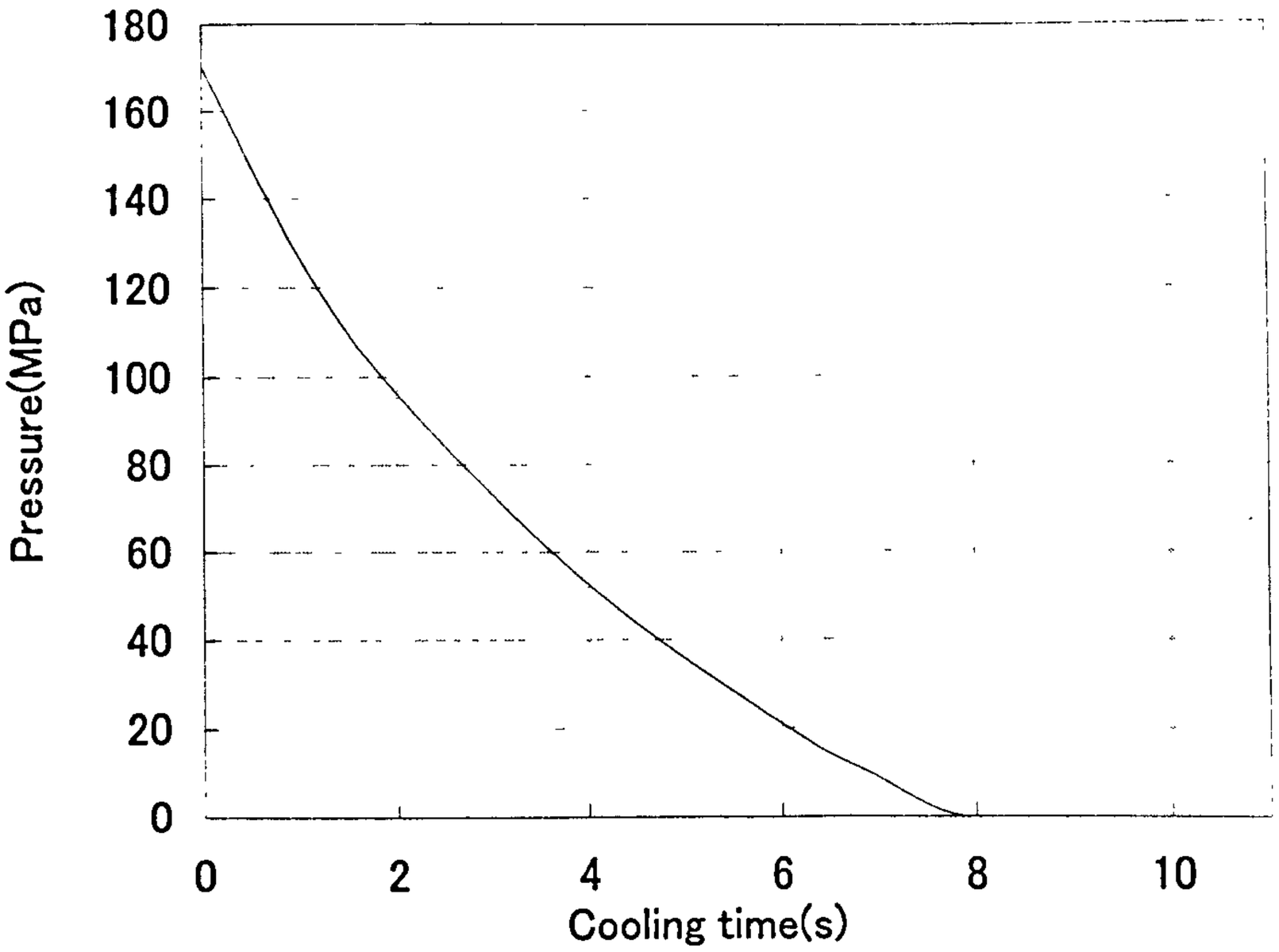

History of the pressure within half of the bar for different cooling times.

Fig. 4.6.2.5 Pressure history

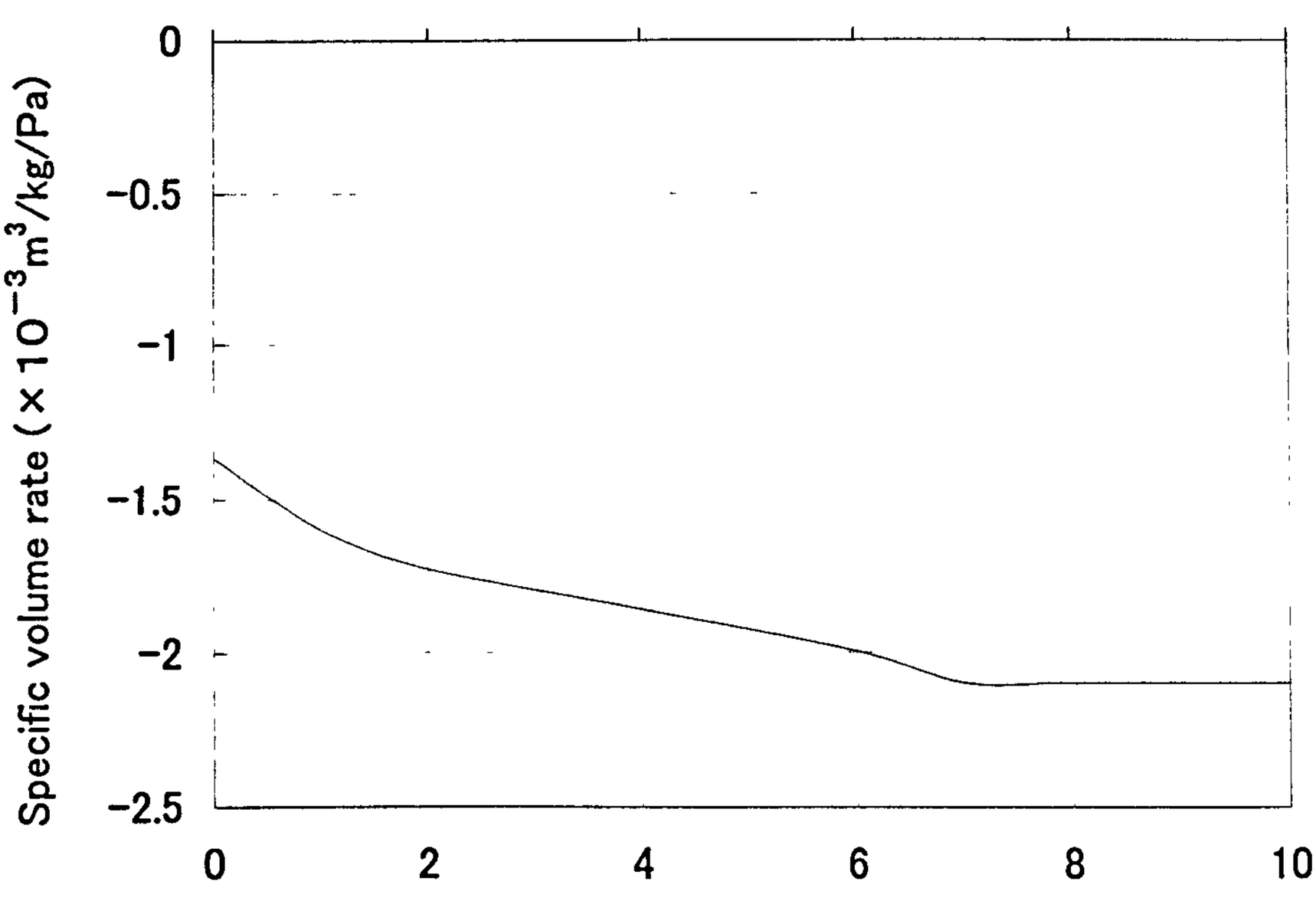

History of the specific volume rate within half of the bar for different cooling times.

Fig. 4.6.2.6 Specific volume rate

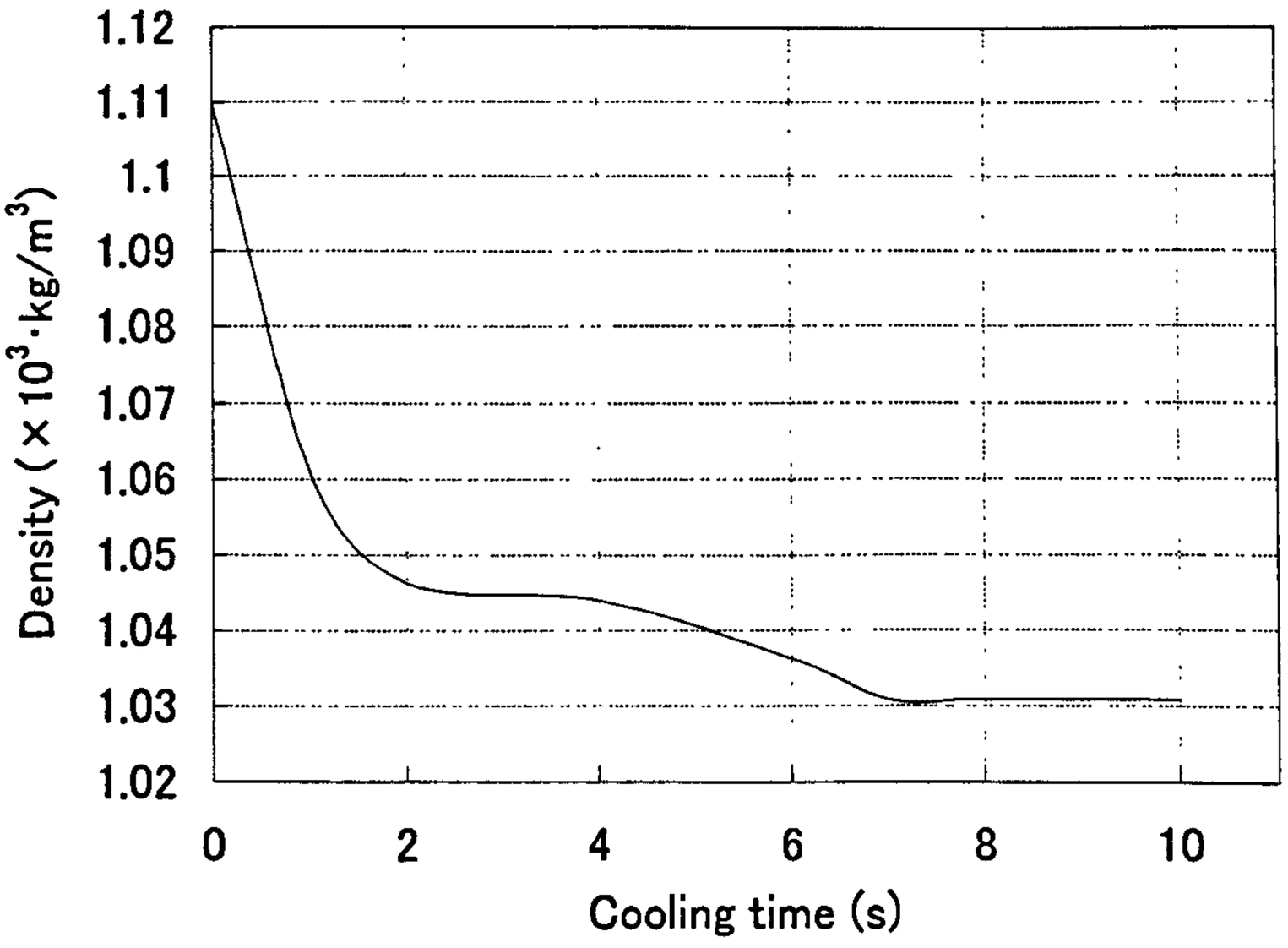

History of the density within the half of the bar for different cooling times.

Fig. 4.6.2.7 History of the density

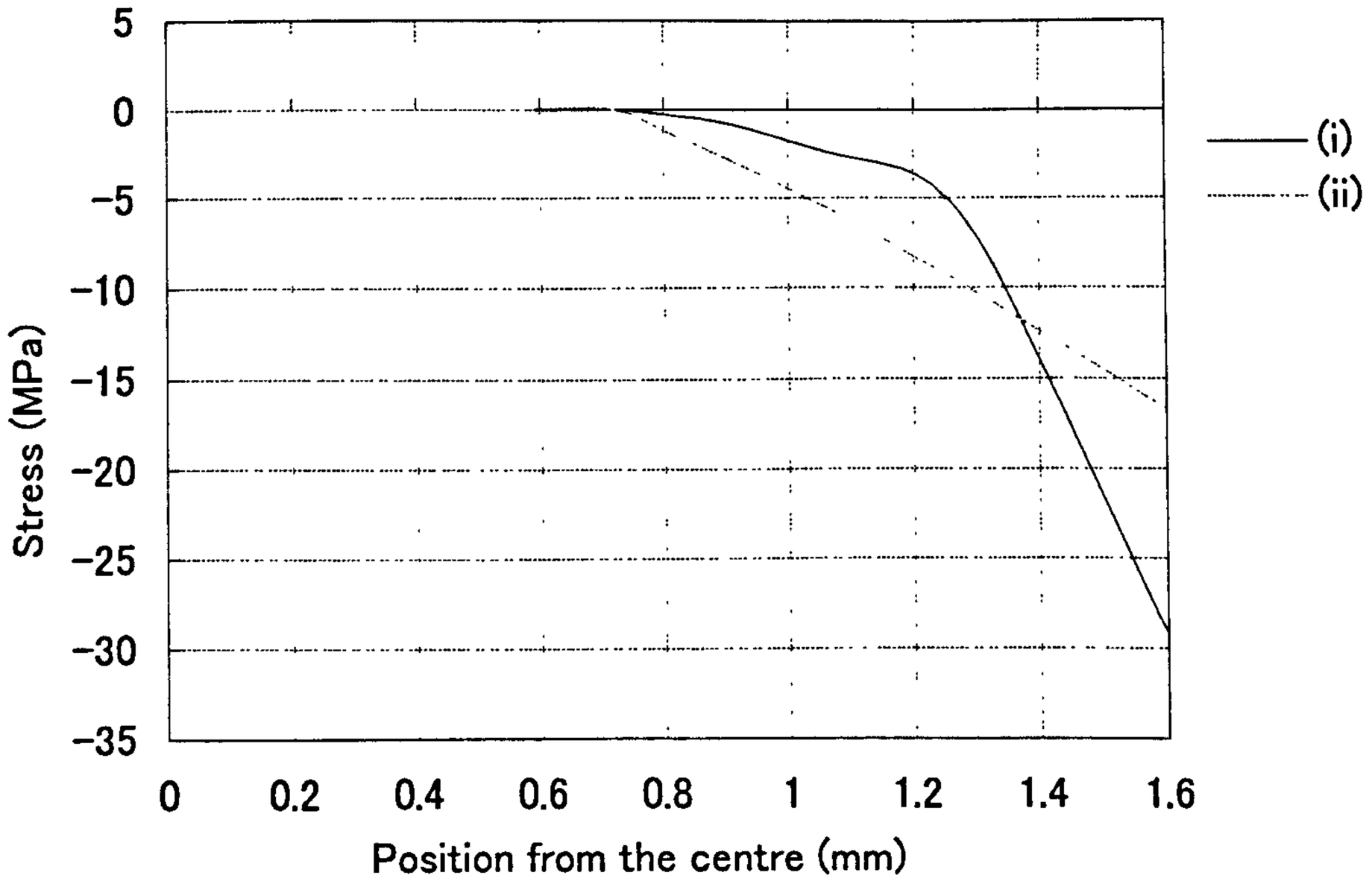

Temperature and pressure induced stresses. (i) Pressure induced stress.
(ii) Temperature induced stress in the mould.

Fig. 4.6.2.8 Temperature (in mould) and pressure induced stresses (L004)

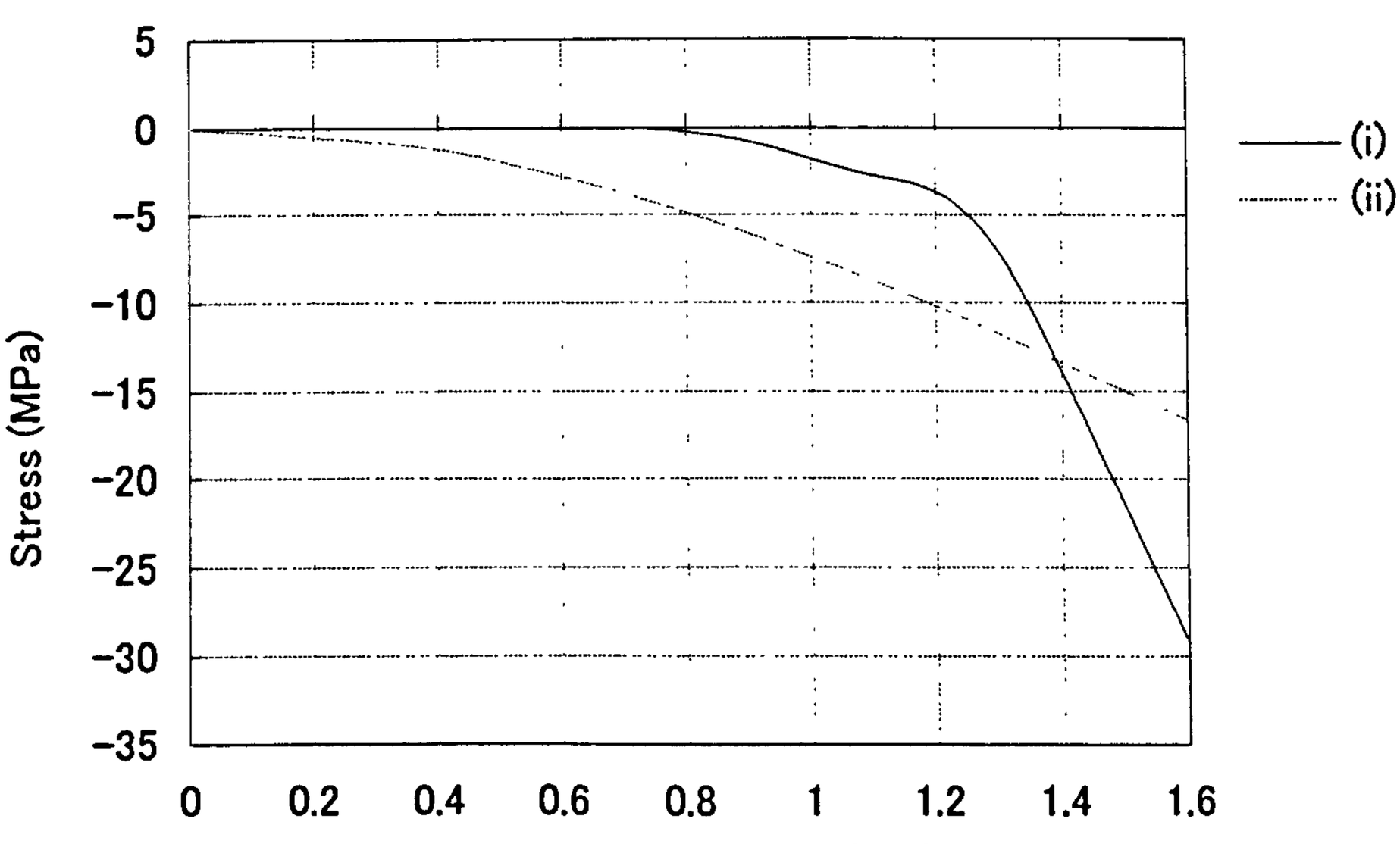

Temperature and pressure induced stresses. (i) Pressure induced stress.
(ii) Temperature induced stress in the mould.

Fig. 4.6.2.9 Temperature (in mould) and pressure induced stresses (L005)

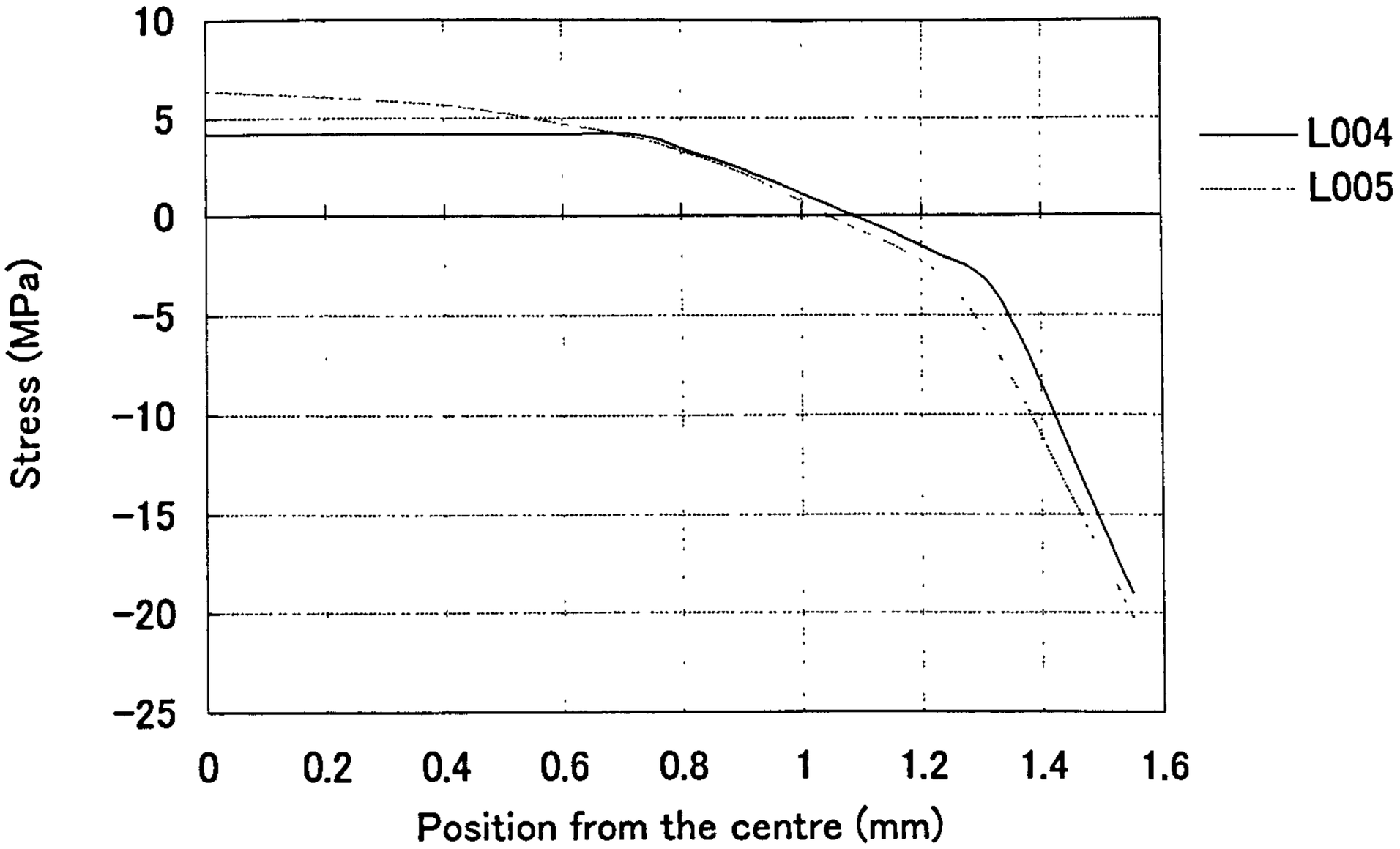

Comparison of effect of mould release agent, using straight bars. (i) Stress obtained without friction constraint (L004). (ii) Stress obtained with friction constraint (L005).

Fig. 4.6.2.10 Comparison of effect of friction constraint, using straight bars

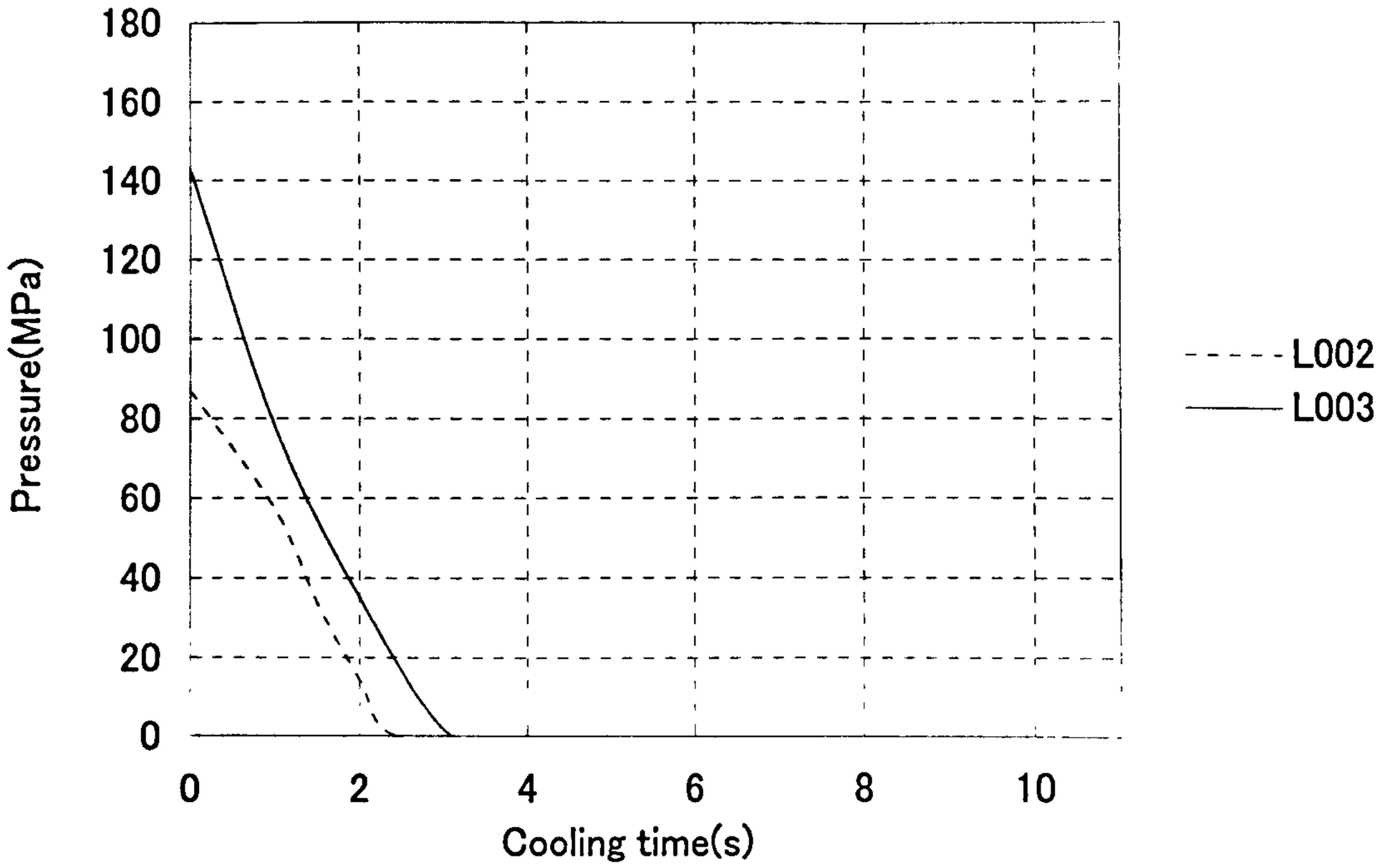

History of the pressure within half of the bar for different injection pressures.

Fig. 4.6.2.11 Pressure history

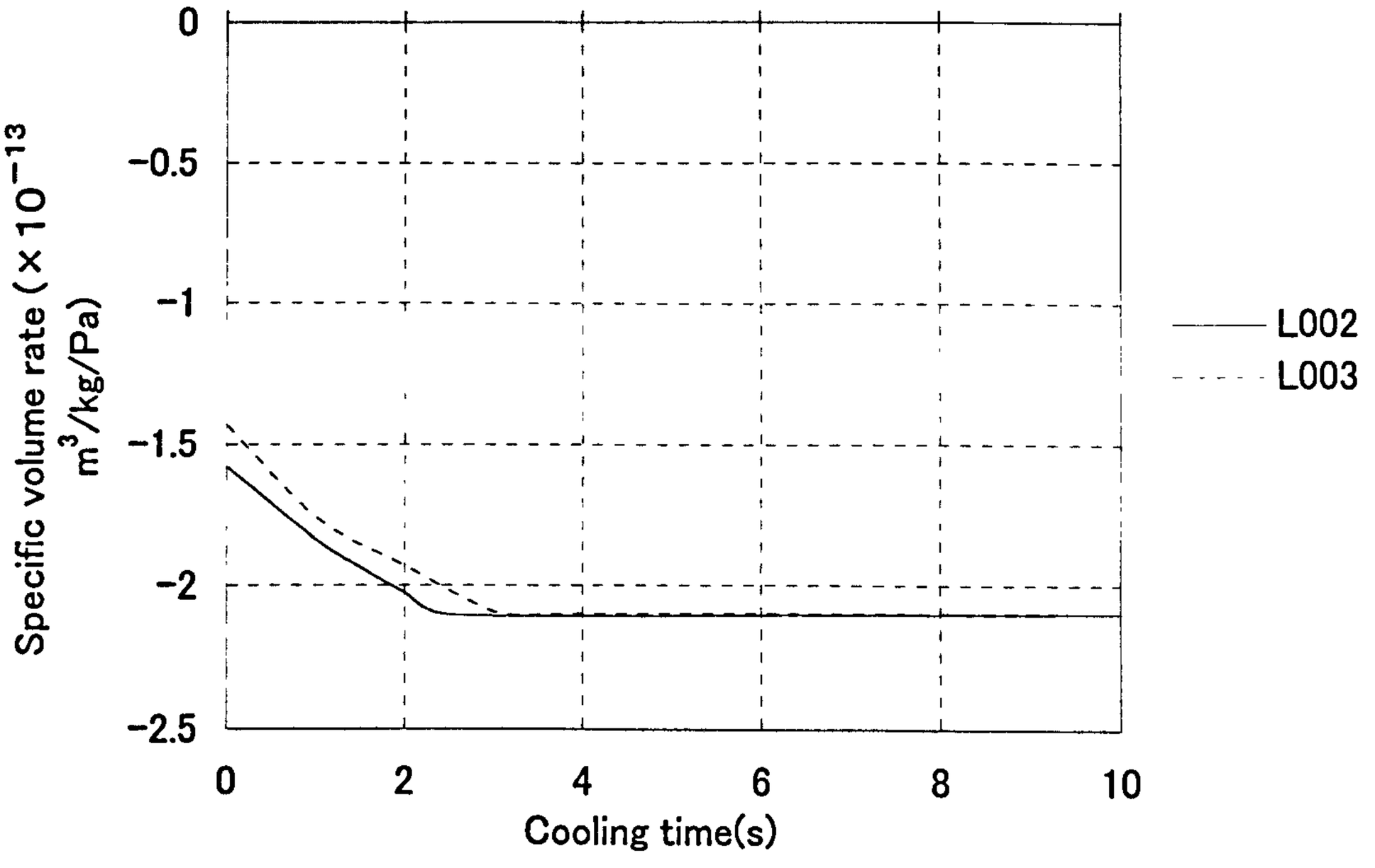

History of the specific volume rate within half of the bar for different injection pressures

Fig. 4.6.2.12 Specific volume rate

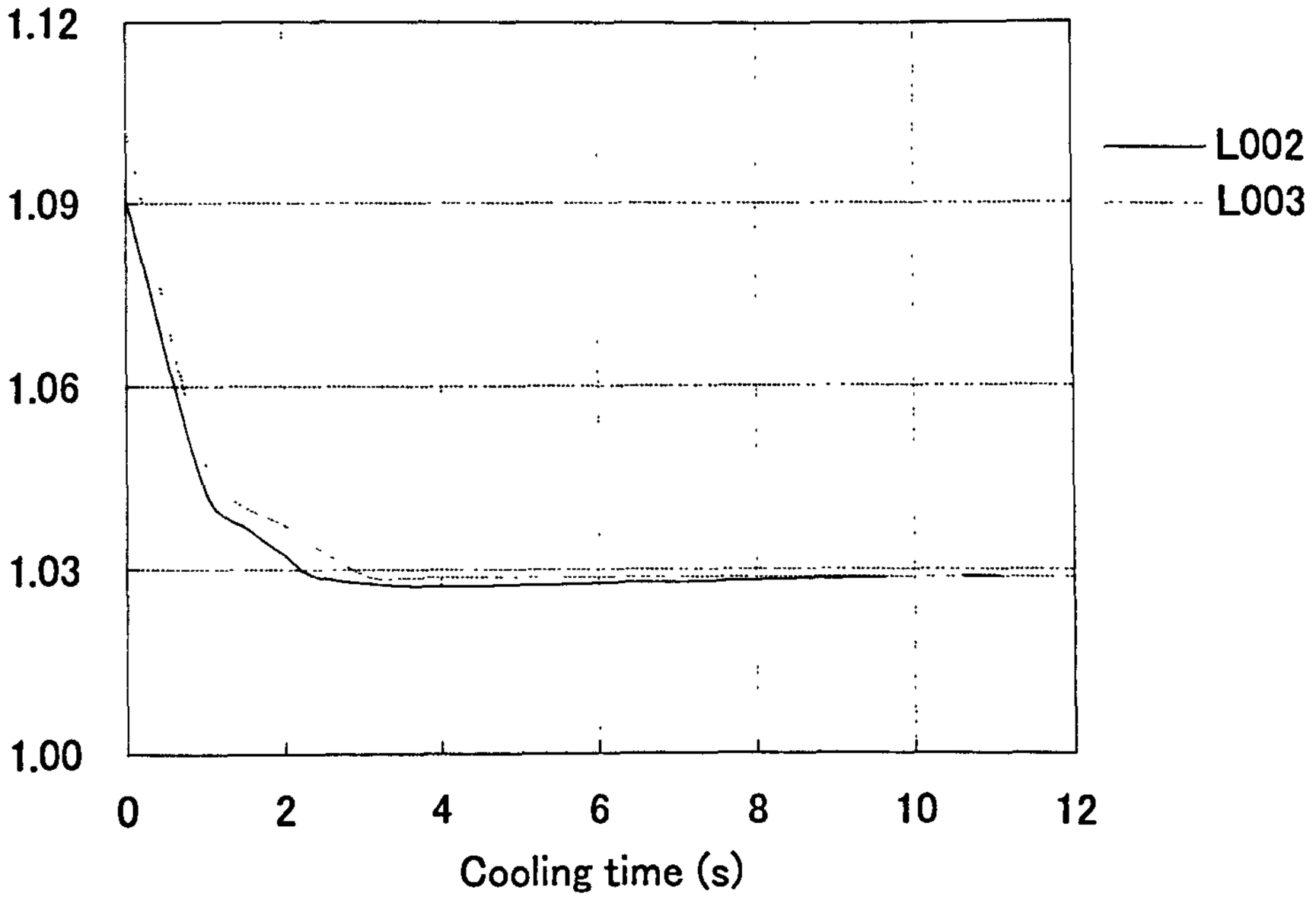

History of the density within half of the bar for different injection pressure.

Fig. 4.6.2.13 History of the density

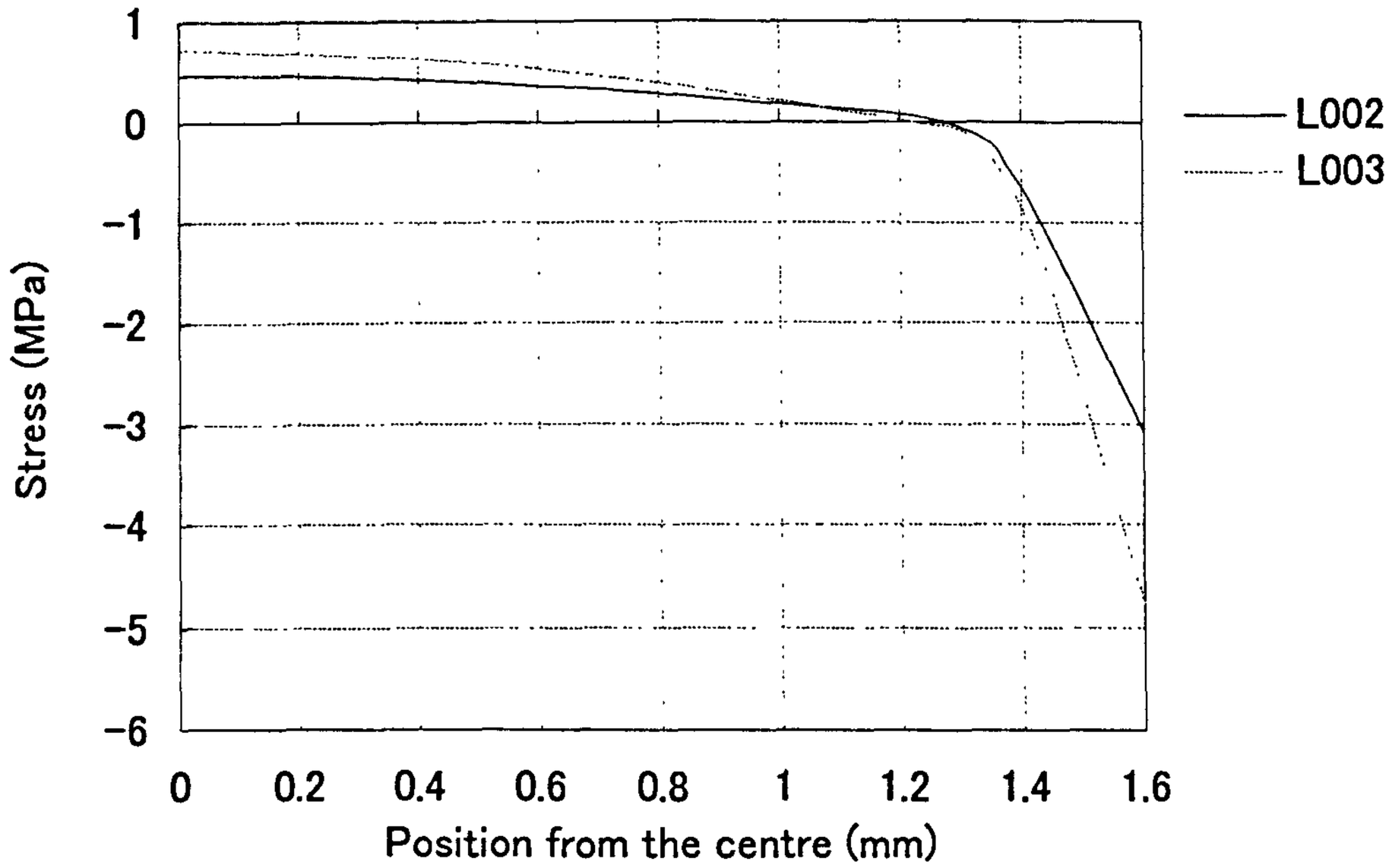

Comparison of effect of injection pressure (i) Stress obtained using 143 MPa injection pressure (L002). (ii) Stress obtained using pressure 87 MPa (L003).

Fig. 4.6.2.14 Comparison of effect of injection pressure

CHAPTER 5

EXPERIMENTAL

5.1 Materials and preparation of samples

5.1.1 Materials

Polystyrene (Dow chemical DE409) was used. The material properties are shown in Table 5.1.1. These data and polystyrene were kindly sent by Dow chemical.

Conductivity	0.138 ($W \cdot m^{-1} \cdot °C^{-1}$)	
Specific Heat	1811 ($J \cdot kg^{-1} \cdot °C^{-1}$)	
Melt Density	887 ($kg \cdot m^{-3}$)	
Solid Density	1049.82 ($kg \cdot m^{-3}$)	
Ejection Temperature	102 (°C)	
No Flow Temperature	130 (°C)	
Tensile Modulus Parallel	3400 (MPa)	
Tensile Modulus Perpendicular	3400 (MPa)	
Poisson Ratio	0.35	
Viscosity		
Temperature (°C)	Shear rate (s^{-1})	Viscosity (Pa·s)
200	1000	168.1
220	100	529.2
220	1000	121.2
220	10000	21.8
240	100	347.4
240	1000	87.4
Specific Volume		
Temperature (°C)	Pressure (MPa)	Specific Volume (m^3/kg)
0	0	948
0	160	919
20	0	953
20	160	921
103.2	0	972
160.3	160	937
210	0	1036
210	160	952
250	0	1060
250	160	965

Table 5.1.1 Properties of DE409

5.1.2 Injection moulding

The Samples were prepared using a Butler-Smith 100/60 reciprocating screw machine with a single end gated tool. The material was moulded into ASTM D638 type I tensile test bars (190×12.7×3.2 mm, Fig. 5.1.1) and straight test bars (190×12.7×3.2 mm, Fig. 5.1.2) with a deep gate system (2.5 mm) and a shallow gate system (0.5 mm). The moulding conditions are shown in Fig. 5.1.3 and Table 5.1.2.

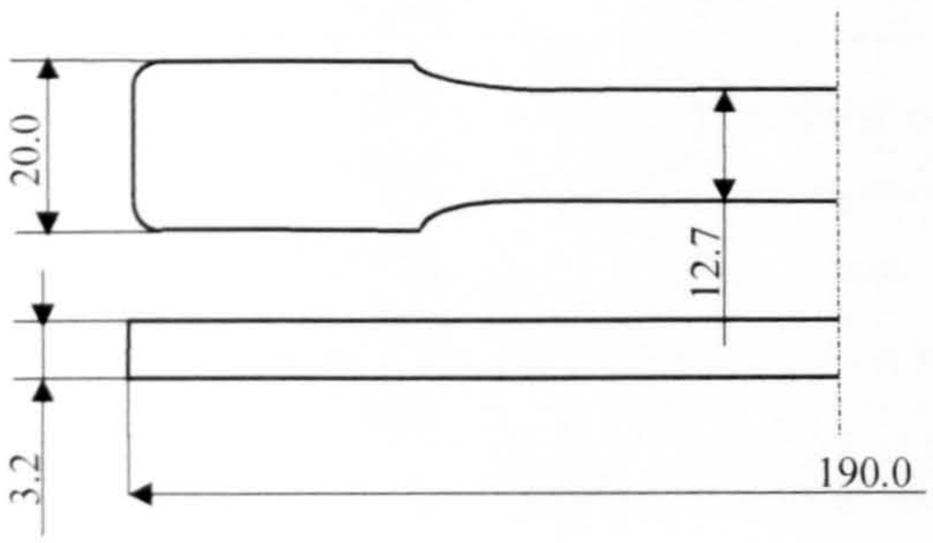

(The dimensions are in mm)

Fig.5.1.1 Geometry of tensile bars.

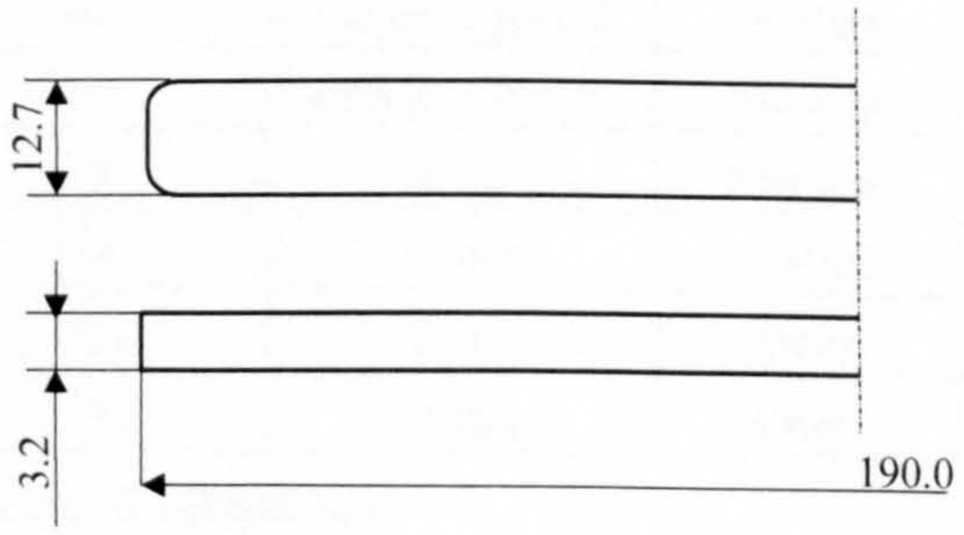

(The dimensions are in mm)

Fig.5.1.2 Geometry of straight bars.

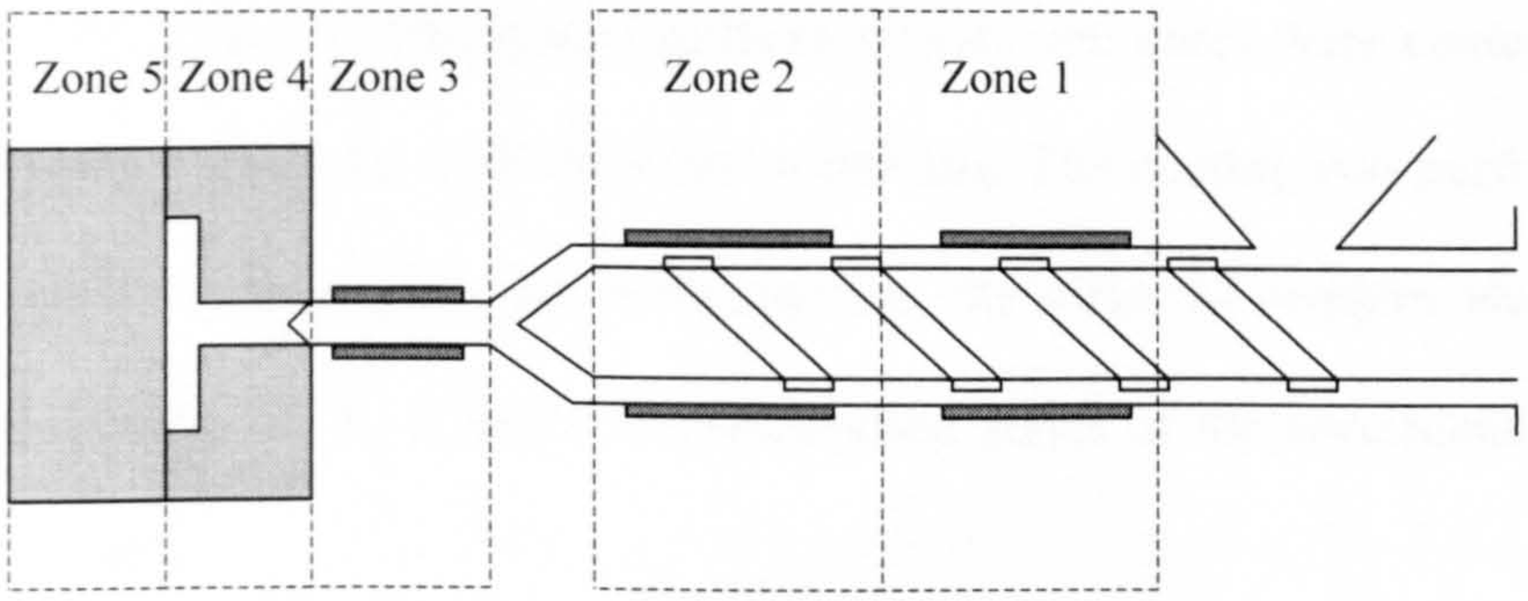

Fig. 5.1.3 Position of the cooling and heating system

Injection pressure (MPa)	Temperature (°K)					Injection Time (s)	Cooling Time (s)
	Zone 1	Zone 2	Zone 3	Zone4	Zone 5		
170	443 (190 °C)	443 (190 °C)	443 (190 °C)	315 (42 °C)	315 (42 °C)	11.0	12.01

Table 5.1.2 Moulding conditions

5.1.3 Preparation conditions for specimens

The over all preparation conditions the samples is shown in Table 5.1.3. Individual treatment of the samples is described later.

Sample	Bar type	Mould release agent	Coolant temperature (K)	Coolant	Gate system
W	Tensile	NO	275	Water	Shallow
MW	Tensile	YES	275	Water	Shallow
E	Tensile	NO	293	Ethylene glycol	Shallow
ME	Tensile	YES	293	Ethylene glycol	Shallow
a	Straight	NO	275	Water	Shallow
b	Straight	YES	275	Water	Shallow
c	Straight	YES	275	Water	Deep
d	Straight	NO	275	Water	Deep

Table 5.1.3 Conditioning of specimens

5.1.3.1 Mould release agent

Mould release agent (Rocol non silicone mould release spray) was used for the series of samples, MW, ME, a, and c. The mould surfaces (cavity and core) were coated by the mould release agent each cycle of the injection moulding. The coating was performed as quickly as possible. In order to avoid contamination, the series of samples were made after series of samples, W, E, a, and d (corresponding series of the specimens without mould release agent).

5.1.3.2 Coolant and coolant temperature

As soon as samples were ejected, they were transferred into a coolant, either ice-water or ethylene glycol for 10 minutes. The transfer was performed as quickly as possible, less than 10 sec after completing mould filling. Other samples made in the same conditions were allowed to cool in air. The samples cooled in air were stored at room

temperature.

Note: 5.1.3.1: In order to avoid the samples are not wetted by water, ethylene glycol was chosen as a coolant because they are coated with mould release agent.

5.2 Residual stress measurement

Residual stresses occur when polymers are injection-moulded, and depend on the injection pressure, the rate of cooling (both in mould and after demoulding) and many other factors. The stress magnitude changes with time, temperature, and the conditions of the environment after being injection moulded.

5.2.1 The layer removal method

The residual stress distribution was determined using the layer removal procedure. An Elliott high-speed milling machine and a single point cutter were used to remove successive layers. The sample bar was held on the machine bed by a vacuum clamp. The path traced out by the cutter was slightly larger than that of the width of the sample so that one sweep was sufficient to remove each successive uniform layer. In order to avoid building up heat, thin uniform layers (0.2 mm in average) were removed from one surface of the sample by the cutter. The cutting was started from the gate direction in order to standardise the surface condition. After each layer was removed, the radius of curvature of the sample was measured using a laser and the optical lever principle[152-157]. Then a plot was developed of curvature versus depth of removal, and this was then used to calculate residual stress, using the Treuting and Read procedure.[148,149,155]

5.2.2 Curvature measurement and calculation

The method was based on optical reflection. A highly-directional laser beam was

directed at different selected points of the sample and curvature was characterised according to the direction of the laser reflections from slivers of glass attached to the surface of the sample using water as adhesive. The arrangement is shown in Fig. 5.2.1.

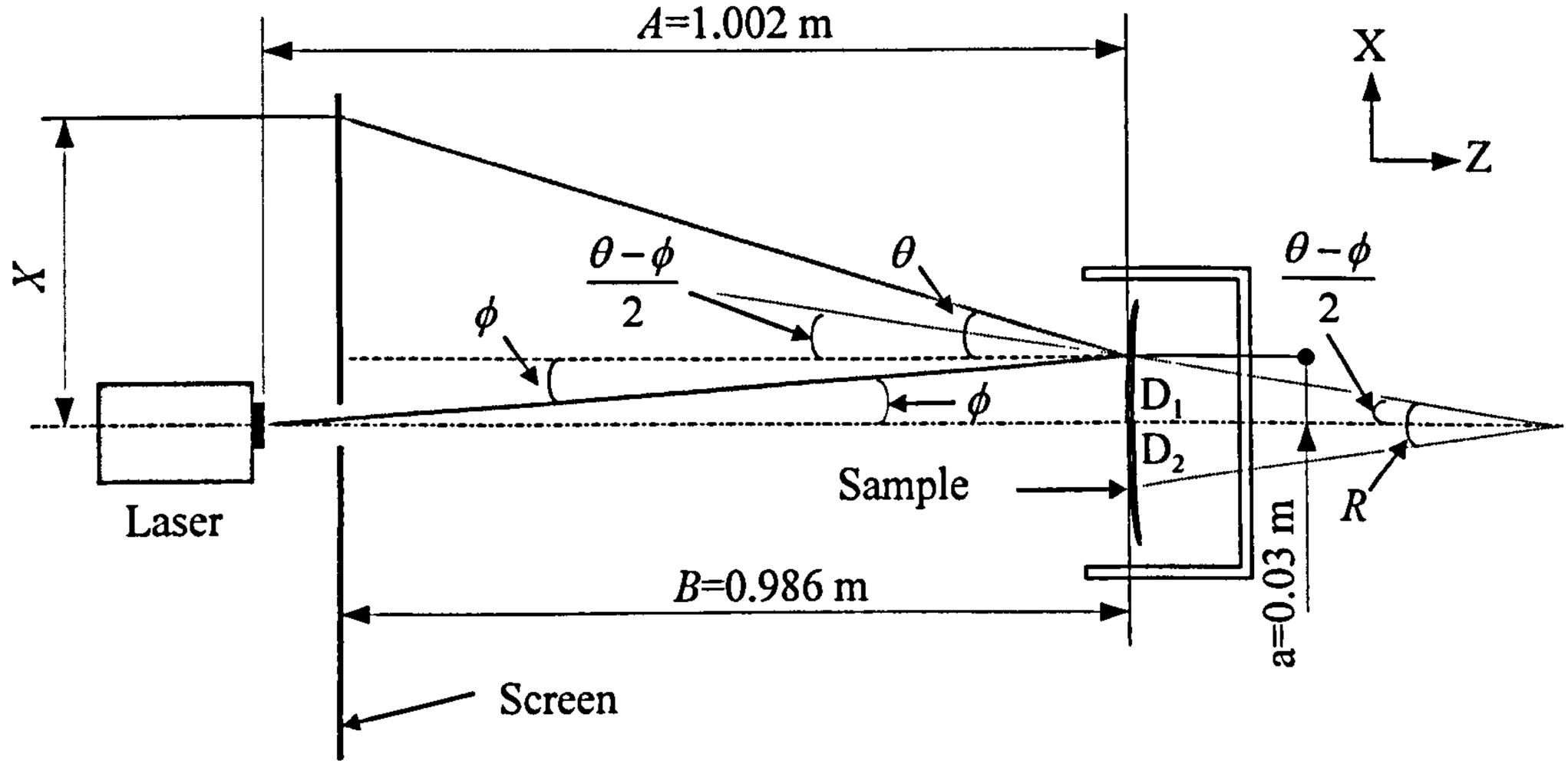

Fig. 5.2.1 Diagram showing laser reflections and construction lines

A (1.002 m) is the distance between the sample and the pivot point about which the laser is rotated during measurements. B (0.986 m) is the distance between the screen and the sample, R is the radius of curvature of the sample, X is a measured distance between the centre of the graduated screen and the reflected light spot and a (0.03 m) is a half of the separation of the marks on the sample.

From Fig. 5.2.1,

$$\sin\left(\frac{\theta-\phi}{2}\right)=\frac{a}{R} \tag{5.2.1}$$

$$\tan\theta=\frac{X-a}{B} \tag{5.2.2}$$

$$\tan\phi = \frac{a}{A} \tag{5.2.3}$$

all the angles involved are small so that we can rewrite equations.

$$\frac{\theta - \phi}{2} = \frac{a}{R} \tag{5.2.4}$$

$$\theta = \frac{X - a}{B} \tag{5.2.5}$$

$$\phi = \frac{a}{A} \tag{5.2.6}$$

Combining the above equations gives:

$$\frac{a}{R} = \frac{x - a}{2B} - \frac{a}{2A} \tag{5.2.7}$$

Re-arranging leads to the final equation:

$$\frac{1}{R} = \frac{A(X - a) - Ba}{2BAa} \tag{5.2.8}$$

5.3 Stress relaxation measurement

Stress relaxation data were required for calculations of the relaxation of residual stress in the moulded bars after the bars had cooled to room temperature.

The stress relaxation tests were conducted using Lloyd tensile testing machine T5003 set to maintain a constant strain (Fig. 5.3.1) at a constant temperature (293 K). A cross head speed of 20mm/min was used to apply the initial deformation. The sample was loaded to the selected stress, the cross head movement stopped and the change in the stress with time was recorded.

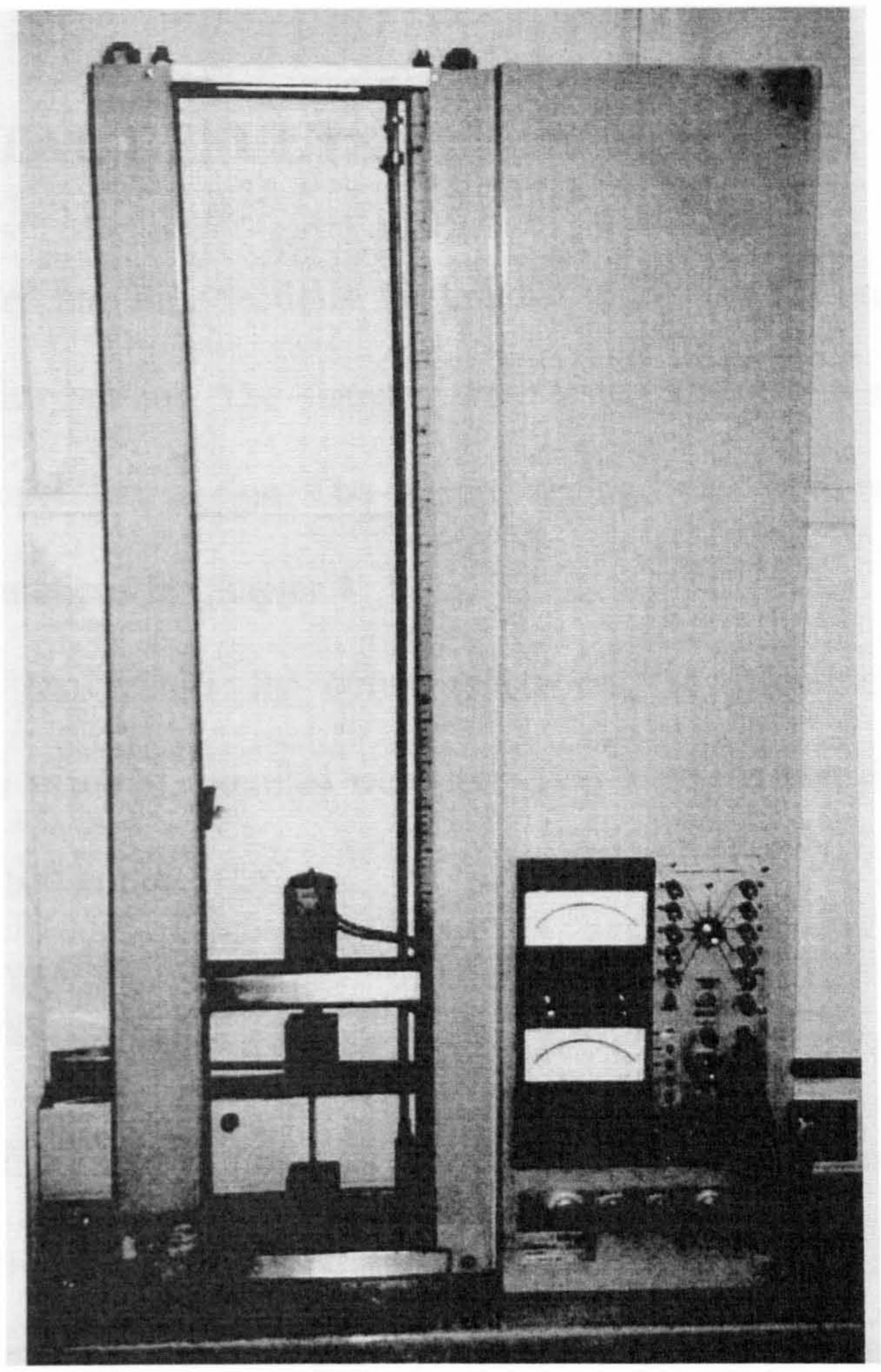

Fig. 5.3.1 Lloyd tensile testing machine T5003

CHAPTER 6

EXPERIMENTAL RESULTS

The results are divided into nine sections. Section 6.1 to Section 6.8 contain the results for residual stress distributions. The samples were tested after the residual stress had decayed in room temperature ageing. The elapsed ageing times were recorded in order to apply to the computations in Chapter 4.

Section 6.9 covers the results for stress relaxation. To examine the relaxation characteristics of the material, samples were tested on a tensile test jig and measured over period of 70 to 100 hours.

6.1 Residual stress

Residual stress distribution measurements were made on different samples. The results have been divided into eight series of samples:

(1) Tensile bars made using a shallow gate system and cooled in ice water (W)

(2) Tensile bars made using mould release agent and a shallow gate system and cooled in ice water (MW)

(3) Tensile bars made using a shallow gate system and cooled in ethylene glycol (E)

(4) Tensile bars made using mould release agent and a shallow gate system and cooled in ethylene glycol (ME)

(5) Straight bars made using a shallow gate system and cooled in ice water, (a)

(6) Straight bars made using mould release agent and a shallow gate system and cooled in ice water (b)

(7) Straight bars made using a deep gate system and cooled in ice water, (c)

(8) Straight bars made using mould release agent and a deep gate system and cooled in ice water (d)

Note 1: The material data on Table. 5.1.1 (Section 5.1.1) were taken to calculate the residual stress.

6.1.1 Comparison of the effect of different cooling temperatures and coolants, using tensile bars (W and E)

These experiments aimed to analyse the effect of different cooling temperatures and thermal properties of different cooling mediums. The results are shown in Fig. 6.1 (p. 144), Fig. 6.2 (p. 144) and Table 6.1. Fig. 6.1 shows curvature measurements as a function of material removed in one half of the bar cooled in ice water, using tensile bars and a shallow gate system (W). The two curves in Fig. 6.2 correspond to cooling in two different mediums just after the injection moulding: ice water (solid line, 275 K) and ethylene glycol (broken line, 293 K). For both analyses the curvature versus depth-removed plots were straight lines, corresponding to parabolic stress distributions. Thus the residual stresses for the two specimens were everywhere proportional[150]. The magnitude of stress in bars cooled in ice water was 1.15 times higher than the value in bars cooled in ethylene glycol.

Sample	Maximum stress (MPa)	Minimum stress (MPa)	Thickness (mm)
W	2.6	-5.2	3.11
E	2.3	-4.6	3.12

Table 6.1

6.1.2 Comparison of the effect of different cooling temperatures and coolants, using tensile bars and mould release agent (MW and ME)

The objective of these experiments was to investigate the effect of different cooling temperatures and thermal properties of cooling mediums. This section also deals with

the effect of the friction (friction constraint) between the mould surfaces and the surfaces of the samples, using mould release agent. The results are shown in Fig. 6.3 (p. 145) and Table 6.2. There are two curves in Fig. 6.3, corresponding to cooling in two different mediums just after the injection moulding: ice water (solid line, 275 K) and ethylene glycol (broken line, 293 K). The residual stress magnitude for the bars which were cooled in ice water was every where 1.18 times higher than the value produced in bars cooled in ethylene glycol.

Sample	Maximum stress (MPa)	Minimum stress (MPa)	Thickness (mm)
MW	2.5	-5.0	3.12
ME	2.15	-4.3	3.12

Table 6.2

6.1.3 Comparison of the effect of mould release agent, using tensile bars (water cooling) (W and MW)

These experiments aimed to analyse the effect of the friction between the mould surfaces and the surfaces of the samples, using mould release agent. The results are shown in Fig. 6.4 (p. 145) and Table 6.3. The two curves in Fig. 6.4 represent W (solid line, without mould release agent) and MW (broken line, using mould release agent). The two curves were virtually the same.

Sample	Maximum stress (MPa)	Minimum stress (MPa)	Thickness (mm)
W	2.6	-5.2	3.12
MW	2.5	-5.0	3.12

Table 6.3

6.1.4 Comparison of the effect of mould release agent, using tensile bars (cooled using ethylene glycol) (E and ME)

The objective of these experiments was to investigate the effect of the friction (friction constraint) between the mould surfaces and the surfaces of the samples, using mould release agent. The results are shown in Fig. 6.5 (p. 146) and Table 6.4.

There are two curves in Fig. 6.5, corresponding to E (solid line, without mould release agent) and ME (broken line, using mould release agent).

The curves were virtually the same.

Sample	Maximum stress (MPa)	Minimum stress (MPa)	Thickness (mm)
E	2.3	-4.6	3.12
ME	2.15	-4.3	3.12

Table 6.4

6.1.5 Comparison of the effect of different gate systems, using straight bars (a and d)

These experiments aimed to analyse the effect of different gate systems. The results are shown in Fig. 6.6 (p. 146) and Table 6.5. The two curves in Fig. 6.6 represent different gate systems: a (solid line, shallow gate system) and d (broken line, deep gate system). The residual stress magnitude for the bars which used the shallow gate system was everywhere 1.39 times higher than the value in bars produced using the deep gate system.

Sample	Maximum stress (MPa)	Minimum stress (MPa)	Thickness (mm)
a	3.2	-6.4	3.20
d	2.3	-4.6	3.21

Table 6.5

6.1.6 Comparison of the effect of different gate systems, using straight bars and mould release agent (b and c)

The objective of these experiments was to investigate the effect of different gate systems using mould release agent. The results are shown in Fig. 6.7 and Table 6.6. There are two curves in Fig. 6.7 (p. 147), corresponding to b (solid line, shallow gate system) and c (broken line, deep gate system). The curves were virtually the same.

Sample	Maximum stress (MPa)	Minimum stress (MPa)	Thickness (mm)
b	1.6	-3.2	3.20
c	1.65	-3.3	3.21

Table 6.6

6.1.7 Comparison of the effect of mould release agent, using straight bars and shallow gate system (a and b)

These experiments aimed to analyse the effect of the friction (friction constraint) between the mould surfaces and the surfaces of the samples, using the shallow gate system. The results are shown in Fig. 6.8 (p. 147) and Table 6.7. The two curves in Fig. 6.8 represent a (solid line, without mould release agent) and b (broken line, with mould release agent). The residual stress magnitudes in the bars without mould release agent were 1.96 times higher than those in bars value produced using mould release agent.

Sample	Maximum stress (MPa)	Minimum stress (MPa)	Thickness (mm)
a	3.2	-6.4	3.20
b	1.6	-3.2	3.20

Table 6.7

6.1.8 Comparison of the effect of mould release agent, using straight bars and deep gate system. (c and d)

The objective of these experiments was to investigate the effect of the friction (friction constraint) between the mould surfaces and the surfaces of the samples, using deep gate system. The results are shown in Fig. 6.9 (p. 148) and Table 6.8. There are two curves in Fig. 6.9, corresponding to c (solid line, with mould release agent) and d (broken line, without mould release agent). The residual stress magnitudes in bars without mould release agent were everywhere 1.4 times higher than the values in bars made using mould release agent.

Sample	Maximum stress (MPa)	Minimum stress (MPa)	Thickness (mm)
c	1.65	-3.3	3.21
d	2.30	-4.6	3.21

Table 6.8

6.2 Stress relaxation measurement

The stress relaxation tests were conducted on tensile tests and the relaxation curves were plotted as load - time diagrams in Fig. 6.10 (p. 148).

There are two curves in Fig. 6.10, corresponding to different initial stress, W1 (solid line, at 21 MPa) and W2 (broken line, at 17 MPa).

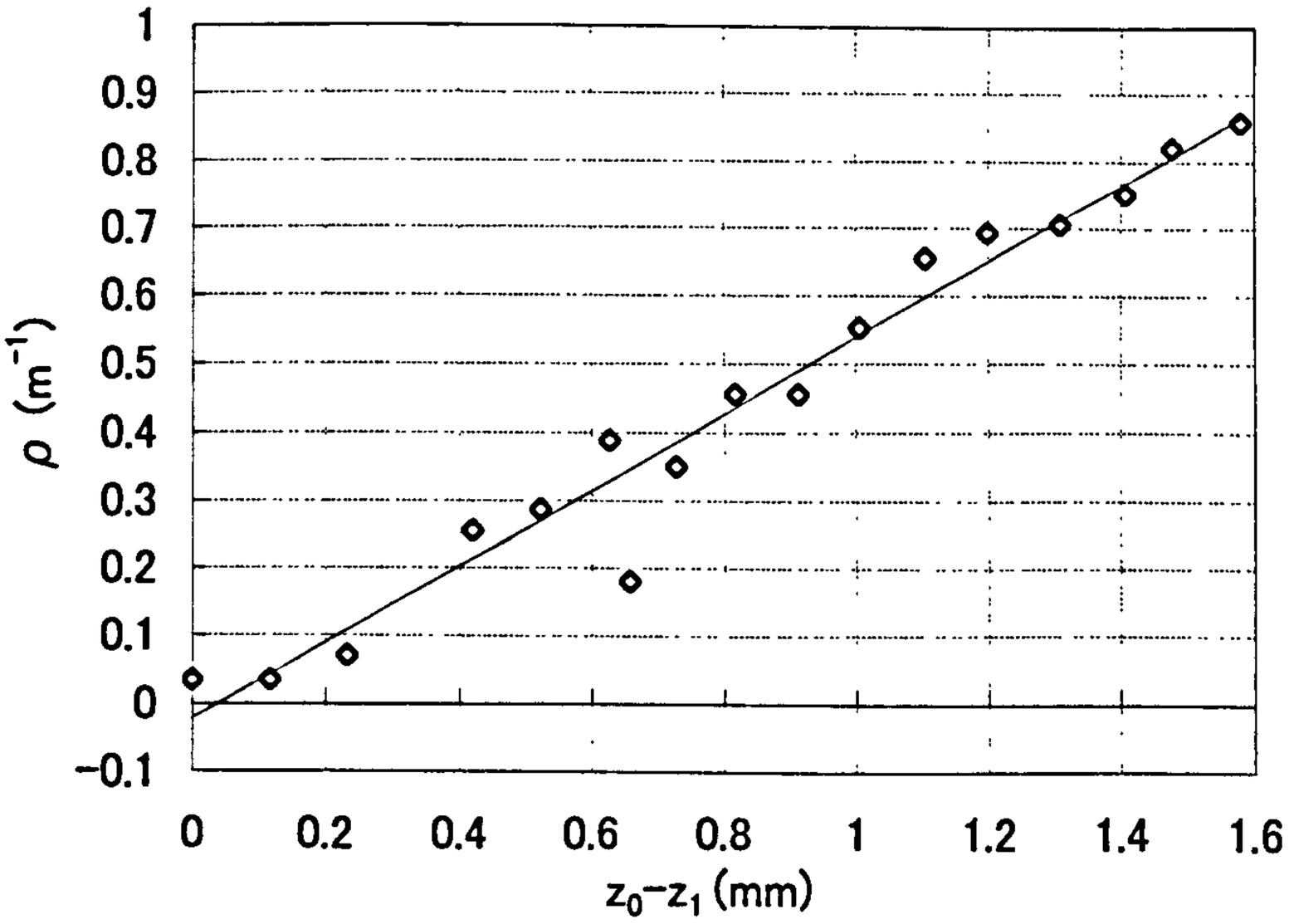

Curvature measurements as a function of material removed in one half of the bar cooled in ice water, using tensile bars and a shallow gate system (W).

Fig. 6.1

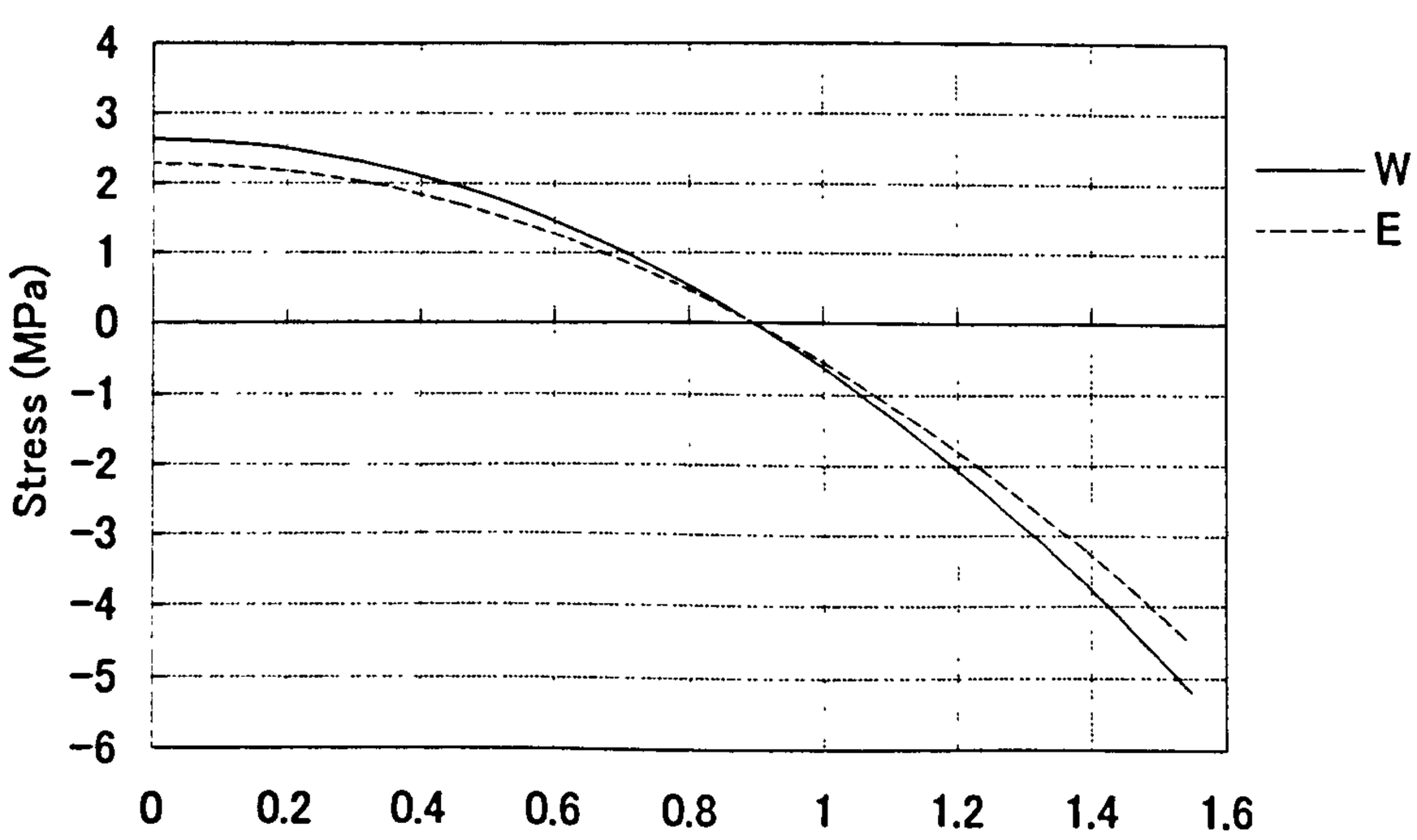

Comparison of the effect of different cooling temperatures and coolants, using tensile bars. (W) Stress obtained using ice water (275 K). (E) Stress obtained using ethylene glycol (293K).

Fig. 6.2

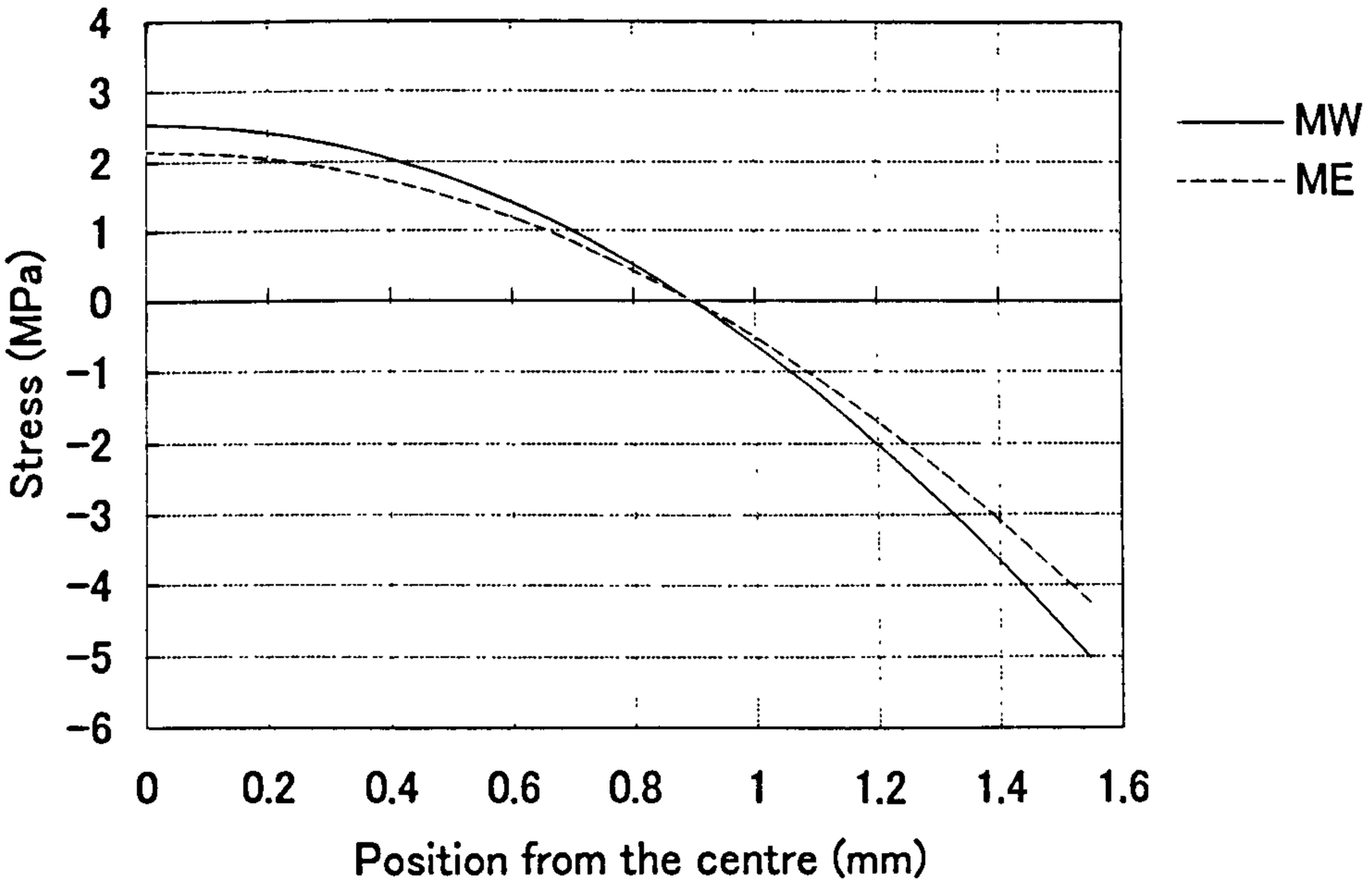

Comparison of the effect of different cooling temperatures and coolants, using tensile bars. Mould release agent was used. (MW) Stress obtained using ice water (275 K). (ME) Stress obtained using ethylene glycol (293 K).

Fig. 6.3

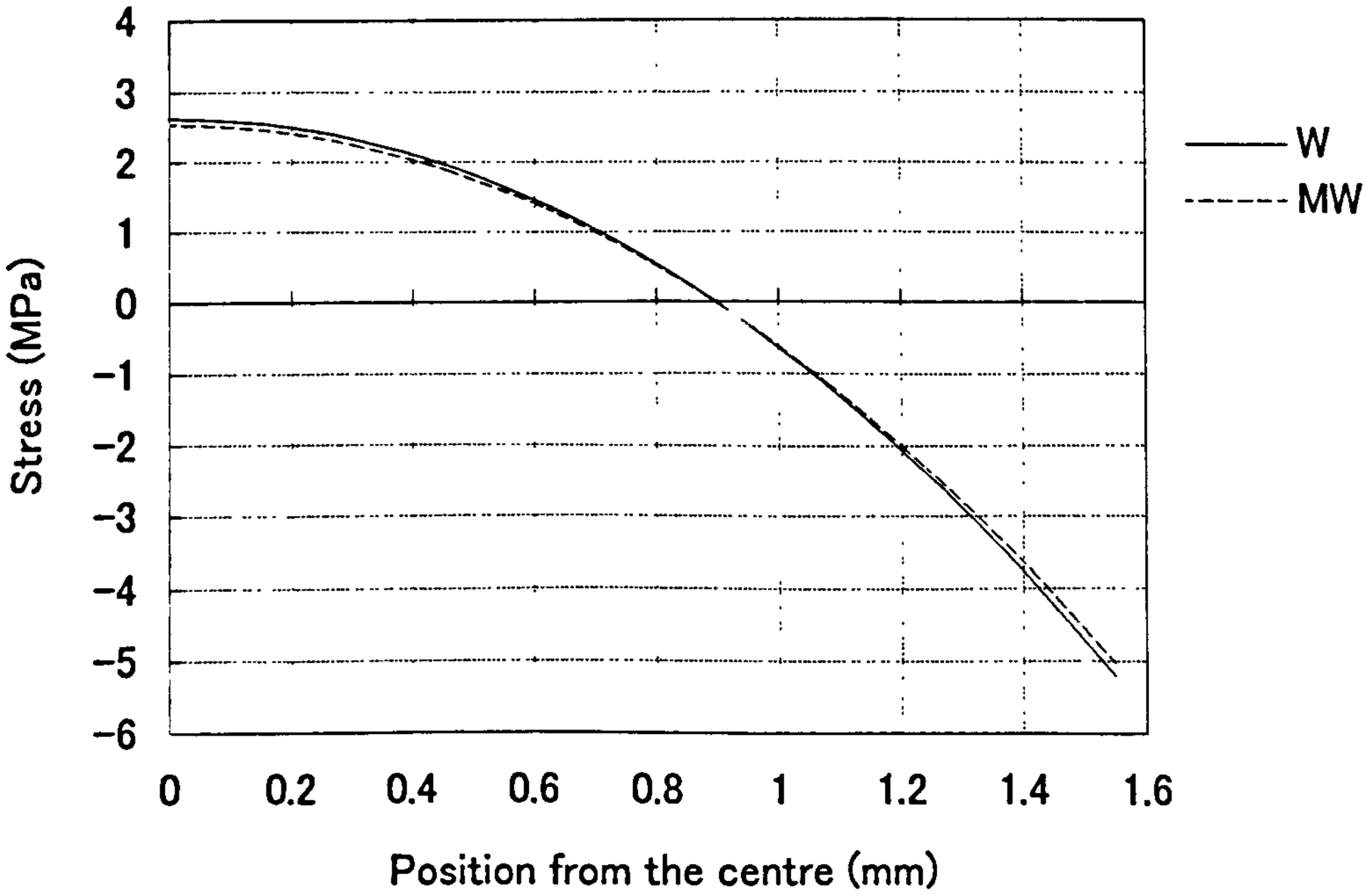

Comparison of the effect of mould release agent, using tensile bars and ice water. (W) Stress obtained without mould release agent. (MW) Stress obtained using mould release agent.

Fig. 6.4

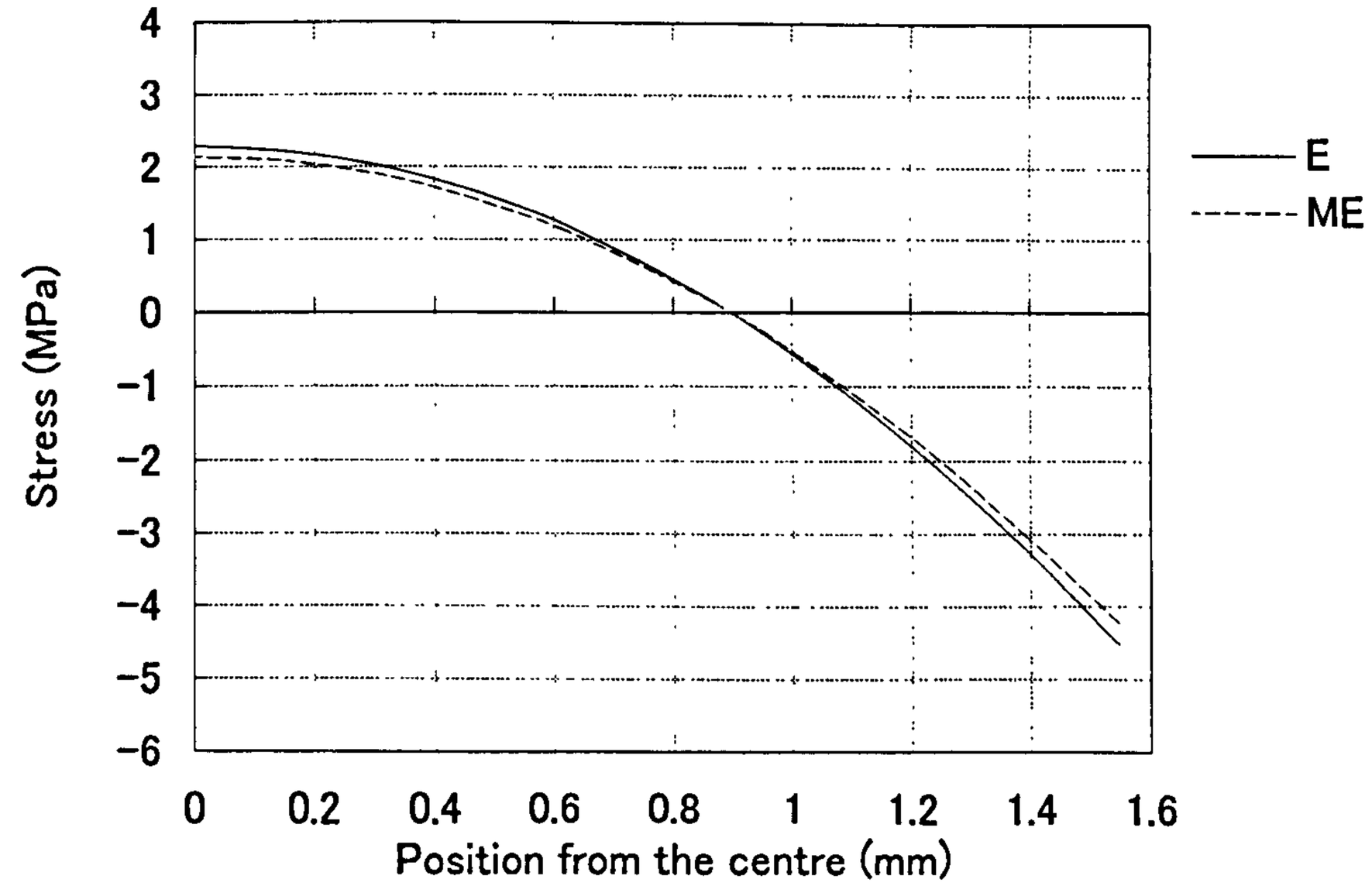

Comparison of the effect of mould release agent, using tensile bars and ethylene glycol. (E) Stress obtained without mould release agent. (ME) Stress obtained using mould release agent.

Fig. 6.5

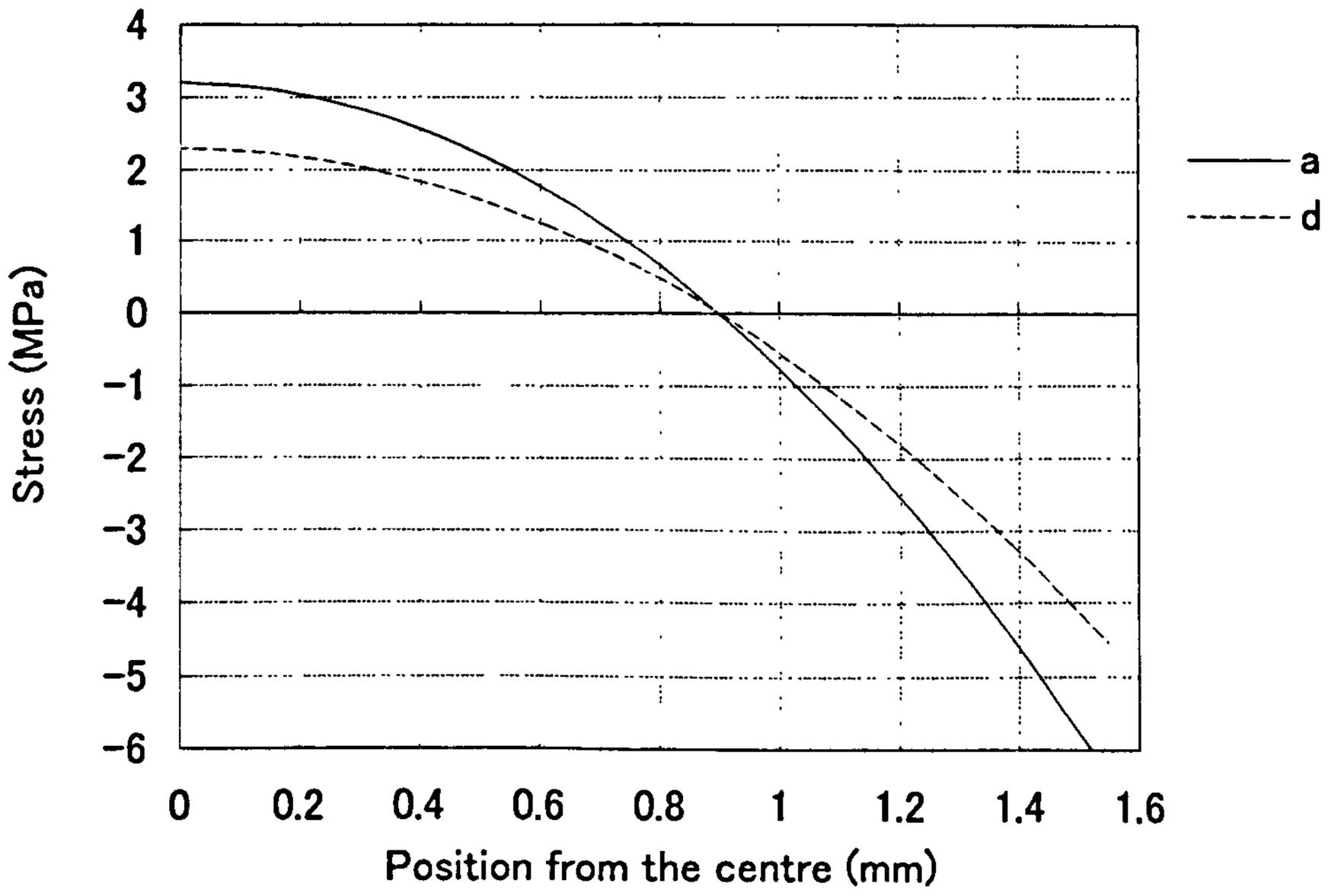

Comparison of the effect of different gate systems, using straight bars. Mould release agent was not used. (a) Stress obtained using shallow gate system. (d) Stress obtained using deep gate system.

Fig. 6.6

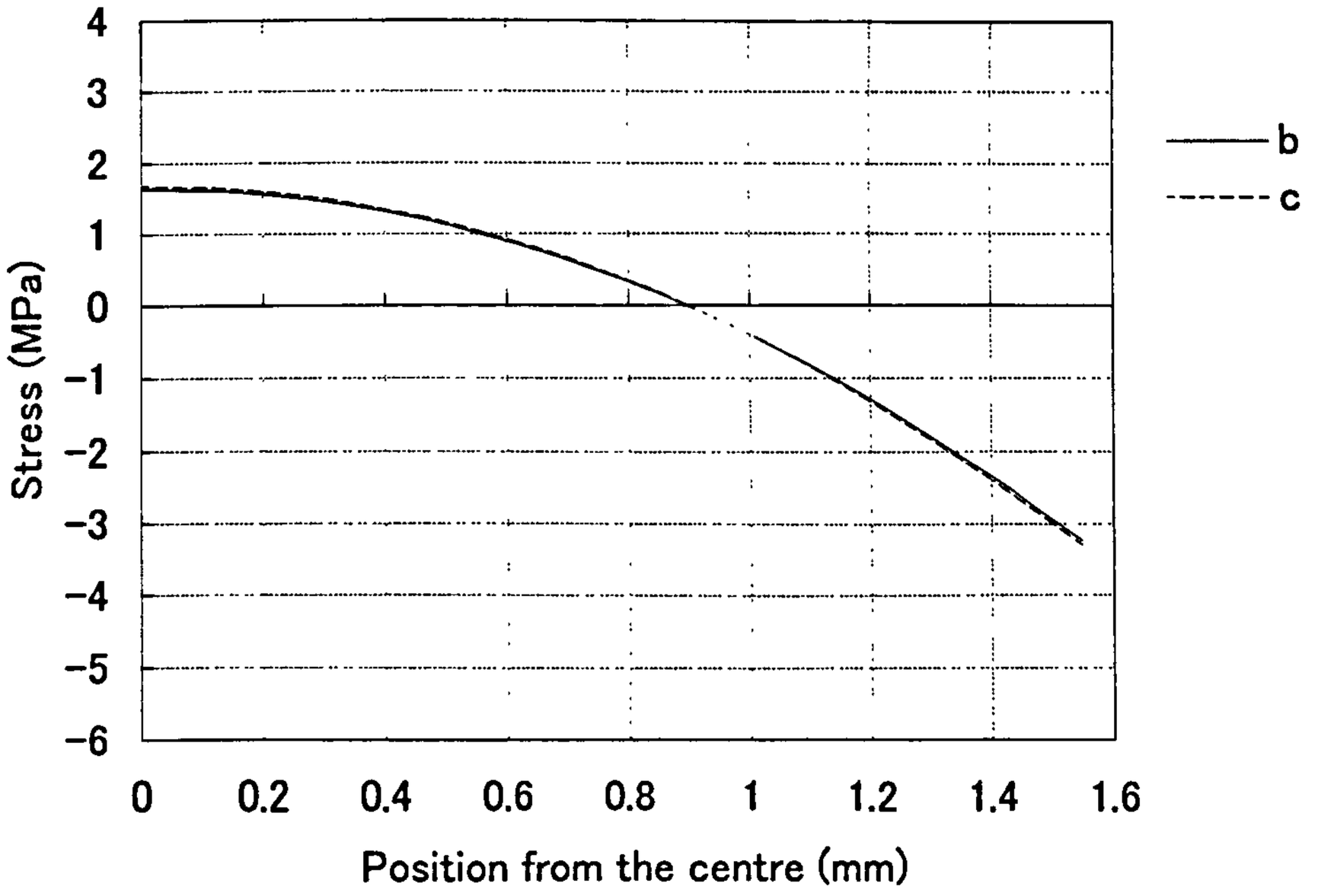

Comparison of the effect of different gate systems, using straight bars and mould release agent. (b) Stress obtained using shallow gate system. (c) Stress obtained using deep gate system.

Fig. 6.7

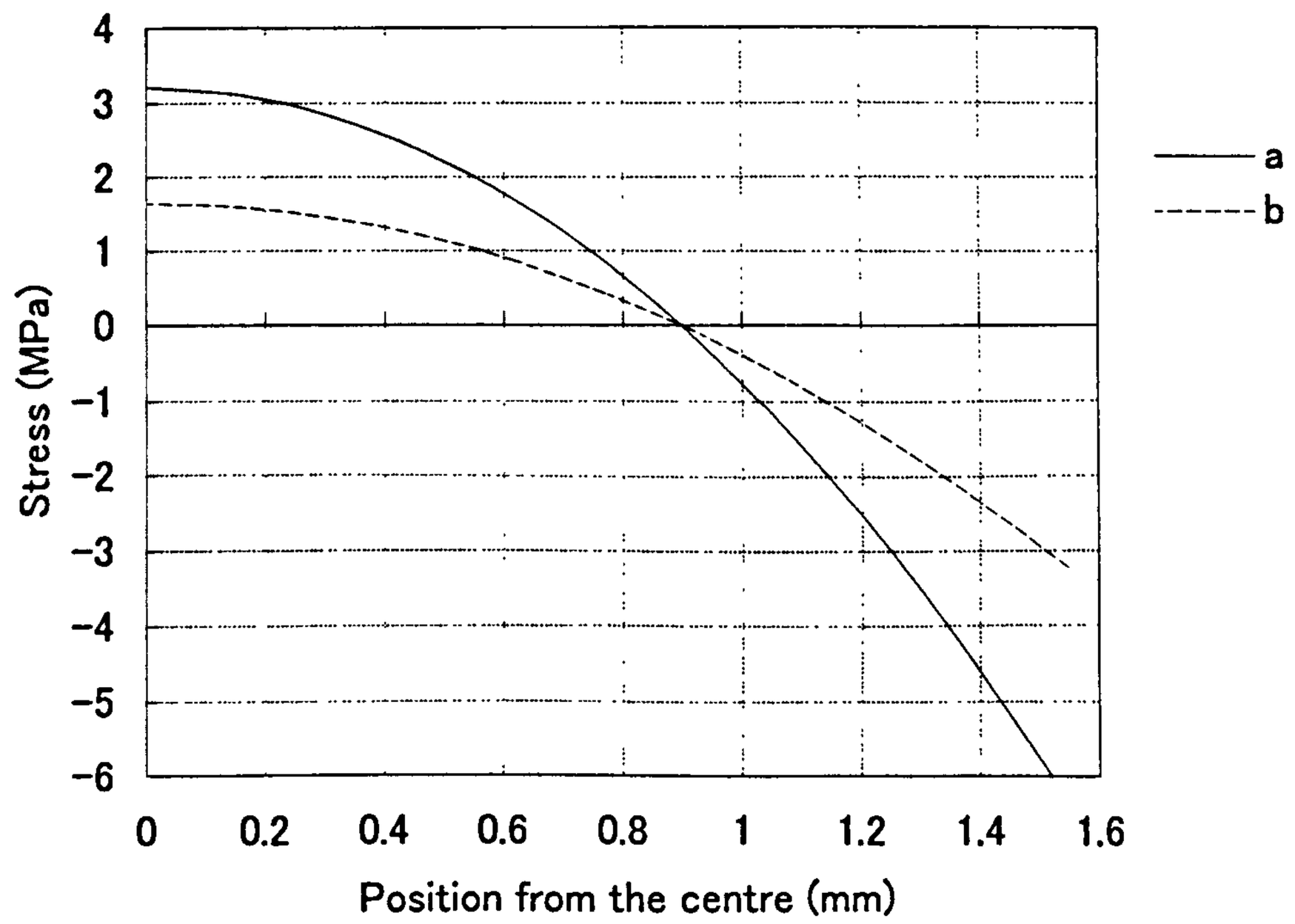

Comparison of the effect of mould release agent, using straight bars and shallow gate system. (a) Stress obtained without mould release agent. (b) Stress obtained using mould release agent.

Fig. 6.8

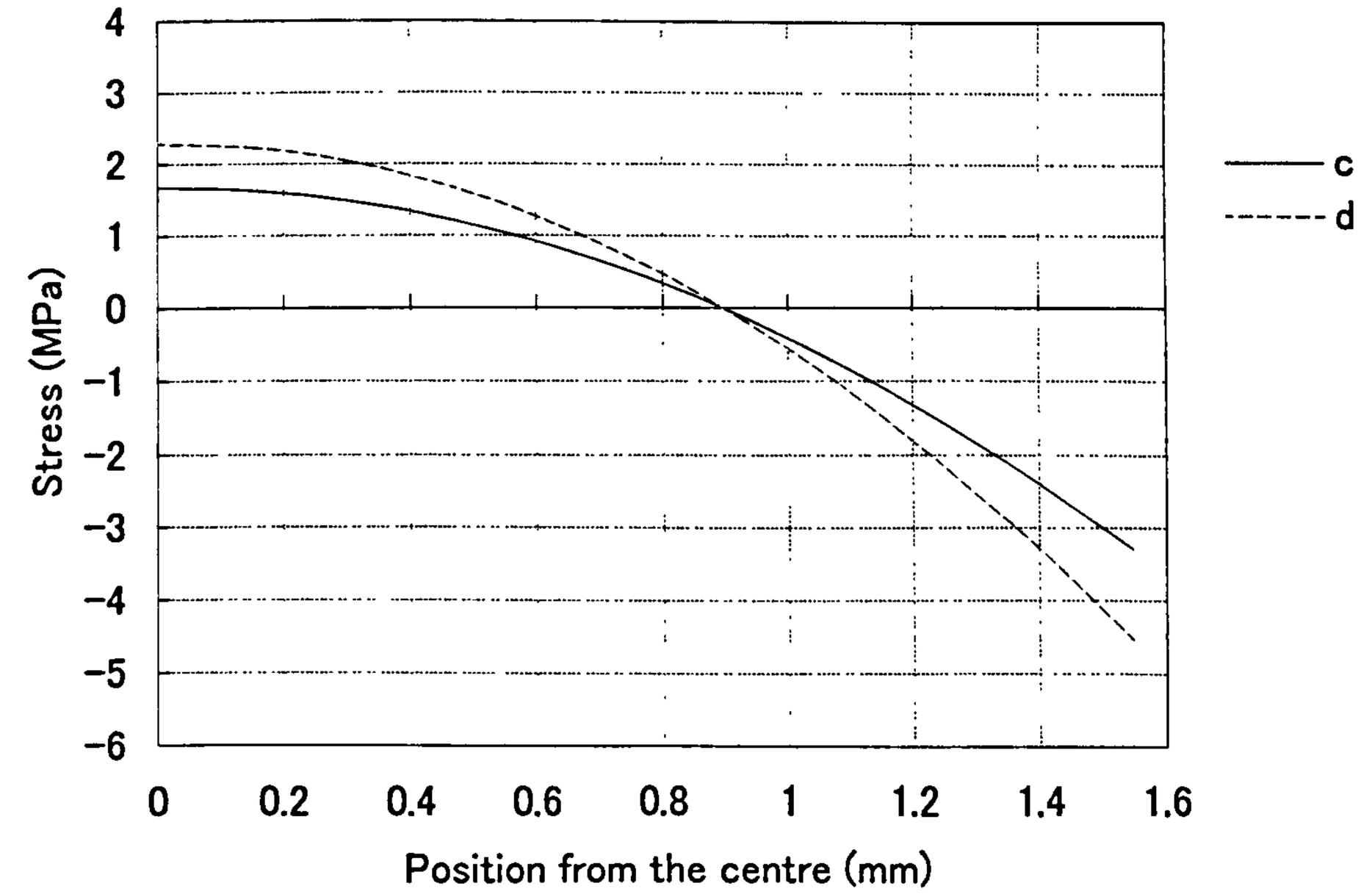

Comparison of the effect of mould release agent, using straight bars and deep gate system.

(c) Stress obtained using mould release agent. (d) Stress obtained without mould

Fig. 6.9

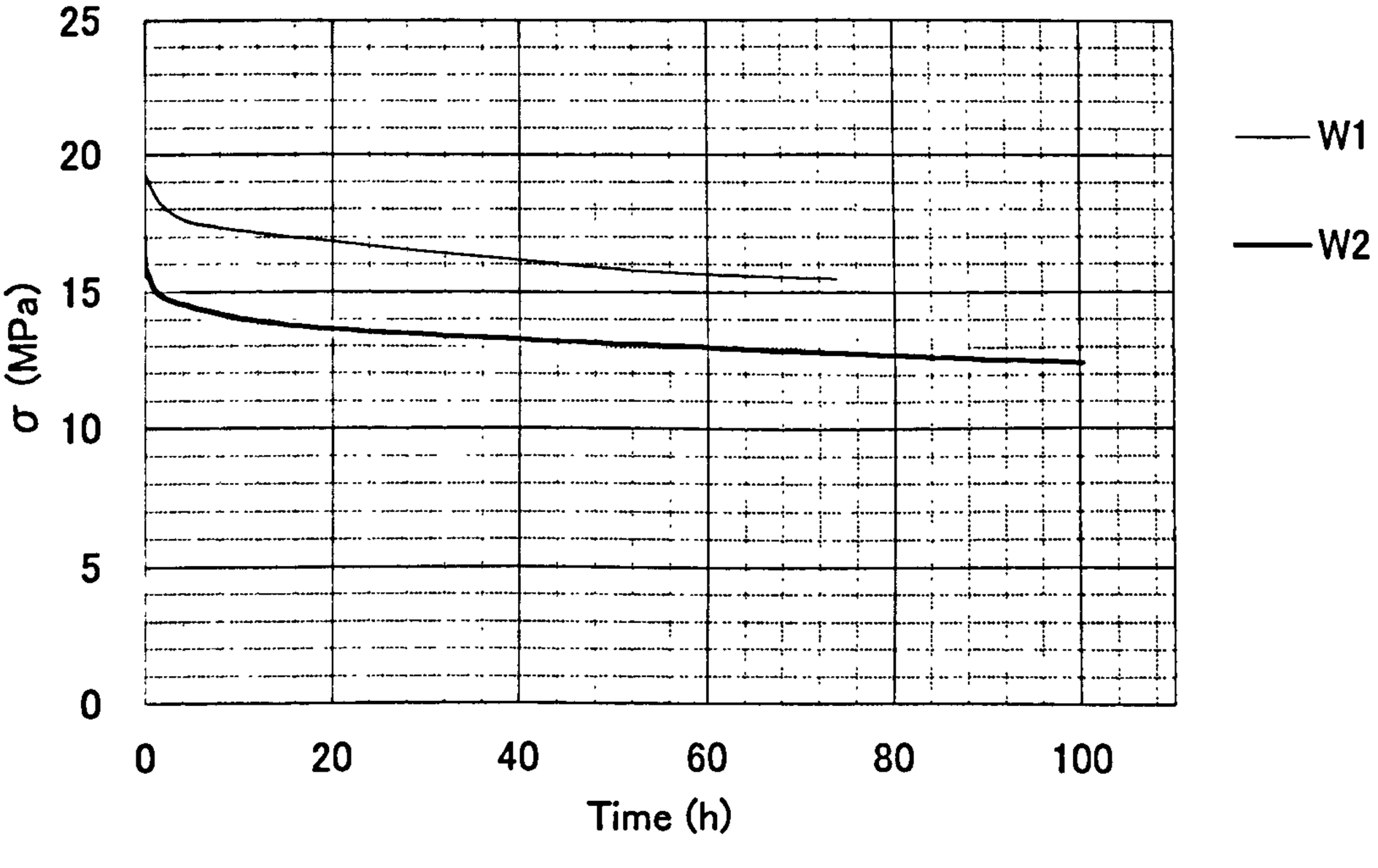

Stress relaxation of injection moulded bars at various initial stresses. (W1) At 21 MPa.

Fig. 6.10

CHAPTER 7

DISCUSSION

A unified theoretical model to calculate the residual stress distributions of the moulding and the post-moulding stages of the entire injection-moulding process has been presented in Chapter 3. The various experiments and the computations have been conducted to determine the effect of different kinematic boundary conditions for the moulding conditions and the post-moulding conditions, due to different process temperatures. The effect of different polymer relaxation times on the residual stress distributions has been examined in Chapter 4, 5 and 6. In the discussion in Section 7.1, the effect of different cooling temperatures after the demoulding are dealt with. Section 7.2 discusses the effect of packing pressure. Section 7.3 deals with the friction constraint effect. Section 7.4 discusses the stress relaxation effect. The effect of the gate system is dealt in Section 7.5.

7.1 Cooling temperature effect

The effect of different cooling temperatures after the demoulding are discussed in this section. Computations considering the effect of different cooling temperatures after the demoulding and comparison between the computed results and experimental measurements have not been found in the literature and it is believed that such results are presented for the first time in this thesis.

7.1.1 liquid nitrogen and ice water

Fig. 7.1.1 (p. 160) and Table 7.1.1 show the measured and the computed residual stress

distributions using method A (based on Struik's method). The labels in Fig 7.1.1 refer to the computed stress obtained using the temperature of liquid nitrogen (K019), the computed stress obtained using the temperature of ice water (K020), the observed stress obtained using liquid nitrogen (N) and the observed stress obtained using ice water (I). The observed residual stress magnitude for the bars which were cooled in liquid nitrogen was everywhere 4.6 times higher than in the bars cooled in ice water. The computed residual stress magnitude for the bars which were cooled in liquid nitrogen was 13.7 times the computed magnitude for bars cooled in ice water on average. The observed residual stress magnitude for the bars which were cooled in liquid nitrogen was 6 times that of the computed magnitude on average. The observed residual stress magnitude for the bars which were cooled in ice water was 2.2 times that of the computed magnitude on average. All four stress distributions have compressive stresses at the surfaces and tensile stresses in the core of the sample. The positions of the maxima are better predicted than those of the minima. The calculated stress distributions shown in Fig 7.1.1 were in qualitative agreement with the experimental results.

	K019	N	K020	I
Maximum stress (MPa)	24.6	17.0	1.6	4.0
Minimum stress (MPa)	-42.7	-28.2	-3.3	6.6

Table 7.1.1

Fig. 7.1.2 (p. 160) and Table 7.1.2 show the measured stress and the computed residual stress distributions using method B. The labels in Fig 7.1.2 refer to the computed stress obtained using the temperature of liquid nitrogen (L006), the computed stress obtained using the temperature of ice water (L007), the observed stress obtained using liquid

nitrogen (N) and the observed stress obtained using ice water (I). The computed residual stress magnitude for the bars which were cooled in liquid nitrogen was 7.2 times the computed magnitude in the bars cooled in ice water on average. The observed residual stress magnitude for the bars which were for the bars cooled in liquid nitrogen was 0.6 times that of the computed magnitude on average. The observed residual stress magnitude for the bars which were cooled in ice water was 1.1 times that of the computed magnitude on average. All four stress distributions have compressive stresses at the surfaces and tensile stresses in the core of the sample. The positions of the maxima are better predicted quantitatively. However, the compressive stress near the surfaces are under predicted.

	L006	N	L007	I
Maximum stress (MPa)	22.1	17.0	1.1	4.0
Minimum stress (MPa)	-47.8	-28.2	-8.6	-6.6

Table 7.1.2

As described in Sections 3 and 4, Method A (based on Struik's method) refers to boundary conditions which are based on local cooling rate and incremental temperature changes whereas using method B (taking account of the pressure profile) starts by calculating the pressure profile and is based on the specific volume rate from the differentiation of the Tait equations by pressure. The strain as a function of pressure is calculated using the specific volume and the density. The predictions of residual stress distributions using method B show slightly better agreement with the experimental results than the method A. This is as would be expected from Section 4.4.2.1 (temperature distributions) and Table 4.6.2.1 in Section 4 (process controls) since the procedure using method B deals with the process controls (particularly detailed pressure profiles) in a better manner than method A.

The calculations predict much large residual stress magnitudes at the surfaces of samples when the samples are cooled in liquid nitrogen than the corresponding experimental results[86]. A possible reason for this is that when the samples are cooled by liquid nitrogen, bubbles appear near the surfaces due to the evaporation of liquid nitrogen. This causes the cooling condition to be milder than that modelled in the calculations. In order to verify this reason, using liquid nitrogen slush (solid nitrogen-liquid nitrogen mixture) would be effective. The use of a better agreement between experimental conditions and boundary conditions for calculations would result in a better prediction of residual stresses.

7.1.2 Ice water and room temperature

Fig 7.1.3 (p. 161) and Table 7.1.3 show the measured stress and the computed residual stress distributions using method A. The labels in Fig 7.1.3 refer to the computed stress obtained using temperature of ice water (K0172), the computed stress obtained using room temperature (K018), the observed stress obtained using ice water (W) and the observed stress obtained using room temperature (E). The observed residual stress magnitude for the bars which were cooled in ice water was everywhere 1.1 times the value produced in bars cooled in a room temperature. The computed residual stress magnitude for the bars which were cooled in ice water was everywhere 1.03 times the computed magnitude for the bars cooled in ice water. The observed residual stress magnitude for the bars which were cooled in ice water was 0.34 times that of the computed magnitude on average. The observed residual stress magnitude for the bars which were cooled using a room temperature was 0.32 times the computed magnitude on average. All four stress distributions have compressive stresses at the surfaces and tensile stresses in the core of the sample. The calculated stress distributions shown in

Fig 7.1.3 were in qualitative agreement with the experimental results. However, the compressive stresses near the surfaces were over predicted and the tensile stresses in the core were under predicted.

	K0172	W	K018	E
Maximum stress (MPa)	6.2	2.6	6.0	2.3
Minimum stress (MPa)	-15.8	-5.2	-15.5	4.6

Table 7.1.3

7.2 Packing pressure effect

Fig. 7.2.1 (p. 161) and Table 7.2.1 show the measured stress and the computed residual stress distributions using the WLF equations. The labels in Fig 7.2.1 refer to the computed stress obtained using 143 MPa of injection pressure (L002), the computed stress obtained using 87 MPa of injection pressure (L003) and the observed stress obtained using both the pressures 143 MPa and 87 MPa (Exp). The computed residual stress magnitude for the bars which were made using 143 MPa was 0.68 times the computed magnitude using 87 MPa on average. The observed residual stress magnitudes for the bars which were made using both the pressure 143 MPa and 87 MPa was 0.83 times the computed magnitude using 143 MPa and 0.55 times the computed magnitude using 87 MPa on average. All four stress distributions have compressive stresses at the surfaces and tensile stresses in the core of the sample. The calculated stress distributions shown in Fig 7.2.1 were in qualitative agreement with the experimental results. However, the compressive stresses near the surfaces were under predicted.

	L002	L003	Experiment
Maximum stress (MPa)	0.5	0.7	1.0
Minimum stress (MPa)	-3.1	-4.8	-2.0

Table 7.2.1

Zoetelief, Douven and Ingen Housz[80] calculated that considerable tensile stress develops at the surface of injection moulded products during the holding and packing stage. They reported that the tensile stress is caused by the high mould pressure that occurs during the process. However, they did not compare the effect of different packing pressures on residual stress magnitude. Bushko and Stokes[69-72] computed residual stresses accounting for the additional material that is forced into the volume created by cooling and by the time-dependent packing pressure compressing the molten material and the solidified layers, which are pushed against the mould walls. They indicated that for low packing pressures for which the cavity pressure drops to zero before the complete thickness undergoes the glass transition, the residual stresses do change with pressure. For high pressures, for which cavity-pressure histories differ only by a constant until the complete thickness has undergone the glass transition, increases in packing pressure have no effect on the residual stresses, therefore showing that the magnitude of packing pressure affects shrinkage and the residual stresses are affected by the packing-pressure changes before complete transition to the glassy state.

In the studies described in this thesis, when barrel temperatures were adjusted to maintain production of visually satisfactory mouldings from polystyrene, the residual stress distributions were not very sensitive to changes in injection pressure in the range 37 - 143 MPa[155]. This result seems to indicate that there might be a compensating effect.

7.3 Friction constraint effect

Fig. 7.3.1 (p. 162) and Table 7.3.1 show the measured stress and the computed residual stress distributions using method B. These computations and comparison between the computed results and the experimental have been attempted for the first time in the research described in this thesis. The labels in Fig 7.3.1 refer to the computed stress obtained without friction constraint (L004), the computed stress obtained with friction constraint (L005), the observed stress obtained without mould release agent and using the straight bars (a) and the observed stress obtained using mould release agent and the straight bars (b). The observed residual stress magnitude for the bars produced without mould release agent was everywhere 0.5 times the value produced using mould release agent. The computed residual stress magnitude without friction constraint was 0.66 to 0.94 times that when using friction constraint. The observed residual stress magnitude for the bars produced without mould release agent was 0.38 to 0.17 times the computed magnitude without friction constraint. The observed residual stress magnitude for the bars produced using mould release agent was 0.5 to 0.32 times the computed magnitude without friction constraint. All four stress distributions have compressive stresses at the surfaces and tensile stresses in the core of the sample. The calculated stress distributions shown in Fig 7.3.1 were in qualitative agreement with the experimental results. However, the compressive stresses near the surfaces were under predicted.

	L004	b	L005	a
Maximum stress (MPa)	4.2	1.6	6.4	3.2
Minimum stress (MPa)	-19.0	-3.2	-20.2	-6.4

Table 7.3.1

Fig. 7.3.2 (p. 162) and Table 7.3.2 show the measured stress and the computed residual

stress distributions using the method A. The labels in Fig 7.3.2 refer to the computed stress obtained without friction constraint (K013), the computed stress obtained with friction constraint (K0171), the observed stress obtained without mould release agent and using the straight bars (a) and the observed stress obtained using mould release agent and the straight bars (b). The computed residual stress magnitude without friction constraint was 0.33 to 0.42 times that when using friction constraint. The observed residual stress magnitude for the bars produced without mould release agent was 0.64 to 0.43 times the computed magnitude without friction constraint. The observed residual stress magnitude for the bars produced using mould release agent was 0.46 to 0.36 times the computed magnitude without friction constraint. The calculated stress distributions shown in Fig 7.3.2 (p. 162) were in qualitative agreement with the experimental results. However, the compressive stresses near the surfaces were under predicted. As can be seen from Figs. 7.3.1 and 7.3.2, the predictions of residual stress distributions using method B show slightly better qualitative agreement with the experimental result than those obtained using method A.

	K013	b	K0171	a
Maximum stress (MPa)	2.5	1.6	7.0	3.2
Minimum stress (MPa)	-7.4	-3.2	-17.8	-6.4

Table 7.3.2

The residual stress distributions were not very sensitive to the pressure or change of mould release agent if tensile bars with end tabs were used. This is because the shoulders of the samples are still kinematically constrained by the mould, even when using the mould release agent. The calculated stress distributions were in qualitative agreement with the experimental results however they were not in quantitative agreement. The reasons for this could be that, the calculations use a two stage model

(constrained boundary conditions before the pressure drops to zero and unconstrained boundary conditions after the pressure becomes zero) while in the experiment, there should exist three stages ((i) constrained boundary conditions before the pressure drops towards a certain pressure; (ii) friction constraints once the pressure has dropped below this, continuously until the pressure becomes zero; (iii) unconstrained boundary conditions after the pressure becomes zero) which remove the intimate contact of the moulding with the mould cavity walls.

7.4 Stress relaxation effect

Fig. 7.4.1 (p. 163) shows the measured and the calculated stresses as functions of time and compares them with values obtained by fitting Eq. 4.5.1 in Chapter 4. The labels in Fig 7.4.1 refer to the calculated stress obtained using 21 MPa of initial stress (W1 Calc), the observed stress obtained using 21 MPa of initial stress (W1), the calculated stress obtained using 17 MPa of initial stress (W2 Calc) and the stress obtained using 17 MPa of initial stress (W2). The fits of the calculated stress relaxation curves were in quantitatively good agreement with the experimental results. All residual stress calculations from Sections 7.1 to 7.4 were made using Eq. 4.5.1 for different elapsed times after mouldings have been made. The introduction of stress relaxation in this thesis reduced disagreements between the experimental results and the computed residual stresses.

7.5 Gate system effect

Fig 7.5.1 (p. 163) and Table 7.5.1 show the measured residual stress distributions. The labels in Fig 7.1.3 refer to the stress obtained without mould release agent and using the shallow gate system (a), the stress obtained using mould release agent and the shallow

gate system (b), the stress obtained using mould release agent and the deep gate system (c), and the stress obtained without mould release agent and the deep gate system (d). The observed residual stress magnitude for the bars produced without mould release agent and using the shallow gate was everywhere 0.5 times the value produced using mould release agent. The observed residual stress magnitude for the bars produced without mould release agent and using the shallow gate was virtually the same as the value produced using mould release agent and the deep gate system. The reason for this result is that, as the melt solidifies in the mould, at some stage the through thickness stress at the mould surfaces drop to zero. After this stage, the sample surfaces are no longer in intimate contact with the mould surfaces. When the deep gate system is used, as the gate freeze time is longer than for the shallow gate system, the sample surfaces remain in intimate contact with the mould cavity walls for much longer even when mould release agent was used.

	a	b	d	c
Maximum stress (MPa)	3.2	1.6	2.3	1.65
Minimum stress (MPa)	-6.4	-3.2	-4.6	-3.3

Table 7.5.1

7.6 General discussion

All the calculated results except L007[Note 7.6] over predicted on the residual stress magnitudes. The results of the other researches[69-74,80,89] show the same tendencies. Also Bushko and Stokes[70] described that the WLF equation is known to be a poor approximation for the shift function below T_g. The use of a better model for the shift function below T_g would result in a better prediction of residual stresses. However, a better approximation than the WLF and the KWW equations has not appeared in the

literature.

Note 7.6: If the stress relaxation effect (Section 7.4) is not applied to L007, The residual stress magnitude was over predicted.

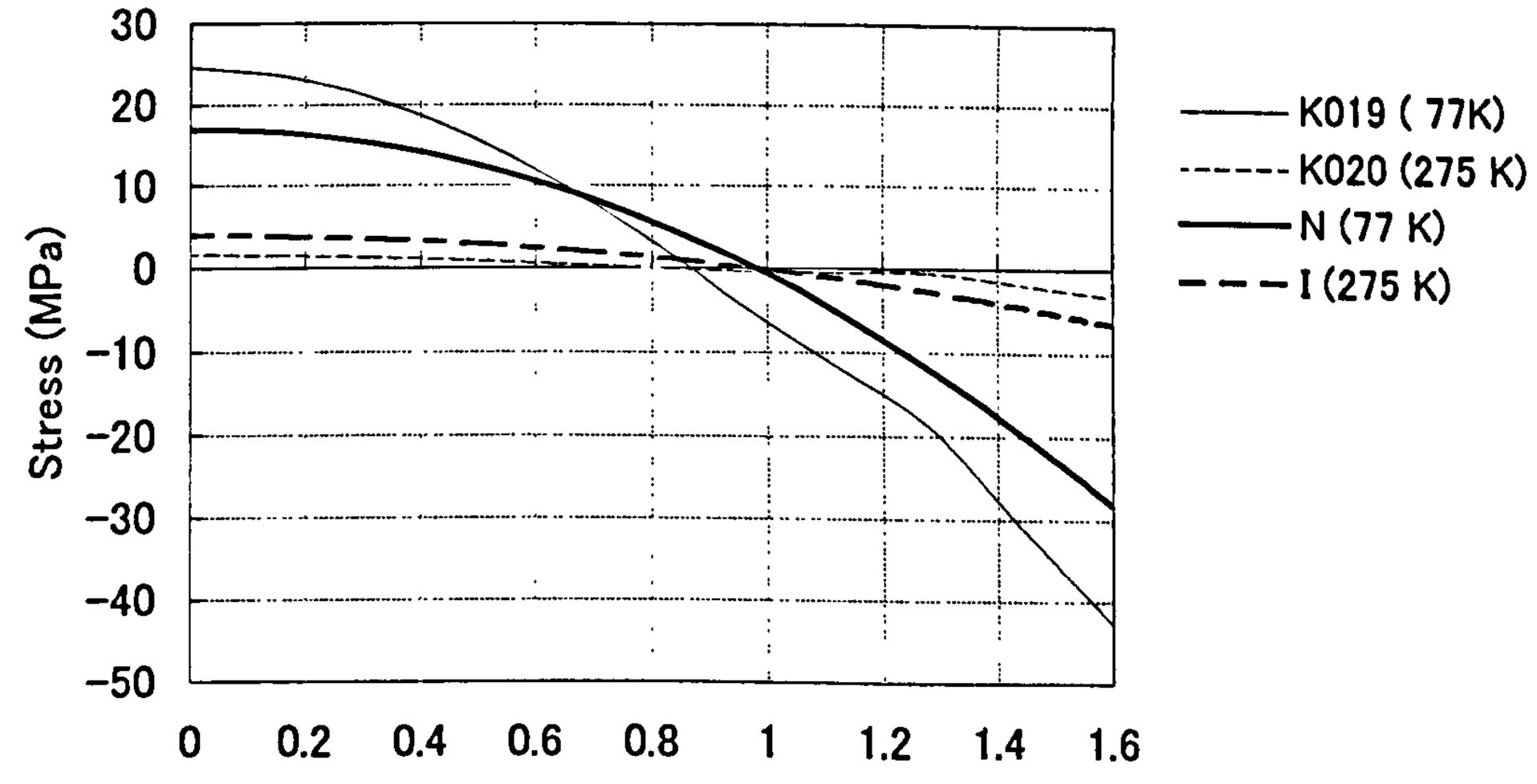

Comparison of the effect of different cooling temperatures, using tensile bars. (K019) Computed stress obtained using liquid nitrogen. (K020) Computed stress obtained using ice water. (N) Observed stress obtained using liquid nitrogen. (I) Observed stress obtained using ice water.

Fig. 7.1.1 Comparison of the different cooling temperature, using free quench method

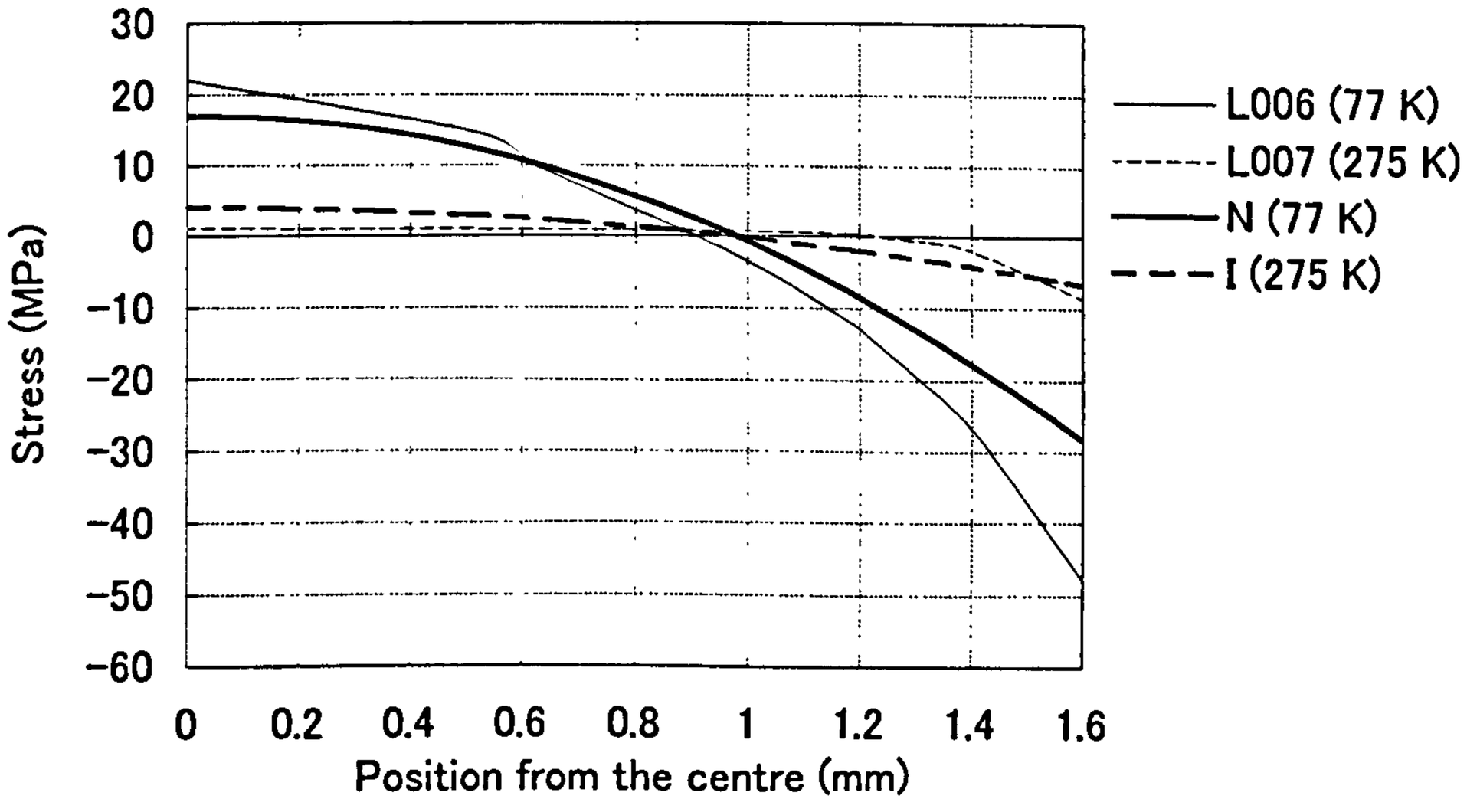

Comparison of the effect of different cooling temperatures, using tensile bars. (L006) Computed stress obtained using liquid nitrogen. (L007) Computed stress obtained using ice water (L007). (N) Observed stress obtained using liquid nitrogen. (I) Observed stress obtained using ice water.

Fig. 7.1.2 Comparison of the different cooling temperatures, using the WLFequations

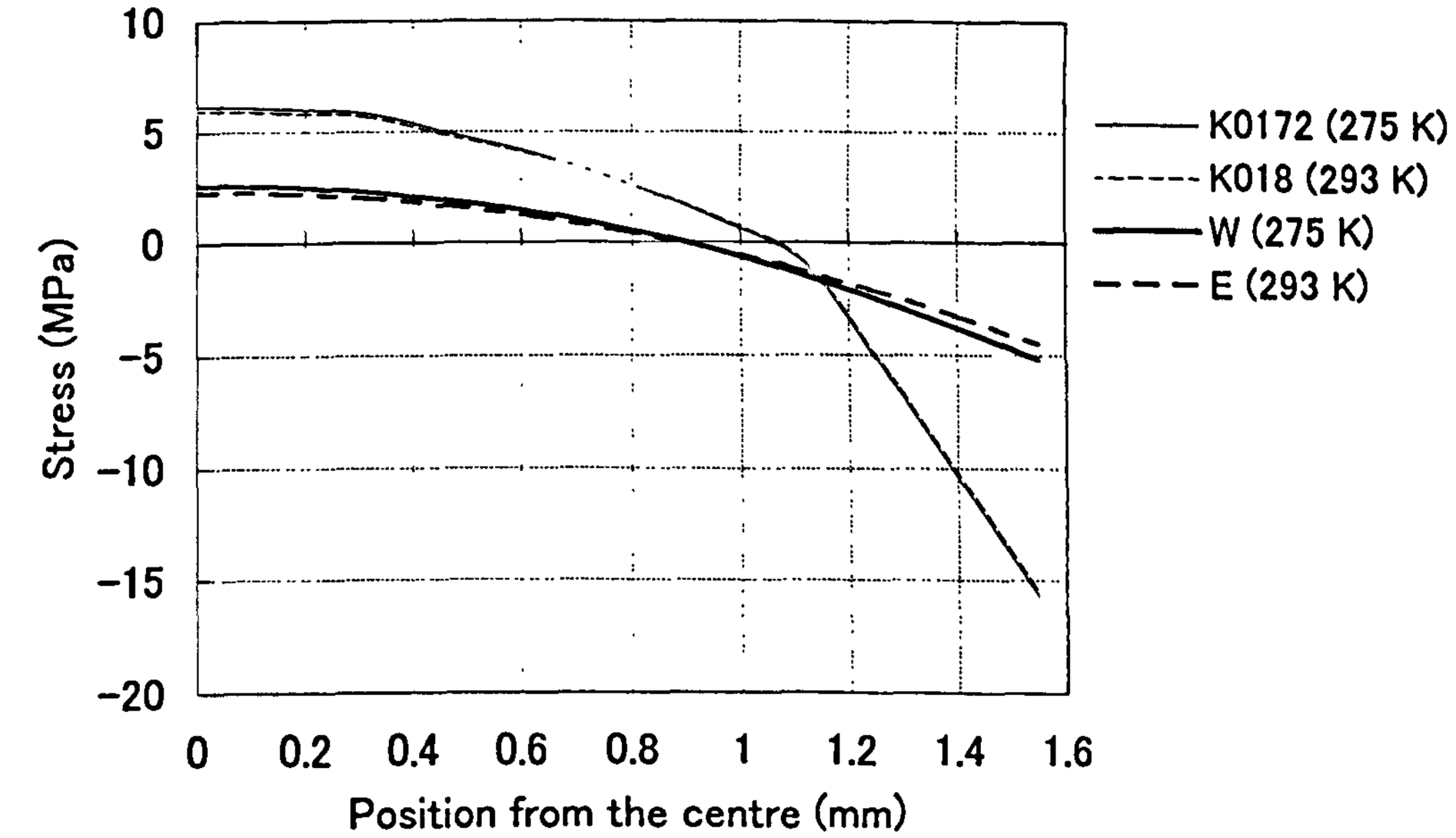

Comparison of the effect of different cooling temperatures, using tensile bars. (K0172) Stress obtained using ice water. (K018) Stress obtained using room temperature. (W) Observed stress obtained using ice water (275 K).
(E) Observed stress obtained using ethylene glycol (293 K).

Fig. 7.1.3

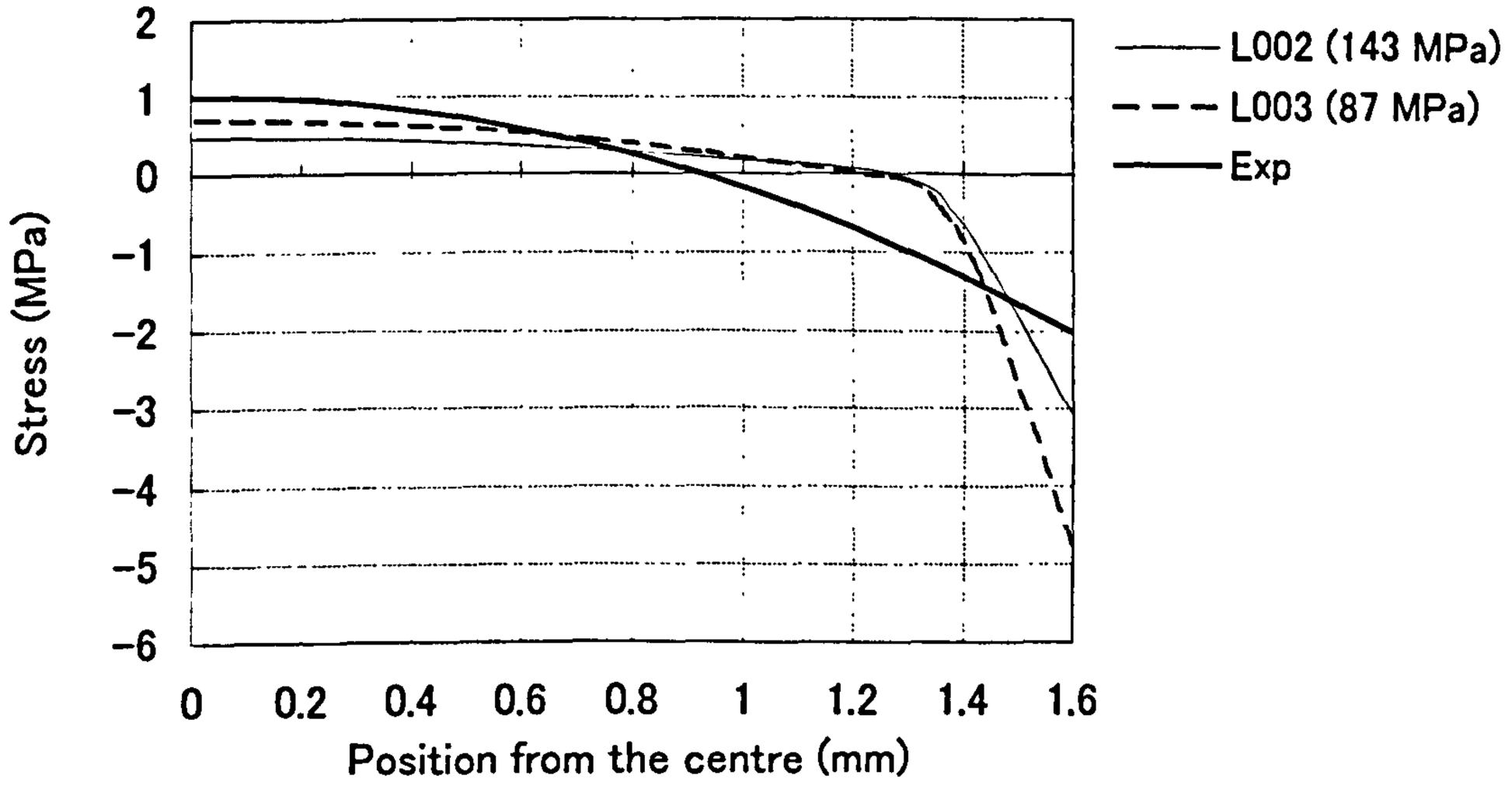

Comparison of the effect of injection pressure (i) Stress obtained using 143 MPa of injection pressure (L002). (ii) Stress obtained using 87 MPa of injection pressure (L003). (Exp) Observed stress obtained using both the pressure 143 MPa and 87MPa.

Fig. 7.2.1

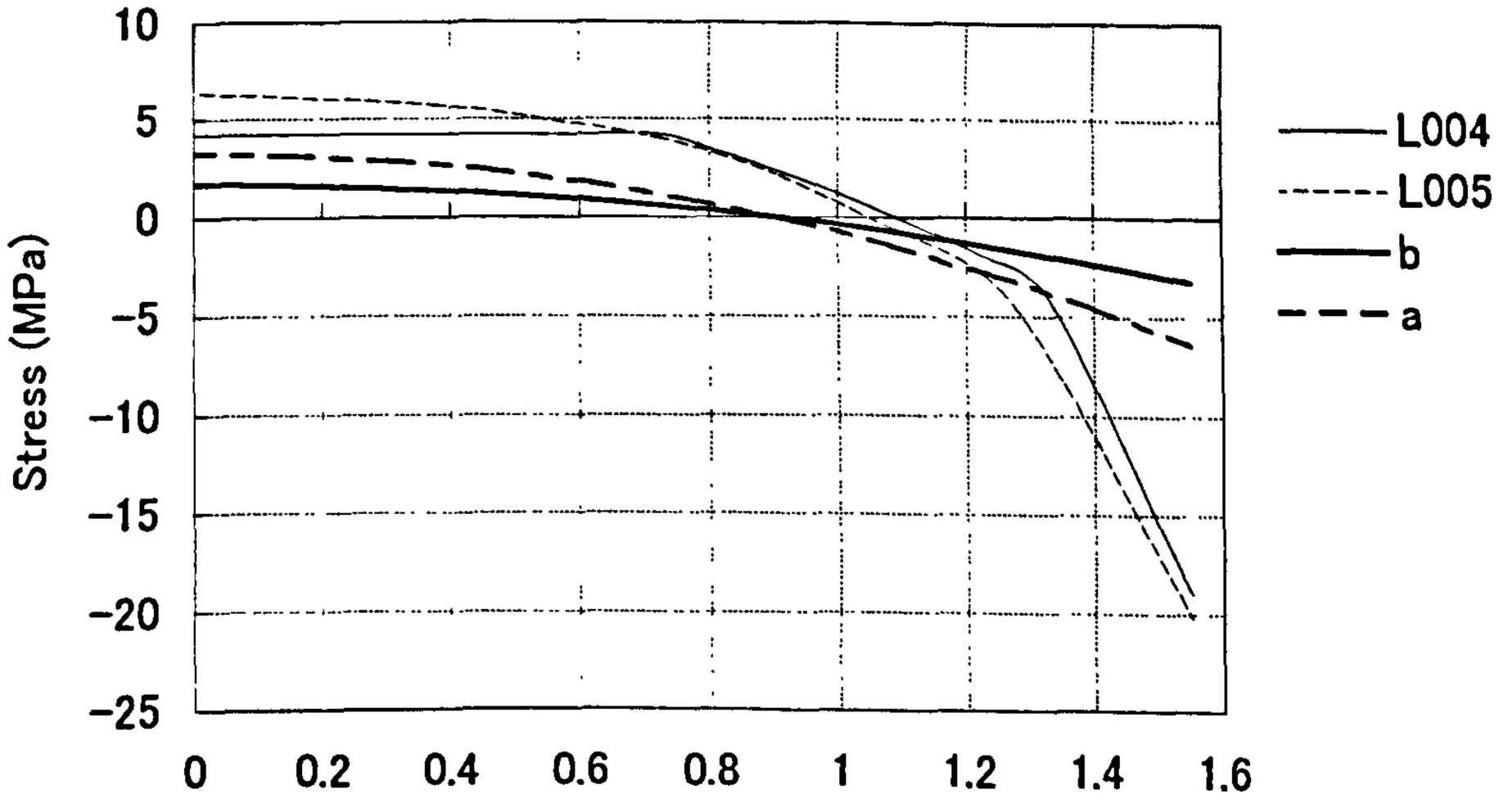

Comparison of the effect of mould release agent, using the straight bars. (L004) Computed stress obtained without friction constraint. (L005) Computed stress obtained with friction constraint, using straight bars and shallow gate system. (a) observed stress obtained without mould release agent. (b) Observed stress obtained using mould release agent.

Fig. 7.3.1

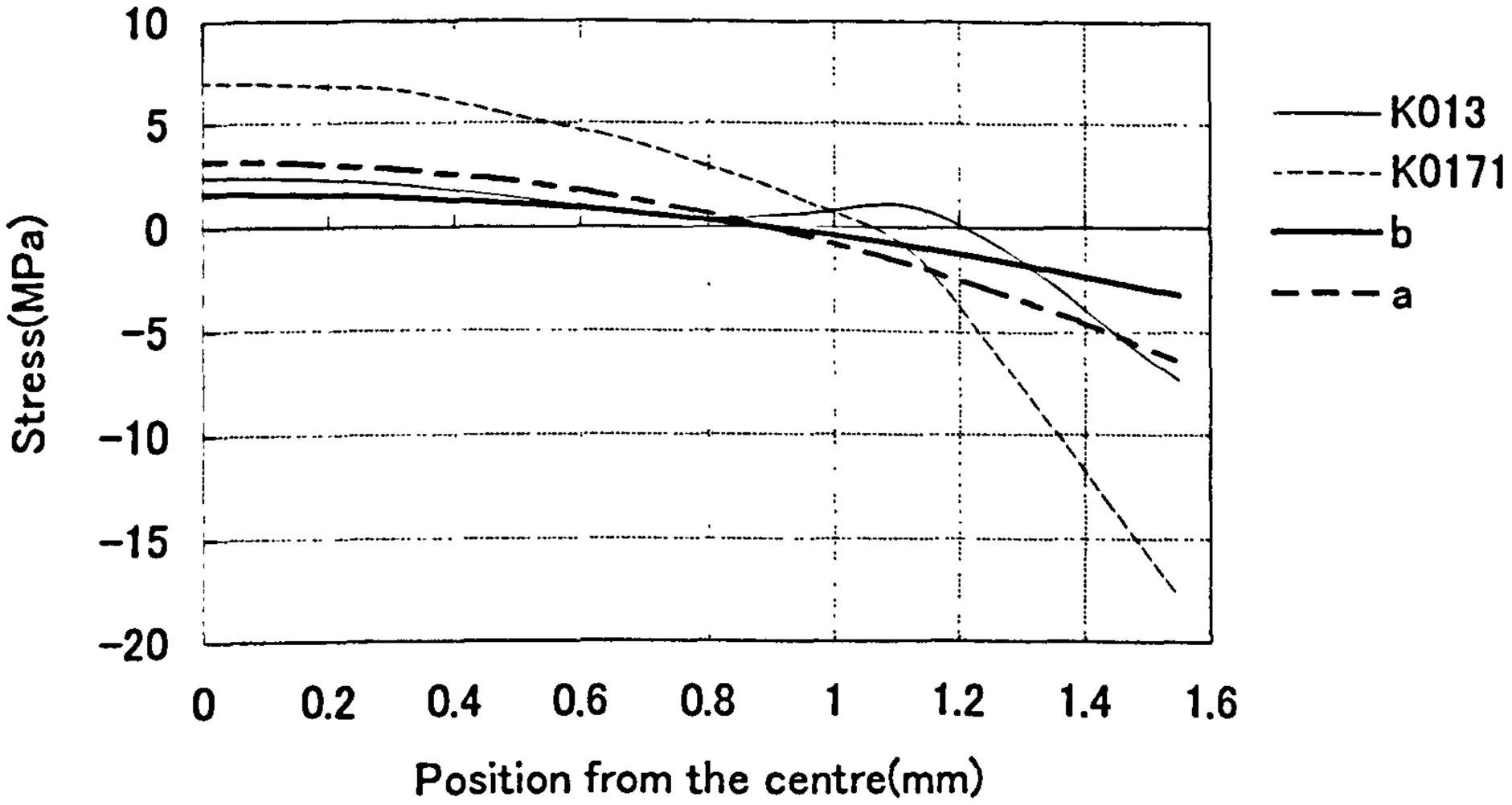

Comparison of the effect of mould release agent, using the straight bars. (K013) Computed stress obtained without friction constraint. (K0171) Computed stress obtained with friction constraint. (a) Observed stress obtained without mould release agent. (b) Observed stress obtained using mould release agent.

Fig.7.3.2

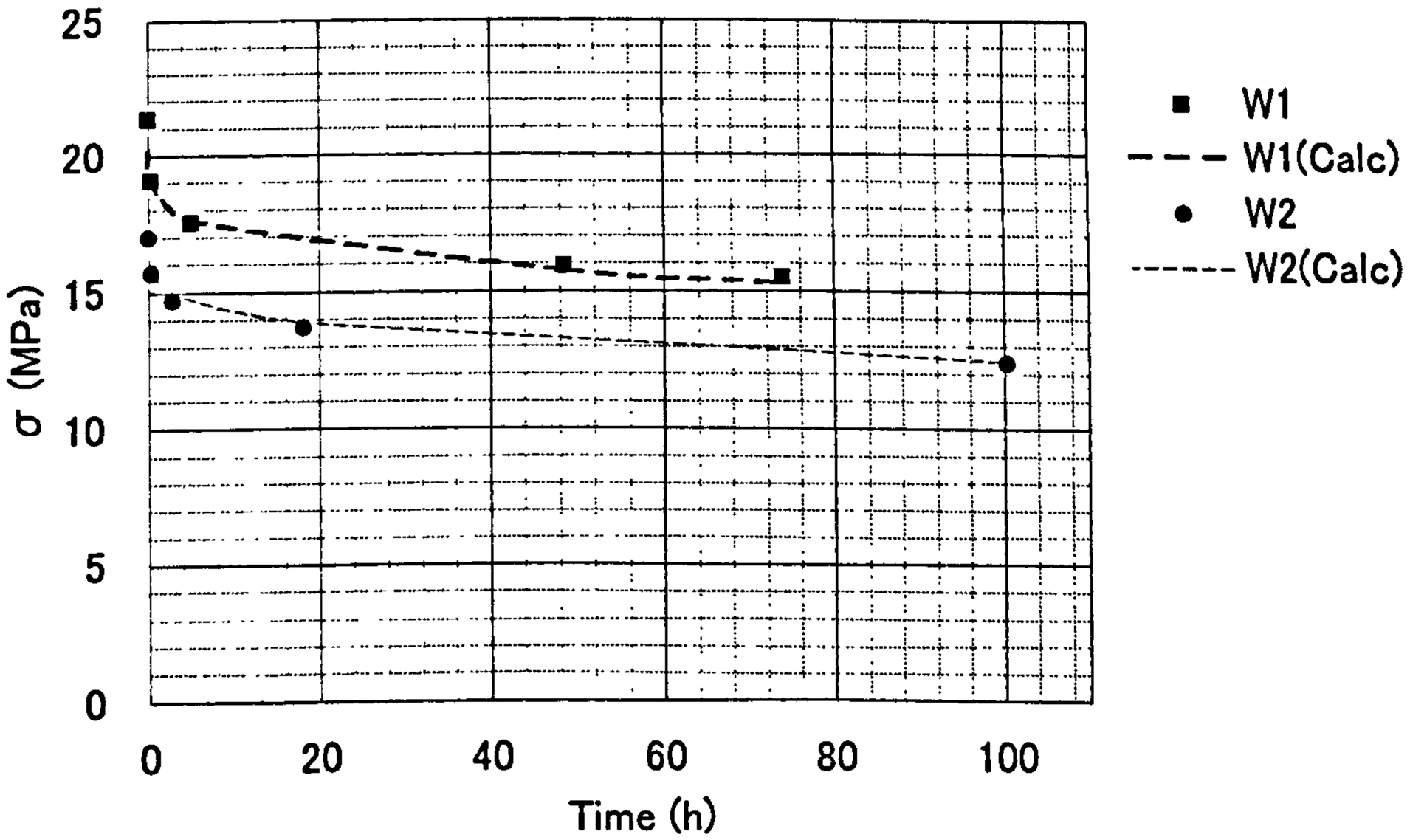

Stress relaxaton of the injection moulded bars at various intial stresses. (W1) Observed stresses at 21 MPa. (W1 Calc) Computed stresses at 21 MPa (W2) Observed stresses at 17 MPa. (W2 Calc) Computed stresses at 17 MPa

Fig. 7.4.1

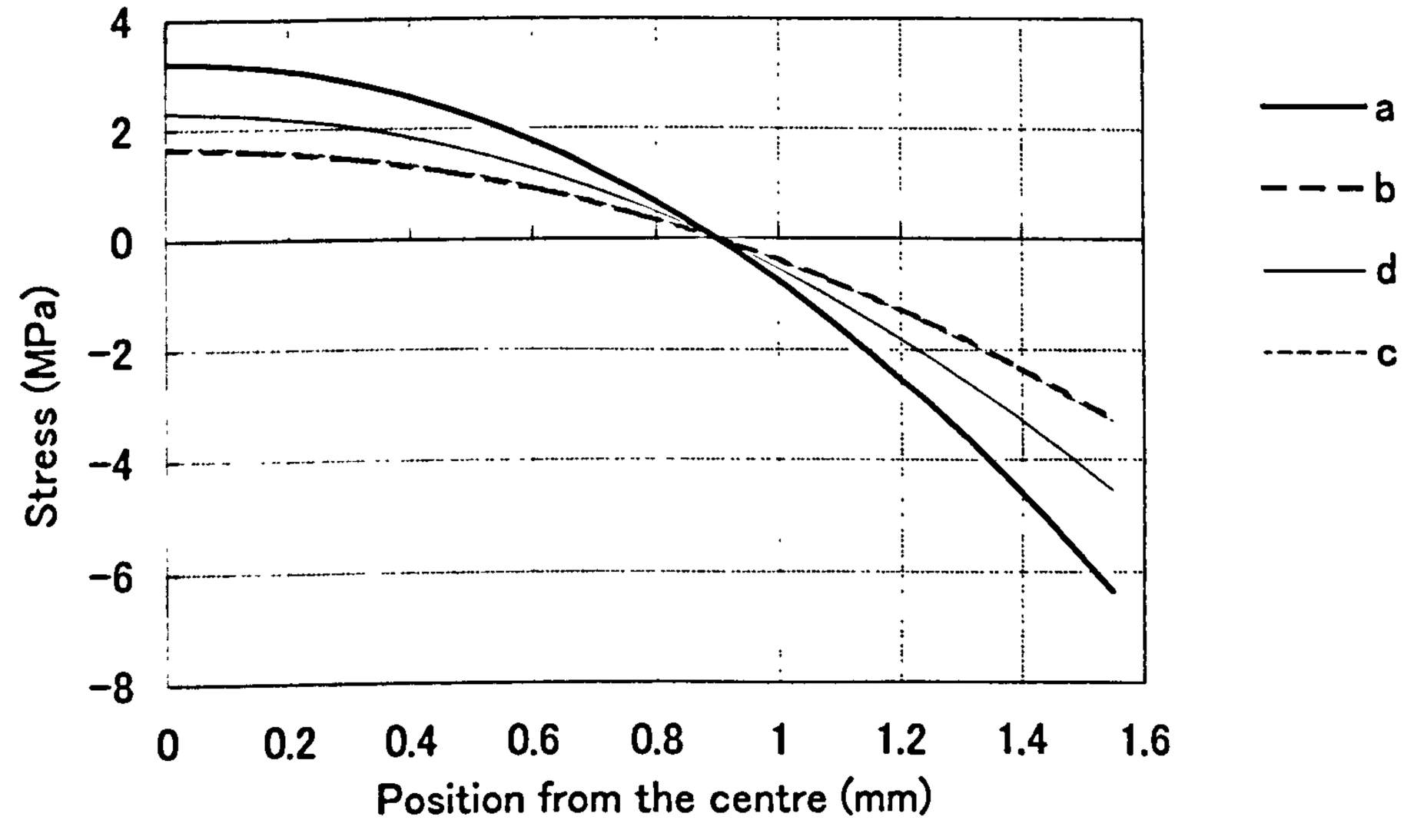

Comparison of the effect of the gate system, using the straight bars: (a) Stress obtained without mould release agent and using shallow gate system; (b) Stress obtained using mould release agent and shallow gate system. (c) Stress obtained using mould release agent and deep gate system; (d) Stress obtained without mould release agent and using deep gate system.

Fig. 7.5.1

CHAPTER 8

CONCLUSIONS

A unified theoretical model to calculate the residual stresses in moulding and post-moulding stages of the entire injection-moulding process is presented in this thesis.

The predicted residual stress distributions over the entire moulding and post-moulding history have been found to be in generally good agreement with the corresponding experimental results under various processing conditions and post-moulding changes. In particular, kinematic boundary conditions for the moulding conditions and the post-moulding conditions, due to different temperatures and relaxation times of the polymer, have been found to be critical ingredients in the calculation of the residual stress distributions.

The improved method of computation has predicted correctly the dependence of residual stress distribution on cooling conditions after de-moulding and on the pressure or absence of constraints on movement of the moulding within the mould prior to ejection. Although quantitative agreement is not exact, the agreement over a range of conditions are superior to that given in other publications in the literature.

8.1 Cooling temperature effect

Large residual stress distributions can be generated in samples if they are cooled rapidly in liquid nitrogen after injection moulding. Calculations predict very large residual stress magnitudes when samples are cooled in liquid nitrogen. This residual stress is caused by the high cooling rate after demoulding. The predicted residual stress distributions are found to be in good agreement with the corresponding experimental

results. Using method B (taking account of the pressure profile; see Section 4.4 (p. 90)) show slightly better agreement with the experimental results than method A (based on Struik's method; see Section 4.3 (p. 81)).

8.2 Friction constraint effect

The residual stress magnitude can be reduced in samples if they are not constrained by mould surfaces, as when using straight bars and mould release agent. Calculations predict lower residual stress magnitudes when samples are not constrained by the mould surfaces. The residual stress distributions are not very sensitive to the pressure or change of mould release agent if tensile bars with end tabs are used. This is because the shoulders of the samples are still kinematically constrained by the mould, even when using the mould release agent. The predicted residual stress distributions are found to be in quantitatively good agreement with the corresponding experimental results. Using method B equations show slightly better agreement with the experimental results than method A.

8.3 Packing pressure effect

When barrel temperatures were adjusted to maintain production of visually satisfactory mouldings from polystyrene, the residual stress distributions were not very sensitive to changes in injection pressure in the range 37 - 143 MPa[157]. This result seems to indicate that there might be a compensating effect. Calculations confirmed that residual stress distributions are not very sensitive to changes in injection pressure in the range 37 - 143 MPa, when using the temperatures corresponding to the experimental moulding conditions in the earlier study. Comparison of the residual stress magnitudes obtained in experiments and in the calculations did not show good agreement. This may be affected

by high melt temperature.

8.4 Stress relaxation effect

In most thermoplastics creep and stress relaxation proceed at fairly significant rates at room temperature. Therefore, it is expected that residual stress relaxes during ageing at room temperature. Calculations have to be made for different elapsed times after demoulding because residual stress measurements are not usually made just after mouldings have been made. All the computed results given in this thesis take into account the residual stress relaxation. This method reduces the disagreements between experimental results and computed results.

REFERENCES

[1] Boundy R. H., Boyer R. F., "Styrene its polymers, copolymers and Derivatives", Hafner Publishing co., 1970

[2] Kavesh S., Schultz J. M., Polym. Eng. Sci., 9, 5 (1969)

[3] Karasz F. E., MacKnight W. J., Macromolecules 1, 537 (1968)

[4] Ferry J. D., "Viscoelastic Properties of Polymers", Wiley, New York, 1970

[5] Leuchs O., "The Classifying of High polymers" Butterworth, London, 1968

[6] Lodge A. S., Meissner J., Rheol Acta **12**, 41 (1973)

[7] Chang R-Y., Chiou S-Y., Polym. Eng., Sci. **35**, 1733 (1995)

[8] Liu S-J., Polym. Eng. Sci., **36**, 807 (1996)

[9] Flaman A. A. M., Polym. Eng. Sci. **33** 193 (1993)

[10] Chang R-Y., Tsaur B. D., Polym. Eng. Sci., **33**, 1222 (1995)

[11] Markovsky A., Soules T. F., Chen V., Vukcevich M. R., J. Rheol. **31** 785 (1987)

[12] Nowick A. S., In B.Chalmers, Progress in Metal Physics, Interscience, New York p.1. (1953)

[13] Van Krevelen D.W., "Properties of polymers", Elsevier, 1990.

[14] Struik L. C. E., "Physical Ageing in Amorphous Polymers", in: "Failure of Plastics" Brostow W. and Corneliussen R. D., Eds., Hanser, Munich, 1986

[15] Struik L. C. E., "Physical Ageing in Amorphous Polymers and other Materials", Elsevier, Amsterdam, 1978.

[16] Struik L. C. E., "Internal Stresses, Dimensional Instabilities and Molecular Orientations in Plastics", John Wiley & Sons (1990).

[17] McCrum N. G., Read N. G., Williams G., "Anelastic and Dielectric Effects in Polymeric Solids", Wiley, London, 1967

[18] Struik L. C. E., Dorfmuller T., Williams G., in "Molecular Dynamics and Relaxation Phenomena in Glasses", Eds., Lecture Notes in Physics, **277**, Springer, Berlin (1987)

[19] Gortemaker F. H., Janschitz-Kriegl H., Delft Prog. Rep., Series **A1**, 73 (1974)

[20] Gortemaker F. H., Janschitz-Kriegl H. and Nijenhuis K., Rheol Acta, **15**, 487 (1976)

[21] Rouse P. E., J.Chem.Phys., **21**, 1272 (1953)

[22] McCrum N. G., Read B.E., Williams G., "Anelastic and Dielectric Effects in Polymeric Solids", John Wiley & Sons Ltd (1967)

[23] Kirkwood J. K. and Fuoss R. M., J. Chem. Phys., **9**, 329 (1941)

[24] Yamafuji K. and Ishida Y., Kolloid Z., **15**, 183 (1962)

[25] Bueche F., J. Polymer Sci., **54**, 597 (1961)

[26] Doolittle A. K., J. Appl. Phys., **54**, 597 (1951)

[27] Doolittle A. K., J. Appl. Phys., **23**, 236 (1951)

[28] Kovacs A. J., Fortschr Hochpolymer Forsch., **3**, 394 (1964)

[29] Menges G., Thienel P., Polym. Eng. Sci., **17**, 758 (1977)

[30] Oyanagi Y., Sato S., Kubota K., Seikei kakko, **4**, 340 (1990)

[31] Spencer R. S., Gilmore G.D., J. Appl. Phys., **20**, 502 (1949)

[32] Spencer R. S., Gilmore G.D., J. Appl. Phys., **21**, 523 (1950)

[33] Kamal H. R., Levan N.T., Polym. Eng. Sci., **19**, 1162 (1975)

[34] Smith R. P., J. Polymer Sci., 8, 1337 (1970)

[35] Tait P. G., Phys. Chem. **2**, 1 (1888)

[36] Simha R., Wilson P.S., Olabisi O., Kolloid Z., **251**, 402 (1973)

[37] Hartman B., Haque M. A., Appl. Polym. Sci., **30,** 1553 (1985)

[38] Hartman B., M. Haque A., Appl. Polym. Sci., **58,** 2831 (1985)

[39] Simha R., Somcynsky T., Macromolecules, **2,** 342 (1969)

[40] Pastine D. J., Warfield R.W., Polymer, **22,** 1754 (1981)

[41] Chiang H. H., Tech. Rept. No. 62, Cornell Injection Molding Program, Cornell

[42] Debye P., Math. Vorlesungen Univ.Göttingen **6,** 19 (1964)

[43] Kardos A., Forsch. Geb. Ingenieurw. **5B,** 14 (1934)

[44] Sakiadis B. Coates C. J., A. I. Ch. E. J. **1,** 275 (1955)

[45] Sakiadis B. Coates C. J., A. I. Ch. E. J. **2,** 88 (1955)

[46] Dainton F. S., Evans D. M., Hoare F. E., Melia T.P., Polymer, **3** 286 (1962)

[47] Passaglia E., Kevorkian R., Appl. Phys., **34,** 90 (1963)

[48] Gee D. R., Melia T. P., Makromol. chem. **132,** 195 (1970)

[49] White J. R., Academic review in KBS Plastics, RAPRA Technology Ltd., Shrewsbury (1996)

[50] Thompson M. and White J. R., Polym. Eng. Sci, **24,** 227 (1984)

[51] Adams L H. and Williamson E. D., J. Franklin Institute, **190,** 835 (1920).

[52] Leaderman H., "viscoelasticity Phenomena In Amorphous High Polymeric Systems", Chap. 1 in Rheology. Vol. 2, pp. 1-61, F. R. Enrich, ed., Academic Press, New York. (1958).

[53] Moreland L. W. and Lee E. H., Trans. Soc. Rheol, **4,** 233 (1960)

[54] Lee E. H. and Rogers T. G., Trans. ASME, J. Appl Mech., **30,** 127 (1963)

[55] Lee E. H., Rogers T. G., and T. C. Woo, J. American Ceram. Soc., **48,** 480 (1965)

[56] Narayanaswamy O. S., Gardon R., J. Am. Ceram. Soc., 52, 554 (1969)

[57] Bürkle D., Kunststoffe **65**, 25 (1975) [Engl. trans.: Kunststoffe: German Plastics **65(1)**, 9 (1975)]

[58] Knappe W., Kunststoffe **51**, 562 (1961) [Engl. trans.: Kunststoffe: German Plastics **51(9)**, 561 (1961)

[59] Struik L. C. E., Polym. Eng. Sci, **18**, 799 (1978)

[60] Isayev A. I., Crouthamel D. L., Polym. Plast. ,Technol. Eng. **22**, 177 (1984)

[61] Eduljee R. F., Gillespie J. W. Jr, McCollough R. L., Thermoplast J., Compos. Mater. **2**, 319 (1989)

[62] Chang R-Y., Tsaur B. D., Polym. Eng. Sci. **33**, 1222 (1995)

[63] Titomanlio G., Brucato V. M. B., Kamal M. R., Intern. Polym. Processing **1**, 55 (1987)

[64] Brucato V. M. B., Piaccarolo S., Titomanlio C., Mater. Eng. **1**, 597 (1989)

[65] Wimberger-Friedl R., J. Polym. Sci., **32**, 595 (1994)

[66] Williams J. G., Plast. Rubber Process. Appli., **1**, 369 (1981)

[67] Lee C. S., Dubin Sarkar A. K., Squire K. R., Vorres C. L, Yuhas D. E., and Blechl J., SPE ANTEC Tech. Paper, **36**, 375 (1990)

[68] Santhanam N., PhD thesis, Cornell University, Ithaca, N.Y. Also Cornell Injection Moulding Program (CIMP) Technical Report No.71 (1992)

[69] Bushko W. C., Stokes V. K., Polym. Eng. Sci, **35**, 351 (1995)

[70] Bushko W. C., Stokes V. K., Polym. Eng. Sci, **35**, 365 (1995)

[71] Bushko W. C., Stokes V. K., Polym. Eng. Sci, **36**, 322 (1996)

[72] Bushko W. C., Stokes V. K., Polym. Eng. Sci, **36**, 659 (1996)

[73] Jansen K. M. B., Intern. Polym. Proc. **1**, 82(1994)

[74] Jansen K. M. B., Titomanlio G., Polym. Eng. Sci, 36, 2029 (1996)

[75] Aggarwala B. D., Saibel E., Phys. and Chem. of Glasses, 2, 137 (1961)

[76] Boley B. A., Wiener J. H. 'Theory of Thermal Stress', Wiley, London, 1960.

[77] Timoshenko A. J., Goodier J. N., 'Theory of Elasticity', McGraw-Hill, New York, 1951

[78] Tadmor Z., J. Appl. Polym. Sci. 18, 1753 (1974)

[79] Baaijens F. P. T, Douven L. F. A., Appl. Sci. Res. 48, 141 (1991)

[80] Zoetlief W. F., Douven L. F. A., Ingen Housz A. J., Polym. Eng. Sci. 36, 1886 (1996)

[81] Hindle C. S., White J. R., Dawson D., Thomas K., Polym. Eng. Sci. 32 157 (1992)

[82] El-Rafey E., Abdelkader A., Kandil S. H., J. Appl. Polym. Sci. :Appl. Polym. Symp. 55 129 (1994)

[83] Liou M. J., Suh N. P., Polym. Eng. Sci. 29, 441 (1989)

[84] Siegmann A., Buchman A., Kenig S., Polym. Eng. Sci. 22, 560 (1982)

[85] Sandilands G. J. and White J. R., Polymer, 21, 338 (1980)

[86] Kwok E. S., Li Tong, White J. R., Polym. Eng. Sci. 36, 651 (1996)

[87] Pham H. T., Bosnyak C. P., Sehanobish K., Polym. Eng. Sci. 33, 1634 (1993)

[88] Allan P. S., Mortazavi M. I., Plast. Rubb. Proc. Applics. 5, 71 (1985)

[89] Titomanlio G., Drucato V., Kamal M.R., Int. Polym. Process, 1, 55 (1987)

[90] Amano K., Seikei kakko, 21, 114 (1988)

[91] Coates P. D., Haynes A. R, Speight R.G., Polymer, 35 3831(1994)

[92] Coates P. D., Rose R. M., Wilkinson B., Plast. Rub. Comp. Proc. Appl., 23, 295 (1995)

[93] Speight R. G., Coates P. D., J. B. Hull, C. Peters, J. Proc. Mech. Eng., 211, 115

(1997)

[94] Chiang H. H., Hieber C.A., Wang K.K., Polym. Eng. Sci., **31**, 139 (1991)

[95] Wagner A. H., Kalyon D.M., Polym. Eng. Sci., **36** 1897 (1996)

[96] Greener J., Polym. Eng. Sci., **26**, 534 (1986)

[97] McKinney J. E., Simha R., J Res. Nat. Bur. Stand. Section A, **81**, 283 (1977)

[98] Brown I. G., Wetton R. E., Richardson M. J., Saville N.G., Polymer, **19**, 659 (1978)

[99] Prest W. M. Jr., O'Reilly J. M., Roberts F. J. Jr., Mosher R. A., Polym. Eng. Sci., **21**, 1181 (1981)

[100] Oels H-J., Rehage G., Macromolecules, **10**, 1036 (1977)

[101] Greener J., Polym. Eng. Sci., **26**, 85 (1986)

[102] Sandilands G. J., White J. R., J. Appl .Polym. Sci. **30**, 4771 (1985)

[103] White J. R., Mater. Sci. Eng. **45**, 35 (1980)

[104] White J. R ., Rheol. Acta. **20**, 23 (1981)

[105] El-Rafey E., Kandil S. H., Abdelkader A., Kunststoffe **81** 710 (1991) [Engl. trans.: Kunststoffe: German Plastics **81**(8) 20(1991)]

[106] Haworth B., White J. R., J. Mater. Sci. **16**, 3263 (1981)

[107] Struik L. C. E., Polym. Eng. Sci. **17**, 165 (1977)

[108] Qayyum M. M., White J. R., J. Mater. Sci. **20**, 2557 (1985)

[109] Qayyum M. M., White J. R., J. Appl. Polym. Sci. **43**, 129 (1991)

[110] Qayyum M. M., White J. R., J. Mater. Sci. **21**, 2391 (1986)

[111] Pearson J. R. A., Mechanical Principles of Polymer Processing. Pergamon Press. Oxford (1966)

[112] Harry D. H., Parrott R. G., Polym. Eng. Sci., **10**, 209 (1970)

[113] Kamal M. R., Kenig S., Polym. Eng. Sci., 12, 294 (1972)

[114] Kamal M. R., Kenig S., Polym. Eng. Sci., 12, 302 (1972)

[115] Stevenson J. F., Galskoy A., Wang K. K., Chen I., Reber D. H., Polym. Eng. Sci., 17, 706 (1977)

[116] Kamal M. R., Kuo Y., Doan P. H., Polym. Eng. Sci.,15, 863 (1975).

[117] Kuo Y., Kamal M. R., AIChEJ., 22. 661 (1976)

[118] Broyer E., Gutfinger C., Tadmor Z., Trans. Soc. Rheol., 19, 423 (1975)

[119] Hieber C. A., Shen S.F., J. Non-Newt. Fluid Mech., 7, 1 (1980)

[120] Hieber C. A., Socha L. S., Shen S. F., Wang K. K., Isayev A. I., Polym. Eng. Sci., 23, 20 (1983)

[121] Schlichting H., Boundary-Layer Theory. 6th ed., McGraw-Hill, New York (1968)

[122] Argysis J. H., "Energy Theorems and Structural Analysis" Aircraft Engineering 26, (1954)

[123] Turner M. J., Clough R. W., Martin H. C., Topp L. J., " Stiffness and deflection Analysis of Complex Structures", J. of Aero. Sci. 23, 805(1956)

[124] Noor A., "Survey of Some Finite Element Software Systems", in Kardestuncer H. and Norrie D. H. (editor), " Finite Element Method Hand Book" McGraw Hill, New York, (1987)

[125] Bathe K. J., "Finite Element Procedures", Prentice Hall, Englewood, New Jersey (1996)

[126] Krishnamachari S. I., "Applied Stress Analysis of Plastics", Van Nostrand Reinhold, New York, 1993

[127] Wang V. W., Hieber C. A., Wang K.K., J. Polym. Eng., 7, 21 (1986)

[128] Chung T. S., Ryan M. E., Polym. Eng. Sci., **21**, 271 (1981)

[129] Chung T. S., Ide Y., J. Appl. Polym. Eng. Sci., **28**, 2999 (1983)

[130] Schmidt T. W. and Menges G., SPE ANTEC Tech. Papers. **32**, 92 (1986)

[131] Hieber C. A., in Injection and Compression Molding Fundamentals, A. I. Isayev, ed., ch. 1, Marcel Dekker, New York (1987)

[132] Titomanlio G., Piccarolo S., Levati G., J. Appl. Polym. Sci., **35**, 1483 (1988)

[133] Wang K. K., Himasekhar K, Chiang H. H, , Jong W. R., Wang V. W., SPE ANTEC '91 (1991) 267

[134] Himasekhar K., Lottey J., Wang K. K., ASME J. Eng. Ind., **114** 213 (1992)

[135] Chiang H. H., Himasekhar K, Santhanam N., Wang K. K., ASME. J. Eng. Mater. Tech., **37**, 115 (1993)

[136] Akay M., Ozden S. , Tansey T., Polym. Eng. Sci. **36**, 1839 (1996)

[137] Ni S. J., Wang K. K., SPE ANTEC '93 1612 (1993)

[138] Gennari A. G., SPE ANTEC '93 3436(1993)

[139] De Frahan H. H., Verleye V., Dupret F, Crochet M. J., Polym. Eng. Sci. **32**, 254 (1992)

[140] Matsuoka T., Takabatake J-I., Inoue Y, Takahashi H., Polym. Eng. Sci. **30**, 957 (1990)

[141] Matsuoka T., Polypropylene: Structure, Blends and Composites, Vol.3: Composites, Ed. Karger-Koksis J., Chapman & Hall, London, 113 (1995)

[142] Lockett F. J., Plast. Rubb. -Proc **5**, 85 (1980)

[143] Bay R. S., Tucker C. L. III, Polym. Compos. **13** 317 (1992)

[144] Bay R. S., Tucker C. L. III, Polym. Compos. **13**, 332 (1992)

[145] Advani S. G., Tucker C. L. III, J. Rheol. **31**, 751 (1987)

[146] Folgar F., Tucker C. L. III, J. Reinf. Plast. Compos. 3 (1984) 98

[147] Advani S. G., Tucker C. L. III, J. Rheol. 31 (1987) 751

[148] White J. R., Residual stresses in polymers, Encyclopedia of Mater. Sci. and Eng. Suppl. Vol. 1 Ed. R.W. Cahn, Pergamon, Oxford, 471(1988)

[149] Treuting R. G., Read W.T., J.Appl.Phys., **22,** 130 (1951)

[150] White J. R., Polym. Testing, **4**, 165 (1984)

[151] Akay M., Ozden S., Polym. Testing, **13**, 323 (1994)

[152] Coxon L. D., White J. R., J. Mater. Sci., 14, 1114 (1979)

[153] Coxon L. D., White J. R., Polym. Eng. Sci., 20, 230 (1980)

[154] Paterson M. W. A., PhD thesis, University of Newcastle upon Tyne, U.K. (1989)

[155] Haworth B., C.S. Hindle, G.J. Sandilands, J.R. White, Plast. Rubb. Proc. Applics., 2, 59(1982)

[155] Crosby S. M., White J.R., Plast. Rubb. Proc. Appl., **12** 159 (1989)

[156] Conduction of Heat in Solids, Carslaw H. S., Oxford At the Clarendon Press (1959)

[157] Boley B. A. and Wiener J. H., 'Theory of Thermal Stresses', Wiley, London, 1960.

[158] Timoshenko S., and Goodier J. N., 'Theory of Elasticity', McGraw-Hill, New York.

[159] Struik L. C. E., Polym. Eng. Sci, **18**, 799 (1978)